2014

Hyperthin Organic Membranes for Gas Separations

Minghui Wang
Lehigh University

Hyperthin Organic Membranes for Gas Separations

by

Minghui Wang

A Dissertation

Presented to the Graduate and Research Committee

of Lehigh University

in Candidacy for the Degree of

Doctor of Philosophy

in

Polymer Science and Engineering

Lehigh University

May, 2014

Approved and recommended for acceptance as a dissertation in partial fulfillment of the requirements for the degree of Doctor of Philosophy.

Name: Minghui Wang

Dissertation Title: Hyperthin Organic Membranes for Gas Separations

_____
Defense Date

_____
Steven L. Regen, Dr., Advisor

_____
Accepted Date

Committee Members

_____
Steven L. Regen, Dr., Chair

_____
Gregory S. Ferguson, Dr.

_____
James E. Roberts, Dr.

_____
Lloyd M. Robeson, Dr.

Copyright Permissions

The material contained in Chapters 3, 4, 5 and 6 has been published prior to submittal of this dissertation. The proper copyright permission was obtained from each journal before submittal of this document, with the publication cited at the beginning of the chapter.

Acknowledgments

I wish to express my gratitude to Dr. Steven L. Regen, my dissertation advisor, for all his guidance and thoughtful suggestions throughout my Ph.D. study. I would also like to thank the members of my dissertation committee, Dr. Lloyd M. Robeson, Dr. Gregory S. Ferguson and Dr. James E. Roberts for their contributions to the studies discussed in this dissertation. In addition, I would also like to extend my thankfulness to all the faculty and staff members in the Department of Chemistry, Lehigh University, for their help during these years, especially Dr. Ned D. Heindel.

Special thanks should be given to Dr. Vaclav Janout in our group for synthesizing most of the surfactants for this research and for teaching me how to do organic synthesis. I would also like to thank Dr. Yao Wang for teaching me all the necessary techniques needed for this research. I also thank Dr. Song Yi for his contribution to part of this research. Furthermore, I thank all of the past and present members of the Regen group for their helpful advice and support.

Special gratitude is also due to Ms. Jie Fu in Dr. Bruce E. Koel's Group in Princeton University for her help with XPS measurement in this study.

Finally, I would like to thank my wife Ms. Nisha Zhu and my whole family for their love, encouragement and constant support.

Table of Contents

List of Tables

List of Figures

Abstract

Gas separation is practically important in many aspects, *e.g.*, clean energy production and global warming prevention. Compared to other separation technologies like cryogenic distillation and pressure swing adsorption, membrane separation is considered to be more energy efficient. For practical purposes, the ultimate goal is to construct membranes producing high flux and high gas permeation selectivity at the same time. Based on the inverse relationship between flux and membrane thickness, it is clear that fabricating highly selective membranes as thin as possible could increase the flux through the membrane without sacrificing selectivity. But it has proven to be challenging to manufacture selective membranes in the hyperthin (< 100nm) region. [Note: 100 nm is the typical dense layer thickness of commercial membranes to separation gases.] In this dissertation, the focus is on the development of hyperthin selective membranes that were supported by poly(1-trimethylsilyl-1-propyne) (PTMSP), using Langmuir-Blodgett (LB) and Layer-by-Layer (LbL) deposition methods.

A "gluing" strategy has been successfully introduced into LB films by our laboratory recently, in which LB monolayers are ionically crosslinked with polyelectrolytes. This success stimulated the pursuance of LB films with improved gas separation properties by: (i) examining calix[n]arene-based surfactants with different sizes (ii) using polymeric surfactants as LB forming materials, and (iii) optimizing the condition of the subphase containing polyelectrolytes. Both a strong polyelectrolyte poly(4-styrene sulfonate) (PSS) and a weak polyelectrolyte poly(acrylic acid) (PAA) were used to create glued LB bilayers. The gas permeation through PSS or PAA-glued LB bilayers made of calix[n]arenes was found to be dominated by solution-diffusion rather than molecular-

sieving mechanism. The porous nature of calix[n]arene-based surfactants also turned out to be unnecessary for constructing LB films with high gas selectivities, because a single PAA-glued LB bilayer made of a nonporous polymeric surfactant (*ca.* 7 nm) was found to exhibit a much higher H_2/CO_2 selectivity (200), which reached the "upper bound". The key factors that are likely to affect the quality of the glued LB bilayers were: (i) the degree of ionic crosslinking between surfactants and polyelectrolytes, (ii) charge repulsion and (iii) hydrogen bonding among the polyelectrolyte chains. In principle, employing a surfactant bearing a large number of ionic sites (*e.g.*, a polymeric surfactant) that can increase the degree of ionic crosslinking and a weak polyelectrolyte (*e.g.*, PAA) that can be optimized to minimize the charge repulsion and maximize the hydrogen bonding should afford glued LB films with high gas selectivities. The current finding also indicated that the PAA layer filled in between two surfactant monolayers served as the main gas barrier.

In a related study, polyelectrolyte multilayers (PEMs) (*ca.* 14 nm in thickness), which were made from structurally matched (*i.e.*, two oppositely charged polyelectrolytes having identical backbones) and unmatched polyelectrolytes pairs, both showed high CO_2/N_2 selectivities (*ca.* 100-150). However, the permeabilities of PEMs derived from structurally matched polyelectrolytes were significantly higher than that from an unmatched pair. The larger solubility of CO_2 with respect to N_2 in these PEMs should be the reason lead to the high CO_2/N_2 permeation selectivities.

Chapter 1

Background and Specific Aims

1.1 Gas Separation Background

The attempt to isolate single gas species can be traced back to the 18th century, when O_2 and N_2 were discovered by Joseph Priestly and Daniel Rutherford, respectively.[1,2] However, it wasn't until the second half of the 19th century that serious efforts was made to liquefy the industrially important gas, O_2, in response to the increasing demand for high quality steel. The main reason is that O_2 can be used to increase the smelting of ore.[3] In 1895, Carl Linde patented the idea of separating O_2 by cryogenic distillation, but he didn't successfully manufacture his final device until early in the 20th century.[4-6] Since then, many gaseous species have been isolated and purified for various purposes, mainly by cryogenic distillation.[7]

1.1.1 The Need of Separating Gases

Currently, almost every known gas is being isolated for different reasons.[8] In this section, only four gases of interest are introduced. Pure oxygen finds its importance in the medical and life-support fields.[9] Furthermore, oxygen is also critical in the steel industry as well as in the chemical industry.[3]

Another important gas is nitrogen, which is the major component of our atmosphere. Nitrogen can be used as the replacement of air to provide an inert atmosphere when oxidation is undesirable.[10] Moreover, liquid nitrogen is widely applied as a refrigerant to provide an ultra-low temperature environment.[8,10]

In addition to oxygen and nitrogen, the separation of hydrogen from nitrogen in the ammonium-production process has been commercialized since 1980.[11] Recently, the separation of hydrogen from carbon dioxide has also become of considerable interest.[12-25] Hydrogen has been used in the petroleum and chemical industry for a long time.[26] It is also considered to be especially attractive as a clean source of energy, as its product is only water when used in fuel cells.[27] For these reasons, developing improved methods of separating hydrogen has become of major interest.[14-18] Currently, steam-methane reforming in combination with the water-gas shift reaction represents the most economical technique for the production of hydrogen.[28,29] Since the hydrogen that is produced in this way contains a significant amount of CO_2 (up to *ca.* 20%), the removal of CO_2 from H_2 is of particular interest.[14]

At present, flue gas (mainly CO_2 and N_2), which is generated from power plants, accounts for the majority of man-made CO_2 emissions.[22-24] Because of concern of global warming, there is also considerable interest in developing improved methods for separating and capturing CO_2 from flue gas.

1.1.2 Non-Membrane Technologies for Gas Separations

Before the emergence of membrane technology,[11,30-36] there were two main technologies used for separating gases; *i.e.*, cryogenic distillation[8,37] and sorption methods[38-42]. These two methods are briefly discussed in the following sections.

1.1.2.1 Cryogenic Distillation[8, 37]

Cryogenic distillation separates gases based on the differences in boiling point. It was first employed by Carl Linde to separate O_2/N_2 in the early part of the 20th century.[4-6] A

two-column system was used to ensure the purity of the final products. Similar systems can also be applied to isolate argon and other gases.[8]

The attractiveness of this method lies with its ability to produce large quantities of high-purity gases.[11] If operated on a large scale, the cost of the final gas that is obtained is usually less expensive than when produced by other methods. However, the cryogenic processes has a large capital cost, mostly due to the cost of large compressors and expansion turbines. Moreover, the need to cool the gases to below their boiling points requires a large consumption of energy. Although a variety of modest modifications have been made to the cryogenic method to improve its overall energy efficiency, the need for taking advantage of liquid/gas phase transition processes remains, as do significant energy requirements.

1.1.2.2 Sorption Methods: Amine scrubbing[25,42], Temperature Swing Adsorption[39], Pressure Swing Adsorption[15,38] and Vacuum swing Adsorption[40, 41]

Amine scrubbing has been used on a small scale to capture CO_2 from flue gas from coal-fired power plants.[42] In a typical process, a 20% or 30% monoethanolamine (MEA) aqueous solution is used as the absorbent (scrubber) to absorb CO_2 from flue gas. The scrubber is regenerated later by releasing CO_2 at elevated temperature (100 to 120 ℃). The advantage of the amine scrubbing process lies in its simplicity and its maturity. However, a large capital investment, a constant loss of MEA during recycling, and a large amount of energy that is required for the regeneration step are the major disadvantages. In addition, amine scrubbing processes are limited to the capture of acidic gases.

Temperature swing adsorption (TSA)[39], pressure swing adsorption (PSA)[15,38] and vacuum swing adsorption (VSA)[40, 41] are alternative methods for separating gases, in

which solid adsorbents are used to capture one of the gaseous components. This gas is then released by increasing the temperature (for TSA) or reducing the pressure (for PSA and VSA). For PSA, the inlet gas mixture is compressed to a higher pressure to ensure efficient adsorption by the adsorbent. The pressure is then reduced to the ambient pressure for desorption of adsorbates.[15,38] For VSA, this releasing step is further enhanced by lowering the pressure of the column to sub-atmospheric pressure after adsorption has been completed at the higher pressure.[40, 41] Of these three technologies, TSA is considered to be a good choice for CO_2 capture from post-combustion flue gas, because of the possibility of utilizing low-grade heat from the power plant as a source of energy for regenerating the adsorbents.[20] In contrast, PSA is better suited for pre-combustion CO_2 capture, because the gas mixtures are inherently pressurized after the conversion reactions.[20] The PSA process has been commercialized as an onsite nitrogen generator by a number of companies For example, Air Products has been producing high purity nitrogen (up to 99.9995%) based on the PSA method since the 1980s.[43] The adsorbents that are employed are usually highly porous materials such as zeolites, activated carbon, silica gel, alumina and carbon molecular sieves (CMS).[43] The limitation of these adsorption-based gas separation methods lies in the efficiency of adsorbents and the large energy consumption that is needed for the regeneration process. Currently, a new class of adsorbents, generally referred to as Metal Organic Frameworks (MOF), is attracting a lot of attention as potential substitutes.[20]

In addition to these two traditional technologies for gas separations, membrane-based methods have emerged as an attractive alternative over the past 30 years.[11,31,44] This

method is based on the principle that gases have different permeabilities across a given membrane material. A detailed introduction is given in the next section.

1.2 Gas Separations by Use of Membranes.

The use of membranes to separate gases is a relatively new technology, although the study of gas permeation through membranes has a long history. Graham's law of effusion developed by Thomas Graham in first half of 19th century is one example.[45,46] Later, owing to the availability of synthetic polymer membranes, the solution-diffusion model of gas permeation was developed from the 1940s to the 1950s.[47] Nevertheless, the first commercial use of membranes for gas separations only appeared in 1980 with the introduction of a hydrogen selective Prism technology by Monsanto.[48] Soon after Prism's successful debut, other companies such as Dow and Grace Membrane Systems, started to manufacture membranes for gas separations.[11]

1.2.1 Mechanisms of Membrane-Based Gas separations [11, 49-51]

Figure 1.1 shows two gaseous permeants (*i* and *j*) diffusing across a polymeric membrane. Here, the flux (*J*) of each gas is related to its permeability coefficient (*P*), the pressure gradient (Δp) that is applied across the membrane, and the thickness of the membrane (l), as shown in equation (1).[50] Rearrangement to equation (2) expresses this relationship in terms of a normalized flux or "permeance", P/l. The membrane's permeation selectivity, α, is then defined by the ratio of the two permeabilities or the two permeances (equation 3).[50]

$$\boldsymbol{J}\left(\frac{\boldsymbol{cm^3}}{\boldsymbol{cm^2 \cdot s}}\right) = \frac{\boldsymbol{P \cdot \Delta p}}{\boldsymbol{l}} \quad \textbf{(1)}$$

$$\frac{\boldsymbol{P}}{\boldsymbol{l}}\left(\frac{\boldsymbol{cm^2}}{\boldsymbol{cm^2 \cdot s \cdot cmHg}}\right) = \frac{\boldsymbol{J}}{\boldsymbol{\Delta p}} \quad \textbf{(2)}$$

$$\alpha_{ij} = \frac{(\frac{P}{l})_i}{(\frac{P}{l})_j} \quad (3)$$

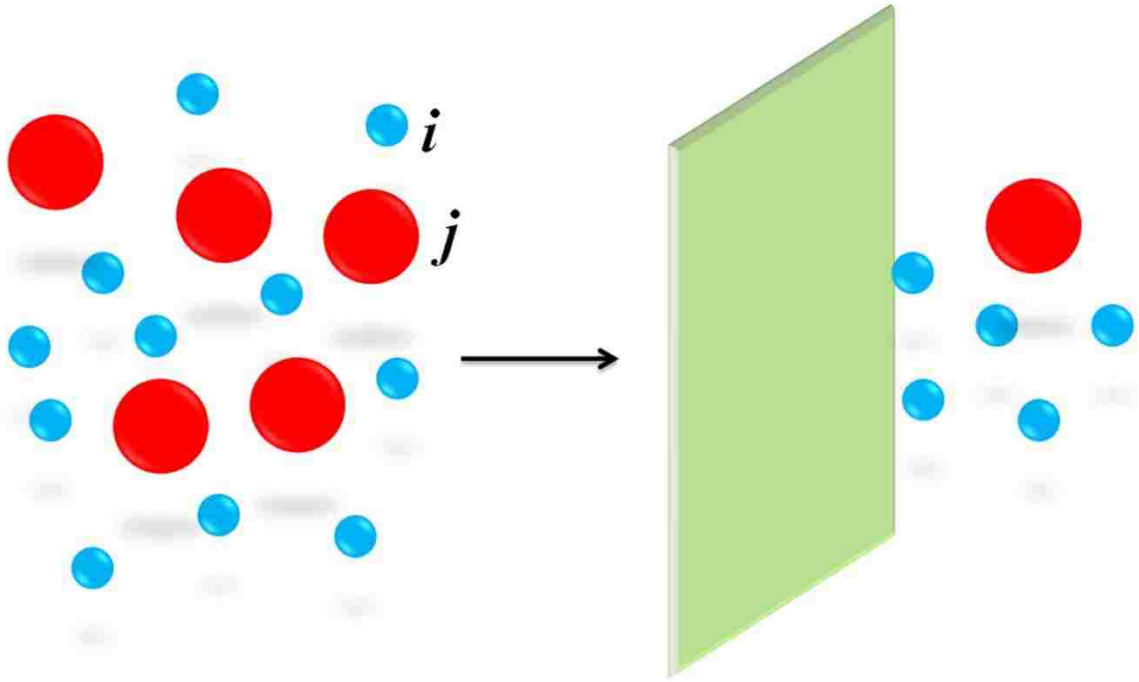

Figure 1.1 Schematic illustration of two gaseous permeants (*i* and *j*) diffusing across a membrane.

Figure 1.2 shows two types of membranes that are commonly used for gas separations: porous membranes (mainly inorganic)[44,52-55] and dense membranes (mainly polymeric).[31] Depending on the size of the pores within these porous membranes, there are four possible mechanisms of permeation: convective flow (>100 nm), Knudsen diffusion (*ca.* 2-100 nm), molecular sieving (*ca.* 0.3-0.5 nm) and surface adsorption and diffusion (*ca.* < 10 nm).[11,34,51] For dense membranes, the main mechanism for gas transport is considered to follow the solution-diffusion model.[11,31,47]

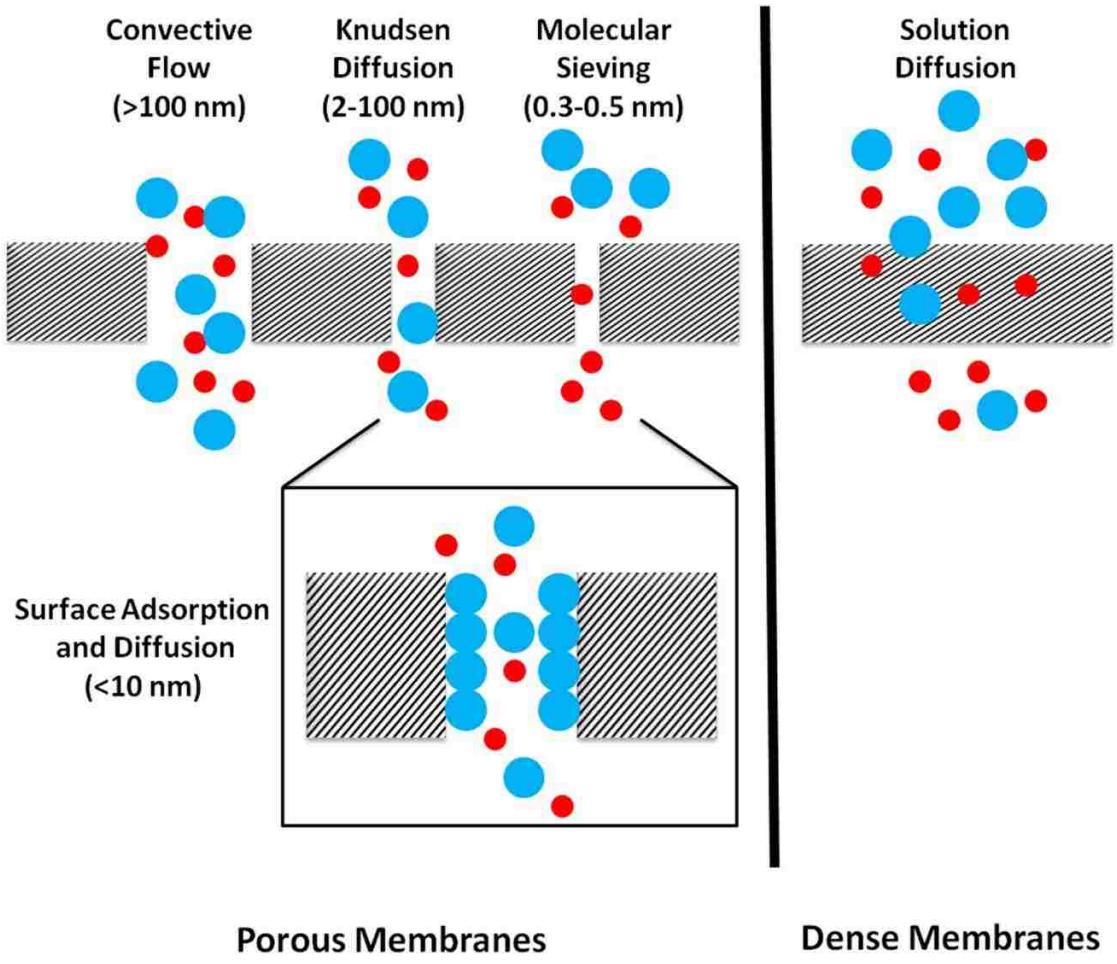

Figure 1.2 Schematic illustration showing gases permeating through porous and dense membranes.

1.2.1.1 Convective Flow[11,34,51]

As illustrated in Figure 1.2, when the pore diameter is larger than 100 nm, convective flow dominates, and this can be described by Poiseuille's law according to equation (4)[11]:

$$J = \frac{r^2 \cdot \varepsilon}{8\eta} \times \frac{[p_0 - p_l][p_0 + p_l]}{l \cdot RT} \quad (4)$$

Here J is the gas flux, η is the viscosity of the gas, r is the pore radius, ε is the porosity of the membrane, l is the pore length and p_o and p_l represent the absolute pressure of gas species at the beginning of the pore (x=0) and at the end of the pore (x=l). In addition, R

is the ideal gas constant and *T* is temperature. From equation (4), the gas selectivity for two gaseous permeants *i* and *j* can be expressed by equation (5):

$$\alpha_{ij} = \frac{\eta_j}{\eta_i} \quad \textbf{(5)}$$

Separations by convective flow have little gas selectivity, because the viscosity η of different gaseous species is very small.[56]

1.2.1.2 Knudsen Diffusion[11,51,57]

If the diameter of the pores is in the range of 2 to 100 nm, Knudsen diffusion generally dominates.[34, 36] In a Knudsen flow, the gas molecules have more collisions with pore walls than with other gas molecules.[36] The flux of the gas is then given by equation (6)[11]:

$$J = \frac{4r\varepsilon}{3} \times \left(\frac{2RT}{\pi M}\right)^{\frac{1}{2}} \times \frac{p_0 - p_l}{l \cdot RT} \quad \textbf{(6)}$$

Here *M* is the molecular weight of the gas molecule. As is apparent, the permeability of a gas (*i*) *via* Knudsen diffusion is proportional to $(M_i)^{-1/2}$. The selectivity of such membranes ($\alpha_{i/j}$) for gases (*i*) and (*j*) is then given by equation (7)[11,36]:

$$\alpha_{ij} = \sqrt{\frac{M_j}{M_i}} \quad \textbf{(7)}$$

This expression is consistent with Graham's law of effusion.[46]

1.2.1.3 Molecular Sieving Effect[11, 36, 51]

For light gases, when the pore diameter of a microporous membrane reaches a size that is comparable to the kinetic diameter of the gas molecules (*ca.* 0.3 to 0.5 nm), the molecular sieving effect can become the major mechanism of transport; *i.e.*, the membrane allows the passage of only gas molecules that are small enough to pass through the pores, while it blocks the passage of larger gas molecules.[11, 36, 51] The

sorption effect is normally ignored when molecular sieving effect is dominating.[11] The flux and diffusion coefficient that are associated with molecular sieve membranes can be expressed as equations (8) and (9), respectively[36,58]:

$$\boldsymbol{J = \frac{\Delta p}{l \cdot RT} \cdot D_0 \cdot \exp\left(\frac{-E_a}{RT}\right)} \quad \textbf{(8)}$$

$$\boldsymbol{D_0 = g_d d_p \lambda^2 \frac{kT}{h} \exp\left(\frac{S_{a,d}}{R}\right)} \quad \textbf{(9)}$$

Here J is flux, D_0 is the diffusion coefficient of the membrane, E_a is the activation energy for permeation, g_d is probability that a molecule can make a jump in the right direction given that jump length is d_p, k and h are Boltzmann's and Planck's constants, respectively, and $S_{a,d}$ is the activation entropy for diffusion. Based on these relationships, it is clear that increasing temperatures will increase the flux of all gaseous species, and decrease the gas selectivity.[36]

1.2.1.4 Surface Adsorption and Diffusion[35,59]

In addition to the above three mechanisms, surface adsorption and diffusion should also be taken into account, when microporous membrane have pore diameters that are less than 10 nm.[11] When the pore size decreases to *ca.* 5 to 10 nm, the total surface area within membranes increases to more than 100 m^2/cm^3. As a result, a significant amount of gas molecules can be adsorbed onto the pore walls, and these adsorbed gas molecules can move by a process of surface diffusion.[11] This is particularlly relevant for separations of CO_2 and other condensable gases from uncondensable gases, because the surface adsorption and diffusion effect is usually more significant for condensable gases. In some case, CO_2 and other condensable gases can block the diffusion of uncondensable gases.[11,36,59]

1.2.1.5 The Solution-Diffusion Model

The solution-diffusion model for gas transport applies to dense non-porous polymeric membranes as shown in Figure 1.2.[11,31, 47] Unlike porous membranes, dense polymeric membranes have no permanent pores that are much larger than the permeating gas molecules. However, they do have dynamic transient gaps, which result from the thermal motions of polymer chains. These transient gaps allow gas molecules to diffuse through polymeric membranes.[60] When the gaseous permeants pass through such membranes, they first adsorb and dissolve into the membrane surface and then dissolve into the bulk membrane. The gas molecules then diffuse through the membrane down a concentration gradient.[11, 47] Gas separations are achieved based on overall differences in permeation rates for the different permeants.

The flux of gas across the membrane in the integrated Fick's law form is expressed as equation (10)[11, 47]:

$$\boldsymbol{J = D \times S \cdot \frac{\Delta p}{l}} \qquad \textbf{(10)}$$

Here *S* is the solubility of a gas in a membrane. The permeability of a gas crossing through a membrane is then defined by equation (11)[11, 47]:

$$\boldsymbol{P = D \times S} \qquad \textbf{(11)}$$

Combining equation (11) with equation (10) then gives equation (1). Based on equation (11), the gas selectivity can also be expressed as[11, 47]:

$$\boldsymbol{\alpha_{ij} = \left(\frac{D_i}{D_j}\right) \times \left(\frac{S_i}{S_j}\right)} \qquad \textbf{(12)}$$

This means that the gas selectivity is the product of relative gas diffusivity and relative gas solubility in the membrane.

For gas transport across polymeric membranes, the diffusivity of a permeant can vary by several orders of magnitude depending on the particular membrane material. However, the difference in the solubility of the same gas in these different polymeric membranes is usually within a factor of 10. This difference implies that gas transport is more sensitive to the packing and flexibility of the polymer chains than their solubility in the polymer.[11]

The permeation of gases through polymeric membranes is usually described as an activated process.[36,61,62] Thus the permeability and diffusion coefficient of the gas in a polymeric membrane can be expressed by equations (13) and (14), respectively[36,62]:

$$\boldsymbol{P = P_{\Phi} exp(\frac{-E_p}{RT})} \quad \textbf{(13)}$$

$$\boldsymbol{D = D_{\Phi} exp(\frac{-E_d}{RT})} \quad \textbf{(14)}$$

Here E_p is the activation energy for permeation, E_d is the activation energy for diffusion, and P_Φ and D_Φ are temperature independent constants. Based on the activated process and the solution-diffusion mechanism, a correlation between relative gas diffusivity and the size difference of two gaseous permeants can be expressed as shown in equation (15) [61]:

$$\boldsymbol{ln\left(\frac{D_i}{D_j}\right) = \frac{1-a}{RT} \cdot c \cdot (d_j^2 - d_i^2)} \quad \textbf{(15)}$$

Here, a and c are constants, and, d_i and d_j are the kinetic diameters of the two gaseous permeants. Thus the relative diffusivity of a pair of gases is directly related to the size difference of two permeants.[61]

In addition to the activated process, the diffusion of gases across polymeric membranes has also been described by use of a free-volume model.[63] In brief, the free volume is

considered as the unoccupied space that exists between the polymer chains. It is the difference between the membrane's specific volume and the polymer chain's occupied volume.[11] The amount of free volume is then quantified by the percentage of fractional free volume v_f, as shown in equation (16)[11]:

$$\boldsymbol{v_f = \frac{v - v_0}{v}} \quad \textbf{(16)}$$

Here, v is the specific volume of polymer, which is equal to the reciprocal of polymer density, and v_0 is the volume that is occupied by the polymer molecules, themselves. The diffusivity of gas in the membrane is related to the fractional free volume, v_f , by equation (17)[63]:

$$\boldsymbol{D = A \cdot \exp\left(\frac{-B}{v_f}\right)} \quad \textbf{(17)}$$

Here, A and B are both adjustable parameters. As a result, rubbery polymeric membranes usually have a larger gas diffusivity than glassy membranes because of the larger fractional free volume.[11] However, not all glassy polymers have lower free volume than rubbery polymers. For example, poly[1-(trimethylsilyl)-1-propyne] (PTMSP) has one of the largest fractional free volumes (about 30%) of all known organic polymers.[64]

The free-volume theory can also be used to describe the physical aging process of a polymer membrane.[65-67] Based on the free volume theory, the free volume can diffuse in polymeric membranes *via* the thermal motion of the polymer segments. Thus, over time, the free volume will diffuse towards the surface of a membrane and escape the membrane. This explains why a membrane becomes less permeable over time (*i.e.*, the physical aging process). The physical aging process is expected to be faster in thin

membranes because the free volume needs to diffuse less distance to the surface to escape.[65-67]

1.2.2 Membranes of Interest

Currently, both inorganic membranes and polymeric membranes are being investigated for various gas-separation purposes.[31,34,52] Compared to polymeric membranes, however, the choice of inorganic membranes is limited. Inorganic membranes include dense noble metal membranes for hydrogen separation,[68,69] porous zeolite membranes[52,53,70] and carbon molecular sieve membranes[55] for natural gas sweetening (*i.e.*, a process to concentrate methane and to remove impurities such as H_2S and CO_2[71]) and carbon dioxide removal.[52] The inorganic membranes are of interest mainly owing to their robustness at elevated temperature. Nevertheless, the very high capital cost to manufacture such membranes limit their potential for being commercialized.[72] In addition, due to the inherent brittleness of inorganic membranes, they need to be relatively thick to achieve acceptable selectivities. As a result, the flux across such membranes is relatively small when compared to membranes made from organic polymers.[72]

In contrast to inorganic membranes, organic polymeric membranes are relatively inexpensive and generally easy to manufacture and handle.[72] For these reasons that have attracted more attention than inorganic membranes. Table 1.1 shows a summary of commercialized polymeric membranes and their applications. These membranes are usually fabricated into hollow fiber modules or spiral wound modules for end applications.[11,31] In addition to these well-established membrane systems and applications, new polymeric materials are being sought for new applications, such as

CO_2/H_2 and CO_2/N_2 separations for the production of hydrogen and for the removal of CO_2 from flue gas.[16,73]

Table 1.1[a] Commercial membranes for gas separations[11,31,71,74]

Application	Gas Pair	Membranes (Company)
Hydrogen separation	H_2/N_2, H_2/CO and H_2/CH_4	Polyimide (Medal of Air Liquide), Polysulfone (Permea of Air Products), Cellulose acetate (Separex of UOP), Polyimide (Ube)
Natural gas sweetening	CO_2/CH_4	Cellulose acetate (Separex of UOP), Cellulose acetate (Cynara of Cameron), Polyimides (Medal of Air Liquide), Perfluoro silicone rubber (MTR)
Nitrogen enrichment	N_2/O_2	Tetrabromobisphenol A polycarbonate (Generon), Polyimides and Polysulfone (Praxair), Polyimide and polyamide (Medal)
Air dehydration	Air/H_2O	Polysulfone (Cactus of Air Products), Polyimides (Ube)

[a]Information gathered from reference 11, 31, 71 and 74.

1.2.2.1The Upper Bound

Figure 1.3 shows a Robeson's empirical upper-bound plot for H_2/CO_2.[75] In this plot, H_2/CO_2 permeation selectivity is plotted as a function of H_2 permeability $P(H_2)$. The two straight lines that are shown represent the combination of the highest permeation selectivities and the highest permeabilities that had been recorded as of 1991 and 2008, respectively. The negative slopes reflect a "trade-off" between the permeation selectivity and permeability; that is, those polymeric membranes that exhibit greater permeation selectivities usually show lower gas permeabilities and *vice versa*. The red unfilled circles represent the numerous polymers measured up to 2008. The relation between permeability P_i of the more permeable gas and permeation selectivity α_{ij} of two gaseous permeants in the upper bound can then be expressed as equation (18)[75]:

$$P_i = k\alpha_{ij}^n \quad (18)$$

Here *k* is the front factor and *n* is the slope of the log-log plot.

Since the publication of first upper-bound plot in 1991, considerable effort has been made to create new polymers that have permeation properties that lie in the right upper corner of the upper-bound plot (in the direction of the blue arrow in Figure 1.3). At present, polymers of intrinsic microporosity (PIMs) represent the state-of-art polymers for gas separation, which have moderate gas selectivities and high permeabilities.[76,77]

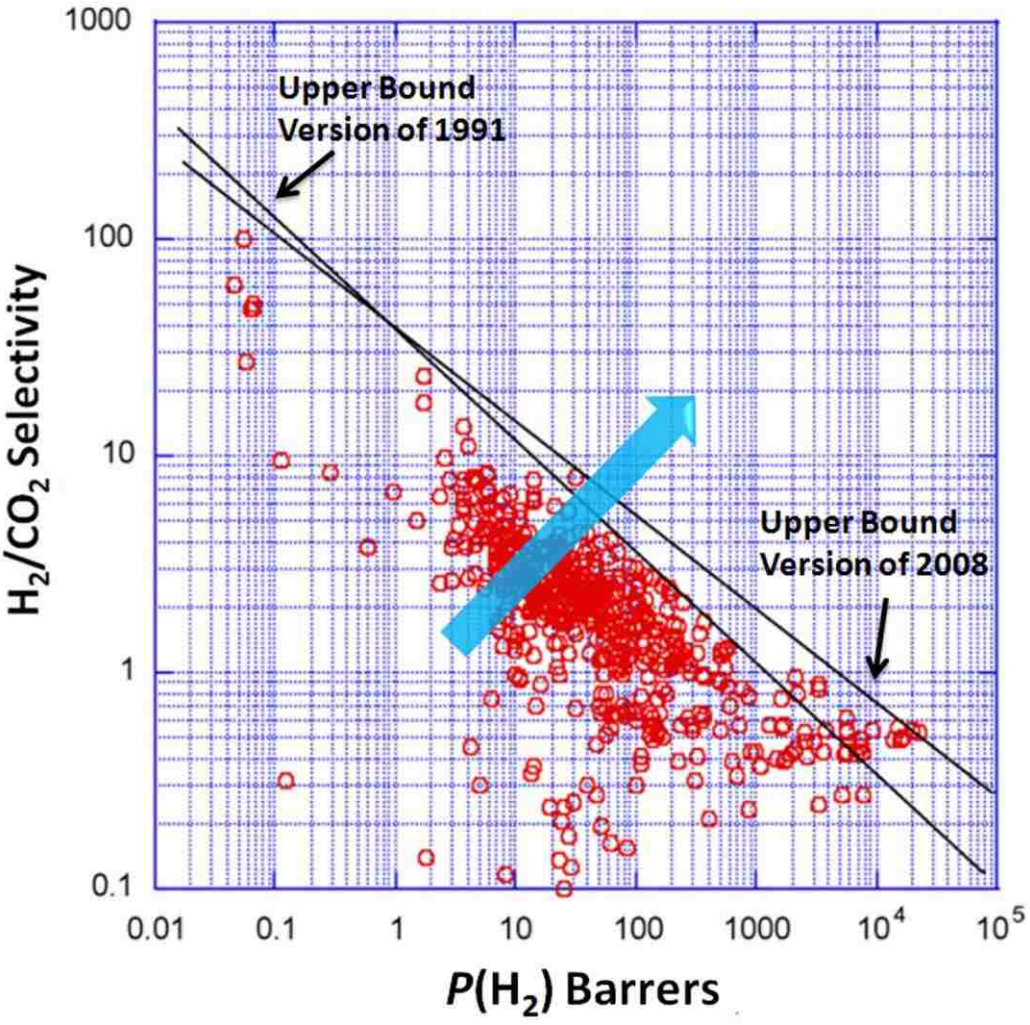

Figure 1.3 The upper-bound plot for H_2/CO_2. Adapted from reference 75, Copyright (2008), with permission from Elsevier.

1.2.2.2 Asymmetric Membranes

The main object of all gas separations is to *obtain high flux and high permeation selectivities*. Based on equation (1), there are three options that are available to increase membrane flux: a) increase the permeability of membrane; b) increase the pressure difference from upper stream and downstream; c) decrease the membrane's thickness. As is apparent, option a) generally lowers the permeation selectivity of the membrane based on the upper-bound plot; *i.e.*, the trade-off that is characteristic of the solution-diffusion model. Option b) is unattractive since it increases the operational cost that is involved. Thus, option c), is especially attractive since it can lead to increased flux with retention of gas permeation selectivity.

Since the decrease of thickness usually results in the decrease of the mechanical strength, asymmetric membranes have been manufactured to overcome this drawback.[11] Figure 1.4 shows a typical structure of an asymmetric membrane, which contains two layers: a) a permeation-selective layer and b) a highly permeable non-selective porous support. According to the series-resistance model, the relationship between the permeance of the composite membrane and the permeance of each layer can be expressed as equation (19)[78]:

$$\frac{\mathbf{1}}{(\frac{\boldsymbol{P}}{\boldsymbol{l}})_{\boldsymbol{Composite}}} = \frac{\mathbf{1}}{(\frac{\boldsymbol{P}}{\boldsymbol{l}})_{\mathbf{1}}} + \frac{\mathbf{1}}{(\frac{\boldsymbol{P}}{\boldsymbol{l}})_{\mathbf{2}}} \qquad \textbf{(19)}$$

This model assumes that the gas-permeation resistance (the reciprocal of gas permeance) of the composite membrane is equal to the sum of the gas permeation resistance of the two layers.[78] Based on this model, the intrinsic gas permeance of the thin skin layer can be calculated by measuring the permeance of the composite and that of the support layer, separately.

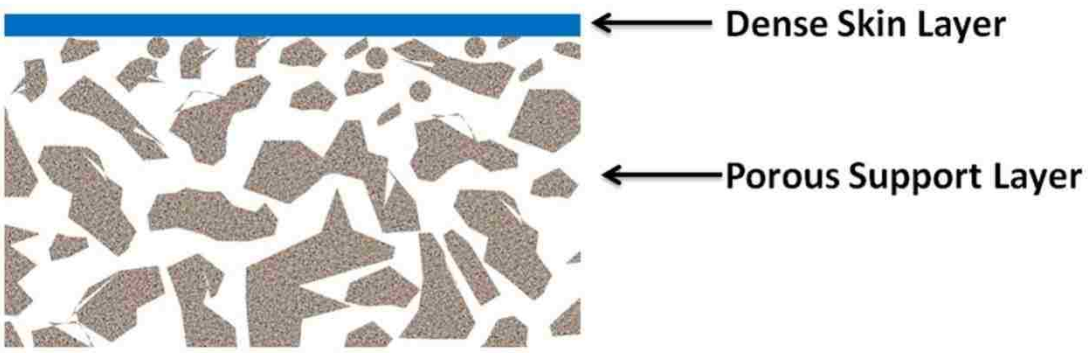

Figure 1.4 Illustration of an asymmetric membrane.

The Main Methods for Creating Asymmetric Membranes

The main methods for creating asymmetric membranes are phase inversion and interfacial polymerization.[11,33,79]

For a typical phase-inversion process, the cast polymer solution is immersed in water after a brief solvent evaporation.[11,79] At the water/solvent interface, the absorption of water and loss of solvent cause the polymer to rapidly precipitate at the interface, thus forming a dense skin layer. Such a process is slower in the bulk phase, allowing the polymer in the bulk phase to have more time to form porous structures.

For interfacial polymerization, a microporous film made of polysulfone is first impregnated with an aqueous amine solution. The film is then treated with a multivalent crosslinking agent in an organic solvent that is immiscible with water. As a result, an ultrathin skin layer forms at the interface of two solutions.[11,33]

Challenges

According to equation (1), it is desirable to fabricate asymmetic membranes using permeation selective layers that are as thin as possible. However, at present, fabricating asymmetric membranes with defect free permeation selective layers less than 100 nm has

proven to be challenging.[80] A "caulking" technique is normally employed to repair defects by using an additional ultra-permeable rubbery layer on top of the skin layer.[11] However, it is desirable to eliminate the defects without the need of applying this additional layer.

1.3 Techniques Employed in Our Laboratory for Fabricating Hyperthin Membranes

Langmuir-Blodgett (LB) and layer-by-layer (LbL) deposition of polyelectrolytes are routinely employed in our laboratory to produce asymmetric membranes having permeation-selective layers with thicknesses that are less than 100 nm, that is, "hyperthin" membranes.[50]

1.3.1 The Langmuir-Blodgett (LB) Method

The Langmuir-Blodgett (LB) method was first introduced by Katherine Blodgett in the 1930s.[81,82] A typical LB deposition process is shown in Figure 1.5. Here, an amphiphilic surfactant molecule (*e.g.*, fatty acid) is first spread onto the air/water interface to form a monolayer, and the monolayer then compressed to a desired surface pressure and subsequently transferred onto a solid support by passing a support vertically through the monolayer. Additional monolayers can be deposited onto the support by passing the support, vertically again, through the monolayer. Most LB films that are fabricated are of the Y-type in which the monolayers are in a head-to-head and tail-to-tail arrangement as shown in Figure 1.5.

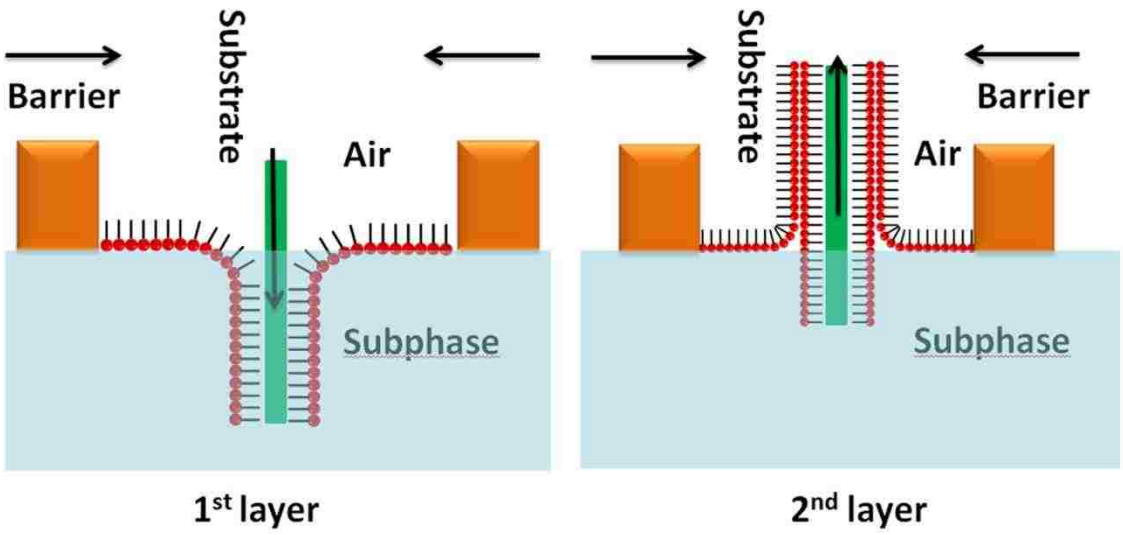

Figure 1.5 Schematic Illustration of the formation of a Y type LB bilayer.

Langmuir-Blodgett (LB) films have been of interest for applications involving nonreflective glass coatings[81-83], chemical sensors[84,85], electronics,[86,87] as well as gas separations.[50, 88-90] The materials used for making LB films has expanded from traditional fatty acids to newly emerged nanoparticles, nanowires, nanotubes and most recently graphene and graphene oxide materials.[86,87,91]

The use of LB films as permeation-selective membranes was first proposed by Katherine Blodgett in her pioneering studies.[83] In particular, she stated that LB films might be employed as "sieves or filters for the segregation of previously `non-filterable' substances of molecular magnitudes. It is only necessary for such filtration that the particles or molecules to be filtered be of a size greater than the dimensions of the molecular voids formed in the film structure."[83] Despite numerous attempts to utilize LB films for gas separations, most studies have found that their permeation selectivities were close to values that would be predicted based on Graham's law of effusion, reflecting the existence of defects. For example, for He/N_2, the selectivity will be the inverse ratio of

square root molecular weight, which is 2.6.[78,90] In one rare instance, a permeation selectivity exceeding Graham's law of effusion was reported, based on a LB film that was constructed from 40 monolayers (*ca.* 58 nm) of a polymeric surfactant. In this case, a He/N_2 selectivity of *ca.* 23 was reported.[92]

Many of the studies that have been carried out by our research group involving LB films were based on the hypothesis that calix[6]arene-based surfactants could lead to molecular sieving (Figure 1.6).[50] Thus, the calix[6]arene-based surfactant was chosen based on its porous structure and its potential to produce "perforated monolayers" that function as molecular sieves.[93,94]

Single LB bilayers of calix[6]arene-based surfactants with and without a "glue" (*i.e.*, a polymeric counterion present in the subphase that can crosslink the surfactant molecules) have been extensively investigated by our group.[50] Thus, various polyelectrolytes[95,96] and polyelectrolyte concentrations,[97] pH[98] and ionic strengths[99] have been investigated. For example, it was shown that a very high He/N_2 selectivity (close to 1000) and a high He/CO_2 selectivity (reaching 150) can be achieved using poly(acrylic acid) (PAA) as a glue for crosslinking a calix[6]arene-based LB bilayer.[96,98] Whether a molecular sieving mechanism was dominating, however, was not firmly established.

With a primary aim of obtaining LB bilayers having improved gas permeation selectivity, and also obtaining a better understanding of the basic science behind the gas permeation through LB films, I prepared poly(4-styrene sulfonate) (PSS) glued and PAA-glued LB bilayers made from calix[n]arene-based surfactants (n=4, 5 and 6) and also a polymeric surfactant. Single PAA-glued LB bilayers based on the polymeric surfactant showed impressive H_2/CO_2 selectivities (*e.g.*, H_2/CO_2 selectivitities of 200). Whether

porous surfactants are really necessary to achieve such selectivity, and whether molecular sieving is operating, will be discussed in detail in the body of this dissertation.

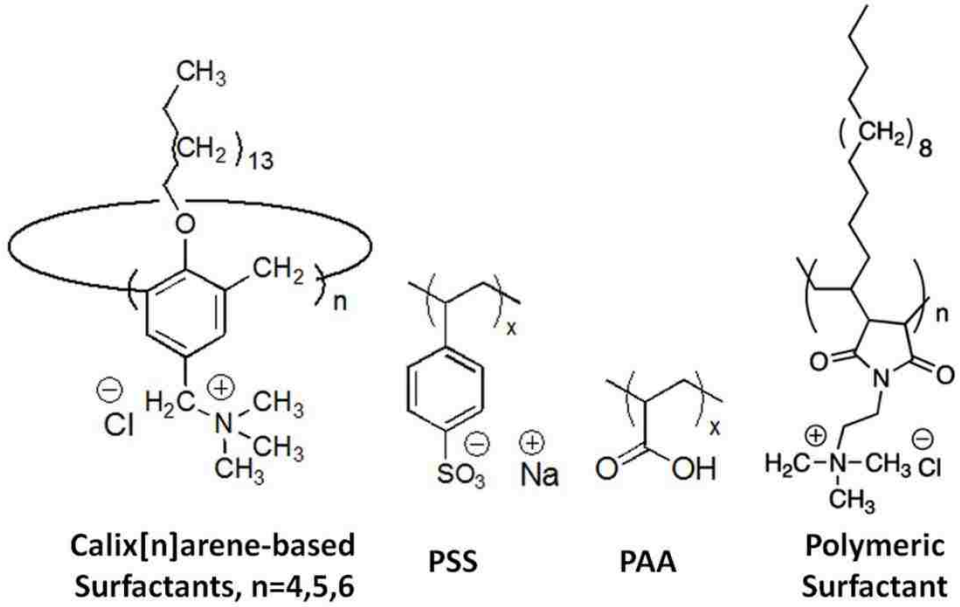

Figure 1.6 Structures of calix[n]arene-based surfactants, a polymeric surfactant and polyanions (PSS and PAA) used in this research.

1.3.2 Layer-by-layer (LbL) Deposition of Polyelectrolytes.

The Layer-by-Layer (LbL) deposition process was initiated by Iller in 1966 and further developed by Decher *et al.* in the early 1990s.[100,101] A typical deposition process is shown in Figure 1.7. Thus, the substrate is first dipped into a polyelectrolyte solution 1, followed by a washing step (pure water), and then dipped into an oppositely charged polyelectrolyte solution 2, followed by another washing step. This process is then repeated multiple times to achieve a desired membrane thickness.

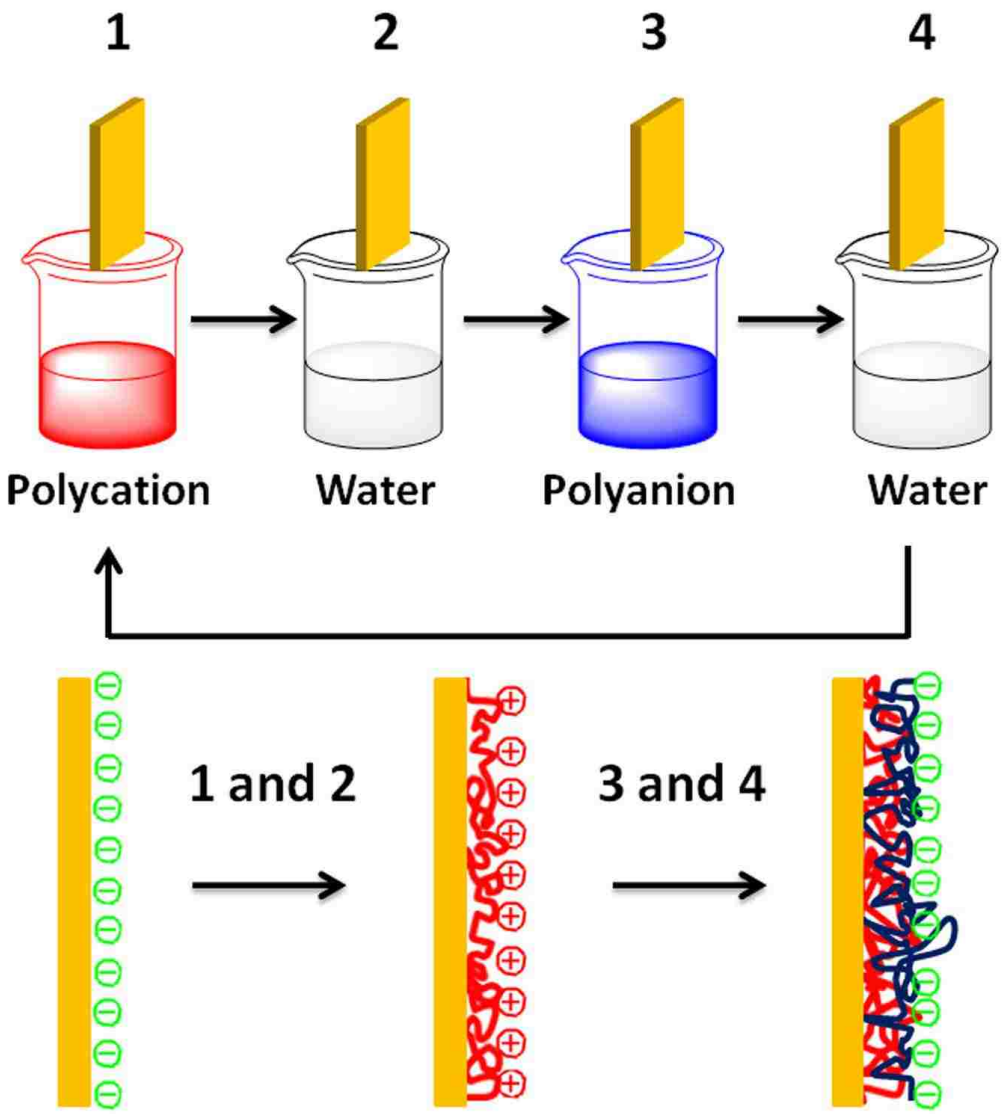

Figure 1.7 Schematic illustration of polyelectrolytes LbL deposition.

The LbL method has attracted considerable attentions over the past 20 years.[102] Various materials have been employed to build LbL multilayer structures based on electrostatic forces[103], hydrogen bonding[104], coordination bonding[105,106] or covalent bonding[107]. In addition, the newly emerged spray and spin-assisted LbL methods have made the deposition process faster to carry out.[108,109]

Because of its simplicity and versatility, multilayers that are derived from LbL method have found applications in various fields.[110-114] However, research on the gas barrier properties of polyelectrolytes multilayers (PEMs) derived from LbL method has been limited. McCarthy investigated PEMs constructed by poly(allylamine hydrochloride) (PAH) and PSS supported on surface oxidized poly(4-methyl-1-pentene). A H_2/N_2 selectivity of 121 was reached at 200 monolayers, corresponding to a thickness of *ca.* 200 nm.[115] Later, Bruening created ultrathin covalently bonded PEMs from PAH and PAA. The resulting membranes that were *ca.* 50 nm in thickness had CO_2/CH_4 selectivities as high as 68, and O_2/N_2 selectivities equal to 6.9.[116] Recently, Grunlan has made PEMs from weak polyelectrolytes, clay and graphene oxides to create O_2 barriers.[117-119]

In our laboratory, several polyelectrolytes pairs have been employed to create PEMs with impressive CO_2/N_2 selectivity (>100), especially in view of their thicknesses, which were *ca.* 13 nm.[120,121] The primary amine groups in PAH were suspected as a possible origin of the high CO_2/N_2 selectivity, because primary amine groups can promote the facilitated transport of CO_2 through membranes.[122]

In this dissertation, PEMs without primary amine groups have been investigated. Figure 1.8 shows the structure of the polyelectrolytes used. The origin of their high CO_2/N_2 selectivity (in the range of 100 to 150) and the effect of "structural matching" (*i.e.*, where the polycation and polyanion have the identical polymer backbone) on the gas permeation properties of PEMs are discussed in the body of the dissertation.

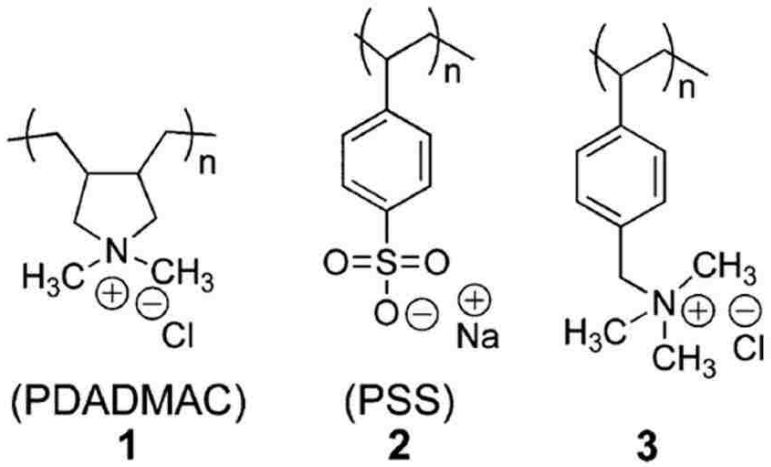

Figure 1.8 Structures of polycations **PDADMAC** and **3**, and polyanion **PSS**, used to construct polyelectrolyte multilayers *via* the Layer-by-Layer method.

1.4 Specific Aims of This Research

In Figures 1.9 and 1.10 are shown two types of hyperthin membranes that have been investigated in this dissertation; *i.e.*, single LB bilayers and PEMs. Here steps 1 to 3 that are shown in Figure 1.9 represent an effort to tighten LB bilayers. This effort will be discussed in Chapters 3, 4 and 5, respectively, where the specific aims were:

1) To determine if calix[n]arenes act as molecular sieves.

2) To determine whether porous surfactants are necessary for making tight LB bilayers.

3) To understand what factors contribute to the tightening of LB bilayers.

4) To determine if the gas permeation properties of a single LB bilayer can reach the upper bound.

The specific aims of the studies that have focused on hyperthin PEMs and are discussed in Chapter 6 (Figure 1.10), are:

1) To study the effects of molecular weight, ionic strength and "structural matching" on the gas permeation properties of PEMs.

2) To understand the origin of high CO_2/N_2 selectivities of PEMs.

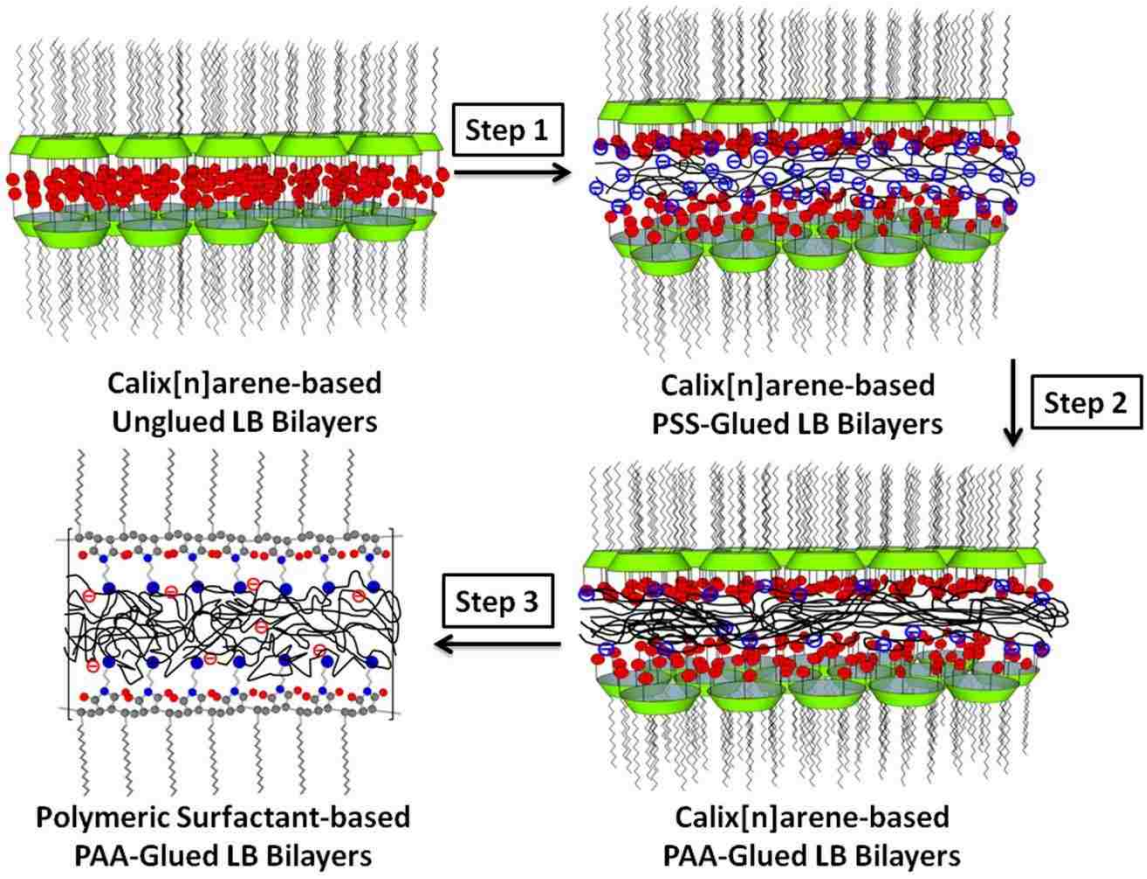

Figure 1.9 Stylized illustrations of LB bilayers.

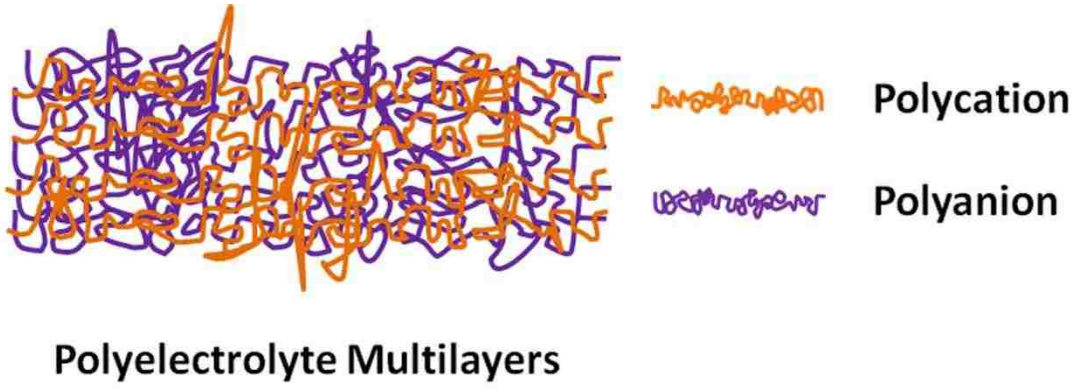

Figure 1.10 Stylized illustration of polyelectrolyte multilayers.

1.5 References

1. Cook, G. A.; Lauer, C. M., *The encyclopedia of the chemical elements*. Reinhold Book Corporation: New York, 1968.
2. Weeks, M. E., The discovery of the elements. IV. Three important gases. *J. chem. Educ.*, **1932,** 9, (2), 215-245.
3. Emsley, J., *Nature's building blocks: An A-Z guide to the elements*. Oxford University Press: Oxford, England, UK, 2001.
4. Linde, C. V. Apparatus for producing low temperatures, the liquefaction of gases, and the separation of the constituents of gaseous mixtures. US Patent 728173 A, 1903.
5. Linde, C. V. Process of producing low temperatures, the liquefaction of gases, and the separation of the constituents of gaseous mixtures. US Patent 727650 A, 1903.
6. Linde, C. V. Apparatus for producing pure nitrogen and pure oxygen. US Patent 795525 A, 1905.
7. Smith, A. R.; Klosek, J., A review of air separation technologies and their integration with energy conversion processes. *Fuel Process. Technol.*, **2001,** 70, (2), 115-134.
8. Kerry, F. G., *Industrial gas handbook: Gas separation and purification*. CRC Press: 2007.
9. Morgenthaler, G. W.; Fester, D. A.; Cooley, C. G., An assessment of habitat pressure, oxygen fraction, and eva suit design for space operations. *Acta Astronautica* **1994,** 32, (1), 39-49.
10. Harding, C. J.; Johnson, D. A.; Janes, R., *Elements of the p Block*. Royal Society of Chemistry: Cambridge, 2002.
11. Baker, R. W., *Membrane technology and applications*. 3rd ed.; John Wiley & Sons: Chichester, West Sussex: 2012.

12. Adhikari, S.; Fernando, S., Hydrogen membrane separation techniques. *Ind. Eng. Chem. Res.*, **2006,** 45, (3), 875-881.

13. Marban, G.; Vales-Solis, T., Towards the hydrogen economy? *Int. J. of Hydrogen Energy*, **2007,** 32, (12), 1625-1637.

14. Ockwig, N. W.; Nenoff, T. M., Membranes for hydrogen separation. *Chem. Rev.*, **2007,** 107, (10), 4078-4110.

15. Yang, S. I.; Choi, D. Y.; Jang, S. C.; Kim, S. H.; Choi, D. K., Hydrogen separation by multi-bed pressure swing adsorption of synthesis gas. *Adsorption-J. Int. Adsorpt. Soc.*, **2008,** 14, (4-5), 583-590.

16. Shao, L.; Low, B. T.; Chung, T. S.; Greenberg, A. R., Polymeric membranes for the hydrogen economy: Contemporary approaches and prospects for the future. *J. Membr. Sci.*, **2009,** 327, (1-2), 18-31.

17. Kim, H. W.; Yoon, H. W.; Yoon, S. M.; Yoo, B. M.; Ahn, B. K.; Cho, Y. H.; Shin, H. J.; Yang, H.; Paik, U.; Kwon, S.; Choi, J. Y.; Park, H. B., Selective gas transport through few-layered graphene and graphene oxide membranes. *Science* **2013,** 342, (6154), 91-95.

18. Li, H.; Song, Z. N.; Zhang, X. J.; Huang, Y.; Li, S. G.; Mao, Y. T.; Ploehn, H. J.; Bao, Y.; Yu, M., Ultrathin, molecular-sieving graphene oxide membranes for selective hydrogen separation. *Science* **2013,** 342, (6154), 95-98.

19. Ramdin, M.; de Loos, T. W.; Vlugt, T. J. H., State-of-the-art of CO_2 capture with ionic liquids. *Ind. Eng. Chem. Res.*, **2012,** 51, (24), 8149-8177.

20. Sumida, K.; Rogow, D. L.; Mason, J. A.; McDonald, T. M.; Bloch, E. D.; Herm, Z. R.; Bae, T. H.; Long, J. R., Carbon dioxide capture in metal-organic frameworks. *Chem. Rev.*, **2012,** 112, (2), 724-781.

21. Dawson, R.; Cooper, A. I.; Adams, D. J., Chemical functionalization strategies for carbon dioxide capture in microporous organic polymers. *Polym. Int.*, **2013,** 62, (3), 345-352.

22. D'Alessandro, D. M.; Smit, B.; Long, J. R., Carbon dioxide capture: Prospects for new materials. *Angew. Chem. Int. Ed.,* **2010,** 49, (35), 6058-6082.

23. Yu, C. H.; Huang, C. H.; Tan, C. S., A review of CO_2 capture by absorption and adsorption. *Aerosol Air Qual. Res.,* **2012,** 12, (5), 745-769.

24. Wilcox, J., *Carbon capture*. Springer: 2012.

25. Lecomte, F.; Broutin, P.; Etienne, L., *CO_2 capture: Technologies to reduce greenhouse gas emissions*. Editions Technip: Paris, 2010.

26. Dehghani, A.; Bridjanian, H.; Farshi, A., Selection separation method for hydrogen and light hydrocarbons gases from waste-gas streams of a petroleum refinery. *Pet. Sci. Technol.,* 30, (21), 2196-2207.

27. Edwards, P. P.; Kuznetsov, V. L.; David, W. I. F.; Brandon, N. P., Hydrogen and fuel cells: Towards a sustainable energy future. *Energy Policy* **2008,** 36, (12), 4356-4362.

28. Xu, J. G.; Froment, G. F., Methane steam reforming, methanation and water-gas shift .1. Intrinsic kinetics. *Aiche J.,* **1989,** 35, (1), 88-96.

29. Oliveira, E. L. G.; Grande, C. A.; Rodrigues, A. E., Methane steam reforming in large pore catalyst. *Chem. Eng. Sci.,* **2010,** 65, (5), 1539-1550.

30. Bernardo, P.; Drioli, E.; Golemme, G., Membrane gas separation: A review/state of the art. *Ind. Eng. Chem. Res.,* **2009,** 48, (10), 4638-4663.

31. Sanders, D. E.; Smith, Z. P.; Guo, R. L.; Robeson, L. M.; McGrath, J. E.; Paul, D. R.; Freeman, B. D., Energy-efficient polymeric gas separation membranes for a sustainable future: A review. *Polymer,* **2013,** 54, (18), 4729-4761.

32. Lau, C. H.; Li, P.; Li, F. Y.; Chung, T. S.; Paul, D. R., Reverse-selective polymeric membranes for gas separations. *Prog. Polym. Sci.,* **2013,** 38, (5), 740-766.

33. Lalia, B. S.; Kochkodan, V.; Hashaikeh, R.; Hilal, N., A review on membrane fabrication: Structure, properties and performance relationship. *Desalination* **2013,** 326, 77-95.

34. Khatib, S. J.; Oyama, S. T., Silica membranes for hydrogen separation prepared by chemical vapor deposition (CVD). *Sep. Purif. Technol.,* **2013,** 111, 20-42.

35. Feng, C. Y.; Khulbe, K. C.; Matsuura, T.; Ismail, A. F., Recent progresses in polymeric hollow fiber membrane preparation, characterization and applications. *Sep. Purif. Technol.,* **2013,** 111, 43-71.

36. Pabby, A. K.; Rizvi, S. S. H.; Sastre, A. M., *Handbook of membrane separations: Chemical, pharmaceutical, food, and biotechnological applications*. CRC Press: 2008.

37. Davidian, B. Apparatus and process for separating air by cryogenic distillation. US 20130133364 A1, 2013.

38. Jasra, R. V.; Choudary, N. V.; Bhat, S. G. T., Separation of gases by pressure swing adsorption. *Sep. Sci. Technol.,* **1991,** 26, (7), 885-930.

39. Petkovska, M.; Tondeur, D.; Grevillot, G.; Granger, J.; Mitrovic, M., Temperature-swing gas separation with electrothermal desorption Step. *Sep. Sci. Technol.,* **1991,** 26, (3), 425-444.

40. Kumar, R., Vacuum swing adsorption process for oxygen production - A historical perspective. *Sep. Sci. Technol.,* **1996,** 31, (7), 877-893.

41. Chou, C. T.; Chen, C. Y., Carbon dioxide recovery by vacuum swing adsorption. *Sep. Purif. Technol.,* **2004,** 39, (1-2), 51-65.

42. Rochelle, G. T., Amine scrubbing for CO_2 capture. *Science* **2009,** 325, (5948), 1652-1654.

43. Lewis, R.; Ivanova, S., Producing nitrogen *via* pressure swing adsorption. *CEP: An AIChE Publication* **2012**, (June), 38-42.

44. Shimekit, B.; Mukhtar, H.; Ahmad, F.; Maitra, S., Ceramic membranes for the separation of carbon dioxide - A review. *Trans. Indian Ceram. Soc.,* **2009,** 68, (3), 115-138.

45. Wisniak, J., Thomas Graham. I. Contributions to thermodynamics, chemistry, and the occlusion of gases. *Educ. Qu ́m.,* **2013,** 24, (3), 316-325.

46. Mohazzabi, P. and Cumaranatunge, L., Graham's law of effusion in dense systems with nonuniform interactions, *Can. J. Phys.*, **2003,** 81, 1121-1129.

47. Wijmans, J. G.; Baker, R. W., The solution-diffusion model - A review. *J. Membr. Sci.*, **1995,** 107, (1-2), 1-21.

48. Henis, J. M. S.; Tripodi, M. K., A novel-approach to gas separations using composite hollow fiber membranes. *Sep. Sci. Technol.*, **1980,** 15, (4), 1059-1068.

49. Pandey, P.; Chauhan, R. S., Membranes for gas separation. *Prog. Polym. Sci.*, **2001,** 26, (6), 853-893.

50. Wang, M. H.; Janout, V.; Regen, S. L., Gas transport across hyperthin membranes. *Acc. Chem. Res.*, **2013**, 46, (12), 2743-2754

51. Oyama, S. T.; Yamada, M.; Sugawara, T.; Takagaki, A.; Kikuchi, R., Review on mechanisms of gas permeation through inorganic membranes. *J. Jpn. Pet. Inst.*, **2011,** 54, (5), 298-309.

52. Anderson, M.; Wang, H. B.; Lin, Y. S., Inorganic membranes for carbon dioxide and nitrogen separation. *Rev. Chem. Eng.*, **2012,** 28, (2-3), 101-121.

53. Caro, J.; Noack, M.; Kolsch, P.; Schafer, R., Zeolite membranes - state of their development and perspective. *Microporous Mesoporous Mater.*, **2000,** 38, (1), 3-24.

54. Dong, J.; Lin, Y. S.; Kanezashi, M.; Tang, Z., Microporous inorganic membranes for high temperature hydrogen purification. *J. Appl. Phys.*, **2008,** 104, (12), 17.

55. Ma, X. H.; Swaidan, R.; Teng, B. Y.; Tan, H.; Salinas, O.; Litwiller, E.; Han, Y.; Pinnau, I., Carbon molecular sieve gas separation membranes based on an intrinsically microporous polyimide precursor. *Carbon* **2013,** 62, 88-96.

56. Habre, W.; Asztalos, T.; Sly, P. D.; Petak, F., Viscosity and density of common anaesthetic gases: implications for flow measurements. *Brit. J. Anaesthesia* **2001,** 87, (4), 602-607.

57. Shindo, Y.; Hakuta, T.; Yoshitome, H.; Inoue, H., Gas-diffusion in microporous media in Knudsen regime. *J. Chem. Eng. Jpn.*, **1983,** 16, (2), 120-126.

58. Singh, A.; Koros, W. J., Significance of entropic selectivity for advanced gas separation membranes. *Ind. Eng. Chem. Res.,* **1996,** 35, (4), 1231-1234.

59. Hassan, M. H.; Way, J. D.; Thoen, P. M.; Dillon, A. C., Single-component and mixed-gas transport in a silica hollow-fiber membrane. *J. Membr. Sci.,* **1995,** 104, (1-2), 27-42.

60. Schmeling, N.; Konietzny, R.; Sieffert, D.; Rolling, P.; Staudt, C., Functionalized copolyimide membranes for the separation of gaseous and liquid mixtures. *Beilstein J. Org. Chem.,* **2010,** 6, 789-800.

61. Freeman, B. D., Basis of permeability/selectivity tradeoff relations in polymeric gas separation membranes. *Macromolecules* **1999,** 32, (2), 375-380.

62. Kesting, R. E. and Fritzsche A. K., *Polymeric gas separation membranes.* John Wiley & Sons, Inc: New York, 1993.

63. Alentiev, A. Y.; Yampolskii, Y. P., Free volume model and tradeoff relations of gas permeability and selectivity in glassy polymers. *J. Membr. Sci.,* **2000,** 165, (2), 201-216.

64. Baschetti, M. G.; Doghieri, F.; Freeman, B.; Sarti, G. C., Transient and steady-state effective diffusivity in high free volume glassy polymers. *J. Membr. Sci.,* **2009,** 344, (1-2), 144-154.

65. Rowe, B. W.; Freeman, B. D.; Paul, D. R., Physical aging of ultrathin glassy polymer films tracked by gas permeability. *Polymer* **2009,** 50, (23), 5565-5575.

66. Rowe, B. W.; Pas, S. J.; Hill, A. J.; Suzuki, R.; Freeman, B. D.; Paul, D. R., A variable energy positron annihilation lifetime spectroscopy study of physical aging in thin glassy polymer films. *Polymer* **2009,** 50, (25), 6149-6156.

67. Rowe, B. W.; Freeman, B. D.; Paul, D. R., Influence of previous history on physical aging in thin glassy polymer films as gas separation membranes. *Polymer* **2010,** 51, (16), 3784-3792.

68. Dolan, M. D.; Dave, N. C.; Ilyushechkin, A. Y.; Morpeth, L. D.; McLennan, K. G., Composition and operation of hydrogen-selective amorphous alloy membranes. *J. Membr. Sci.,* **2006,** 285, (1-2), 30-55.

69. Yun, S.; Oyama, S. T., Correlations in palladium membranes for hydrogen separation: A review. *J. Membr. Sci.,* **2011,** 375, (1-2), 28-45.

70. Lin, Y. S.; Kumakiri, I.; Nair, B. N.; Alsyouri, H., Microporous inorganic membranes. *Sep. Purif. Methods,* **2002,** 31, (2), 229-379.

71. Baker, R. W.; Lokhandwala, K., Natural gas processing with membranes: An overview. *Ind. Eng. Chem. Res.,* **2008,** 47, (7), 2109-2121.

72. Lu, G. Q.; da Costa, J. C. D.; Duke, M.; Giessler, S.; Socolow, R.; Williams, R. H.; Kreutz, T., Inorganic membranes for hydrogen production and purification: A critical review and perspective. *J. Colloid Interface Sci.,* **2007,** 314, (2), 589-603.

73. Liu, S. L.; Shao, L.; Chua, M. L.; Lau, C. H.; Wang, H.; Quan, S., Recent progress in the design of advanced PEO-containing membranes for CO_2 removal. *Prog. Polym. Sci.,* **2013,** 38, (7), 1089-1120.

74. Baker, R. W., Future directions of membrane gas separation technology. *Ind. Eng. Chem. Res.,* **2002,** 41, (6), 1393-1411.

75. Robeson, L. M., The upper bound revisited. *J. Membr. Sci.,* **2008,** 320, (1-2), 390-400.

76. Carta, M.; Malpass-Evans, R.; Croad, M.; Rogan, Y.; Jansen, J. C.; Bernardo, P.; Bazzarelli, F.; McKeown, N. B., An efficient polymer molecular sieve for membrane gas separations. *Science* **2013,** 339, (6117), 303-307.

77. Du, N. Y.; Park, H. B.; Robertson, G. P.; Dal-Cin, M. M.; Visser, T.; Scoles, L.; Guiver, M. D., Polymer nanosieve membranes for CO_2-capture applications. *Nat. Mater.,* **2011,** 10, (5), 372-375.

78. Rose, G. D.; Quinn, J. A., Composite membranes - permeation of gases through deposited monolayers. *Science* **1968,** 159, (3815), 636-637.

79. Guillen, G. R.; Pan, Y. J.; Li, M. H.; Hoek, E. M. V., Preparation and characterization of membranes formed by nonsolvent induced phase separation: A review. *Ind. Eng. Chem. Res.,* **2011,** 50, (7), 3798-3817.

80. Ismail, A. F.; Yean, L. P., Review on the development of defect-free and ultrathin-skinned asymmetric membranes for gas separation through manipulation of phase inversion and rheological factors. *J. Appl. Polym. Sci.,* **2003,** 88, (2), 442-451.

81. Blodgett, K. B., Films built by depositing successive monomolecular layers on a solid surface. *J. Am. Chem. Soc.,* **1935,** 57, (6), 1007-1022.

82. Blodgett, K. B., Monomolecular films of fatty acids on glass. *J. Am. Chem. Soc.,* **1934,** 56, (2), 495-495.

83. Blodgett, K. B. Film structure and method of preparation. 1940.

84. Giancane, G.; Valli, L., State of art in porphyrin Langmuir-Blodgett films as chemical sensors. *Adv. Colloid Interface Sci.,* **2012,** 171, 17-35.

85. Moriizumi, T., Langmuir-Blodgett films as chemical sensors. *Thin Solid Films* **1988,** 160, (1-2), 413-429.

86. Tao, A. R.; Huang, J. X.; Yang, P. D., Langmuir-Blodgettry of nanocrystals and nanowires. *Acc. Chem. Res.,* **2008,** 41, (12), 1662-1673.

87. Li, X. L.; Zhang, G. Y.; Bai, X. D.; Sun, X. M.; Wang, X. R.; Wang, E.; Dai, H. J., Highly conducting graphene sheets and Langmuir-Blodgett films. *Nat. Nanotechnol.,* **2008,** 3, (9), 538-542.

88. McCullough, D. H.; Regen, S. L., Don't forget Langmuir-Blodgett films. *Chem. Commun.,* **2004**, (24), 2787-2791.

89. Higashi, N.; Kunitake, T.; Kajiyama, T., Efficient oxygen enrichment by a Langmuir-Blodgett-film of the polyion complex of a double-chain fluorocarbon amphiphile. *Polym. J.,* **1987,** 19, (2), 289-291.

90. Rose, G. D.; Quinn, J. A., Gas transport through supported Langmuir-Blodgett Multilayers. *J. Colloid Interface Sci.,* **1968,** 27, (2), 193-&.

91. Acharya, S.; Hill, J. P.; Ariga, K., Soft Langmuir-Blodgett technique for hard nanomaterials. *Adv. Mater.*, **2009,** 21, (29), 2959-2981.

92. Riedl, T.; Nitsch, W.; Michel, T., Gas permeability of Langmuir-Blodgett (LB) films: Characterisation and application. *Thin Solid Films* **2000,** 379, (1-2), 240-252.

93. Yan, X.; Hsu, J. T.; Regen, S. L., Selective dampening of the gas permeability of a Langmuir-Blodgett film using moist permeants. *J. Am. Chem. Soc.*, **2000,** 122, (48), 11944-11947.

94. Conner, M.; Janout, V.; Regen, S. L., Molecular-sieving by a perforated Langmuir-Blodgett film. *J. Am. Chem. Soc.*, **1993,** 115, (3), 1178-1180.

95. Yan, X.; Janout, V.; Hsu, J. T.; Regen, S. L., The gluing of a Langmuir-Blodgett bilayer. *J. Am. Chem. Soc.*, **2003,** 125, (27), 8094-8095.

96. Li, J. W.; Janout, V.; Regen, S. L., Glued Langmuir-Blodgett bilayers having unusually high He/CO_2 permeation selectivities. *Langmuir* **2005,** 21, (5), 1676-1678.

97. Li, J. W.; Janout, V.; Regen, S. L., Glued Langmuir-Blodgett film: An unexpected dependency of gluing on polyelectrolyte concentration. *Langmuir* **2004,** 20, (6), 2048-2049.

98. Li, J. W.; Janout, V.; McCullough, D. H.; Hsu, J. T.; Truong, Q.; Wilusz, E.; Regen, S. L., Exceptional gas permeation selectivity of a glued Langmuir-Blodgett bilayer by pH control. *Langmuir* **2004,** 20, (19), 8214-8219.

99. Wang, Y.; Stedronsky, E.; Regen, S. L., Probing the gas permeability of an ionically cross-linked Langmuir-Blodgett bilayer with a "Touch" of salt. *Langmuir* **2008,** 24, (12), 6279-6284.

100. Iler, R. K., Multilayers of colloidal particles., *J. Colloid Interface Sci.*, 1966, 21, 569-594.

101. Decher, G., Fuzzy nanoassemblies: Toward layered polymeric multicomposites. *Science* **1997,** 277, (5330), 1232-1237.

102. Decher, G.; Schlenoff, J. B., *Multilayer thin films*. Wiley-VCH Verlag &Co.: Weinheim, 2012.

103. Chapel, J. P.; Berret, J. F., Versatile electrostatic assembly of nanoparticles and polyelectrolytes: Coating, clustering and layer-by-layer processes. *Curr. Opin. Colloid Interface Sci.,* **2012,** 17, (2), 97-105.

104. Kharlampieva, E.; Sukhishvili, S. A., Hydrogen-bonded layer-by-layer polymer films. *Polym. Rev.,* **2006,** 46, (4), 377-395.

105. Doron-Mor, I.; Cohen, H.; Cohen, S. R.; Popovitz-Biro, R.; Shanzer, A.; Vaskevich, A.; Rubinstein, I., Layer-by-layer assembly of ordinary and composite coordination multilayers. *Langmuir* **2004,** 20, (24), 10727-10733.

106. Lan, Y. R.; Xu, L. M.; Yan, Y.; Huang, J. B.; de Keizer, A.; Besseling, N. A. M.; Stuart, M. A. C., Promoted formation of coordination polyelectrolytes by layer-by-layer assembly. *Soft Matter* **2011,** 7, (7), 3565-3570.

107. Huang, C. J.; Chang, F. C., Using click chemistry to fabricate ultrathin thermoresponsive microcapsules through direct covalent layer-by-layer assembly. *Macromolecules* **2009,** 42, (14), 5155-5166.

108. Mundra, P.; Otto, T.; Gaponik, N.; Eychmuller, A., Automated setup for spray assisted layer-by-layer deposition. *Rev. Sci. Instrum.,* **2013,** 84, (7), 5.

109. Fadhillah, F.; Zaidi, S. M. J.; Khan, Z.; Khaled, M.; Rahman, F.; Hammond, P., Development of multilayer polyelectrolyte thin-film membranes fabricated by spin assisted layer-by-layer assembly. *J. Appl. Polym. Sci.,* **2012,** 126, (4), 1468-1474.

110. Skorb, E. V.; Andreeva, D. V., Layer-by-Layer approaches for formation of smart self-healing materials. *Polym. Chem.,* **2013,** 4, (18), 4834-4845.

111. Boudou, T.; Crouzier, T.; Ren, K. F.; Blin, G.; Picart, C., Multiple functionalities of polyelectrolyte multilayer films: New biomedical applications. *Adv. Mater.,* **2010,** 22, (4), 441-467.

112. Gribova, V.; Auzely-Velty, R.; Picart, C., Polyelectrolyte multilayer assemblies on materials surfaces: From cell adhesion to tissue engineering. *Chem. Mater.,* **2012,** 24, (5), 854-869.

113. De Koker, S.; Hoogenboom, R.; De Geest, B. G., Polymeric multilayer capsules for drug delivery. *Chem. Soc. Rev.*, 41, (7), 2867-2884.

114. Xiang, Y.; Lu, S. F.; Jiang, S. P., Layer-by-layer self-assembly in the development of electrochemical energy conversion and storage devices from fuel cells to supercapacitors. *Chem. Soc. Rev.*, 41, (21), 7291-7321.

115. Levasalmi, J. M.; McCarthy, T. J., Poly(4-methyl-1-pentene)-supported polyelectrolyte multilayer films: Preparation and gas permeability. *Macromolecules* **1997,** 30, (6), 1752-1757.

116. Sullivan, D. M.; Bruening, M. L., Ultrathin, gas-selective polyimide membranes prepared from multilayer polyelectrolyte films. *Chem. Mater.*, **2003,** 15, (1), 281-287.

117. Yang, Y. H.; Bolling, L.; Priolo, M. A.; Grunlan, J. C., Super gas barrier and selectivity of graphene oxide-polymer multilayer thin films. *Adv. Mater.*, **2013,** 25, (4), 503-508.

118. Priolo, M. A.; Gamboa, D.; Holder, K. M.; Grunlan, J. C., Super gas barrier of transparent polymer-clay multilayer ultrathin films. *Nano Lett.*, **2010,** 10, (12), 4970-4974.

119. Yang, Y. H.; Haile, M.; Park, Y. T.; Malek, F. A.; Grunlan, J. C., Super gas barrier of all-polymer multilayer thin films. *Macromolecules* **2011,** 44, (6), 1450-1459.

120. Wang, Y.; Stedronsky, E.; Regen, S. L., Defects in a polyelectrolyte multilayer: The inside story. *J. Am. Chem. Soc.*, **2008,** 130, (49), 16510-+.

121. Wang, Y.; Janout, V.; Regen, S. L., Creating poly(ethylene oxide)-based polyelectrolytes for thin film construction using an ionic linker strategy. *Chem. Mater.*, **2010,** 22, (4), 1285-1287.

122. Shishatskiy, S.; Pauls, J. R.; Nunes, S. P.; Peinemann, K. V., Quaternary ammonium membrane materials for CO_2 separation. *J. Membr. Sci.*, **2010,** 359, (1-2), 44-53.

Chapter 2

Experimental Methods

This chapter provides detailed experimental procedures employed in the dissertation research. Unless otherwise stated, all the chemicals and reagents were obtained from commercial sources and used without further purification.

2.1 Surfactants and Polyelectrolytes

The syntheses of calix[n]arene-based surfactants (**Calix4**, **Calix5** and **Calix6**), polymeric surfactant POMTMA and polycation, poly(4-styryl-methylene trimethylammonium chloride) PSTAC shown in Figure 2.1 were carried out by our colleague, Dr. Vaclav Janout (Lehigh University). Detailed procedures have previously been reported.[1-6] The procedure for the synthesis of the polymeric surfactant $POMOCH_3$ has been reported too.[5]

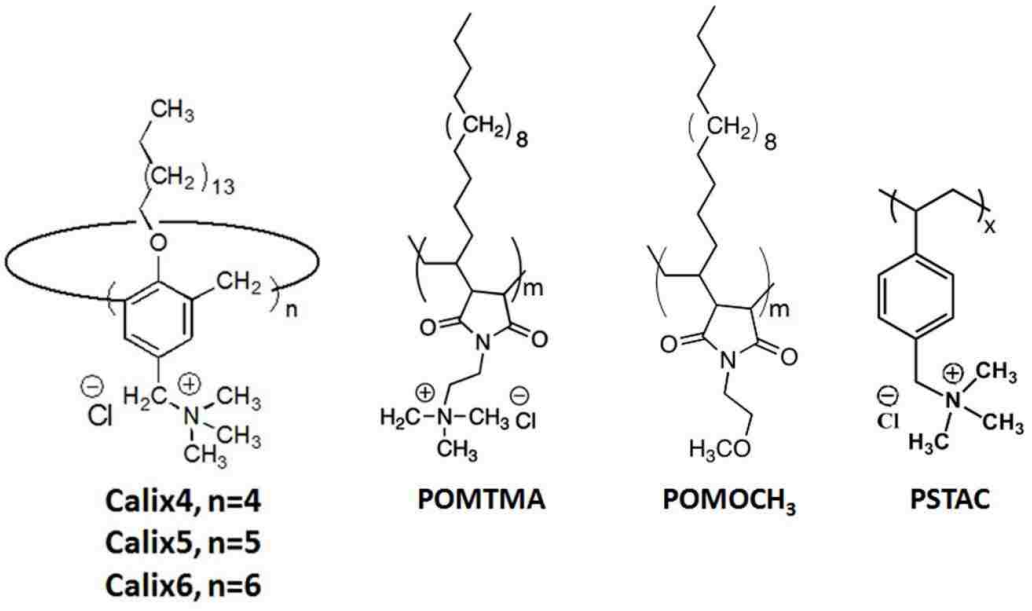

Figure 2.1 Structures of calix[n]arene-based surfactants, polymeric surfactants POMTMA and $POMOCH_3$, and polycation PSTAC.

2.2 Preparation of Substrates

To mechanically support the hyperthin membranes fabricated by the Langmuir-Blodgett (LB) and layer-by-layer (LbL) deposition methods, two substrates were prepared. Poly[1-(trimethylsilyl)-1-propyne] (PTMSP) cast films were chosen as the substrates for gas permeation property measurements, because a PTMSP cast film has ultra-high permeability toward all the gases, and because it has a continuous surface.[7] To measure the topography and thickness of the hyperthin membranes, silicon wafers that were silylated with *n*-octadecyltrichlorosilane (OTS) were employed as analogs of PTMSP. These two substrates both have advancing contact angles for water that are larger than 110 º. The structures of PTMSP and OTS are shown in Figure 2.2.

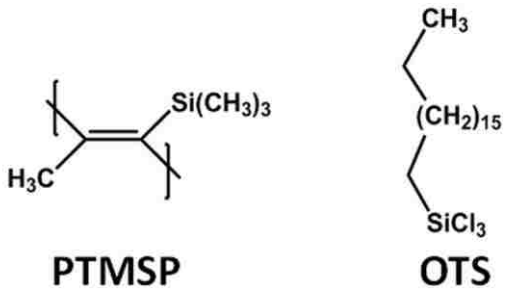

Figure 2.2 Structures of PTMSP and OTS.

2.2.1 Preparation of Poly[1-(trimethylsilyl)-1-propyne] (PTMSP) Cast Films

Supports that were made from PTMSP were prepared by using a solution casting technique in a clean room. PTMSP was purchased from Gelest Inc. Morrisville, PA, and used without further purification. A typical casting apparatus (Figure 2.3) consisted of a Pyrex glass square (8" ×8" ×1/8". McMaster Car Supply Company, New Brunswick, NJ), a steel centering ring seal (14 cm, Kurt J. Lesker Co., Allentown, PA), and five (2.10" o.d. × 1.64" i.d. × 0.010") low carbon steel washers (Boker's, Inc., Allentown, PA). The

Pyrex glass square, ring seal, and five washers were cleaned with chloroform, methanol, and acetone with the aid of kimwipes prior to use (Kimberly Clark, Canada).

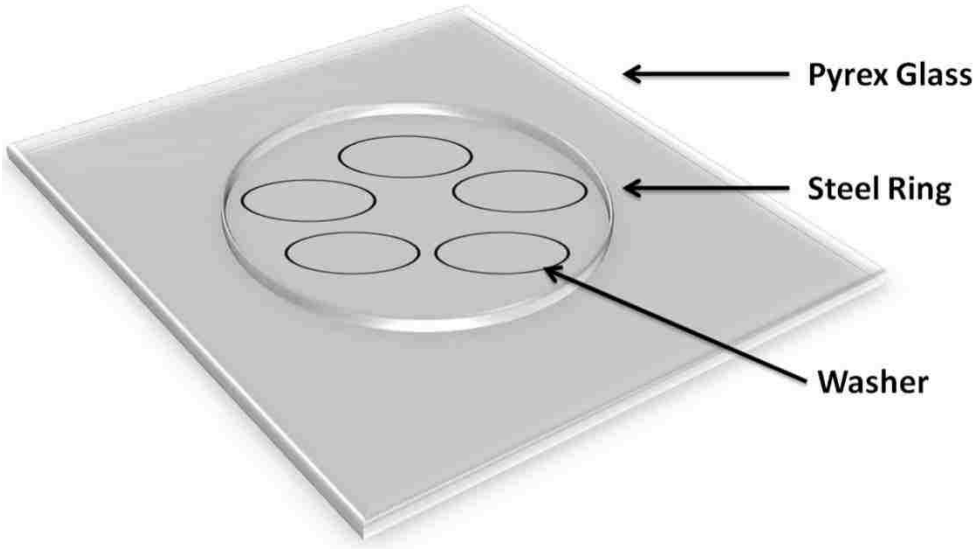

Figure 2.3 Illustration of a PTMSP solution casting apparatus.

The ring seal was bound to the glass square using a 5% toluene solution (HPLC grade) of PTMSP as "glue" 5 h before the casting was started. Five steel washers were then placed symmetrically within the ring seal/glass square casting unit. A PTMSP/toluene casting solution (*ca.* 480 mg/30 mL), which had been stirred for at least 4 h, was filtered using 25 mm GD/X disposable syringe filter (0.45 um pore size, Whatman Inc. Florham Park, NJ) and then poured into the ring seal. The entire apparatus was then covered with 15 large pieces of filter paper (Whatman qualitative circles, 18.5 cm, Whatman Inc. Florham Park, NJ) in order to keep the casting unit dust-free, and also to control the solvent evaporating speed. All the filter papers were cleaned with a stream of nitrogen before using. Gas bubbles in the casting solution that formed after pouring were removed by a syringe needle before putting any filter paper on the casting unit, to avoid forming defects in the cast films.

The toluene was allowed to evaporate for at least 15 h, leaving a PTMSP film across the steel washers and glass square. A surgical blade (S/P Surgical Blades, Baxter Diagnostics, Deerfield, IL) was then used to cut out the individual washers. Approximately 30 mL of water were poured into the ring seal to help separate the washers bearing the PTMSP support from the glass surface. The PTMSP cast films were then placed individually into tin containers (diameter 2.38 inch, height 0.75 inch, House of Cans, Lincolnwood, IL) with Whatman filter paper (Whatman quantitative circles, diameter 55 mm, Whatman Inc., Florham Park, NJ) placed underneath and allowed to dry for at least 24 h. The resulting PTMSP cast films, which had a typical thickness of *ca.* 30 μm, were placed in antistatic bags for at least 15 min prior to the fabrication of composite membranes. A "good" PTMSP membrane adheres tightly to the steel washer and has a uniform surface by visual inspection.

2.2.2 Preparation of OTS Silylated Silicon Wafer

Silicon wafers (150 mm, facet 100, boron, P type, MEMC Electronic Materials, currently known as SunEdison Inc., St. Peters, MO) were cut into 13 x 25 mm pieces and immersed in a piranha solution (made from concentrated H_2SO_4 and 30% H_2O_2 at 70/30, v/v) at 80 ℃ for 4 h (**Caution**: "piranha solutions" react violently with many organic materials and should be handled with great care). The wafers were then rinsed with deionized Milli-Q water, and dried under a stream of nitrogen. The resulting surface was then measured by ellipsometry and had a typical SiO_2 film thickness of *ca.* 2.0 nm. The advancing contact angles of water on this surface, as measured by goniometry, were less than 10°. Silylation of these wafers was carried out immediately (to avoid organic contamination) by immersing them in a 10 mM anhydrous hexane solution (25 mL) of *n*-

octadecyltrichlorosilane (OTS) for 20 min at room temperature (in air). This OTS solution was stirred for at least 4 h in air prior to treating the oxidized silicon wafer. Additional 125 mL of hexane were then poured into the flask and decanted to stop the silylation reaction. The wafers were then rinsed with 150 mL of hexane and 150 mL of chloroform (or dichloromethane) three times and dried under a stream of nitrogen. The advancing contact angles of these OTS-modified silicon wafers with respect to water were greater than 110 º. Typically, the thickness of this OTS layer was *ca.* 2.5 nm, as determined by ellipsometry.

2.3 Deionized Water

A three-stage unit consisting of one carbon and two mixed-beds (US Filter, Broadview, IL), followed by a Milli-Q Continental Water System (Millipore Corporation, Bedford, MA) containing four-cartridges (one Super-C Carbon cartridge, two Ion-Dx Cartridges, one Organex-Q Cartridge) and a final filter unit (Millitask Filter Unit) were employed to obtain deionized water. This deionized water had a typical resistance of 15-17 MΩ.

2.4 Concentration of Surfactant Solutions

The concentrations of the surfactant solutions that were spread at the air/water interface were determined, precisely, using a Cahn C-35 Electrobalance (Thermo Electron Corporation, Waltham, MA). In a typical measurement, a 50 μL sample of the solution was injected onto an aluminum pan, and the solvent was allowed to evaporate until a constant weight was reached (usually within 15 min). The precise concentrations of the surfactants were determined by dividing the measured weight by the volume of sample solution, and typically ranged between 1 to 2 mg/mL.

2.5 Surfactant Monolayer Properties

Surfactant monolayer properties, including surface pressure-area isotherms and surface viscosities, were measured in a clean room (maintained under a positive pressure) by use of a Langmuir-Blodgett (LB) trough.

2.5.1 Surface Pressure-Area Isotherm

Surface pressure-area isotherms were recorded by a Nima 612D film balance. The LB trough is calibrated according to the instruction manual before any cleaning and experiments were done. This includes the calibration of the pressure sensor, the area between barriers, and the speeds of the barriers and the dipper. Before each experiment, the LB trough was thoroughly cleaned by rinsing the Wilhelmy plate (Figure 2.4) (*i.e.*, a piece of filter paper), with Milli-Q water, wiping the surface and the moving barrier with Kimwipes (Kimberly-Clark, OH), which were wetted by solvents such as dichloromethane and methanol (**Caution**: Human exposure to these solvents should be minimized because of their toxic nature).

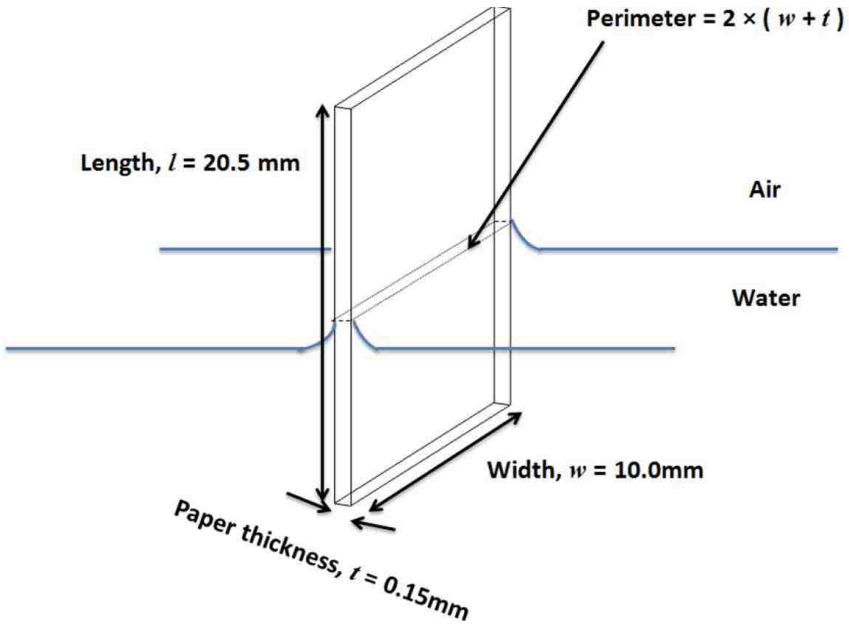

Figure 2.4 The Wilhelmy Plate.

After cleaning the trough, approximately 550 mL of pure water was added to it and the moving barriers were expanded to produce the largest surface area and then compressed to the minimum surface area. At its minimum area, the surface was aspirated to ensure that all surface-active contaminants were removed. This process was repeated, and then all the water was removed by aspiration. The Wilhelmy plate was then installed onto the pressure sensor. The subphase, usually water or aqueous solution of polyelectrolytes, was then added to the trough for surface pressure-area isotherm measurements. To further ensure the absence of surface-active contaminants, the subphase surface was aspirated when barriers were expanded and then compressed to the minimum area. This step was repeated several times until the residue pressure of the subphase was close to 0 mN/m (when barriers were compressed to the minimum area). To maintain the proper level of the subphase solution in the trough, additional solution was added to the trough when needed after repeated aspiration of the subphase surface. When adding more of the subphase solution, this was done by adding it to the aqueous phase that was located outside of the barriers with care. All experiments were carried out using a subphase temperature of 25 ℃.

Using a gas-tight 50-μL Hamilton syringe, equipped with polytetrafluoroethylene (PTFE) tipped plunger, a precise amount of the surfactant (either calix[n]arene-based surfactant or a polymeric surfactant) in a mixed organic solvent (*i.e.*, $CHCl_3$/MeOH 10:1 mixture) (typically 40 μL of a 1 mg/mL solution) was then spread onto the surface of the subphase with the barriers at the maximum area. The residual organic solvent at the air/water interface was then allowed to evaporate for 25 min. The surface pressure-area isotherm was obtained by compressing the barriers at a constant speed, typically 25

cm^2/min, until the monolayer collapsed, as indicated by a sudden loss of surface pressure. The surface pressure-area isotherm cycles were obtained by compressing the monolayer to a specific surface pressure that was beneath the collapse pressure (typically 30 mN/m), and then expanding it to reach 0 mN/m. These compression/expansion cycles were then repeated two times. All the data was recorded by computer and used for making surface pressure *versus* molecular-area plots. The stability of the surfactant monolayer, and also the surfactant molecular areas, were obtained from such plots.

2.5.2 Surface Viscosity Measurements.

Surface viscosity measurements were performed using a Nima Technologies 1212D1 Film Balance equipped with independently moveable barriers and a home-built solid Teflon canal viscometer (19.2 × 4.0 cm), having a centrally located slit that can be adjusted to either 0.60 cm or 0.20 cm), as shown in Figure 2.5. The film balance was calibrated according to the instruction manual before any cleaning and any experiments were done. This includes the calibration of the pressure sensor, the area between barriers, and the speeds of the barriers and the dipper.

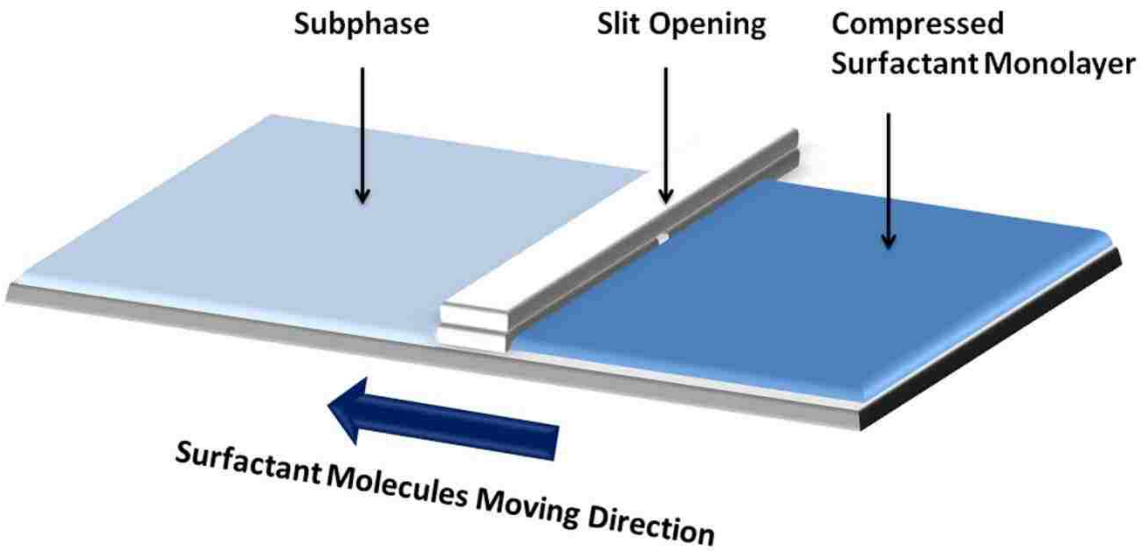

Figure 2.5 Schematic illustration of the surface viscosity measurement.

The cleaning procedure that was used for the LB trough was similar to the procedure used for the surface pressure-area isotherm measurements. In brief, Kimwipes wetted by organic solvents were used to wipe the Teflon-covered trough and home-built Teflon canal viscometer thoroughly several times, followed by aspirating the water surface while compressing the barriers to the minimum area, and then removing all the subphase. The Wilhelmy plate, which is a piece of filter paper (perimeter 20.3 mm), was rinsed by the Milli-Q water, and then installed onto the film balance after adding the desired subphase to the trough at a proper level.

Since the two barriers can move independently, one barrier was moved to a minimum area position and kept at that position. The other barrier was move to the maximum area position first, and then compressed to the minimum area position. Aspiration of the subphase surface was done to ensure the absence of surface-active contaminants. This process was repeated at least two times until the residual surface pressure was close to 0 mN/m, when both barriers were at the minimum area position. The canal viscometer was then placed in front of the moveable barrier; *i.e.*, touching the barrier. All surface viscosity measurements were made at a constant temperature of 25 ℃.

Using a gas-tight 50 μl-Hamilton syringe, equipped with PTFE (polytetrafluoroethylene) tipped plunger, a precise amount of surfactant (either calixarene based surfactant or polymeric surfactant) in a mixed organic solvent (*i.e.*, $CHCl_3$/MeOH 10:1 mixture) (typically 50 μL of a 1 mg/mL solution) was then spread onto the subphase surface with great care, when the moveable barrier was at the maximum area position (the other fixed barrier was at the minimum area position at all times). A monolayer of a given surfactant was obtained after allowing for solvent evaporation over a 25 min period. The surfactant

monolayer was then compressed at a constant speed (typically 25 cm^2/min) to a desired surface pressure (typically, 20 mN/m or 30 mN/m), depending on the monolayer stability and rheology property. The compression was then stopped to allow the monolayer to equilibrate on the subphase at the desired surface pressure for 2 h. Further compression was usually done to ensure that the surface pressure was constantly maintained at the desired value, because the surface pressure of the monolayer tends to decrease slightly, during an ionic crosslinking process. After 2 h, the moveable barrier was rapidly moved to the maximum area position, while the canal viscometer remained in place. As shown in Figure 2.5, the condensed monolayer was exposed to the canal slit, and the surface pressure change was recorded as a function of time. The resulting data was used for plotting surface pressure as a function of time. The surfactant monolayer stability was also obtained from such plots.

2.6 Langmuir-Blodgett (LB) Transfer onto Solid Supports.

After characterizing the monolayer properties of a given surfactant, a condensed monolayer was transferred onto PTMSP or a silicon wafer that had been silylated with octadecyltrichlorosilane (OTS) as shown in Figure 1.5. In a typical process, after thoroughly cleaning the LB trough, the subphase solution (either pure water or an aqueous polyelectrolyte solution) was added to the LB trough, followed by aspirating the surface of the subphase at least two times. A precise amount of surfactant was then spread on the surface of the subphase surface using a Hamilton syringe and the organic solvent allowed evaporating for 25 min.

At the same time, the substrates (either two PTMSP cast membranes or two silicon wafers that have been silylated with OTS) were placed on a support holder in a back-to-

back position. The support holder was also thoroughly cleaned with chloroform (or dichloromethane) and methanol prior to use. In the case of PTMSP supports, the substrate holder consisted of a ceramic ring magnet that was covered with Teflon tape, and connected to a metal rod. Two PTMSP membranes that were attached to steel washers were placed on the holder in a back-to-back position. This holder/PTMSP assembly was then slid into the magnetic circular holder and placed onto an automatic dipper. For silicon wafers, a clamp (with its tip covered by Teflon tape) was employed instead of the magnetic holder. Two OTS-modified silicon wafers were usually clamped in a back-to-back orientation for each LB transfer.

After a solvent evaporation time of 25 min, the surfactant monolayer was compressed to a desired transfer surface pressure (typically 30 mN/m). The film balance was then set to a constant pressure mode and the LB monolayer was allowed to equilibrate for 30 to 60 min. In a typical transfer, the dipping speed (either down-trip or up-trip) was set at 2 mm/min on the dipping menu. The monolayer then was deposited onto the substrate as it was lowered and passed through the air/subphase interface. During this process, ideally, the reduction in the area that is occupied by the surfactant monolayer should equal the geometric surface area of the substrate that passes through this interface. The ratio of this decrease in area divided by the geometric surface area of the support is defined as the transfer ratio. Thus, an ideal transfer is characterized by a transfer ratio of 1.0. Once the substrate is completely submerged in the subphase, the dipper is stopped for about 1 min. To deposit a second monolayer, the substrate was then raised, vertically, from the subphase into air. Additional layers can be obtained by repeating this down-trip and up-trip processes (Figure 1.5). After the LB transfer was completed, the substrate was

removed from the dipper and holder, and then placed onto a test tube rack to dry in ambient laboratory conditions for 2 h. To protect the LB films that were deposited onto silicon wafers, each were stored, individually, in petri dishes (diameter 50mm, Pall life sciences, Port Washington, NY). The treated PTMSP cast films were placed individually into tin containers (diameter 2.38 inch, height 0.75 inch, House of Cans, Lincolnwood, IL) with Whatman filter paper (Whatman quantitative circles, Diameter 55 mm, Whatman Inc., Florham Park, NJ) placed underneath them and allowed to dry for at least 24 h under ambient conditions.

2.7 Polyelectrolyte Multilayers *via* Layer-by-Layer Deposition.

To deposit polyelectrolyte multilayers (PEMs) onto an OTS-modified silicon wafers (or PTMSP casting membranes), a Langmuir-Blodgett monolayer of a **Calix6**, which was ionically crosslinked with poly(sodium 4-styrene sulfonate) (PSS), was first deposited on the substrate to render it hydrophilic.[2] The procedure of the LB monolayer transfer was similar to that described in the last section. In this case, only one down-trip was needed to transfer the PSS-crosslinked LB monolayer of the **Calix6** onto the substrate. The barriers and the dipper were then stopped and the substrate with LB monolayer was left immersed in the subphase for 1 h. Before quickly (*i.e.*, 40 mm/min) removing the substrate with the LB monolayer from the subphase, the residual surfactant monolayer at the air/water interface was removed by aspiration, and the surface pressure was reduced to 0 mN/m by expanding the barriers to the maximum area. The substrate with LB monolayer was then washed with deionized water twice. (*i.e.*, immersed in the deionized water for 5 min without stirring). After washing, the substrate with monolayer was further subjected to conventional layer-by-layer depositions.

Typically, the substrate was immersed, directly, into 200 mL of an aqueous solution of a polycation [*e.g.,* poly(diallyldimethylammonium chloride) (PDADMAC), 15 mM repeat unit concentration] for 15 min. The substrate was then removed and washed twice by immersing in 200 mL of deionized Milli-Q water (600 mL were used for PTMSP casting membranes) for 5 min each, followed by air-drying for 30 min. The substrate was then treated with a 15 mM aqueous solution of PSS for another 15 min and washed in a similar manner. No stirring was used during layer-by-layer deposition. The process was repeated to deposit additional polyelectrolyte layers onto the substrate.

After a desired number of layers were deposited onto the substrate, the membranes were allowed to dry in the laboratory ambient for 2 h before thickness measurements (or 35 h before gas permeation measurements) were made. In addition, a special set-up was made to avoid the polyelectrolyte solution from contaminating the back side of the PTMSP support, which was not covered with LB monolayer. Specifically, two PTMSP membranes with steel washers were always attached in a back-to-back orientation on a home-designed disk magnet holder that was wrapped with PTFE tape, such that only the LB monolayer modified side was exposure to the polymer solutions. The flat surface of the holder assures a tight fit between the holder and PTMSP membranes, which prevents the polyelectrolyte solution from contacting the back side of PTMSP membranes (Figure 2.6).

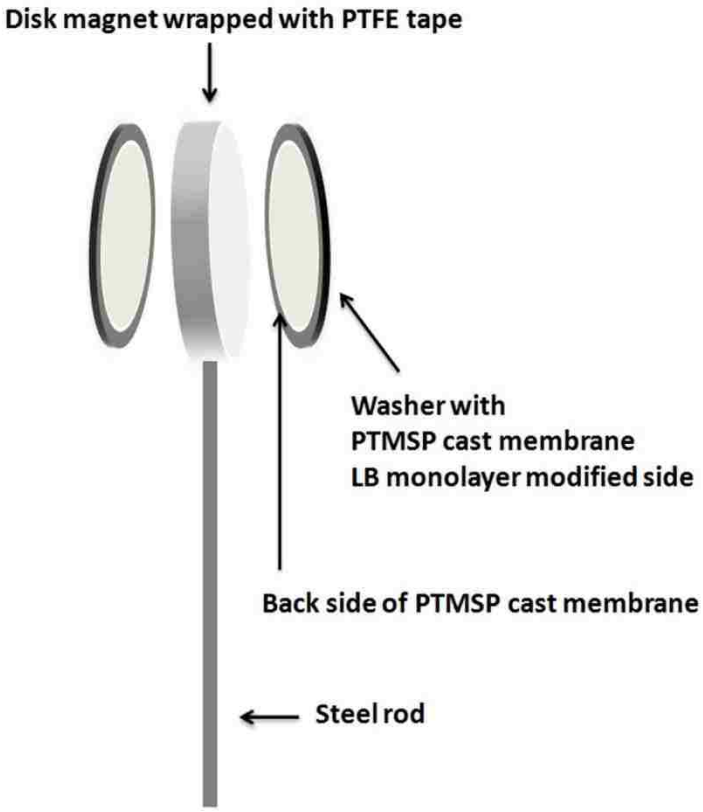

Figure 2.6 Illustration of the holder assembly.

2.8 Membrane Thickness and Topography Determination

The thicknesses of the membranes that were deposited onto OTS-modified silicon wafers were measured by ellipsometry and further confirmed by use of atomic force microscopy (AFM) and step height measurements. In addition, the topographies of the hyperthin membranes were also measured by AFM.

2.8.1 Thickness Measured by Ellipsometry

A V-VASE ellipsometer (J.A. Woollam Co., Inc., Lincoln, NE), equipped with a variable wavelength (250-1700 nm) and variable angle of incidence (15-90 º) system was employed to measure membrane thicknesses. In a typical measurement, two incidence angles (65 º and 75 º) together with four wavelengths (400, 500, 600 and 700 nm) were used to measure a film thickness, with refractive indicesautomatically chosen by the

instrument from its database. For the measurement of the thickness of the OTS layer, the LB films and the polyelectrolyte multilayers, a wavelength of 632.8 nm and an incidence angle of 70 °were used. The refractive indices that were used to estimate the thickness of the OTS, the LB films, and the polyelectrolyte multilayers were 1.46, 1.41, and 1.41, respectively. Measurements were taken at five different regions along the surface of each sample and the mean thickness and the standard deviation were calculated.

2.8.2 Atomic Force Microscopy (AFM)

Two AFM systems were employed in measuring the topography and the thickness of the hyperthin membranes. One was a NanoScope IIIA, Dimension 3000 (Veeco, Santa Barbara, CA). The other was a Solver Next, Multimode SPM (NT-MDT America Inc., Santa Clara, CA). All of the LB films were measured with the NanoScope IIIA, Dimension 3000 system, and all of the polyelectrolyte multilayers were measured by Solver Next Multimode SPM using a tapping mode. A minimum of three different locations along the surface were examined. For each sample, 5×5 and 2×2 μm^2-size images were obtained. Film thicknesses of selected samples were also determined *via* AFM by scratching the surface of OTS-modified silicon wafers bearing hyperthin membranes with a razor blade to remove the surfactant assembly, and measuring step heights. Specific procedures that were used were similar to those described in the literature. (Note: The results from AFM were consistent with OTS still on the surface under such conditions).[8-10]

2.9 Gas Permeation Property Measurements

Five gaseous permeants, helium (He) (Ultra high purity, water < 5 ppm, Airgas Inc. Radnor, PA), hydrogen (H_2) (Ultra high purity, water < 3 ppm, Messer Griesheim

Industires, Inc. Malvern, PA), nitrogen (N_2) (Prepurified, water < 3 ppm, Praxair, Inc., Danbury, CT), oxygen (O_2) (Ultra high purity, water < 5 ppm, Airgas Inc., Radnor, PA), and carbon dioxide (CO_2) ("Bone-dry" grade, water < 10ppm, Airgas, Inc., Radnor, PA), were measured using a home-built gas permeation apparatus (Figure 2.7). The kinetic diameters for He, H_2, N_2, O_2 and CO_2 are 0.260 nm, 0.289 nm, 0.364 nm, 0.346 nm and 0.330 nm, respectively.[11]

Figure 2.7 shows the home-built gas permeation apparatus. The membrane to be measured was placed into the permeation cell between two Viton rubber O-rings (3.45 cm i.d., Scientific Instrument Services, Inc.), with a porous steel support screen (3.70 cm, Millipore Corp.) placed on top. Membranes were always placed in the cell such that the hyperthin membranes faced the upstream of the gas. Using copper tubing, the gaseous permeant travelled from the gas cylinder to an inline filter (15 μm) and elastomer diaphragm regulator (Brooks Instrument, 8601D), which was connected to a Heise gauge port. Another plastic tubing was used to connect the Heise gauge outlet to the permeation cell. The pressure gradient that was applied to each membrane was 10, 20, 30 and 40 psig. After passing through the membrane, the gaseous permeant was directed into a 40 cm-long glass U-tube flowmeter (2 mm i.d.). The volumetric flow rate of the gas was measured by recording the time (t_f - t_i) that was required for a methyl isobutyl ketone solution containing crystal violet to travel a set distance (d_f - d_i), thereby sweeping out a defined volume.

A "purge" process was done after installing a new membrane into the steel cell in order to remove the air inside the steel cell and to remove possible contaminants. In a typical "purge" process, the steel cell was filled with the gas permeant at 40 psig, and then the

inlet gas was cut off, and the gas permeants/air mixture was quickly released by opening a bypass valve. This was repeated at least four times to ensure the air was removed from the steel cell.

Measurements were taken when steady-state values were achieved that, typically, required a minimum of 3 h. At least five volumetric flow rates were recorded for each membrane. The normalized flux was calculated by measuring the mean volumetric flow rate, and dividing that rate by the surface area of the membrane (9.36 cm^2), and by the pressure gradient that was employed. This procedure was repeated for the next permeant gas. In general, the permeation properties were first measured for He, H_2, O_2, N_2, and finally for CO_2. (Note: Not all gas permeants were measured for each study described in this dissertation). To ensure that no damage to the membrane had occurred while these measurements were being made, after the last permeant was investigated (*i.e.*, CO_2), the He or H_2 permeances were measured again and found to be unchanged. [**Caution**: Because of H_2's combustibility, permeance measurements for H_2 should be carried out in a fume hood for safety.]

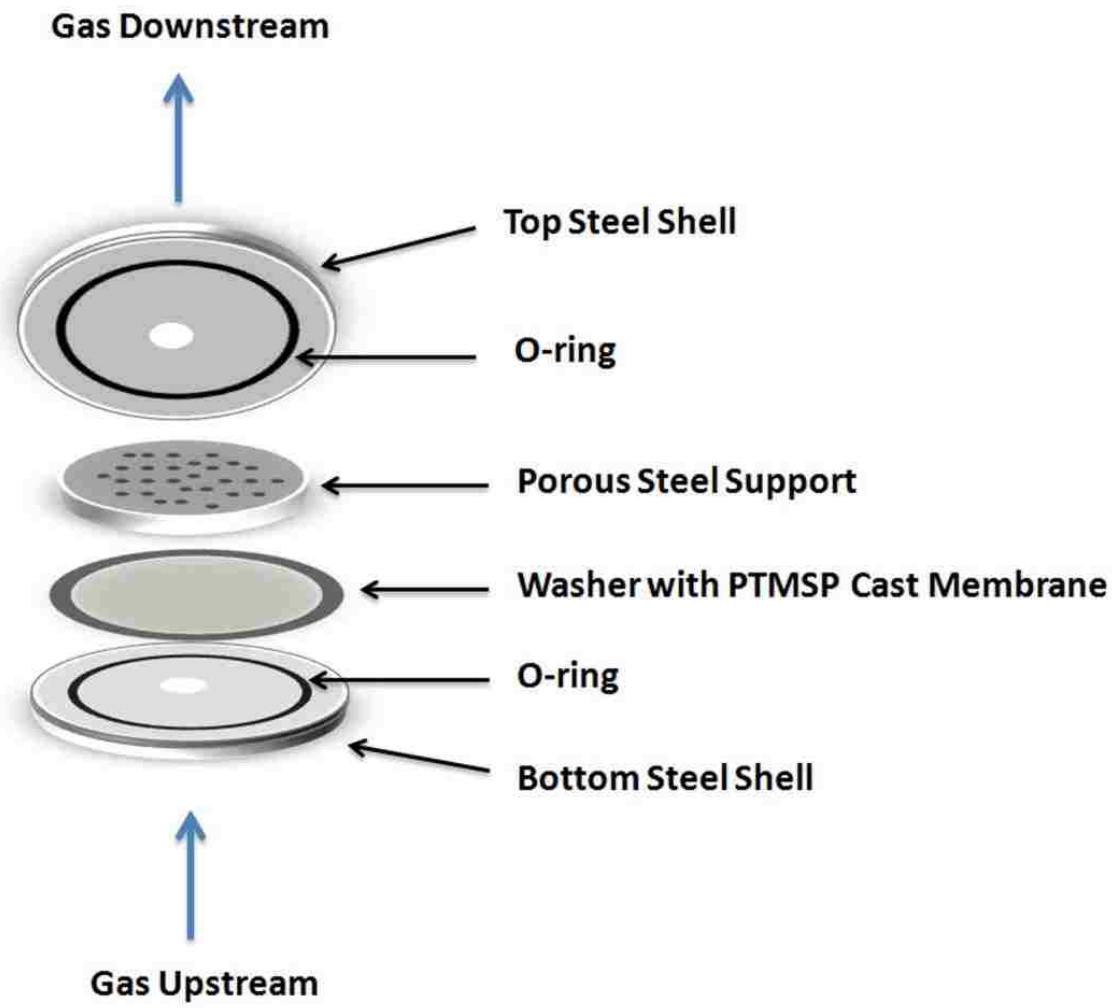

Figure 2.7 Schematic illustration of the home-built apparatus for gas permeation measurements.

2.10 Membrane Wetting Property Measurements.

A Rame-Hart NRL model 100 goniometer (Rame-hart Instrument Co., Succasunna, NJ) was employed to measure the advancing contact angles for the surfaces of interest (Figure 2.8). A Gilmont syringe with a 22-gauge blunt-needle (Rame-hart Instrument Co., Succasunna, NJ) was used for these measurements. Pure Milli-Q water was used to form the drops. To measure the advancing contact angle, a drop of water was placed on the film surface and then the volume of the drop was increased, slowly, to let the edge of

the drop move. The angle was recorded at the point just before the edge of drop moved (*i.e.*, spread out) due the force from the syringe. The volume of the drops was typically *ca.* 1 μL. At least three independent drops were made at three different locations along the substrate surface.

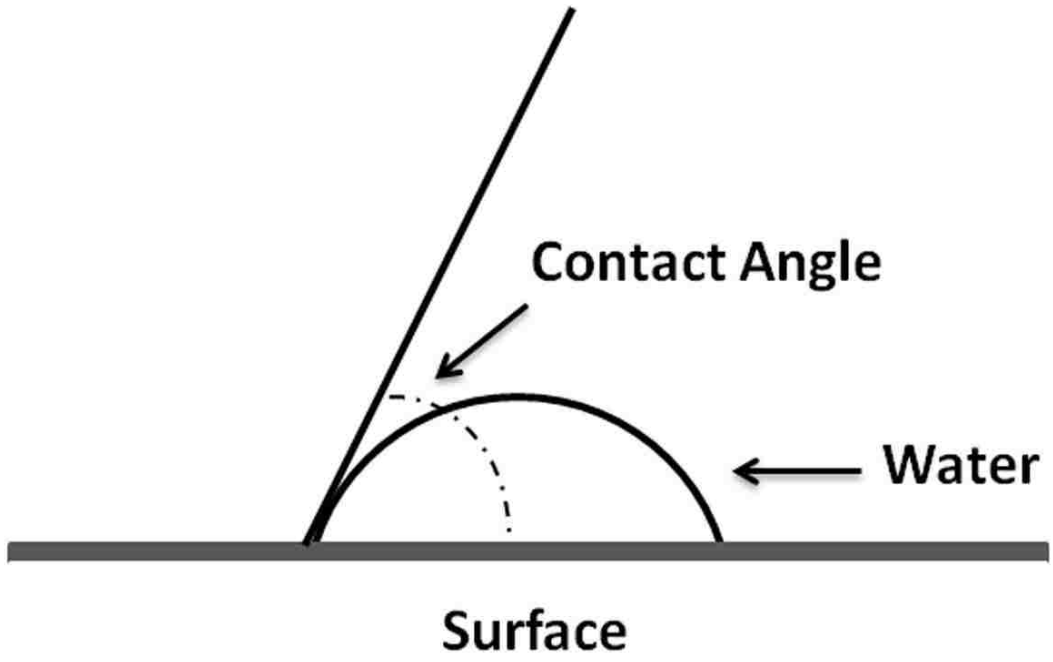

Figure 2.8 Contact-angle schematic.

2.11 X-ray Photoelectron Spectroscopy (XPS) Measurements

To determine the atomic composition of polymeric LB films, X-ray photoelectron spectroscopy (XPS) measurements were carried out using a home-built ultrahigh vacuum (UHV) chamber that is equipped with a 5-channel hemisphere analyzer (SPECS PHOIBOS 100-5 MCD) and a PHI 14-500 dual anode X-ray source. A 200 W Al K-α photon beam ($h\nu$=1468 eV) was used as an incident beam. Take-off angles were varied by rotating the sample manipulator. The total atomic compositions of carbon, oxygen and nitrogen were normalized to 100%. In these experiments, survey scans at 30 °, 49 ° and

90 ° take-off angles were first made over the full range of binding energies (0-1100 eV). The peaks of interest (carbon, oxygen and nitrogen) were then selected and the number of scans determined depending on the peak intensity. These experiments were performed by Ms. Jie Fu at Princeton University.

2.12 References

1. Yan, X.; Janout, V.; Hsu, J. T.; Regen, S. L., The gluing of a Langmuir-Blodgett bilayer. *J. Am. Chem. Soc.,* **2003,** 125, (27), 8094-8095.

2. Li, J. W.; Janout, V.; Regen, S. L., Gluing Langmuir-Blodgett monolayers onto hydrocarbon surfaces. *J. Am. Chem. Soc.,* **2006,** 128, (3), 682-683.

3. Wang, M. H.; Janout, V.; Regen, S. L., Glued Langmuir-Blodgett bilayers from calix[n]arenes: Influence of calix[n]arene size on ionic cross-linking, film thickness, and permeation selectivity. *Langmuir* **2010,** 26, (15), 12988-12993.

4. Wang, Y.; Janout, V.; Regen, S. L., Polymer-enhanced stability of glued Langmuir-Blodgett monolayers. *Macromolecules* **2008,** 41, (3), 497-500.

5. Wang, M. H.; Yi, S.; Janout, V.; Regen, S. L., A 7 nm thick polymeric membrane with a H_2/CO_2 selectivity of 200 that reaches the upper bound. *Chem. Mater.*, **2013,** DOI: 10.1021/cm4028258.

6. Wang, M. H.; Janout, V.; Regen, S. L., Unexpected barrier properties of structurally matched and unmatched polyelectrolyte multilayers. *Chem. Commun.,* **2013,** 49, (34), 3576-3578.

7. Conner, M. D.; Janout, V.; Kudelka, I.; Dedek, P.; Zhu, J. Y.; Regen, S. L., Perforated monolayers: Fabrication of calix[6]arene-based composite membranes that function as molecular-sieves. *Langmuir* **1993,** 9, (9), 2389-2397.

8. McAloney, R. A.; Sinyor, M.; Dudnik, V.; Goh, M. C., Atomic force microscopy studies of salt effects on polyelectrolyte multilayer film morphology. *Langmuir* **2001,** 17, (21), 6655-6663.

9. Wang, Y.; Stedronsky, E.; Regen, S. L., Probing the gas permeability of an ionically cross-linked Langmuir-Blodgett bilayer with a "touch" of salt. *Langmuir,* **2008**, 24, 6279-6284.

10. Sarno, D. M.; Martin, J. J.; Hira, S. M.; Timpson, C. J.; Gaffney, J. P.; Jones, W. E., Enhanced conductivity of thin film polyaniline by self-assembled transition metal complexes. *Langmuir* **2007,** 23, (2), 879-884.

11. Baker, R. W., *Membrane technology and applications*. 3rd ed.; John Wiley & Sons: Chichester, West Sussex, 2012.

Chapter 3

Glued Langmuir-Blodgett Bilayers from Calix[n]arenes for Gas Separations: Use of Poly(4-styrene sulfonate) as a Glue[1]

3.1 Introduction

Langmuir-Blodgett (LB) films have drawn broad interest since their introduction in the early 20th century.[2-10] As suggested by the early pioneer, Katherine Blodgett, LB films have the potential as membranes for molecular separations.[3] However, little success has been achieved to realize this idea. Most LB films show gas permeation selectivities that are close to the value predicted by Graham's law of effusion.[4,5,7]

Our own interest in LB films has focused on their potential as ultrathin selective layers for the separation of gases, which is desired in terms of increasing the overall gas flux.[11] In most of the studies that have been carried out in our laboratories, calix[6]arene-derived surfactants have been employed to construct "perforated" LB films, with a hope that the porous surfactants would behave like molecular sieves during a separation process.[11-13]

In previous work, certain calix[6]arene-based (denoted as **Calix6**) LB films showed significant He/N_2 permeation selectivities and robustness, when they were "glued together" (*i.e.*, ionically crosslinked together) by polyelectrolytes.[13-16] However, whether this porous surfactant is really functioning like a molecular sieve has not been firmly established. A stylized illustration of a "glued" LB bilayer made from a charged porous surfactant and a polymeric counterion is shown in Figure 3.1.

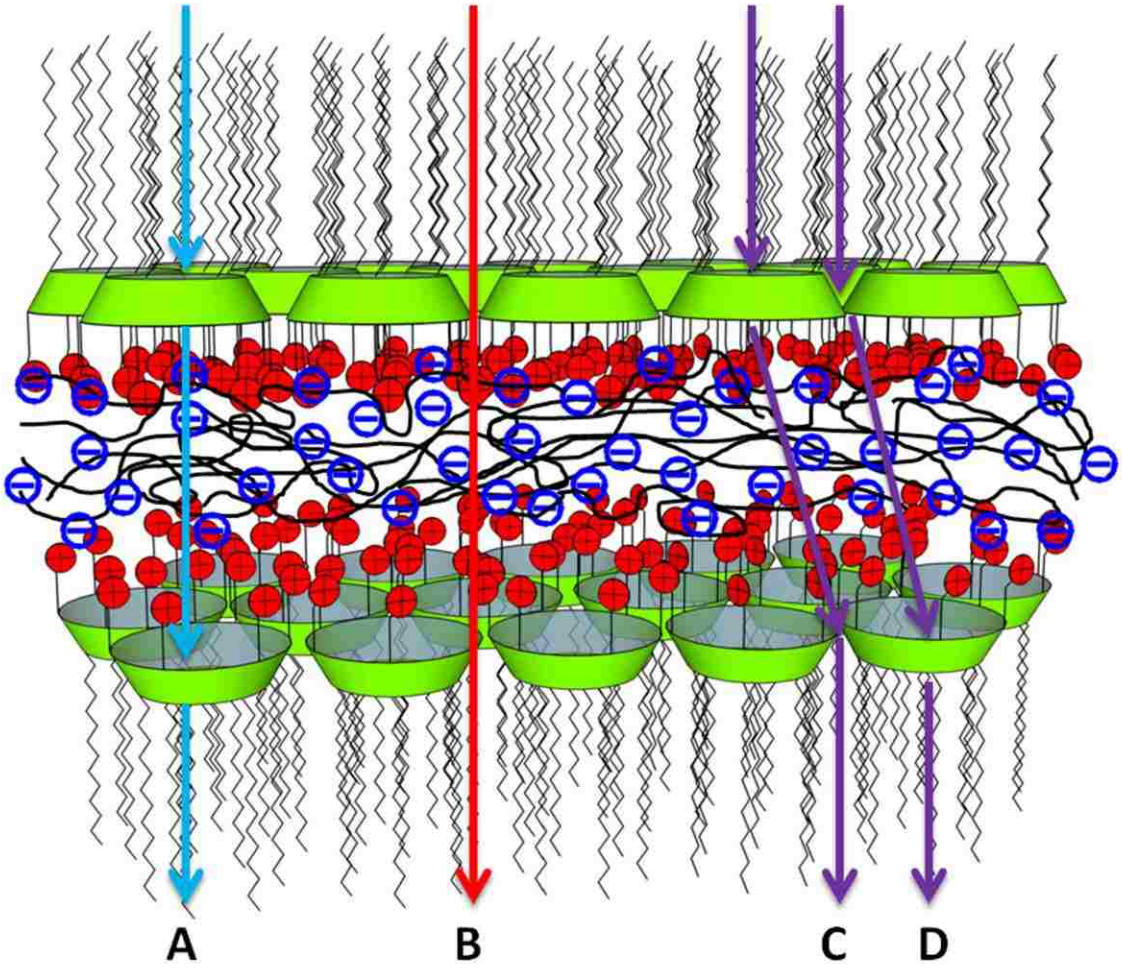

Figure 3.1 A stylized illustration of a LB bilayer derived from a porous surfactant bearing multiple cationic sites that has been glued together with a polymeric anion. Four possible pathways (A to D) for a gas to permeate through the bilayer are also illustrated in this figure. (Note: Although depicted with all-anti conformations, the alkyl chains are likely to be significantly disordered.)

In this chapter, the primary goal was to determine whether poly(4-styrene sulfonate) (PSS) glued LB films made from porous, calix[n]arene-based surfactants do, in fact, operate as molecular sieves. To test for this possibility, we have examined the influence of calix[n]arene size (*i.e.*, with n= 4, 5 and 6) on the permeation properties of PSS-glued single LB bilayers. The cohesiveness of these surfactants in the monolayer state at the air/aqueous subphase, and also the thicknesses of these glued bilayers have also been

investigated, because of the possibility that these two factors may strongly affect the membrane gas permeation performance.

As shown in Figure 3.1, there are four main pathways that gas molecules can potentially pass through such a membrane. Pathway A would represent molecular sieving if the uniform size of the pores inside the surfactant molecules is comparable to the size of gas molecules, which is a key requirement for molecular sieving. Pathway B is unlikely to promote a molecular sieving effect because the size of gaps between surfactant molecules can vary significantly. Pathways C and path D would also represent molecular sieving based on a similar reasoning as path A, but to simplify the discussion, only pathways A and B are discussed in this chapter.

Based on space-filling models, the *maximum* pore diameters for the calix[4]arene, calix[5]arene and calix[6]arene frameworks are *ca.* 0.20 nm, 0.36 nm, and 0.48 nm, respectively. Since the pendant alkyl chains attached to the calix[n]arene frameworks are flexible, they could cover the calix[n]arene's opening, making the effective pore diameters somewhat smaller.[17]

The working hypothesis has been that if gas permeation through pathway A dominates, then for He, CO_2 and N_2 (having kinetic diameters of 0.26 nm, 0.33 nm and 0.36 nm, respectively[18]), none of these permeants should pass through calix[4]arene-based (denoted as **Calix4**) LB bilayers (pore size < 0.20 nm). Therefore, bilayers made from **Calix4** were expected to have the lowest gas permeances and the lowest gas permeation selectivities. For calix[5]arene-based (denoted as **Calix5**) LB bilayers, because their pore size is comparable to that of CO_2, one might expect these bilayers to have a higher gas permeance for He and a relatively low permeance for N_2, resulting in a relatively high

He/N_2 permeation selectivity. In the case of **Calix6** LB bilayers, since the pore size of the surfactant is larger than for all of these gaseous permeants, one might expect them to exhibit the largest gas permeances and only a moderate He/N_2 selectivity. In principle, the permeability of these membranes could also be partially defined by contributions made by a solution-diffusion mechanism across the PSS layer that is incorporated in the LB bilayer. If the findings do not obey these predictions, it would lend support for the belief that molecular sieving is, in fact, not the main mechanism of gas transport, and that pathway B is dominating.[19]

3.2 Membrane Materials.

Calix4, **Calix5** and **Calix6** were synthesized using established methods by our colleague, Dr. Vaclav Janout (Figure 3.2).[14,20] As shown in Figure 3.2, PSS (average M_W *ca.* 70,000, Polysciences, Inc.) was used as the polymeric anion for gluing, and cast films of poly1-(trimethylsilyl)-1-propyne] (PTMSP, Gelest, Inc.) were used as support material.

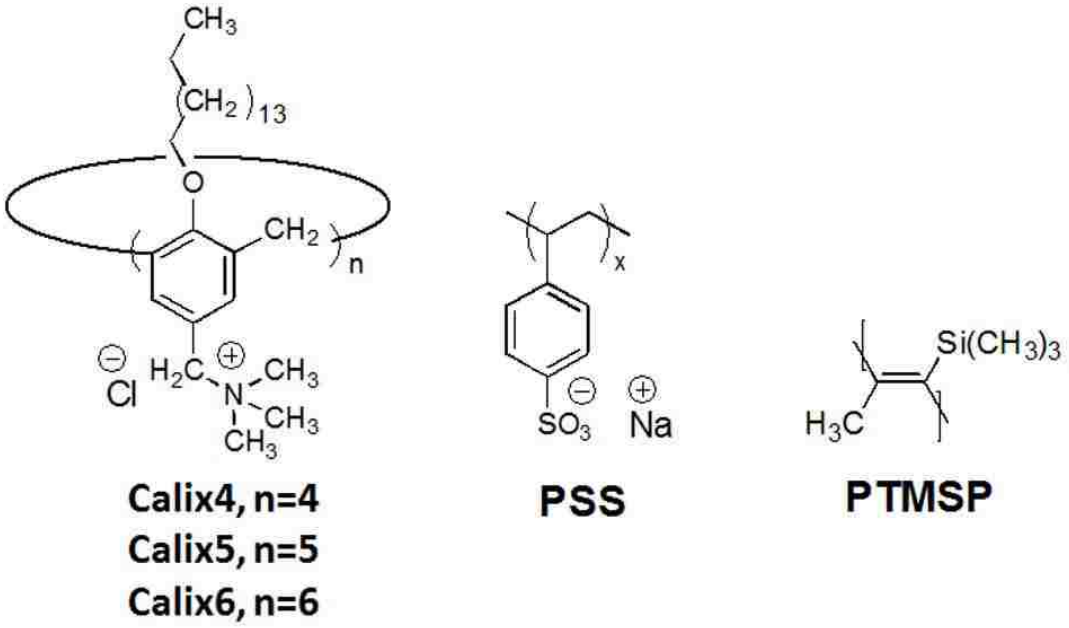

Figure 3.2 Structures of calix[n]arene-based surfactants, PSS and PTMSP.

3.3 Results and Discussion

3.3.1 Monolayer properties

3.3.1.1 Surface Pressure-Area Isotherms.

In Figure 3.3 are shown the surface pressure-molecular area isotherms (taken from isotherm cycles) that were recorded for **Calix4**, **Calix5** and **Calix6** over a pure water subphase or over an aqueous solution containing PSS (5.0 mM repeat unit concentration). As is apparent, the molecular areas occupied by these surfactants were **Calix6** > **Calix5** > **Calix4**. When PSS solution was present, modest differences were found between the first and second compression, but no obvious differences were apparent between the second and third compressions. As shown in Figure 3.3 (A), the first compression always displayed a higher "lift-off" area as well as a higher occupied molecular area before the two isotherms merged at *ca.* 30 mN/m. In contrast, when the subphase was pure water, the difference between the first and subsequent compressions was barely detectable (see Figure 3.3B). These results indicate that during repeated compression and decompression cycles, these surfactant monolayers on a PSS–containing subphase experienced an annealing process.

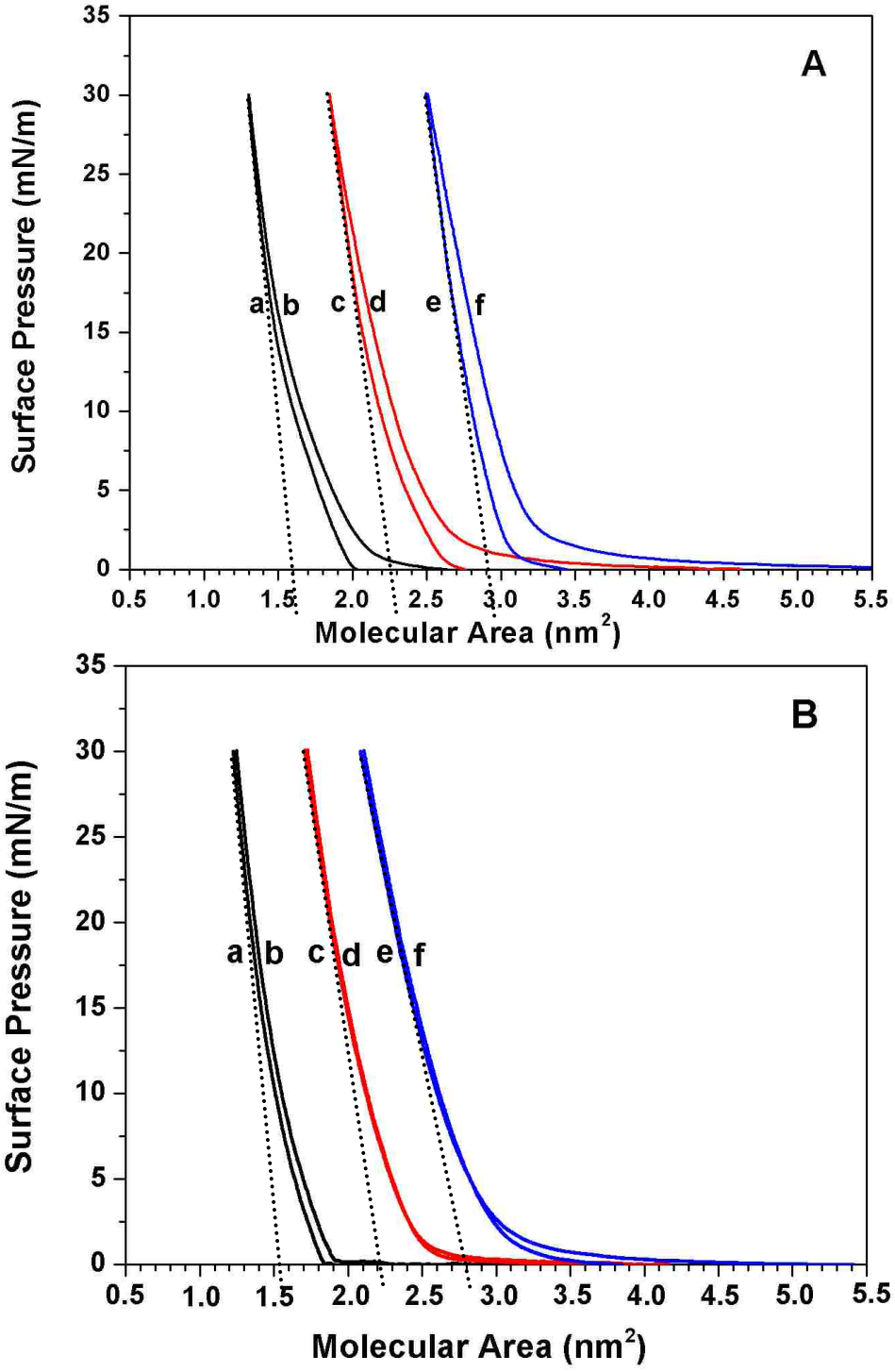

Figure 3.3 Surface pressure-area isotherms recorded for **Calix4** (a, b), **Calix5** (c, d), and **Calix6** (e, f) over: (A) a PSS subphase [5.0 mM repeat units, M_W 70,000] at 25°C; (B) a water subphase. The first compressions are shown as b, d and f; the second and third compressions were the same and are shown as a, c and e.

A comparison of third-compression isotherms for **Calix4**, **Calix5** and **Calix6** over pure water *versus* a subphase containing 5.0 mM PSS is shown in Figure 3.4. It was found that all glued calix[n]arene-based monolayers occupied a greater area than their "unglued" analogs, when the surface pressures were greater than *ca.* 3 mN/m. These results suggest that PSS chains penetrate into these calix[n]arene-based surfactants monolayers. Table 3.1 shows a summary of the molecular areas of calix[n]arenes estimated from Figure 3.3.

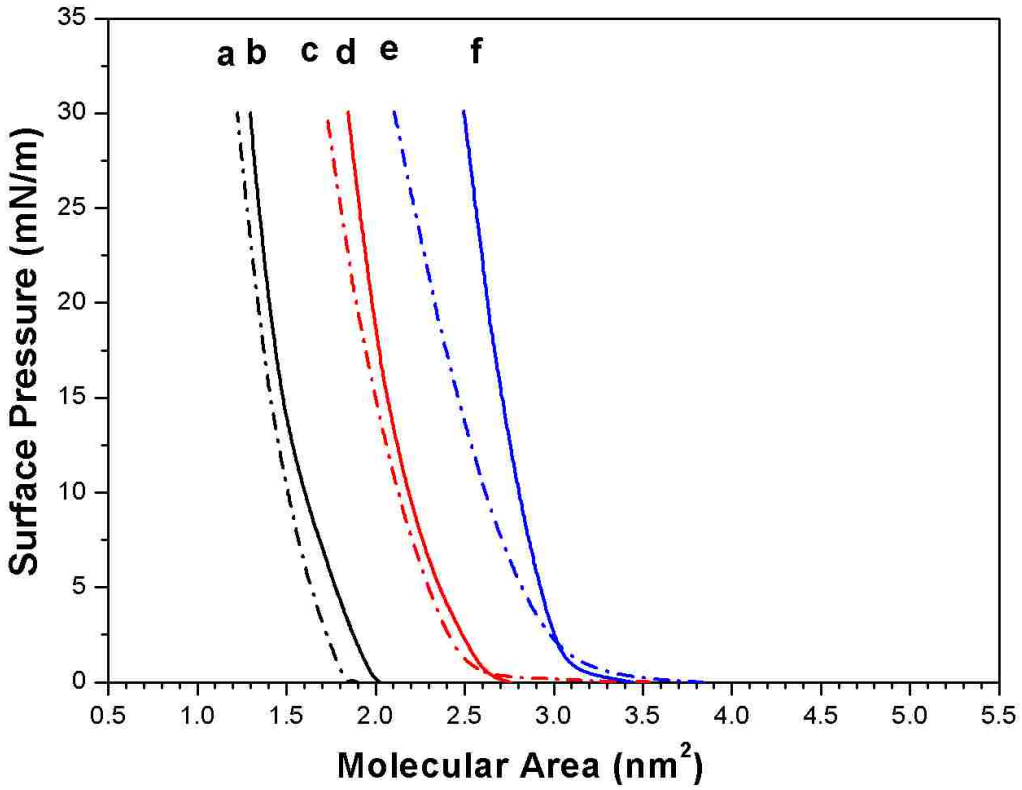

Figure 3.4 Surface pressure-area isotherms (third compression) that were recorded for **Calix4**, **Calix5**, and **Calix6** over pure water (a, c and e, respectively), and over a PSS subphase [5.0 mM repeat units, M_W 70,000] at 25°C (b, d and f, respectively).

Table 3.1 Monolayer properties of calix[n]arenes

Surfactant	Molecular Area[a] (nm^2)	Area per Repeat Unit[b] (nm^2)	Quaternary Ammonium Groups[c] per nm^2	Alkyl Tails[d] per nm^2
Calix4	1.52	0.38	2.63	2.63
Calix5	2.20	0.44	2.27	2.27
Calix6	2.80	0.47	2.13	2.13
Calix4 + PSS	1.60	0.40	2.50	2.50
Calix5 + PSS	2.26	0.45	2.22	2.22
Calix6 + PSS	2.90	0.48	2.08	2.08

[a]Molecular areas of a surfactant determined by drawing a line along the slope of the isotherm of second compression at 30 mN/m as shown in Figure 3.3. [b]Molecular area per repeat unit determined by dividing molecular area of calix[n]arene by n. [c,d]The number of quaternary ammonium groups and alkyl tails per nm^2 is the reciprocal of the molecular area occupied by one repeat unit.

3.3.1.2 Monolayer Cohesiveness.

Surface viscosity measurements were carried out for these calix[n]arene-based monolayers to determine their relative cohesiveness at air/water interface and at the air/PSS solution (5 mM repeat units) interface. The importance of ionic crosslinking can be inferred by comparing the cohesivenesses of unglued monolayers with PSS-glued monolayers. In brief, monolayers were compressed to 30 mN/m, and maintained at this surface pressure for 90 min. The decrease in surface pressure was then recorded as a function of time after the monolayers were exposed to a slit opening of a canal viscometer (the surface pressure outside canal viscometer is 0 mN/m). At the start of the surface viscosity measurements, the area occupied by the monolayer was 1.3, 1.9 and 2.5 nm^2/surfactant molecule for PSS-glued **Calix4**, **Calix5** and **Calix6** monolayers, respectively. For unglued monolayers, these values were 1.2, 1.7 and 2.0 nm^2/molecule, respectively. A summary of our findings is shown in Figure 3.5. The relative surface

viscosities for these glued monolayers were **Calix6** > **Calix5** > **Calix4** as measured by use of both 6 mm and 2 mm slit openings. However, when a 6 mm slit was used, no difference in surface viscosity could be detected between a PSS-glued **Calix4** monolayer and the three unglued monolayers [Figure 3.5 (A)]. It was for this reason that the slit opening was reduced to 2 mm; *i.e.*, to reduce the rate of the surface pressure decrease, so that a greater relative surface viscosity for glued **Calix4** could be observed compared with its unglued analog. Thus, it is clear that all the glued monolayers had a greater cohesiveness as compared with their unglued analogs. This increased cohesiveness can be attributed to ionic crosslinking between surfactants and PSS.

Why does the degree of ionic crosslinking increase as the size of the calix[n]arene increases? A simple explanation is that as the calix[n]arene size increases, its *degree of functionality* (*i.e.*, the number of pendant quaternary ammonium groups per calix[n]arene) also increases. As a consequence, the larger calix[n]arene-based surfactants have a better chance to find oppositely charged PSS anion sites to become crosslinked.

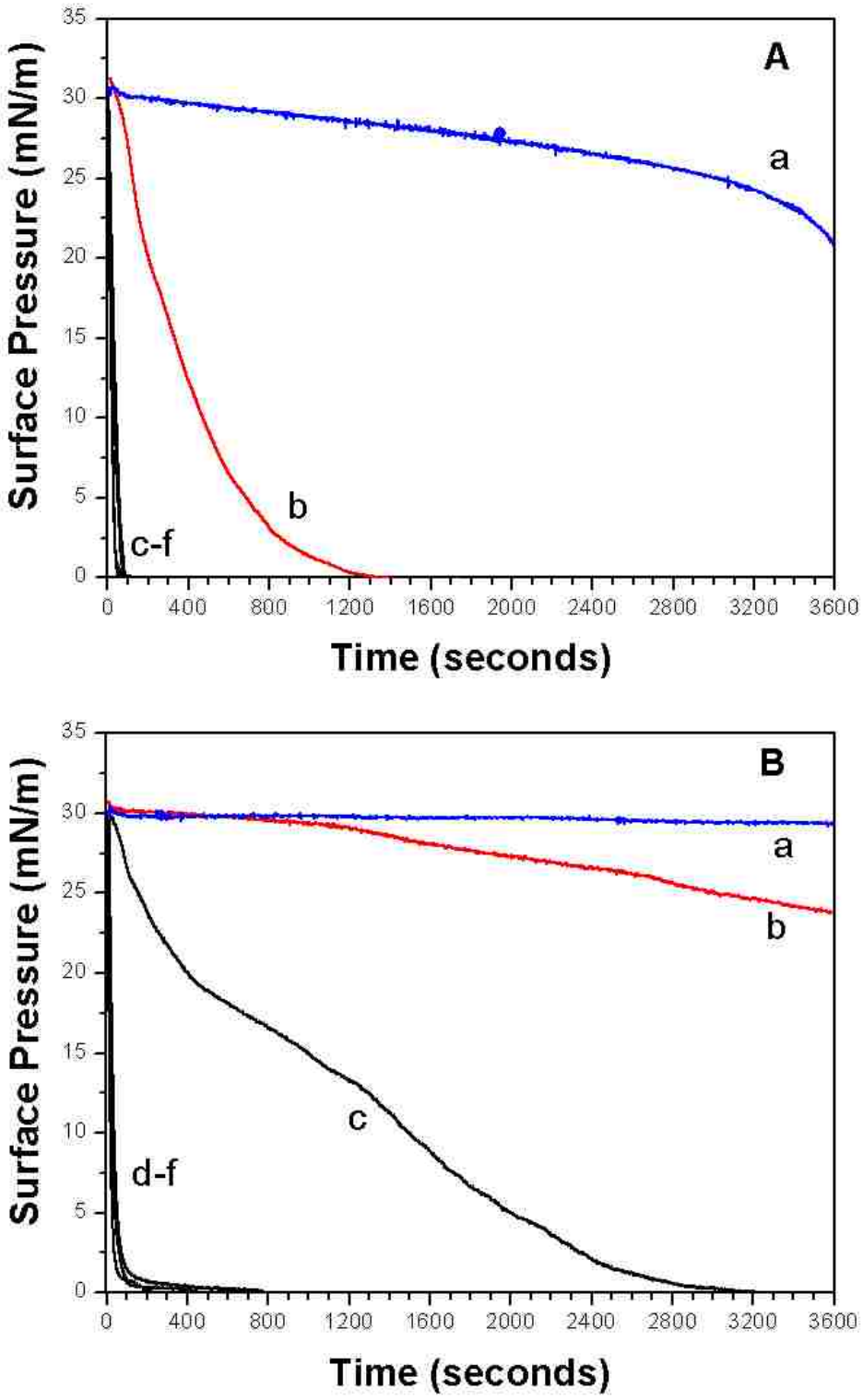

Figure 3.5 Relative surface viscosities determined using a slit opening of (A) 6 mm and (B) 2 mm for monolayers of (a) **3**, (b) **2** and (c) **1** over a PSS subphase [5.0 mM repeat units, M_W 70,000] at 25°C. In the absence of PSS, the surface pressure for **1**, **2** and **3** dropped precipitously (d, e and f) and were indistinguishable with both slit openings.

3.3.2 Thicknesses and Topographies of LB bilayers.

To examine the consequences of calix[n]arene size on the thickness of the PSS layer in glued LB bilayers, glued and unglued single LB bilayers of the three surfactants were deposited onto silicon wafers that were made hydrophobic by treatment with *n*-octadecyltrichlorosilane (OTS). In all cases, the depositions were made using a surface pressure of 30 mN/m and established procedures (see Chapter 2).[16] Film thicknesses were measured by both atomic force microscopy (AFM) and by ellipsometry. As shown in Table 3.2 and Figure 3.7, the step heights measured by AFM (after scratching the surface with a razor blade to remove the glued bilayer) were in excellent agreement with the values determined from ellipsometry. (NOTE: The results from AFM were consistent with OTS still on the surface under such condition).[16,21-24] The topographies of glued and unglued LB bilayers that were observed by AFM before and after scratching are shown in Figure 3.6 and Figure 3.7. The uniformity of the glued bilayers was all excellent as indicated by their topographies, except for glued **Calix4**, which had some noticeable defects [circled in red in Figure 3.6 (b)].

Table 3.2 Membrane thicknesses determined by ellipsometry and AFM

Membrane	Bilayer Thickness[c] (ellipsometry, nm)	Bilayer Thickness (AFM, nm)	RMS Roughness[a] (AFM, nm)	PSS Thickness[b] (AFM, nm)
Calix4	4.3 ± 0.1	4.3 ± 0.5	1.1	---
	(4.3 ± 0.1)			
Calix4 + PSS	6.0 ± 0.1	5.9 ± 0.1	0.3	1.6
	(5.9 ± 0.1)			
Calix5	4.2 ± 0.1	4.1 ± 0.2	0.9	---
	(4.1 ± 0.1)			
Calix5 + PSS	5.6 ± 0.1	5.5 ± 0.1	0.3	1.4
	(5.5 ± 0.1)			
Calix6	4.0 ± 0.1	4.1 ± 0.1	0.3	---
	(4.1 ± 0.1)			
Calix6 + PSS	5.0 ± 0.1	5.1 ± 0.1	0.3	1.0
	(5.1 ± 0.1)			

[a]Root-mean-square roughness determined by AFM. [b]Based on the difference in bilayer thickness in the absence and in the presence of PSS, as determined by AFM measurements. [c]Numbers in parentheses refer to duplicate membranes that were prepared, independently. Error values given for film thicknesses represents one standard deviation based on five AFM and five ellipsometric measurements at different locations along the surface.

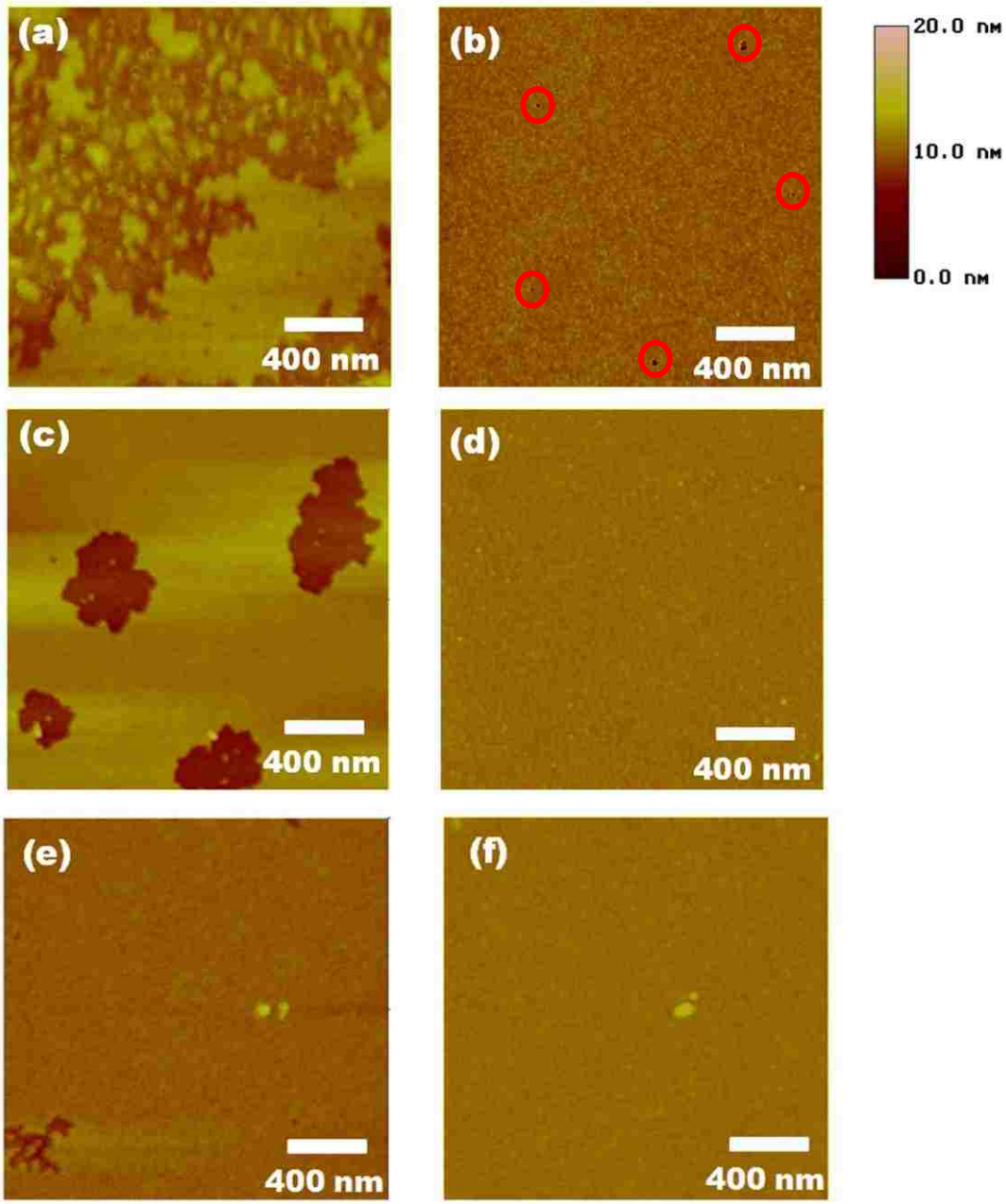

RMS

(a): 1.1 nm	**(b): 0.3 nm**
(c): 0.9 nm	**(d): 0.3 nm**
(e): 0.3 nm	**(f): 0.3 nm**

Figure 3.6 AFM topography (tapping mode, 2×2 μm) and root mean square roughness of unglued LB bilayers of: (a) **Calix4**, (c) **Calix5**, (e) **Calix6**; and PSS-glued LB bilayers of: (b) **Calix4**, (d) **Calix5**, (f) **Calix6**. The *z*-scale is shown on the upper right corner. All LB transfers were made using a speed of 2 mm/min and a surface pressure of 30 mN/m.

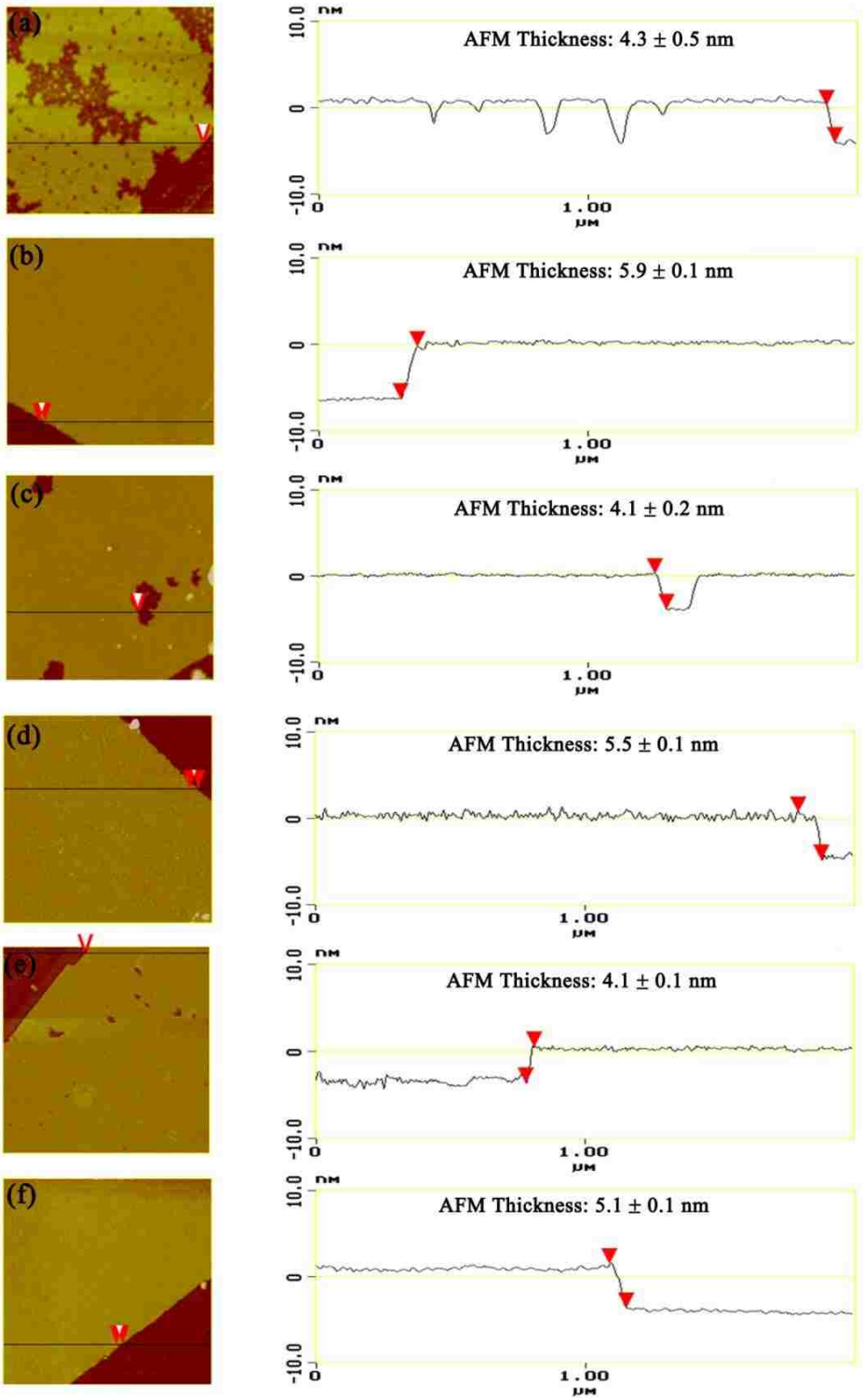

Figure 3.7 Step height images and section profiles (AFM, tapping mode, 2×2 µm) of unglued bilayers of: (a) **Calix4,** (c) **Calix5,** (e) **Calix6;** and glued bilayers of: (b) **Calix4,** (d) **Calix5,** (f) **Calix6.** The *z*-scale is shown to the right. All LB transfers were made using a speed of 2 mm/min and a surface pressure of 30 dyn/cm.

3.3.2.1 Thicknesses of Unglued and PSS-Glued Bilayers as a Function of Calix[n]arene Size.

Table 3.2 and Figure 3.6 show the thicknesses of bilayers in glued or unglued states. The unglued bilayers all showed thicknesses that were close to 4.0 nm (corresponding to a monolayer thickness of *ca.* 2.0 nm). At the same time, the size of calix[n]arene slightly affects the final membrane thicknesses; *i.e.*, the smaller the size of calix[n]arene, the thicker the unglued bilayer. A repeat unit of calix[n]arene is shown in Figure 3.8. The largest distance between head and tail is estimated to be *ca.* 2.5 nm. However, the conformationally flexible alkyl chains may tend to tilt or bend away from an upright position, and thus the real monolayer thickness could be somewhat less than 2.5 nm.

By comparing the thicknesses of glued bilayers and their unglued analogs, it is apparent that increasing the size of calix[n]arene resulted in thinner PSS layers as well as thinner total membrane thicknesses (Table 3.2 and Figure 3.7). One possible explanation is that, at the air/PSS solution interface, **Calix6** had less quaternary ammonium head groups/unit area than **Calix5** and **Calix4**, because **Calix6** had a larger area occupied by its repeat unit (Table 3.1). Thus the amount of PSS that is involved with the crosslinking of the calix[n]arenes at interface may be **Calix6** < **Calix5** < **Calix4**, which could explain these differences in the thickness of the PSS layers.

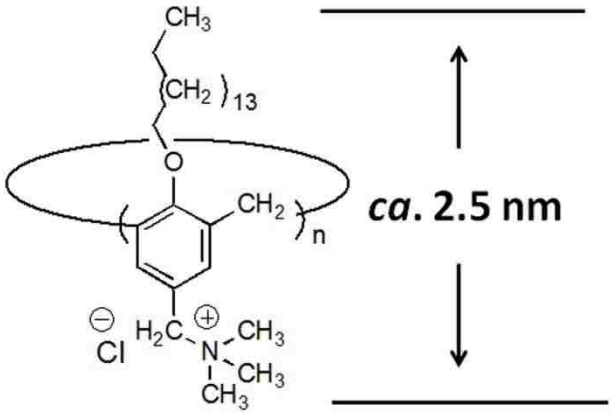

Figure 3.8 The *maximum* length of a calix[n]arene-based surfactant as estimated by GaussView, where the alkyl chains are in an all-*anti* conformation.

3.3.2.2 Topographies of Unglued and PSS-Glued Langmuir-Blodgett Bilayers as a Function of Calixa[n]arene Size.

As shown in Figure 3.6, the glued bilayers had smoother surfaces than their unglued analogs, implying that crosslinking with PSS improves their overall stability; *i.e.*, gluing prevents them from rearranging after deposition onto the silylated silicon wafers. In addition, for unglued bilayers, the smoothnesses were found to improve when the size of calix[n]arene increased. This implies that the bilayers that are formed from the larger calix[n]arene-based surfactants were more stable. For glued bilayers, the topography differences among three surfactants were quite small, but the glued **Calix4** bilayers did have a greater tendency to form defects after deposition [circled in red in Figure 3.6(b)].

3.3.3 Gas Permeation Properties of Unglued and PSS-Glued Bilayers.

To determine the barrier properties of glued and unglued LB bilayers of **Calix4**, **Calix5** and **Calix6**, a series of LB films were deposited onto cast films made from PTMSP. Procedures that were used for these depositions were similar to those used for the deposition onto silylated wafers (see detailed protocols in Chapter 2). Permeance values

(P/l) for each gas are listed in Table 3.3. Here, P is the permeability coefficient and l is the thickness of the composite membrane, where P/l has been calculated by dividing the observed flux (F) by the area of the membrane (A) and by the pressure gradient (Δp) that is used; that is, $P/l = F/(A \times \Delta p)$.[25,26]

Three gaseous permeants He, N_2 and CO_2 were employed in these studies to judge the barrier properties of these glued and unglued LB films. Since the solubility ratio of He/N_2 in organic membranes is normally found to be very similar, the permeation selectivity is expected to be dominated by diffusion.[27-29] This makes the He/N_2 permeation selectivity a very good indicator of diffusional pathways. In addition, CO_2 permeation was measured because the permeation selectivities of He/CO_2 and CO_2/N_2 have practical relevance for hydrogen purification from steam-methane reforming processes and for CO_2 separation from flue gas.[30-32] Here, He was used as a noncombustible surrogate for H_2 since it has similar gas permeation behavior. In contrast to He and N_2, the CO_2 molecule tends to have a high solubility in organic polymer memberanes, which significantly influences its overall transport behavior as described by the solution-diffuion model.[28,29] This tendency was also apparent in the barrier properties of PTMSP cast films (Table 3.3), themselves, where the permeance of CO_2 was found to be larger than He, despite the fact that the size of He is smaller than CO_2.

Table 3.3 Permeances of gases across Langmuir-Blodgett bilayers[a]

Membrane	He	N_2	CO_2	He/N_2	He/CO_2	CO_2/N_2
PTMSP[b]	2.7×10^2	3.0×10^2	1.6×10^3	0.90	0.17	5.3
	(2.4×10^2)	(2.7×10^2)	(1.5×10^3)	(0.89)	(0.16)	(5.6)
Calix4	2.3×10^2	2.4×10^2	1.6×10^3	0.96	0.14	6.7
	(2.6×10^2)	(2.8×10^2)	(1.7×10^3)	(0.93)	(0.16)	(6.1)
Calix5	1.7×10^2	1.1×10^2	9.7×10^2	1.6	0.18	8.8
	(2.0×10^2)	(2.0×10^2)	(1.3×10^3)	(1.0)	(0.15)	(6.5)
Calix6	1.1×10^2	3.8	1.5×10^2	29	0.73	39
	(1.1×10^2)	(7.1)	(1.7×10^2)	(15)	(0.64)	(24)
Calix4 + PSS	1.4×10^2	2.8	1.6×10^2	49	0.85	58
	(1.5×10^2)	(3.2)	(1.9×10^2)	(48)	(0.82)	(58)
Calix5 + PSS	1.2×10^2	0.85	71	1.4×10^2	1.6	84
	(1.3×10^2)	(1.1)	(86)	(1.2×10^2)	(1.6)	(78)
Calix6 + PSS	94	0.59	52	1.6×10^2	1.8	88
	(97)	(0.58)	(44)	(1.7×10^2)	(2.2)	(77)

[a]Permeance values $10^6(P/l)$ ($cm^3/cm^2\cdot s\cdot cmHg$) at ambient temperature were calculated by dividing the observed flux by the area of the membrane (9.36 cm^2) and by the pressure gradient (10 psi) employed, using *ca.* 30 μm thick PTMSP. Numbers in parentheses refer to duplicate membranes that were prepared, independently. Values reported are averages of 5-10 measurements for each sample, which varied by less than 5%. Permeation selectivities that are listed for He/N_2, He/CO_2 and CO_2/N_2 are the ratio of the individual permeances. [b]Bare PTMSP membranes; all other values listed refer to composites of PTMSP and single LB bilayers made from the indicated components.

PTMSP was specifically chosen as the support material because of its ultra-high free volume (*ca.* 30%) and its bimodal intrinsic micropores (0.4 and 0.8 nm respectively), which affords ultra-high permeabilities to all gaseous permeants.[33]

3.3.3.1 Barrier properties of PSS-Glued Bilayers VS Unglued Bilayers

As seen in Table 3.3, the barrier properties of composite membranes constructed from unglued **Calix4** LB bilayers plus PTMSP were essentially the same as that of untreated PTMSP. Unglued bilayers of **Calix5** showed a modest increase in barrier properties to all

of the permeants. In the case of unglued bilayers of **Calix6**, a moderate decrease in the flux of all three gases was observed along with a significant increase in He/N_2 permeation selectivity. On the other hand, all of the glued bilayers that were made from **Calix4, Calix5** and **Calix6** exhibited moderate reductions for the He flux along with substantial reductions for the flux of N_2 and CO_2 relative to the unglued analogs. As a consequence, the permeation selectivities for all of the glued bilayers with respect to He/N_2, He/CO_2, and CO_2/N_2 increased considerably when compared to their unglued analogs. This indicates that tighter membranes (*i.e.*, ones having less defects or smaller average transient gaps) were formed after crosslinking with PSS. The results of these permeation measurements for glued and unglued bilayers are in good agreement with the AFM topography results, in which glued bilayers have been found to be relatively defect-free compared with their unglued analogs.

3.3.3.2 Unglued and PSS-Glued Bilayers Barrier Properties as a Function of Calix[n]arene Size.

As seen in Table 3.3, the trends observed for the barrier properties of glued and unglued bilayers were similar. In both cases the permeances for all of the gases were **Calix4** > **Calix5** > **Calix6**, while the gas selectivities (for He/N_2, He/CO_2 and CO_2/N_2) were always **Calix4** < **Calix5** < **Calix6**. For unglued bilayers, these differences appear to be related to bilayer stability with the larger calix[n]arenes being more stable.

One scenario that could account for the above observations involves the releasing of stress. Thus, all the LB bilayers are likely to have some degree of stress due to repulsion between the charged head groups after deposition. As a result, these LB bilayers would be expected to have some tendency to rearrange to release such stress and allow for reducing the repulsion between the charged head groups. In principle, the amount of the

stress in each bilayer should be **Calix4** > **Calix5** > **Calix6** because the smaller calix[n]arenes have the smaller molecular areas available for each quaternary ammonium head group (Table 3.1). Therefore, the inclination for the unglued bilayers to rearrange should be **Calix4 > Calix5 > Calix6**. A second scenario that one may consider lies with the fact that there are relatively large pores (*ca.* 0.8 nm) in PTMSP, which might only allow the larger surfactants to remain on its surface; *i.e.*, they have less chance to be absorbed into the pores (a "pore absorbing" scenario).[12] As a consequence, the surfactant assembly made from the larger calixarenes may be more stable.

For glued bilayers, the difference in the degree of ionic crosslinking appears to be the most important factor. As discussed above, the degree of crosslinking appeared to be **Calix6** > **Calix5** > **Calix4**. Thus, tighter membranes with greater stability should be formed with the larger calix[n]arenes. As for the "stress releasing" scenario and "pore absorbing" scenario discussed for unglued bilayers, we think they are factors that compete with "ionic crosslinking" in glued bilayers as well. The formation of defects in glued **Calix4** bilayers [see Figure 3.6(b)] lends evidence to this competition. Again, these results agree with the trend of topographies of bilayers shown in Figure 3.6 very well.

3.3.3.3 Why Doesn't A Thicker PSS Layer Lead to Lower Permeances of Gases?

Assuming that the PSS layer itself is making a contribution to the barrier properties, then two factors might account for the overall quality of glued LB bilayers in terms of their gas permeation properties. One factor is the membrane tightness, which should depend on the ionic crosslink density in the PSS-glued bilayer system. The second factor is the membrane's thickness. In general, the permeances of He and N_2 should decrease when the membrane gets tighter and thicker.

As shown in Table 3.2, thicknesses of the glued calix[n]arene bilayers were **Calix4** > **Calix5** > **Calix6**. However, the tightness of the glued bilayers should be **Calix4** < **Calix5** < **Calix6**, as discussed in the last section. Thus the two factors were not working in the same direction, that is bilayers with higher thicknesses had lower tightness or *vice versa*. As a result, if thickness of the glued bilayer is more important, permeances of He and N_2 would be **Calix4** > **Calix5** > **Calix6**. If membrane tightness is more important, permeances of He and N_2 would be **Calix4** < **Calix5** < **Calix6**.

The fact that permeances of He and N_2 of glued calix[n]arene bilayers were **Calix4** < **Calix5** < **Calix6** (Table 3.3) implies that membrane tightness is more important than the membrane thickness for these PSS-glued calix[n]arenes bilayers. This also implies that the PSS layer itself may only make a minor contribution to the barrier properties of glued bilayers. However, to further determine whether it is the whole glued LB bilayer or inserted PSS-layer alone behaving as the main gas barrier, the permeability and gas selectivity data of the pure PSS membrane should be obtained in the future.

3.3.3.4 Is Molecular Sieving Occurring?

The data that we have obtained do not support the hypothesis that glued or unglued calix[n]arene LB bilayers act as molecular sieves. If molecular sieving were occurring, the relative permeances of He and N_2 should be **Calix4** < **Calix5** < **Calix6** and the relative He/N_2 selectivities should be **Calix5** > **Calix6** >> **Calix4** as discussed in the introduction section. However, we have found that the He and N_2 permeances of the glued bilayers are **Calix4** > **Calix5** > **Calix6**, while the He/N_2 selectivities of glued bilayers are **Calix4** < **Calix5** < **Calix6**. These results imply that pathway B dominates the whole permeation process in these membranes and that molecular sieving is not a

significant factor. Further discussion of this problem can be found in the following section.

3.3.3.5 Membrane Performances as Judged by Upper-Bound Plots

To gain further insight into these PSS-glued LB bilayers, the intrinsic permeation properties of membrane made from **Calix6** were included into the Robeson's upper-bound plots.[27-29] These membranes exhibited the higher permeation selectivities. In these plots, the permeation selectivities for He/N_2, CO_2/N_2, and He/CO_2 are plotted as a function of the permeation coefficient of the more permeable gases (*i.e.*, Figures 3.8A, 3.8B and 3.8C, respectively).[27-29] The permeance of PTMSP ($[P/l]_{PTMSP}$) and composite membranes ($[P/l]_{composite}$) were measured separately, and the series resistance model (*i.e.*, $1/[P/l]_{composite} = 1/[P/l]_{PTMSP} + 1/[P/l]_{LB}$) was then used to calculate the intrinsic permeance of the LB bilayers ($[P/l]_{LB}$).[5] The intrinsic permeability coefficients of the LB bilayers were calculated by the equation: $P_{LB} = [P/l]_{LB} \times l_{LB}$, in which l_{LB} is the thickness of the LB bilayers.

As shown in each figure (Figure 3.8 A-C), the line with negative slope represents the "upper bound", which is the combination of the highest permeation selectivity and the highest permeability that has been measured to date for organic polymer-based membranes films that are generally thought to be governed by a solution/diffusion mechanism of transport. The red circles represent the gas permeation properties of all the polymers reported on or before 2008.[29] A "trade-off" relationship between gas permeation selectivity and the gas permeability is apparent in each of these plots; that is, those polymer membranes that exhibit greater permeation selectivities usually show lower gas permeabilities and *vice versa*.

The intrinsic gas permeation properties of glued bilayer of **Calix6**, which are displayed as black filled squares, lie *below* each upper bound. The fact that all three data points lie well below these upper bounds lends support for a *solution-diffusion mechanism of transport and not molecular sieving.* In other words, they support pathway B, in which the gaseous permeants pass through gaps between surfactant molecules.

In addition, according to solution diffusion mechanism, permeation selectivity (α) is defined as the product of diffusivity selectivity (D_i/D_j) and solubility selectivity (S_i/S_j) [*i.e.*, $\alpha=(D_i/D_j)\times (S_i/S_j)$], in which ($D_i/D_j$) is determined by the size difference of two gaseous permeants. In principle, two gas pairs with similar size differences should have similar diffusivity selectivities.[28] The fact that gas selectivities of **Calix6** glued bilayers were $He/CO_2 << CO_2/N_2$, while the size difference between He (0.26 nm) and CO_2 (0.33 nm) is similar to the size difference between CO_2 and N_2 (0.36 nm), implies that the solubility of CO_2 is much higher in these LB bilayers than is the solubility of He and N_2, and that solubility contributions for CO_2 are very significant. (Note: Kinetic diameters of gases determined by zeolite molecular sieves were used to calculate the size differences.[18])

It should be noted that although the intrinsic permeation properties of these glued **Calix6** bilayers lie well below the upper bound of CO_2/N_2, its high CO_2/N_2 selectivity (approaching 100), their extreme thinness (*ca.* 5 nm) suggests that membranes of this type could have practical potential as hyperthin, permeation-selective layers for asymmetric membranes.

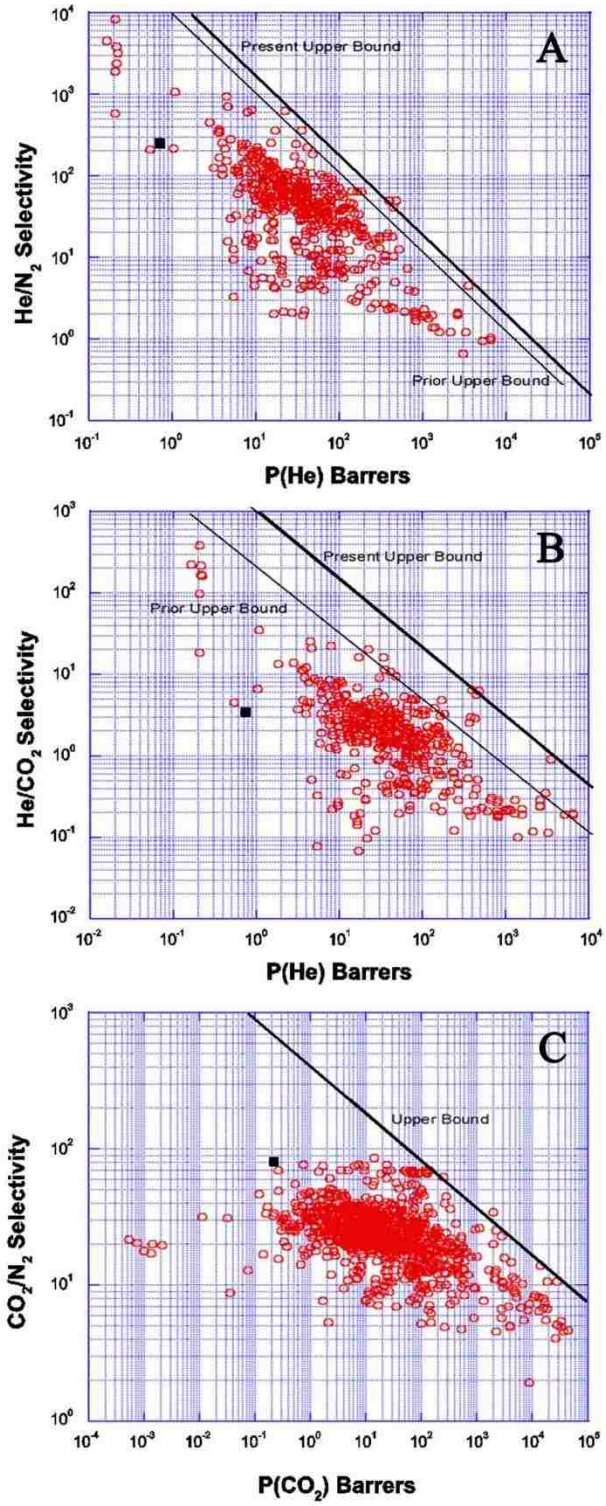

Figure 3.9 Upper-bound plots for: (A) He/N_2 selectivity *versus* He permeability, *P*(He), (B) He/CO_2 selectivity *versus* He permeability *P*(He) and (C) CO_2/N_2 selectivity *versus* CO_2 permeability, $P(CO_2)$. Values lying below the upper bound (■) are for glued bilayers of **Calix6**. The red unfilled circles represent massive amount of polymers that have been reported in the literature where permeation selectivities and permeation coefficients have been recorded. Adapted from reference 29, Copyright (2008), with permission from Elsevier.

3.4 Chapter Summary

In this chapter, LB bilayers of **Calix4**, **Calix5** and **Calix6** have been investigated in PSS-glued and unglued forms. The extent of ionic crosslinking (*i.e.*, gluing) of these three surfactants at the air/PSS aqueous solution interface has been found to increase as the size of the calix[n]arene increases. This has been interpreted in terms of *the degree of functionality of the surfactant*. Comparison of the barrier properties and film thicknesses of glued and unglued LB bilayers implies that the extent of ionic crosslinking is the most important factor controlling the final membrane gas permeation properties. It also implies that PSS layer itself may only make a minor contribution to the barrier properties of a glued LB bilayer. However, whether PSS layer behaves as the main gas barrier or not would be clearer if the gas berrier properties of pure PSS membrane can be obtained and be compared with that of glued LB bilayers in the future. In addition, the current findings support the conclusion that *solution-diffusion and not molecular sieving is the main mechanism* behind the gas permeation for these PSS-glued LB bilayers; *i.e.*, the gaseous permeants pass through gaps between individual porous surfactants and not through the pores within the surfactants. To observe molecular sieving effects in calix[n]arene-based LB bilayer system would appear to require a much higher film quality (*i.e.*, the elimination of residual defects and further tightening of the gaps between the surfactant molecules). This could then force the gaseous permeants to pass through pores of the calix[n]arenes.

3.5 References

1. Wang, M. H.; Janout, V.; Regen, S. L., Glued Langmuir-Blodgett bilayers from calix[n]arenes: Influence of calix[n]arene size on ionic cross-linking, film thickness, and permeation selectivity. *Langmuir* **2010**, 26, (15), 12988-12993.
2. Blodgett, K. B., Films built by depositing successive monomolecular layers on a solid Surface. *J. Am. Chem. Soc.*, **1935**, 57, (6), 1007-1022.
3. Blodgett, K. B. Film structure and method of preparation. **1940**, US Patent No. US 2220860 A.
4. Rose, G. D.; Quinn, J. A., Gas transport through supported Langmuir-Blodgett multilayers. *J. Colloid Interface Sci.*, **1968**, 27, (2), 193-&.
5. Rose, G. D.; Quinn, J. A., Composite membranes - permeation of gases through deposited monolayers. *Science* **1968**, 159, (3815), 636-637.
6. Ulman, A., *An introduction to ultrathin films: From Langmuir-Blodgett to self assembly*. Academic Press: New York, **1991**.
7. Riedl, T.; Nitsch, W.; Michel, T., Gas permeability of Langmuir-Blodgett (LB) films: Characterisation and application. *Thin Solid Films* **2000**, 379, (1-2), 240-252.
8. Li, X. L.; Zhang, G. Y.; Bai, X. D.; Sun, X. M.; Wang, X. R.; Wang, E.; Dai, H. J., Highly conducting graphene sheets and Langmuir-Blodgett films. *Nat. Nanotechnol.* **2008**, 3, (9), 538-542.
9. Tao, A. R.; Huang, J. X.; Yang, P. D., Langmuir-Blodgettry of nanocrystals and nanowires. *Acc. Chem. Res.*, **2008**, 41, (12), 1662-1673.
10. Acharya, S.; Hill, J. P.; Ariga, K., Soft Langmuir-Blodgett technique for hard nanomaterials. *Adv. Mater.*, **2009**, 21, (29), 2959-2981.
11. Wang, M. H.; Janout, V.; Regen, S. L., Gas transport across hyperthin membranes. *Acc. Chem. Res.*, **2013**, 46, (12), 2743-2754

12. Hendel, R. A.; Nomura, E.; Janout, V.; Regen, S. L., Assembly and disassembly of Langmuir-Blodgett films on poly[1-(trimethylsilyl)-1-propyne]: The uniqueness of calix[6]arene multilayers as permeation-selective membranes. *J. Am. Chem. Soc.*, **1997**, 119, (29), 6909-6918.

13. McCullough, D. H.; Regen, S. L., Don't forget Langmuir-Blodgett films. *Chem. Commun.*, **2004**, (24), 2787-2791.

14. Yan, X.; Janout, V.; Hsu, J. T.; Regen, S. L., The gluing of a Langmuir-Blodgett bilayer. *J. Am. Chem. Soc.*, **2003**, 125, (27), 8094-8095.

15. Li, J. W.; Janout, V.; Regen, S. L., Glued Langmuir-Blodgett film: An unexpected dependency of gluing on polyelectrolyte concentration. *Langmuir* **2004**, 20, (6), 2048-2049.

16. Wang, Y.; Stedronsky, E.; Regen, S. L., Probing the gas permeability of an ionically cross-linked Langmuir-Blodgett bilayer with a "Touch" of salt. *Langmuir* **2008**, 24, (12), 6279-6284.

17. Gutsche, C. D., *Calixarenes: An introduction*. 2nd edition ed.; Royal Society of Chemistry: Cambridge, UK, **2008**.

18. Baker, R. W., Membrane technology and applications. 3rd ed.; John Wiley & Sons: Chichester, West Sussex, 2012.

19. Cui, Y.; Kita, H.; Okamoto, K., Preparation and gas separation properties of zeolite T membrane. *Chem. Commun.*, **2003**, (17), 2154-2155.

20. Li, J. W.; Janout, V.; Regen, S. L., Gluing Langmuir-Blodgett monolayers onto hydrocarbon surfaces. *J. Am. Chem. Soc.*, **2006**, 128, (3), 682-683.

21. McAloney, R. A.; Sinyor, M.; Dudnik, V.; Goh, M. C., Atomic force microscopy studies of salt effects on polyelectrolyte multilayer film morphology. *Langmuir* **2001**, 17, (21), 6655-6663.

22. Vercelli, B.; Zotti, G., Polypyrrole self-assembled monolayers and electrostatically assembled multilayers on gold and platinum electrodes for molecular junctions. *Chem. Mater.*, **2006**, 18, (16), 3754-3763.

23. Sarno, D. M.; Martin, J. J.; Hira, S. M.; Timpson, C. J.; Gaffney, J. P.; Jones, W. E., Enhanced conductivity of thin film polyaniline by self-assembled transition metal complexes. *Langmuir* **2007**, 23, (2), 879-884.

24. Wagner, K. C.; Wang, Y.; Regen, S. L.; Vezenov, D. V., Yield strength of glued Langmuir-Blodgett films determined by friction force microscopy. *PCCP*, **2013**, 15, (33), 14037-14046.

25. Koros, W. J.; Fleming, G. K., Membrane-based gas separation. *J. Membr. Sci.*, **1993**, 83, (1), 1-80.

26. Stern, S. A., Polymers for gas separations - the next decade. *J. Membr. Sci.*, **1994**, 94, 1-65.

27. Robeson, L. M., Correlation of separation factor *versus* permeability for polymeric membranes. *J. Membr. Sci.*, **1991**, 62, (2), 165-185.

28. Freeman, B. D., Basis of permeability/selectivity tradeoff relations in polymeric gas separation membranes. *Macromolecules* 1999, 32, (2), 375-380.

29. Robeson, L. M., The upper bound revisited. *J. Membr. Sci.*, **2008**, 320, (1-2), 390-400.

30. Ockwig, N. W.; Nenoff, T. M., Membranes for hydrogen separation. *Chem. Rev.*, **2007**, 107, (10), 4078-4110.

31. Shao, L.; Low, B. T.; Chung, T. S.; Greenberg, A. R., Polymeric membranes for the hydrogen economy: Contemporary approaches and prospects for the future. *J. Membr. Sci.*, **2009**, 327, (1-2), 18-31.

32. Powell, C. E.; Qiao, G. G., Polymeric CO_2/N_2 gas separation membranes for the capture of carbon dioxide from power plant flue gases. *J. Membr. Sci.*, **2006**, 279, (1-2), 1-49.

33. Baschetti, M. G.; Doghieri, F.; Freeman, B.; Sarti, G. C., Transient and steady-state effective diffusivity in high free volume glassy polymers. *J. Membr. Sci.*, **2009**, 344, (1-2), 144-154.

Chapter 4

Poly(acrylic acid) "Glued" Calix[n]arene-Based Langmuir-Blodgett Bilayers for H_2/CO_2 Separation[1]

This chapter includes material that has been reproduced in part with permission from reference 1. Copyright (2011) The Royal Society of Chemistry.

4.1 Introduction

Hydrogen, as an energy carrier, is desired both for its "green" nature and its capability to increase the efficiency of energy usage, which are essential to control global warming and to preserve energy resources.[2-4] Currently, steam-methane reforming processes, in combination with the water-gas shift reaction, represents the most economical technique for the production of hydrogen.[5,6] This process requires the removal of CO_2 from product gas mixtures.[7, 8] Membrane separation methods are considered to be more energy efficient than its competitors such as cryogenic distillation and pressure swing methods.[9-11] Asymmetric membranes are of particular interest, in this regard, because they can produce high flux and high gas selectivities.[12-14] At present, one of the major challenges is to fabricate permeation-selective layers in "hyper-thin" forms (*i.e.*, thinner than *ca.* 100 nm), which are free of defects.[12, 14]

In our laboratory, we have been focusing on the creation of hyperthin defect-free films that are less than 10 nm in thickness by use of the Langmuir-Blodgett (LB) method.[15] Recently, we have demonstrated that single LB bilayers of **Calix6**, which are glued together with poly(acrylic acid) (PAA), and supported on cast films of poly[1-(trimethylsilyl)-1-propyne] (PTMSP), exhibit high He/CO_2 permeation selectivities (see

Figure. 4.1).[16] This earlier finding encouraged us to examine gas permeation properties of PAA-glued calix[n]arene-based bilayers. Since H_2 should have similar permeability as He, high H_2/CO_2 selectivities were expected.

An additional goal of the work that is described in this chapter was to gain further insight into the mechanism of gas permeation across glued LB bilayers. In Chapter 3, we suggested that the quality of PSS-glued LB films needed to be improved by tightening so that gaps between the calix[n]arenes could be removed, thereby allowing for molecular sieving. Since PAA-glued **Calix6** bilayers appeared to be tighter relative to PSS-glued **Calix6**, as judged by He/N_2 selectivities, we were strongly motivated to examine their H_2/CO_2 selectivities.[17, 18] It also seemed reasonable to assume that the quality of PAA-glued **Calix4** bilayers and **Calix5** bilayers would also be improved, significantly.

The working hypothesis that underlies the studies that are described in this chapter is the same as that discussed in Chapter 3; *i.e.*, if molecular sieving were occurring, then the H_2/CO_2 selectivities might be **Calix5** > **Calix6** >**Calix4**, based on the size of the gaseous permeants and the maximum internal diameter of these calix[n]arenes.[19] Also, the relative permeances for H_2 that would be expected would be **Calix6** > **Calix5** > **Calix4**. If the main pathways for diffusion were between transient gaps, however, then a solution-diffusion mechanism would lead to the prediction of observing only modest selectivities that lie beneath the upper bound.

In addition to the gas permeation properties, the monolayer properties, bilayer thicknesses and topographies of PAA glued calix[n]arene-based surfactants have also been carefully examined.

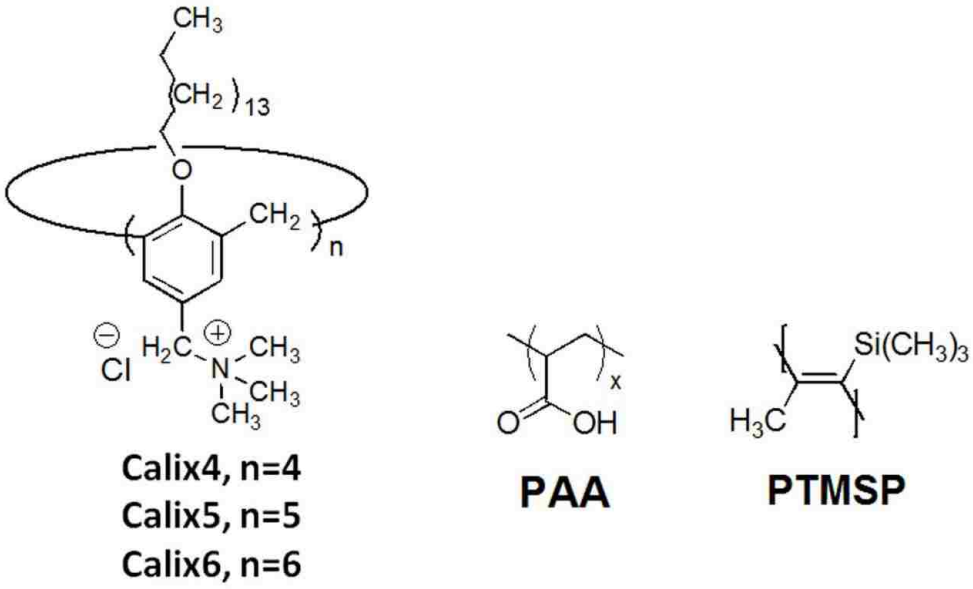

Figure 4.1 Structures of the calix[n]arene-based surfactants, PAA and PTMSP.

4.2 Membranes and Materials

The experimental conditions that were used for the studies that are described in this section were similar to those that were optimized previously, for **Calix6**.[16, 17] The syntheses of **Calix4**, **Calix5** and **Calix6** were carried out by our colleague, Dr. Vaclav Janout, using established methods.[20] Poly(acrylic acid) (PAA) (average M_W *ca.* 240,000), which was used as the polymeric anion for gluing, and poly[1-(trimethylsilyl)-1-propyne] (PTMSP), which was used as support material, were obtained from commercial sources and used directly (see Figure 4.1).

4.3 Results and Discussion

4.3.1 Monolayer properties

4.3.1.1 Surface Pressure-Area Isotherms

Figure 4.2 shows the surface pressure-area isotherm cycles for each calix[n]arene-based surfactant at the air/water interface in the presence and absence of PAA (0.1 mM

repeat units at pH 3.3). As is apparent, the molecular areas were **Calix6** > **Calix5** > **Calix4** in all cases. Unlike PSS glued calix[n]arenes, the differences between first and the following two compressions were much smaller, although larger "lift-off" areas were generally observed in first compressions. These results indicate that the anealing in PAA glued monolayers was less than with the PSS-glued monolayers during repeated compressions and expansions. As shown in Table 4.1, the molecular areas for **Calix4**, **Calix5** and **Calix6**, estimated from second compressions, were *ca.* 2.4 nm^2 (corresponding to 0.60 nm^2/repeat unit), 2.9 nm^2 (corresponding to 0.58 nm^2/repeat unit) and 3.3 nm^2 (corresponding to 0.56 nm^2/repeat unit) respectively. These areas were larger than their unglued analogs as well as their PSS-glued analogs (Table 3.1). These results suggest that the PAA chains penatrate into the surfactant monolayer at the air/PAA solution interface. However, the extent of penetration appears to be larger for the PAA than for the PSS chains.

A possible explanation is that at pH 3.3, the highly protonated PAA chains (*i.e.*, *ca.* 90% of carboxylate groups are protonated, based on a pKa of 4.28 for PAA) have a higher surface activity than the highly charged PSS, because of an overall higher degree of hydrophobicity, which results from protonation.[21,22] As a consequence, one might expect that the PAA chains should penetrate into the gaps between calix[n]arene molecules more effectively than PSS chains, which was evidenced by the larger molecular areas observed in PAA-glued monolayers. A cartoon is shown in Figure 4.3 to describe the extent of penatration of PSS and PAA into gaps among **Calix6** molecules.

Table 4.1 Monolayer properties of calix[n]arenes.

Surfactant	Molecular Area (nm^2)	Area per Repeat Unit (nm^2)	Quaternary Ammonium Groups[c] per nm^2	Alkyl Tails[d] per nm^2
Calix4	1.52	0.38	2.63	2.63
Calix5	2.20	0.44	2.27	2.27
Calix6	2.80	0.47	2.13	2.13
Calix4 + PAA	2.40	0.60	1.67	1.67
Calix5 + PAA	2.90	0.58	1.72	1.72
Calix6 + PAA	3.36	0.56	1.79	1.79

[a]Molecular areas of a surfactant determined by drawing a line along the slope of the isotherm of second compression at 30 mN/m as shown in Figure 4.2. [b]Molecular area per repeat unit determined by dividing molecular area of calix[n]arene by n. [c,d]The number of quaternary ammonium groups and alkyl tails per nm^2 is the reciprocal of the molecular area occupied by one repeat unit.

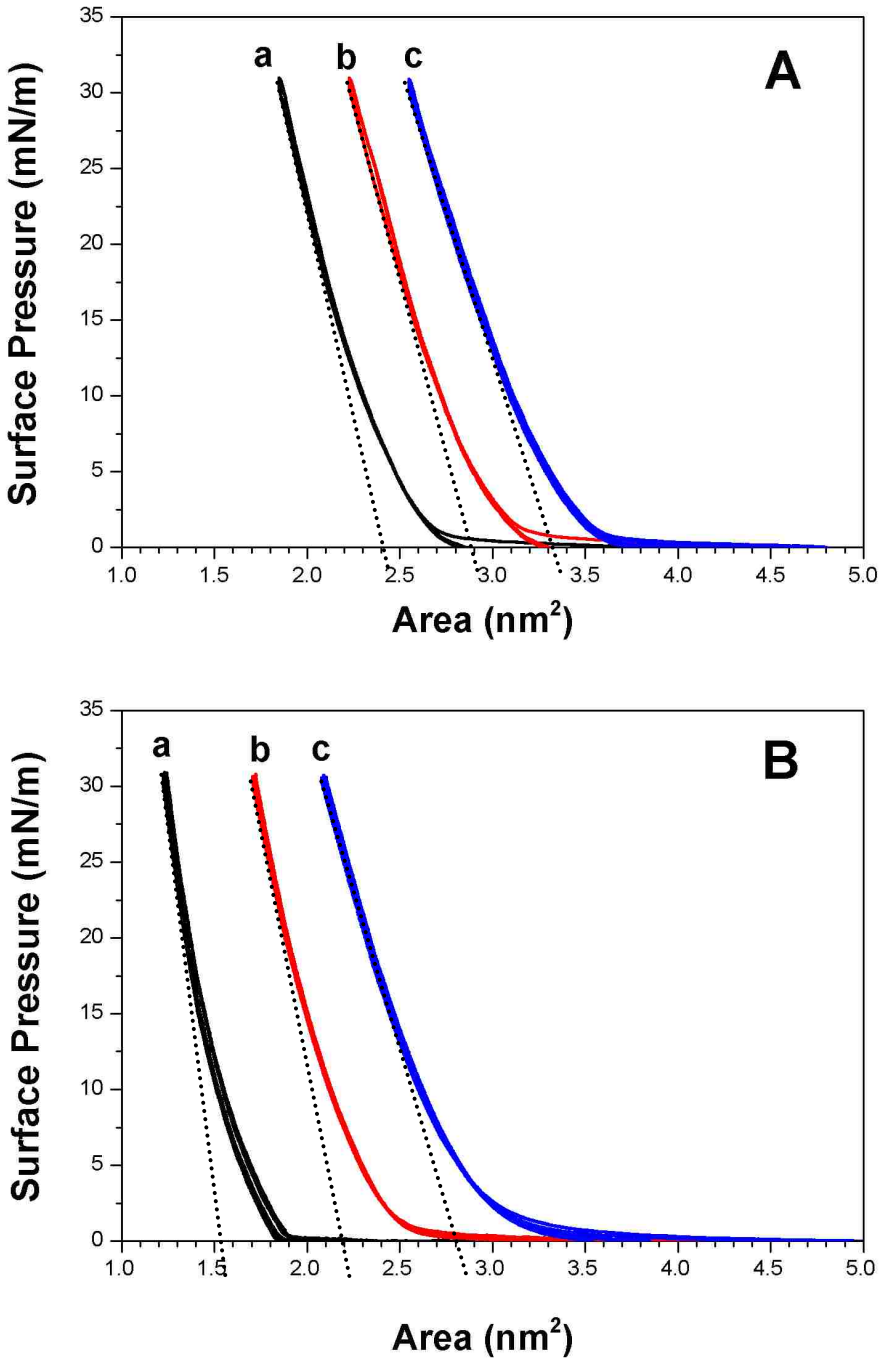

Figure 4.2 Surface pressure-area isotherm cycles recorded: (A) over an aqueous subphase at pH 3.3 (25 ℃) containing PAA [0.1 mM repeat units] and (B) over an pure water subphase at 25 ℃ for (a) **Calix4**, (b) **Calix5** and (c) **Calix6**. [Note: In each isotherm cycle experiment, the calix[n]arene monolayers were compressed to 30 mN/m first, then expanded to 0 mN/m, and this compression/expansion then repeated for an additional two cycles.]

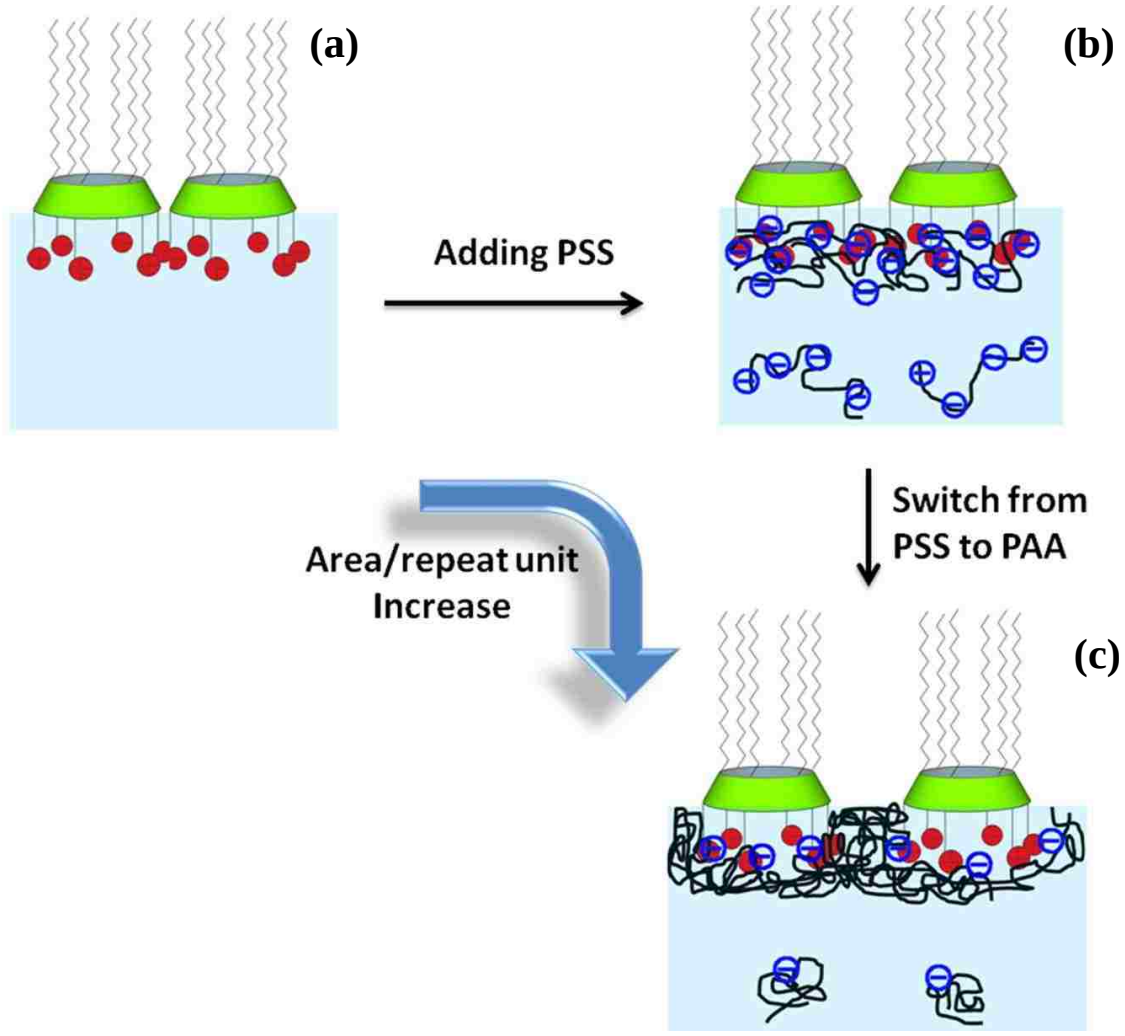

Figure 4.3 Schematic illustrations of **Calix6** monolayers at the air/water interface. Three subphase solutions are shown: (a) pure water, (b) a PSS solution and (c) a PAA solution.

4.3.1.2 Monolayer Cohesiveness

In Figure 4.4 are shown the results from surface viscosity meausrements that were carried out with the three calix[n]arenes at the air/water interface in the presence and absence of PAA (0.1 mM repeat units at pH 3.3). The experimental procedures used were similar to those described in Chapters 2 and 3. In this case, only a slit opening of 6 mm was used with the canal viscometer. The importance of adding PAA into the subphase can thus be revealed by comparing surface viscosities of PAA-glued monolayers with

their unglued analogs. Over the pure water subphase, upon exposure to the 6 mm slit opening of canal viscometer, the surface pressure of the unglued monolayers dropped to 0 mN/m in less than a minute. In the presense of PAA, all three surfactants showed a slow reduction in their surface pressures to 0 mN/m in a more than 30 min period. These findings show the importance of having PAA present in the subphase. Moreover, the viscosities were found to increase as the size of the calix[n]arene increased. The reason for this increase in viscosity is presumed to be similar to that of PSS glued calix[n]arenes; *i.e.*, the degree of crosslinking increases as the size of the calix[n]arene increases due to a higher degree of funcitionality (*i.e.*, quaternary ammonium head groups attached to each calix[n]arene molecule).

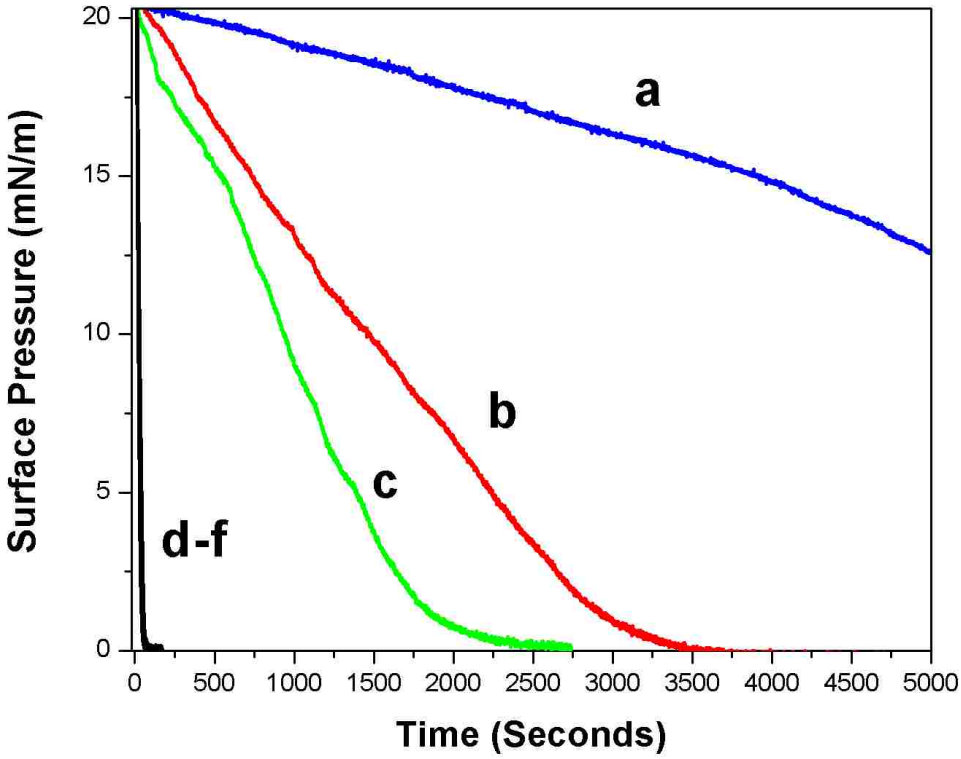

Figure 4.4 Relative surface viscosities determined by use of a canal viscometer with a slit opening of 6 mm for (a) **Calix6**, (b) **Calix5** and (c) **Calix4** over a PAA subphase [0.1 mM repeat units] at pH 3.3 (25 ℃). In the absence of PAA, the surface pressure for **Calix4**, **Calix5** and **Calix6** dropped precipitously (d, e and f) and were indistinguishable.

4.3.2 Thicknesses and Topographies of PAA-Glued LB bilayers

To judge the influence of gluing on film thicknesses and surface topographies, calix[n]arenes Langmuir-Blodgett (LB) bilayers that were glued with PAA were deposited onto silicon wafers that were silylated with *n*-octadecyltrichlorosilane (OTS) using a surface pressure of 30 mN/m. Experimental procedures that were used were similar to that reported.[20] Ellipsometry and atomic force microscopy (AFM) were used to measure the thicknesses and topographies of LB films as described in Chapter 2.[20] Table 4.2 shows a summary of the thicknesses obtained by ellipsometry and by the "AFM razor blade scratching method" (Note: The results from AFM were consistent with OTS still on the surface under such conditions).[23,24] As is apparent, the thicknesses from these two methods were in good agreement. Topographies and step heights of the LB films from AFM measurements are shown in Figure 4.5 and 4.6. Although the PAA-glued LB bilayers made from calix[n]arenes shown in Figure 4.5 were rougher than PSS-glued analogs (see Figure 3.6), no defects were observed in these LB films.

Table 4.2 Thicknesses of PAA-glued bilayers determined by ellipsometry and AFM.

Membrane	Bilayer Thickness[a] (ellipsometry, nm)	Bilayer Thickness (AFM, nm)	RMS Roughness[b] (AFM, nm)
Calix4+PAA	5.8 ± 0.1	5.8 ± 0.2	0.3
	(5.7 ± 0.1)		
Calix5+PAA	5.9 ± 0.1	6.0 ± 0.3	0.7
	(5.9 ± 0.1)		
Calix6+PAA	6.0 ± 0.1	6.1 ± 0.5	1.0
	(6.0 ± 0.1)		

[a]Numbers in parentheses refer to duplicate membranes that were prepared, independently. [b]Root-mean-square roughness determined by AFM. Error values given for film thicknesses represent one standard deviation based on five AFM and five ellipsometry measurements at different locations along the surface.

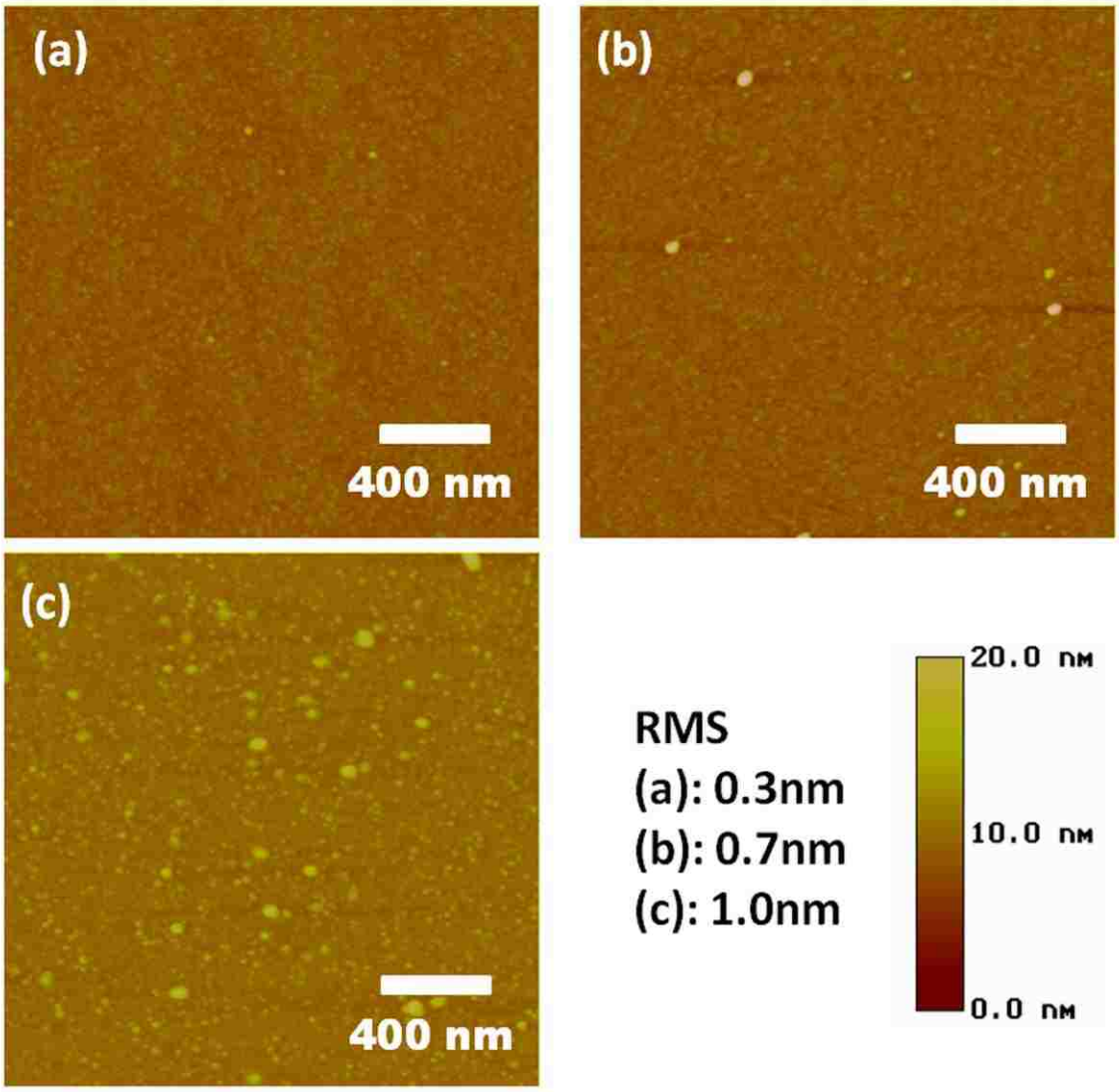

Figure 4.5 AFM topography (tapping mode, 2 × 2 μm) and root mean square roughness of PAA glued LB bilayers of: (a) **Calix4**, (b) **Calix5**, (c) **Calix6**. All LB transfers were made using a speed of 2 mm/min and a surface pressure of 30 mN/m in the presence of 0.1 mM PAA at pH 3.3.

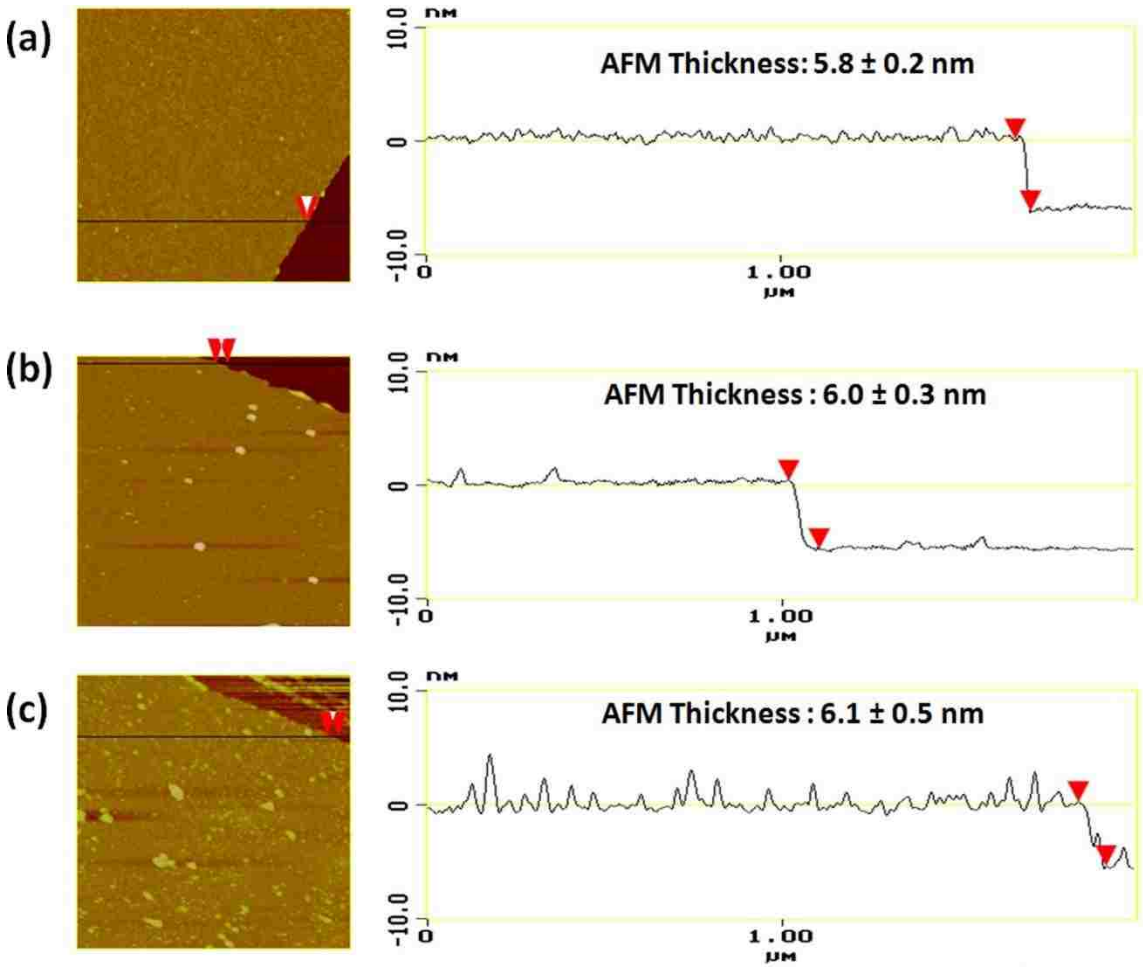

Figure 4.6 Step height images and section profiles (AFM, tapping mode, 2 × 2 μm) of PAA glued bilayers of: (a) **Calix4,** (b) **Calix5,** (c) **Calix6.** The *z*-scale is shown to the right. All LB transfers were made using a speed of 2 mm/min and a surface pressure of 30 mN/m in the presence of 0.1 mM PAA at pH 3.3.

4.3.2.1 Thicknesses of PAA-Glued Bilayers as a Function of Calix[n]arene Size

As shown in Table 4.2 and Figure 4.6, the thicknesses of PAA-glued bilayers of **Calix4**, **Calix5** and **Calix6** were 5.8, 6.0 and 6.1 nm, respectively, which are similar with each other. As discussed in Chapter 3, the bilayer thicknesses increases as the number of ammonium head groups/unit area increases. Thus, these results were consistent with the fact that as the number of ammonium head groups/nm^2 of PAA-glued calix[n]arene-based monolayers increases, their bilayer thickness increases as well (Table 4.1).

4.3.2.2 Topographies of PAA-Glued Bilayers as a Function of Calix[n]arene Size

Figure 4.6 shows the topographies of PAA glued bilayers on OTS silylated silicon wafers. As is apparent, all glued bilayers had defects-free surfaces. A comparison of these results with the topographies of unglued calix[n]arene bilayers indicates that the addtion of PAA in the subphase greatly improved the stability of the LB bilayers. The reason why the roughness of glued bilayers increased as the size of calix[n]arene increases is not presently clear.

4.3.3 Gas Permeation Properties of PAA-Glued Bilayers

A series of PAA-glued LB bilayers of **Calix4**, **Calix5** and **Calix6** LB bilayers were deposited onto cast films made from PTMSP to determine their gas permeation properties. Procedures used for these depositions were similar to those used for the deposition onto silylated silicon wafers (see detailed protocols in Chapter 2). All of the glued LB bilayers that were used for permeation measurements were fabricated, independently, in triplicate. Four gaseous permeants He, H_2, N_2 and CO_2 were employed to judge the barrier properties of these glued LB films. Permeance values (P/l) for each gas are listed in Table 4.3. Here, P is the permeability coefficient and l is the thickness of the composite membrane, P/l has been calculated by dividing the observed flux (F) by the area of the membrane (A) and by the pressure gradient (Δp) that is used; that is, $P/l = F/(A \times \Delta p)$. The permeability of the membranes with respect to H_2 and CO_2 were determined because H_2/CO_2 is of practical interest for the hydrogen purification.[10, 11] Also, the permeabilities of He and N_2 were measured to gain an additional perspective of their barrier properties, and to make a comparison with PSS-glued calix[n]arene bilayers.

Table 4.3 Permeances of gases across Langmuir-Blodgett bilayers[a]

Membrane	He	H_2	CO_2	N_2	He/CO_2	H_2/CO_2	He/N_2
PTMSP[b]	2.7×10^2	7.0×10^2	1.6×10^3	3.0×10^2	0.90	0.17	5.3
	2.7×10^2	7.0×10^2	1.6×10^3	2.9×10^2	0.89	0.16	5.6
Calix4/PAA	31	7.1	0.68	<0.1	46	11	>310
	33	8.8	0.85	<0.1	39	10	>330
	31	8.0	0.88	<0.1	36	9.1	>310
Calix5/PAA	34	9.0	0.33	<0.1	1.0×10^2	28	>340
	31	7.2	0.33	<0.1	95	22	>310
	29	8.4	0.62	<0.1	47	14	>290
Calix6/PAA	28	6.5	0.19	<0.1	152	35	>280
	31	6.9	<0.1	<0.1	>310	>69	>310
	31	7.9	0.19	<0.1	170	43	>310

[a]Permeance values at ambient temperature, $10^6(P/l)$ (cm^3/cm^2-s-cmHg), were calculated by dividing the observed flux by the area of the membrane (9.36 cm^2) and by the pressure gradient (10 psi) employed, using *ca.* 30 μm thick PTMSP. All measurements were made at ambient temperture. Values reported are averages of 5-10 measurements for each sample, which varied by less than 5%. Permeation selectivities that are listed for He/CO_2, H_2/CO_2 and He/N_2 are the ratio of the individual permeances. [b]Bare PTMSP membranes; all other values listed refer to composites of PTMSP and single LB bilayers made from the indicated components.

4.3.3.1 Barrier Properties of PAA-Glued Bilayers as a Function of Calix[n]arene Size

As seen in Table 4.3, PAA-glued calix[n]arene bilayers on PTMSP membranes resulted in substantial reductions for the He, H_2, CO_2 and N_2 permeances. For all PAA glued bilayers, the permeances of the four permeants were always $He > H_2 > CO_2 > N_2$. This ordering clearly reflects their size; *i.e.*, the smaller the permeant, the greater its

permeance. The N_2 fluxes were too small to be detected using a pressure gradient of 10 psi and are indicated as <0.1. Since the N_2 fluxes were essentially undetectable for these PAA-glued calix[n]arene bilayers, it appears that the "transient gaps" within these LB films are smaller than the kinetic diameter of N_2 molecules (0.36 nm).[25]

In addition, the reduction in the flux for CO_2 and N_2 has been found to be much larger than for that of He and H_2 (Table 4.3). As a result, the gas permeation selectivities of PAA-glued bilayers with respect to He/CO_2 and H_2/CO_2 and He/N_2 increased substantially when compared to pristine PTMSP cast films. This clearly indicates that tight membranes (*i.e.*, with few defects or small average transient gaps) were formed when PAA was used as the glue.

As is apparent in Table 4.3, the He permeances for PAA glued bilayers made of **Calix4**, **Calix5** and **Calix6**, were similar to each other. Similar trend was also observed for the H_2 permeances of all of the PAA glued bilayers. On the other hand, the CO_2 permeances for PAA glued calix[n]arene bilayers were **Calix4** > **Calix5** > **Calix6**. As a result, both He/CO_2 and H_2/CO_2 gas selectivities of the PAA glued bilayers were **Calix4** < **Calix5** < **Calix6**. Considering that PAA-glued calix[n]arenes had similar thicknesses (Table 4.2), these results suggest that the larger calix[n]arenes create tighter membranes, which is a likely consequence of a higher degree of ionic crosslinking between calix[n]arenes and PAA within the membranes. The higher number of functionality bore by larger calix[n]arenes can account for this higher degree of crosslinking within these glued bilayers.

4.3.3.2 Barrier Properties of PAA-Glued Bilayers *versus* PSS-Glued Bilayers: A "Self-Healing" Model

As seen in Tables 3.3 and 4.3, the gas permeation selectivities of PAA-glued calix[n]arene bilayers, with respect to He/CO_2 and He/N_2, were always higher than any of the PSS-glued calix[n]arene bilayers. To account for this difference, a "self-healing" model is proposed here. Specifically, at a pH of 3.3, the ionized portions of PAA can ionically crosslink the calix[n]arene molecules and tighten the surfactant assmebly. The remaining protonated portions of PAA are then available for "filling in gaps" between calix[n]arene molecules as well as within the PAA layer, itself.

For the gaps between calix[n]arene molecules, PAA chains can fill these gaps by the hydrophobic interaction with hydrocarbon part of the calix[n]arene. This is fully consistent with the molecular areas of calix[n]arenes that we have observed after PAA has been added to the aqueous subphase (Tables 3.1 and 4.1). One can also envision that protonated segments of PAA can fill in gaps within the PAA layer, itself. Thus, unlike highly charged PSS, the extent of charge repulsion between the PAA chains should be much smaller, which should help to tighten the packing of the PAA chains. In addition, since protonated segments of PAA should be good hydrogen bond donors as well as acceptors,[26] hydrogen bonding should help to tighten the packing of these PAA chains. Thus, partially charged PAA can ionically crosslink surfactant molecules, and partially protonated PAA can fill in the gaps within the assembly (a self-healing process). In the case of PSS, only ionic crosslinking is possible. This interpretation is also supported by the much smaller gas permeances for He, CO_2 and N_2 that have been observed for the PAA-glued membranes as compared with the PSS-glued analogs (Tables 3.3 and 4.3). In

summary, these findings suggest that it is the combination of ionic crosslinking, hydrophobic interactions and hydrogen bonding that lead to high-quality LB films.

4.3.3.3 Is Molecular Sieving Occurring?

As is apparent, the tightness of PAA-glued LB bilayers was significantly greater as compared to the PSS-glued and unglued analogs. Nevertheless, the current data of He, H_2 and CO_2 permeation properties does not support the hypothesis that PAA-glued calix[n]arene-based LB bilayers act as molecular sieves. As discussed in the introduction, if molecular sieving were occurring, the relative permeances of He, H_2 should be **Calix4** < **Calix5** < **Calix6** and the relative selectivities of He/CO_2 and H_2/CO_2 should be **Calix5** > **Calix6** > **Calix4**. However, the He/CO_2 and H_2/CO_2 permeation selectivities we found were **Calix4** < **Calix5** < **Calix6**, while the permeances of such PAA-glued LB bilayers were similar with respect to both He and H_2. These results support the conclusion that these permeants are more likely to pass through gaps between the calix[n]arenes that are filled with PAA (pathway B in Figure 3.1) and that a solution diffusion mechanism is dominating. The higher He/CO_2 and H_2/CO_2 selectivities associated with the larger calix[n]arenes is a likely consequence of a higher degree of ionic crosslinking, resulting in smaller transient gaps within the membrane, and thus higher film quality. Further discussion will be given in the following section.

4.3.3.4 Membrane Performances as Judged by Upper-Bound Plots

Further evidence for a solution-diffusion mechanism being dominant was obtained by calculating the intrinsic permeabilities of PAA-glued bilayers of **Calix6** with respect to He, H_2, CO_2 and N_2 using the series-resistance model (*i.e.*, $1/[P/l]_{composite} = 1/[P/l]_{PTMSP} + 1/[P/l]_{LB}$).[27] By measuring the permeance of PTMSP ($[P/l]_{PTMSP}$) and composite

membranes ($[P/l]_{composite}$) separately, the intrinsic permeance value of the LB bilayers($[P/l]_{LB}$) can be calculated.[27] The intrinsic permeability coefficient of the LB bilayers were calculated by the equation: $P_{LB} = [P/l]_{LB} \times l_{LB}$, where l_{LB} is the thickness of the LB bilayers.

The permeability coefficients for He, H_2, CO_2 and N_2, along with the permeation selectivities of H_2/CO_2, He/CO_2 and He/N_2, were calculated for PAA-glued Calix6 bilayers, and were included in Robeson upper-bound plots for H_2/CO_2, He/CO_2 and He/N_2 (Figure 4.7 A-C).[28-30] The principle of the upper-bound plots has been discussed in Chapter 1 and Chapter 3 in detail. The intrinsic gas permeation properties of the glued bilayers of **Calix6**, which are displayed as black unfilled squares, lie *below* each upper bound. This fact lends support for a *solution-diffusion mechanism of transport and not molecular sieving.* In other words, it appears that pathway B (Figure 3.1) is operating, in which the gaseous permeants pass through gaps between the calix[n]arene molecules.

The fact that the PAA-glued **Calix6** bilayers have H_2/CO_2 selectivities that are higher than almost any of the polymers reported to date makes this class of films of potential interest for H_2/CO_2 separations, especially when one considers that the thickness of these bilayers is only *ca.* 6 nm. In principle, high H_2/CO_2 selectivity and high H_2 flux may be possible, when these LB films are used as the selective layers of asymmetric membranes.

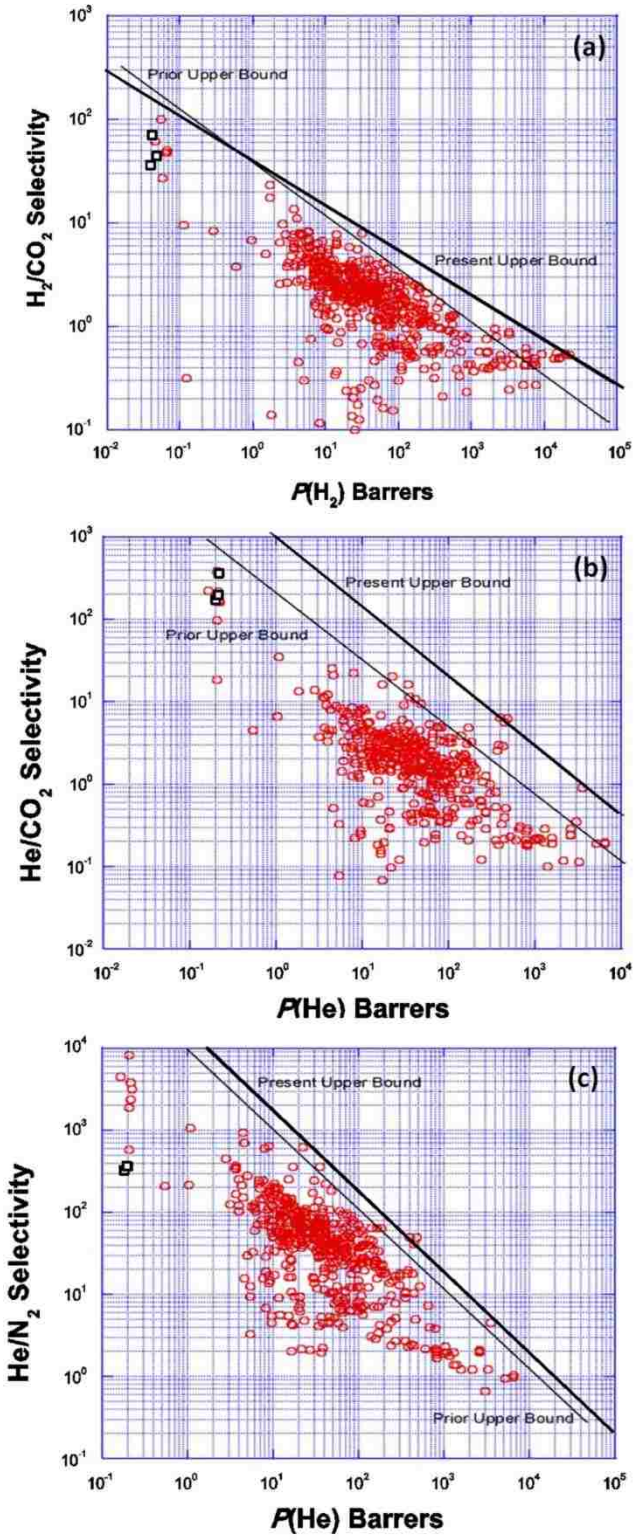

Figure 4.7 Upper-bound plots of H_2/CO_2, He/CO_2 and He/N_2. Values lying below the upper bound (□) are for PAA-glued bilayers of **Calix6**. The red circles represent the polymers that have been reported on or before 2008. Adapted from reference 30, Copyright (2008), with permission from Elsevier.

4.3.3.5 Is the PAA Layer Behaving as the Main Gas Barrier?

To speculate if the PAA layer behaves as the main gas barrier, one needs to compare the gas-permeation properties of PAA-glued LB bilayers of calix[n]arenes with that of PSS-glued analogs (both are defect-free LB films). [Note: The comparison between unglued and PAA-glued LB bilayers of calix[n]arenes is problematic, because unglued calix[n]arenes rearranged easily during of after LB transfer (Figure 3.6) and cannot represent defect-free LB films.]

Assuming that two calix[n]arene layers in a glued LB bilayer are the main gas barriers, then the gas permeation properties of a glued LB bilayer should depend on the size of the gaps between individual calix[n]arene molecules, because gaseous permeants dominately diffuse through these gaps (as discussed in above sections). As shown in Tables 3.1 and 4.1, the molecular area of a PAA-glued calix[n]arene is larger than that of a PSS-glued analog. This result means the size of such gaps increased after replacing PSS with PAA, and a decreased barrier toward all gases should be expected if the main gas barrier is the calix[n]arene layers. However, the PAA-glued LB bilayers turned out to be much stronger gas barriers when compared with PSS-glued analogs (Tables 3.3 and 4.3). Thus, in the case of PAA-glued LB bilayers, it is not calix[n]arene layers, but the PAA layer filled between two calix[n]arene layers serving as the main gas barrier.

A related work showed that LB multilayers made of 6 monolayers of calix[6]arene molecules (functionalized with amidoxime head groups and octyl tails) had a He/N_2 selectivity of ca. 70.[31] This result indicates that a defect-free LB bilayer made of calix[6]arene may have an intrinsic He/N_2 permeation selectivity close to ca. 70. The fact that such a He/N_2 selectivity is much smaller than that of PAA-glued LB bilayer of

calix[6]arene studied in this chapter (> *ca.* 300) and in the literature (He/N_2 selectivity up to 1000[17]), however, lends additional support to the above speculation that PAA layer is the main gas barrier.

To further determine if the main gas barrier is the PAA layer, the intrinsic barrier properties of pure PAA membranes should be obtained in the future to make comparison with these PAA-glued bilayers.

4.4 Chapter Summary

In this chapter, the permeation properties of PAA-glued LB bilayers of **Calix4**, **Calix5** and **Calix6** have been investigated. At a thickness of *ca.* 6 nm, the intrinsic H_2/CO_2 selectivities of PAA-glued **Calix6** bilayers were larger than almost all polymers that have been reported to date. The improved tightness within these PAA-glued LB bilayers, as compared to PSS-glued bilayers, is likely due to the "self-healing" ability of partially ionized PAA chains. Thus, the charged portions of PAA can tighten the LB bilayer by ionic crosslinking, while the protonated portions can fill in the gaps between surfactant molecules as well as the gaps within PAA, itself. The He/CO_2 and H_2/CO_2 selectivities that were found for PAA-LB bilayers increased modestly as the size of the calix[n]arenes increased. This has been attributed to differences in the degree of functionality of the surfactants **Calix4**, **Calix5** and **Calix6**. The permeation data for PAA-glued bilayers obtained in this research support a *solution diffusion mechanism of transport and not molecular sieving*. The fact that the intrinsic permeation properties of PAA-glued **Calix6** bilayers lie below the upper bounds for H_2/CO_2, He/CO_2 and He/N_2 lend additional support for a solution diffusion mechanism. The current finding also implies that the PAA layer filled in between two surfactant monolayers serves as the main gas barrier.

4.5 References

1. Wang, M. H.; Janout, V.; Regen, S. L., Hyper-thin organic membranes with exceptional H_2/CO_2 permeation selectivity: importance of ionic crosslinking and self-healing. *Chem. Commun.*, **2011**, 47, (8), 2387-2389.
2. Kamat, P. V., Meeting the clean energy demand: Nanostructure architectures for solar energy conversion. *J. Phys. Chem. C*, **2007**, 111, (7), 2834-2860.
3. Marban, G.; Vales-Solis, T., Towards the hydrogen economy? *Int. J. Hydrogen Energy*, **2007**, 32, (12), 1625-1637.
4. Alves, H. J.; Bley, C.; Niklevicz, R. R.; Frigo, E. P.; Frigo, M. S.; Coimbra-Araujo, C. H., Overview of hydrogen production technologies from biogas and the applications in fuel cells. *Int. J. Hydrogen Energy*, **2013**, 38, (13), 5215-5225.
5. Xu, J. G.; Froment, G. F., Methane steam reforming, methanation and water-gas shift .1. Intrinsic kinetics. *Aiche J.*, **1989**, 35, (1), 88-96.
6. Oliveira, E. L. G.; Grande, C. A.; Rodrigues, A. E., Methane steam reforming in large pore catalyst. *Chem. Eng. Sci.*, **2010**, 65, (5), 1539-1550.
7. Sircar, S.; Golden, T. C., Purification of hydrogen by pressure swing adsorption. *Sep. Sci. Technol.*, **2000**, 35, (5), 667-687.
8. Yang, S. I.; Choi, D. Y.; Jang, S. C.; Kim, S. H.; Choi, D. K., Hydrogen separation by multi-bed pressure swing adsorption of synthesis gas. *Adsorption-J. Int. Adsorpt. Soc.*, **2008**, 14, (4-5), 583-590.
9. Hinchliffe, A. B.; Porter, K. E., A comparison of membrane separation and distillation. *Chem. Eng. Res. Des.*, **2000**, 78, (A2), 255-268.
10. Ockwig, N. W.; Nenoff, T. M., Membranes for hydrogen separation. *Chem. Rev.*, **2007**, 107, (10), 4078-4110.
11. Shao, L.; Low, B. T.; Chung, T. S.; Greenberg, A. R., Polymeric membranes for the hydrogen economy: Contemporary approaches and prospects for the future. *J. Membr. Sci.*, **2009**, 327, (1-2), 18-31.

12. Hachisuka, H.; Ohara, T.; Ikeda, K., New type asymmetric membranes having almost defect free hyper-thin skin layer and sponge-like porous matrix. *J. Membr. Sci.*, **1996**, 116, (2), 265-272.

13. Kosuri, M. R.; Koros, W. J., Defect-free asymmetric hollow fiber membranes from Torlon (R), a polyamide-imide polymer, for high-pressure CO_2 separations. *J. Membr. Sci.*, **2008**, 320, (1-2), 65-72.

14. Ismail, A. F.; Yean, L. P., Review on the development of defect-free and ultrathin-skinned asymmetric membranes for gas separation through manipulation of phase inversion and rheological factors. *J. Appl. Polym. Sci.*, **2003**, 88, (2), 442-451.

15. Wang, M. H.; Janout, V.; Regen, S. L., Gas transport across hyperthin membranes. *Acc. Chem. Res.*, **2013**, 46, (12), 2743-2754.

16. Li, J. W.; Janout, V.; Regen, S. L., Glued Langmuir-Blodgett bilayers having unusually high He/CO2 permeation selectivities. *Langmuir* **2005**, 21, (5), 1676-1678.

17. Li, J. W.; Janout, V.; McCullough, D. H.; Hsu, J. T.; Truong, Q.; Wilusz, E.; Regen, S. L., Exceptional gas permeation selectivity of a glued Langmuir-Blodgett bilayer by pH control. *Langmuir* **2004**, 20, (19), 8214-8219.

18. Li, J. W.; Janout, V.; Regen, S. L., Glued Langmuir-Blodgett film: An unexpected dependency of gluing on polyelectrolyte concentration. *Langmuir* **2004**, 20, (6), 2048-2049.

19. Gutsche, C. D., *Calixarenes: An introduction*. 2nd edition ed.; Royal Society of Chemistry: Cambridge, UK, **2008**.

20. Wang, M. H.; Janout, V.; Regen, S. L., Glued Langmuir-Blodgett bilayers from calix[n]arenes: Influence of calix[n]arene size on ionic cross-linking, film thickness, and permeation selectivity. *Langmuir* **2010**, 26, (15), 12988-12993.

21. Kurkuri, M. D.; Lee, J. R.; Han, J. H.; Lee, I., Electroactive behavior of poly(acrylic acid) grafted poly(vinyl alcohol) samples, their synthesis using a Ce-

(IV) glucose redox system and their characterization. *Smart Mater. Struct.* **2006**, 15, (2), 417-423.

22. Surface tension measurements made for aqueous solutions 0.1mM PAA at pH 3.3, 5mM PSS and water gave values of 70.8 ± 0.5, 72.2 ± 0.3 and 72.5 ± 0.3 mN/m, respectively (5 measurements, 25 ℃), confirming a greater surface activity of PAA.

23. McAloney, R. A.; Sinyor, M.; Dudnik, V.; Goh, M. C., Atomic force microscopy studies of salt effects on polyelectrolyte multilayer film morphology. *Langmuir* **2001**, 17, (21), 6655-6663.

24. Wang, Y.; Stedronsky, E.; Regen, S. L., Probing the gas permeability of an ionically cross-linked Langmuir-Blodgett bilayer with a "touch" of salt. *Langmuir*, **2008**, 24, 6279-6284.

25. Baker, R. W., Membrane technology and applications. 3rd ed.; John Wiley & Sons: Chichester, West Sussex, 2012.

26. Dong, J.; Ozaki, Y.; Nakashima, K., Infrared, Raman, and near-infrared spectroscopic evidence for the coexistence of various hydrogen-bond forms in poly(acrylic acid). *Macromolecules* **1997**, 30, (4), 1111-1117.

27. Rose, G. D.; Quinn, J. A., Composite membranes - permeation of gases through deposited monolayers. *Science* **1968**, 159, (3815), 636-637.

28. Robeson, L. M., Correlation of separation factor *versus* permeability for polymeric membranes. *J. Membr. Sci.*, **1991**, 62, (2), 165-185.

29. Freeman, B. D., Basis of permeability/selectivity tradeoff relations in polymeric gas separation membranes. *Macromolecules* **1999**, 32, (2), 375-380.

30. Robeson, L. M., The upper bound revisited. *J. Membr. Sci.*, **2008**, 320, (1-2), 390-400.

31. Yan, X.; Hsu, J. T. and Regen, S. L., Selective dampening of the gas permeability of a Langmuir-Blodgett film using moist permeants. *J. Am. Chem. Soc.*, **2000**, 122, 11944-11947

Chapter 5

PAA-Glued Polymeric Langmuir-Blodgett Films For H_2/CO_2 Separation[1]

This chapter includes material that has been reproduced in part with permission from reference 1. Copyright (2013) American Chemical Society.

5.1 Introduction

Membrane technology has attracted considerable attention for the removal of CO_2 from H_2 that is produced by the methane-steam reforming process.[2, 3] Although many classes of organic polymers have been evaluated, most have suffered from low H_2/CO_2 selectivities (*i.e.*, <10) as shown in Robeson's upper-bound plot.[4] An approach that wehave taken in creating high permeance-membranes is based on the use of hyperthin (<100 nm) Langmuir-Blodgett bilayers.[5] However, the intrinsic membrane permeation properties that we have usually observed have placed them beneath the upper bound. In this chapter, we show that single Langmuir-Blodgett (LB) bilayers made from a polymeric surfactant bearing quaternary ammonium head groups, and "glued" (*i.e.*, ionically crosslinked) by poly(acrylic acid) (PAA), which are only 7 nm in thickness, exhibit a remarkable H_2/CO_2 selectivity of 200 (Figure 5.1).

As discussed in Chapters 3 and 4, we have learned that: (i) PAA-glued LB bilayers made from a porous calix[6]arene-based surfactant (**Calix6**) achieved a H_2/CO_2 selectivity of *ca.* 70; (ii) gaseous permeants diffused through gaps between calix[n]arene-based surfactants, which did not act as molecular sieves; (iii) a correlation appeared to exist between permeation selectivity and the number of ionic sites present in the

surfactant (*i.e.*, higher numbers of ionic sites correlated with higher selectivities after the LB bilayers were glued together with a polyelectrolyte).[6-9] These facts suggested that the use of a non-porous *polymeric* surfactant bearing a much larger number of ionic sites could lead to even higher H_2/CO_2 selectivities. The main objective of the work described in this chapter was to test this hypothesis.

At a more fundamental level, the goal of this research was to address three basic questions: (i) Are porous surfactants necessary to create tight LB bilayers? (ii) What factors contribute to the tightening of LB bilayers? (iii) Can the gas permeation properties of a single LB bilayer ever reach the upper bound? To probe these questions, we examined the monolayer properties of a polymer surfactant, the composition of glued bilayers derived from this surfactant and a polymeric glue, the topographies and thicknesses of these bilayers, and their gas permeation properties.

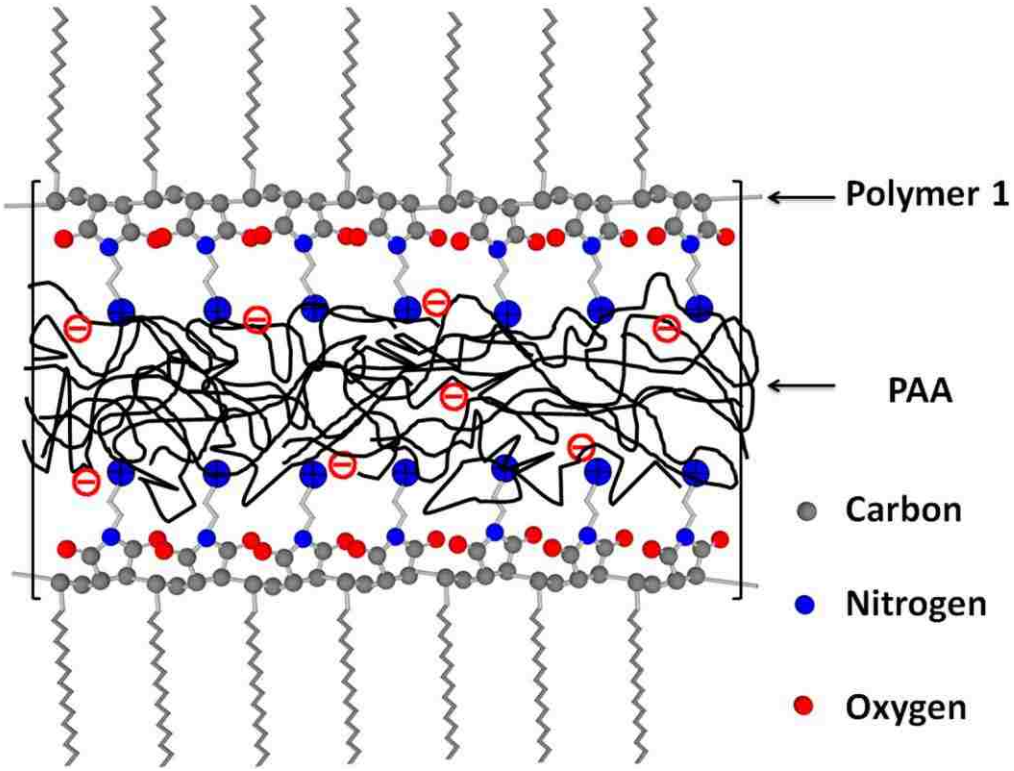

Figure 5.1 Stylized illustration of a glued *all-polymeric* Langmuir-Blodgett (LB) bilayer.

5.2 Membrane and Materials

Langmuir-Blodgett bilayers were fabricated using the polymeric surfactant **1**, which contained a high number of ionic sites, and a non-ionic analog, **2** (control) (Figure 5.2). In addition, LB bilayers made of **Calix6** were also included in this study for purposes of comparison. Poly(acrylic acid) (PAA) (average M_W *ca.* 240,000) was used as the glue, and poly[1-(trimethylsilyl)-1-propyne] (PTMSP) cast film was used as the supporting membrane (see Figure 5.2).

The synthesis of **1** was carried out by our colleague, Dr. Janout Vaclav. The procedures used for the synthesis of both polymers have recently been reported.[1,10] Thus, condensation of poly(maleic anhydride-*alt*-1-octadecene) (**POM**, average M_W *ca.* 40,000, Polysciences) with 2-dimethylaminoethylamine, followed by quaternization with CH_3I afforded **1**. Polymer **2** was synthesized by condensing **POM** with 2-methoxyethylamine.[1]

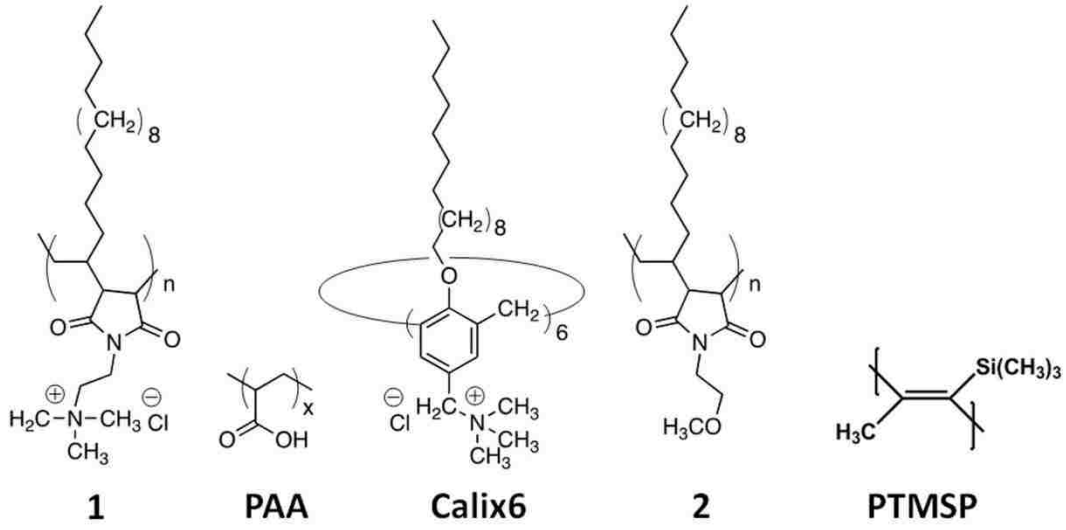

Figure 5.2 Structures of surfactants **1**, **2** and **Calix6**, the polyelectrolyte PAA that was used as the glue, and PTMSP that was used as support material.

5.3 Results and Discussion

5.3.1 Monolayer Properties

5.3.1.1 Surface Pressure-Area Isotherm

In Figures 5.3-5.5 are shown the surface pressure-area isotherms for **1**, **2** and **Calix6** at the air/water interface, in the absence and in the presence of 0.1 mM PAA. (Note: in this comparison, the molecular area per repeat unit was used for each surfactant.) As is apparent, polymers **1** and **2** formed well-behaved monolayers at the air/water interface with collapse pressures higher than 40 mN/m (Figures 5.3-5.5). Figure 5.6 shows the surface pressure-area isotherm cycles for **1**, **2** and **Calix6** in the absence of PAA and in the presence of 0.1 mM PAA at pH 3.0. Minimal annealing for each of the monolayers was observed. The limiting molecular areas per repeat unit for polymer **1**, **2** and **Calix6** at the air/water interface were 0.50 and 0.40 nm^2 and 0.47 nm^2, respectively (Figure 5.6). The slightly larger limiting area of **1** relative to **2** is likely a consequence of the charge repulsion among the pendant quaternary ammonium head groups within **1**.

In addition, similar to what we have found for **Calix6**, the limiting area of polymer **1** increased by *ca.* 20% in the presence of 0.1 mM PAA at pH 3.0 (Figure 5.6). This increase can be ascribed to ionic crosslinking between **1** and PAA, and the high surface activity of PAA at low pH. In contrast, the limiting area of polymer **2** was barely changed after adding PAA into the subphase (Figure 5.6), which is likely due to the lack of strong association between polymer **2** and PAA.

Also, as shown in Figure 5.3, decreasing the pH of the PAA-containing subphase increased the compressibility of monolayers of polymer **1** at the air/water interface (*i.e.*, the slope of surface-pressure area isotherm decreased as the pH was reduced). This

behavior may be due to a reduction in the degree of ionic crosslinking between polymer **1** and PAA. We speculate that ionic crosslinking between **1** and PAA is probably needed to retain PAA at the air/water interface at high surface pressure. Thus, the reduction in the degree of ionic crosslinking may cause more PAA to be squeezed back into the subphase at high surface pressure, which leads to a higher compressibility.

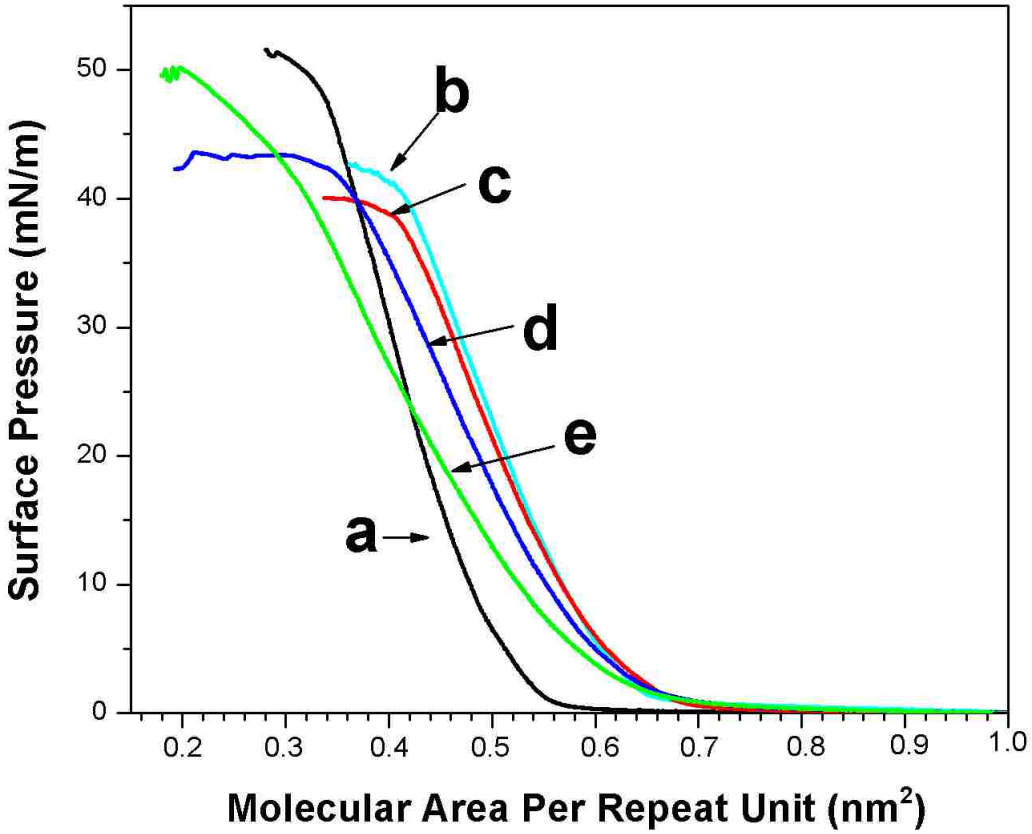

Figure 5.3 Surface pressure-area isotherms for polymer **1** (repeat unit) over the aqueous subphases: (a) in the absence of PAA; (b) in the presence of 0.1 mM PAA at pH 3.5; (c) at pH 3.0; (d) at pH 2.5 and (e) at pH 2.0.

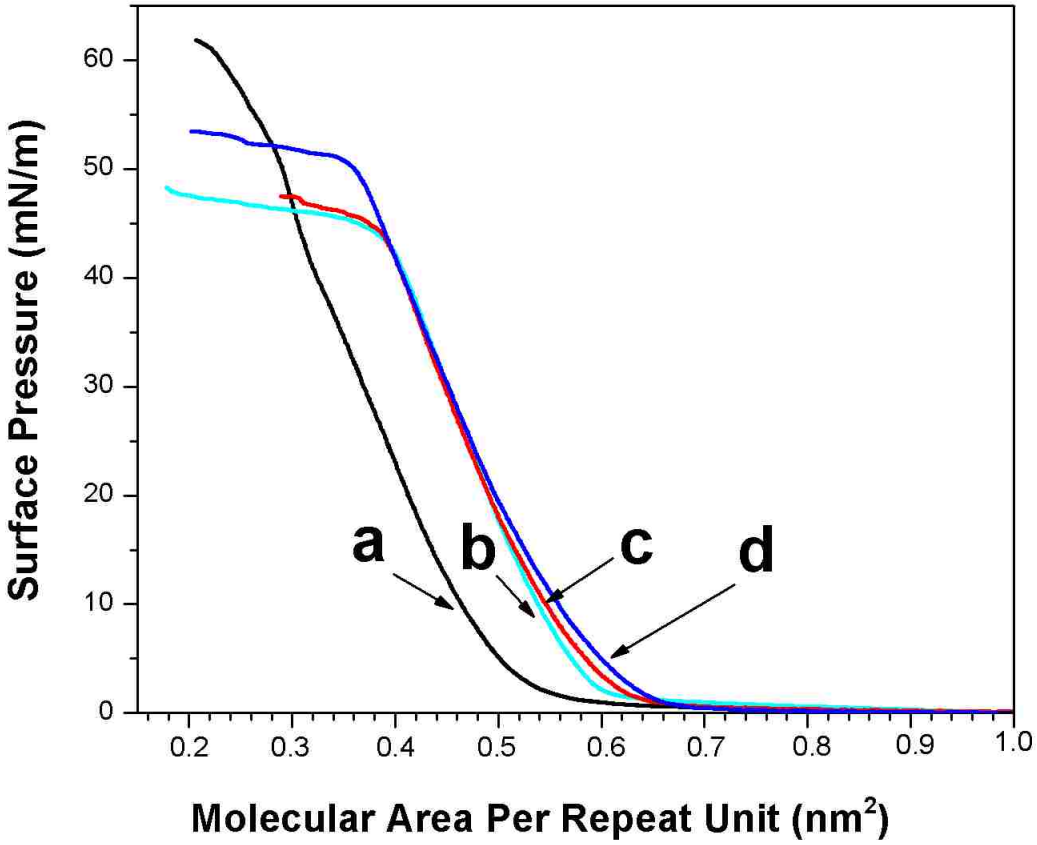

Figure 5.4 Surface pressure-area isotherms for **Calix6** (repeat unit) over the aqueous subphases: (a) in the absence of PAA; (b) in the presence of 0.1 mM PAA at pH 3.5; (c) at pH 3.0; and (d) at pH 2.5.

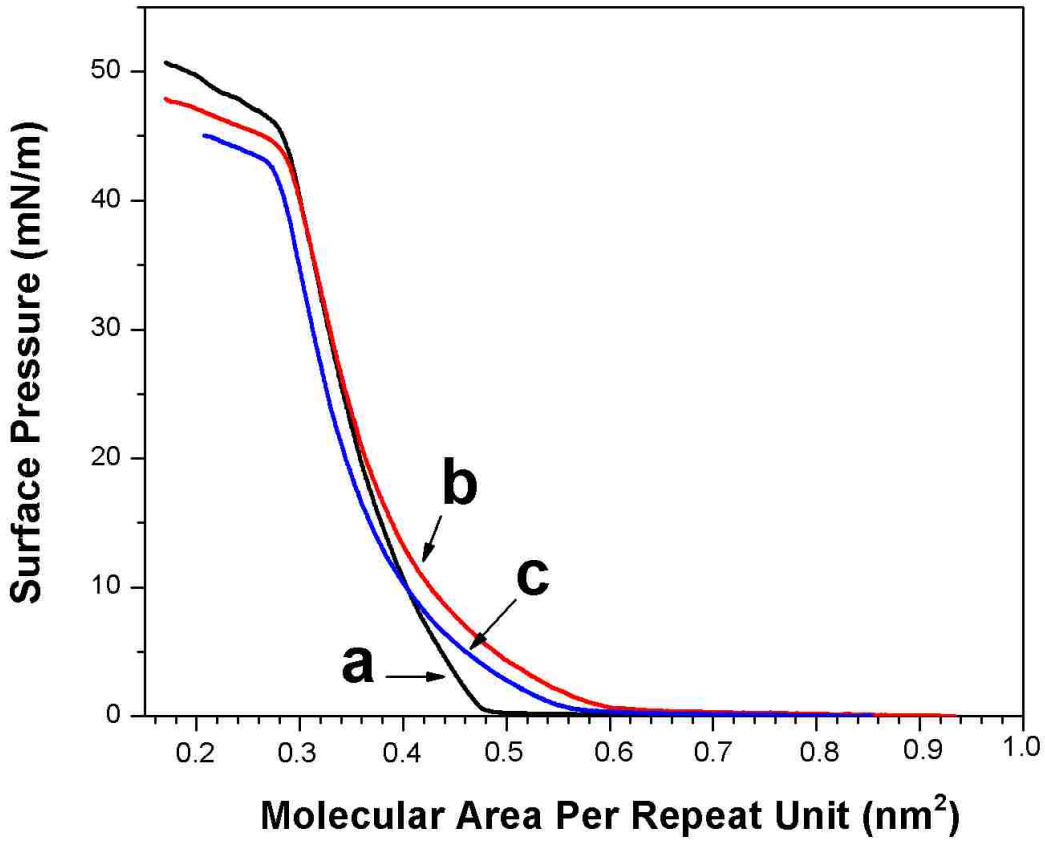

Figure 5.5 Surface pressure-area isotherms for polymer **2** (repeat unit) over the aqueous subphases: (a) in the absence of PAA; (b) in the presence of 0.1 mM PAA at pH 3.0 and (c) at pH 2.5.

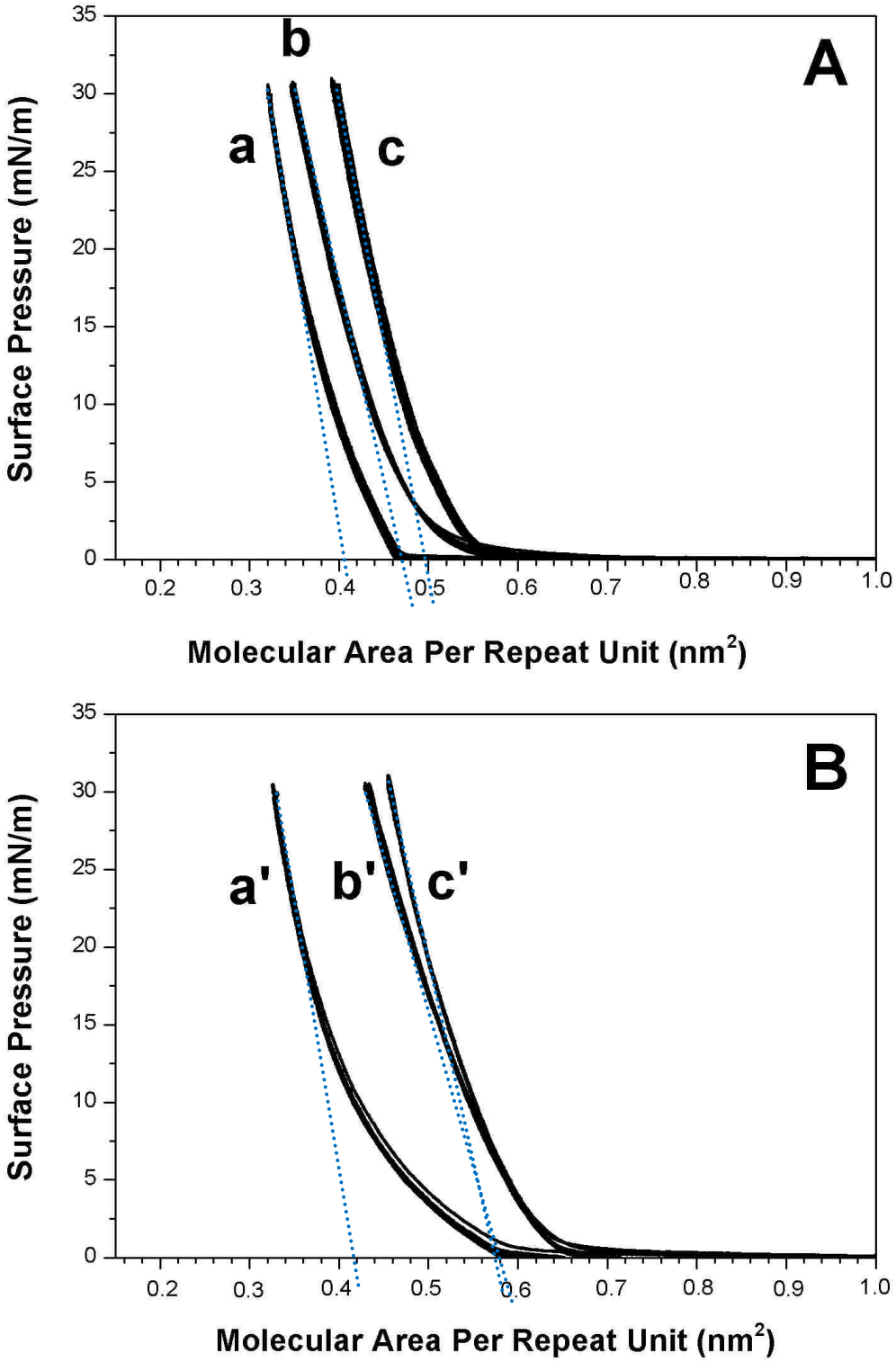

Figure 5.6 Surface pressure-area isotherm cycles (A) in the absence of PAA for: (a) **2** (repeat unit), (b) **Calix6** (repeat unit) and (c) **1** (repeat unit), and (B) in the presence of 0.1mM PAA at pH 3.0 for (a') **2** (repeat unit), (b') **Calix6** (repeat unit) and (c') **1** (repeat unit).

5.3.1.2 Monolayer Cohesiveness

The relative surface viscosities for monolayers of **1**, **2** and **Calix6** over pure water and over aqueous subphases containing 0.1 mM PAA (repeat unit concentration) at different pH values are summarized in Figures 5.7 and 5.8. These viscosities reflect their relative monolayer cohesivenesses at the air/water interface. The procedures used for measuring these surface viscosities were similar to that described in previous chapters. In this case, only a 6 mm-slit opening was used for these measurements. As is apparent, negligible surface viscosities were observed for all monolayers over pure water and for polymer **2** over 0.1 mM PAA at pH 3.0 and 2.5 [Figure 5.7 (k-o)]. In contrast, the monolayer surface viscosities for **1** and **Calix6**, increased when PAA was included in the subphase [Figure 5.7 (a-j)]. As shown in Figure 5.8, a maximum in monolayer viscosities for both **1** and **Calix6** was reached at pH 3.0. At pH values greater than or less than 3.0 the surface viscosities of these surfactants were reduced. This implies that other factors in addition to the degree of ionic crosslinking between surfactants and PAA is contributing to the cohesiveness of these monolayers.

Figure 5.9 shows the factors are likely to contribute to the cohesiveness of monolayers of **1** over a PAA subphase. In principle, decreasing the pH of an aqeuous solution containing PAA from 4.0 to 2.0 should decrease the degree of ionic crosslinking between surfactants and PAA, thereby decreasing the monolayer's cohesiveness. At the same time, decreasing the pH should reduce the charge repulsion within PAA chains and increase hydrogen bonding within PAA chains, which should increase the overall monolayer cohesiveness. These opposing factors can account for a maximum in monolayer cohesiveness that was observed for **1** and **Calix6**.

In addition, at each pH value tested, the relative monolayer viscosities were found to be **1**>**Calix6**>>**2** (Figures 5.7 and 5.8). This follows the same ordering as number of ionic sites that is present in per surfactant molecule (Figure 5.9).

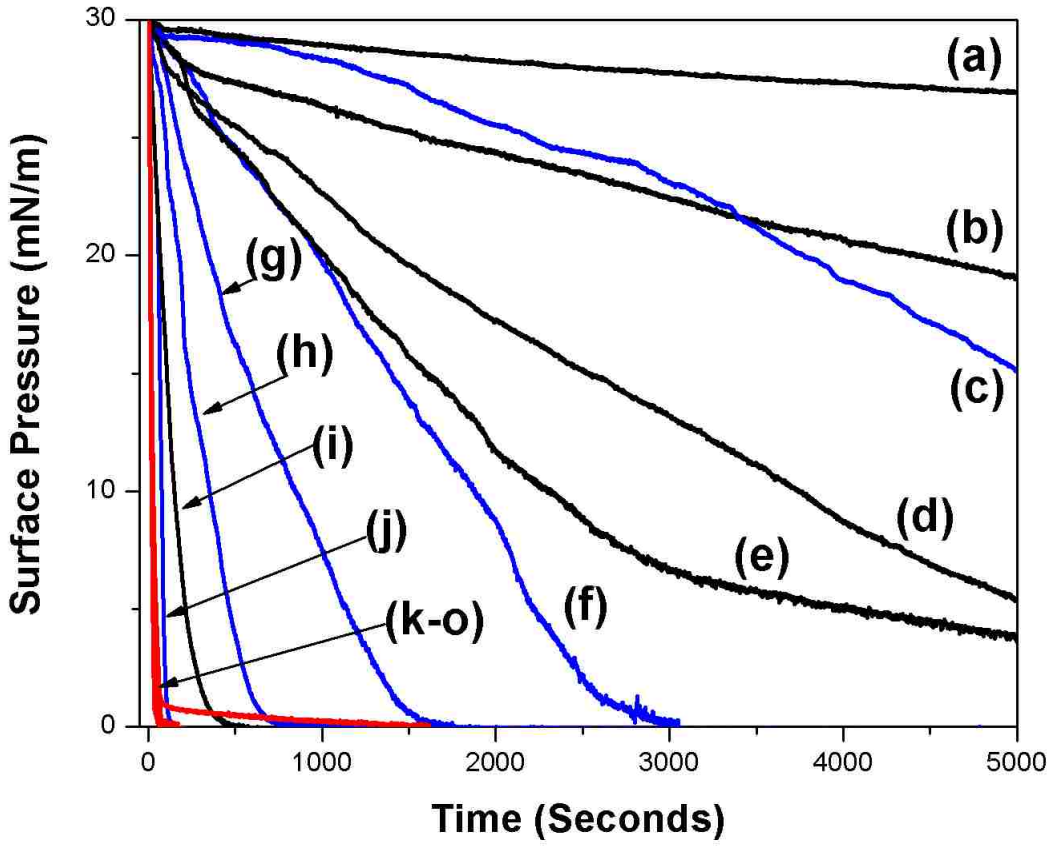

Figure 5.7 Relative surface viscosities measured by use of a canal viscometer with a slit opening of 6 mm for **1** (in black solid lines) over 0.1 mM PAA at (a) pH 3.0; (b) pH 3.5; (d) pH 2.5; (e) pH 4.0 and (i) pH 2.0, and for **Calix6** (in blue solid lines) over 0.1 mM PAA: at (c) pH 3.0; (f) pH 3.5; (g) pH 4.0; (h) pH 2.5 and (j) pH 2.0. The relative surface viscosities for **1**, **2** and **Calix6** over pure water, and also for **2** over 0.1mM PAA at pH 3.0 and pH 2.5, were indistinguishable and were shown in (k-o).

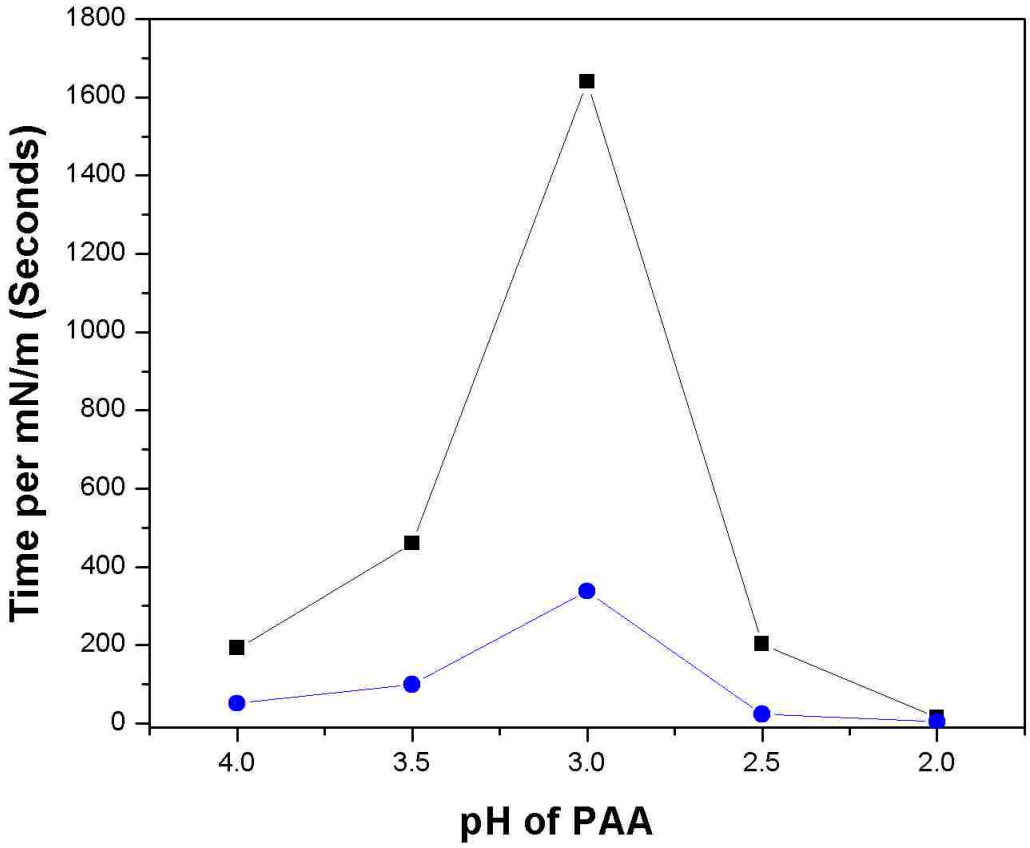

Figure 5.8 Rate of decrease in surface pressure as a function of pH for **1** (black filled square) and **Calix6** (blue filled circle) over 0.1mM PAA. Efflux rates were taken as the slopes of the decay curves (in Figure 5.5) averaged over the range P_o (the initial surface pressure) to *ca.* ½ P_o.

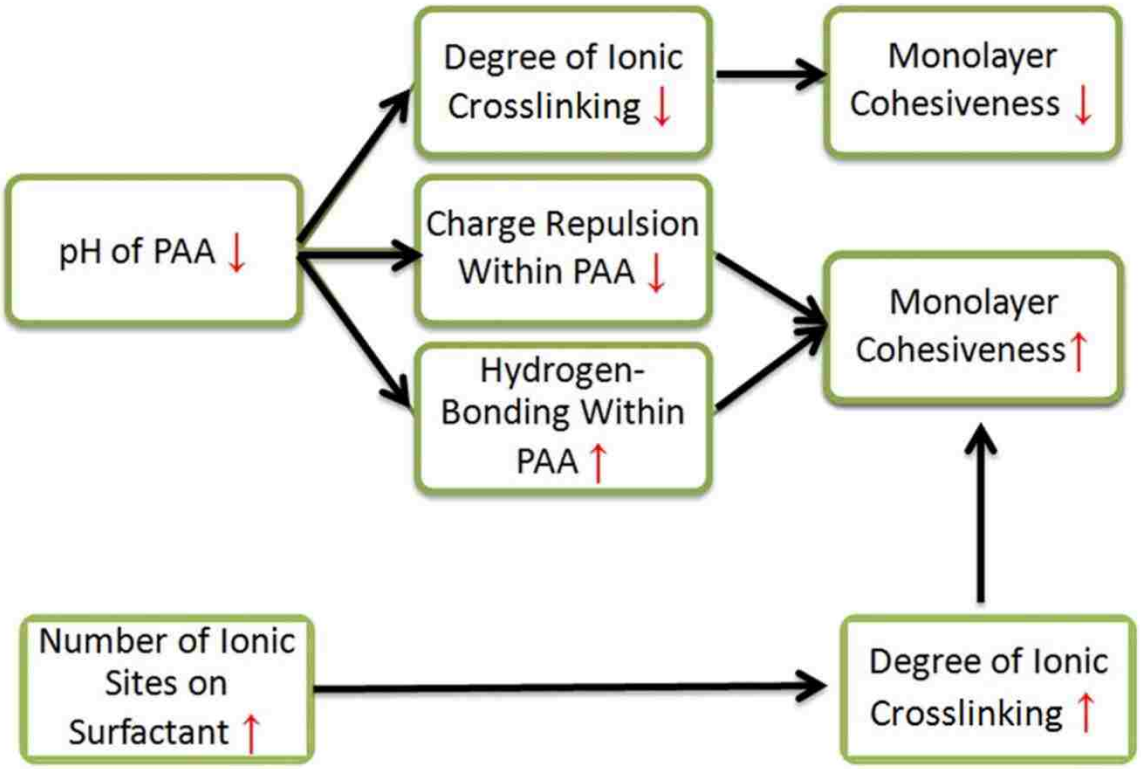

Figure 5.9 Factors that are likely to influence the cohesiveness of PAA-glued monolayers of **1**.

5.3.2 Thicknesses and Topographies of LB bilayers

To measure the thicknesses and the topographies of Langmuir-Blodgett (LB) films, single unglued and PAA-glued LB bilayers that were made from polymers **1**, **2** and **Calix6** were deposited onto silicon wafers that were silylated with *n*-octadecyltrichlorosilane (OTS), using established procedures.[1] Table 5.1 shows the thicknesses and surface roughnesses determined by ellipsometry and atomic force microscopy (AFM). Film thickness were also determined by use of AFM, based on step heights that were measured after removing the LB bilayers by scratching with a razor blade (Figure 5.11). (Note: The results from AFM were consistent with OTS still on the surface under such conditions).[11,12] As is apparent, the thicknesses from these two

methods were in good agreement. The surface topographies of unglued and PAA-glued LB bilayers of **1**, **2** and **Calix6** are shown in Figure 5.10.

Table 5.1 Thicknesses of unglued and PAA-glued bilayers determined by ellipsometry and by AFM

Membrane	Bilayer Thickness (ellipsometry, nm)	Bilayer Thickness (AFM, nm)	RMS Roughness (AFM, nm)
Calix6	4.0 ±0.1	--	1.0
1	4.1 ±0.1	--	1.6
2	4.1 ±0.1	--	0.5
Calix6/PAA-3.5[a]	5.0 ±0.1	--	--
1/PAA-3.5[a]	5.0 ±0.1	--	0.6
Calix6/PAA-3.0[b]	6.1 ±0.2	6.2 ±0.3	0.9
1/PAA-3.0[b]	6.2 ±0.2	6.4 ±0.3	0.5
2/PAA-3.0[b]	5.4 ±0.1	--	1.1
Calix6/PAA-2.5[c]	7.0 ±0.1	7.2 ±0.4	0.7
1/PAA-2.5[c]	7.0 ±0.2	7.2 ±0.3	0.4
2/PAA-2.5[c]	5.8 ±0.1	--	1.8
1/PAA-2.0[d]	7.3 ±0.2	--	0.5

Gluing conditions: [a]at pH 3.5; [b]at pH 3.0; [c]at pH 2.5 and [d]at pH 2.0. Error values given for film thicknesses represent one standard deviation based on 5 AFM and 5 ellipsometric measurements at different locations along the surface. (NOTE: At pH 2.0, the LB transfer ratio for **1** on the down-trip was *ca.* 0.7 ±0.1, while the up-trip was *ca.* 1.5 ±0.1. All other transfer ratios were within 1.0 ±0.1).

5.3.2.1 Thicknesses of Unglued and PAA-Glued LB Bilayers as A Function of the Number of Ionic Sites Presented on the Surfactants

As shown in Table 5.1, the thicknesses of unglued LB bilayers made of **1**, **2** and **Calix6** were all *ca.* 4.0 nm. For PAA-glued LB bilayers, at each pH used, the thicknesses were

Calix6 ≈ **1** > **2**. For instance, at pH 3.0, the ellipsometric thicknesses of PAA-glued LB bilayers made of **Calix6**, **1** and **2** were *ca.* 6.0, 6.1 and 5.4 nm, respectively. The fact that PAA-glued bilayers of **Calix6** and **1** showed larger thicknesses than **2** indicates that the presence of ionic sites on a surfactant enhances the association between PAA and the ionic surfactant, thus increasing the amount of PAA that is adsorbed by the monolayer. These results also indicate that increasing the number of ionic sites above six/surfactant does not lead to increased film thicknesses.

5.3.2.2 Thicknesses of PAA-Glued LB Bilayers as a Function of the pH

As is apparent, for each surfactant, the thicknesses of PAA-glued LB bilayers increased as the pH of the PAA-containing aqueous subphase decreased. For instance, PAA-glued LB bilayers of **1** at pH 3.5, pH 3.0, pH 2.5 and pH 2.0 had thicknesses at *ca.* 5.0, 6.0, 7.0 and 7.3 nm, respectively. As discussed in Chapter 4, these results may be due to the increase of hydrogen bonding and a reduction in charge repulsion within PAA chains as the pH is decreased because both factors should increase the extent of adsorption of PAA by these surfactants.

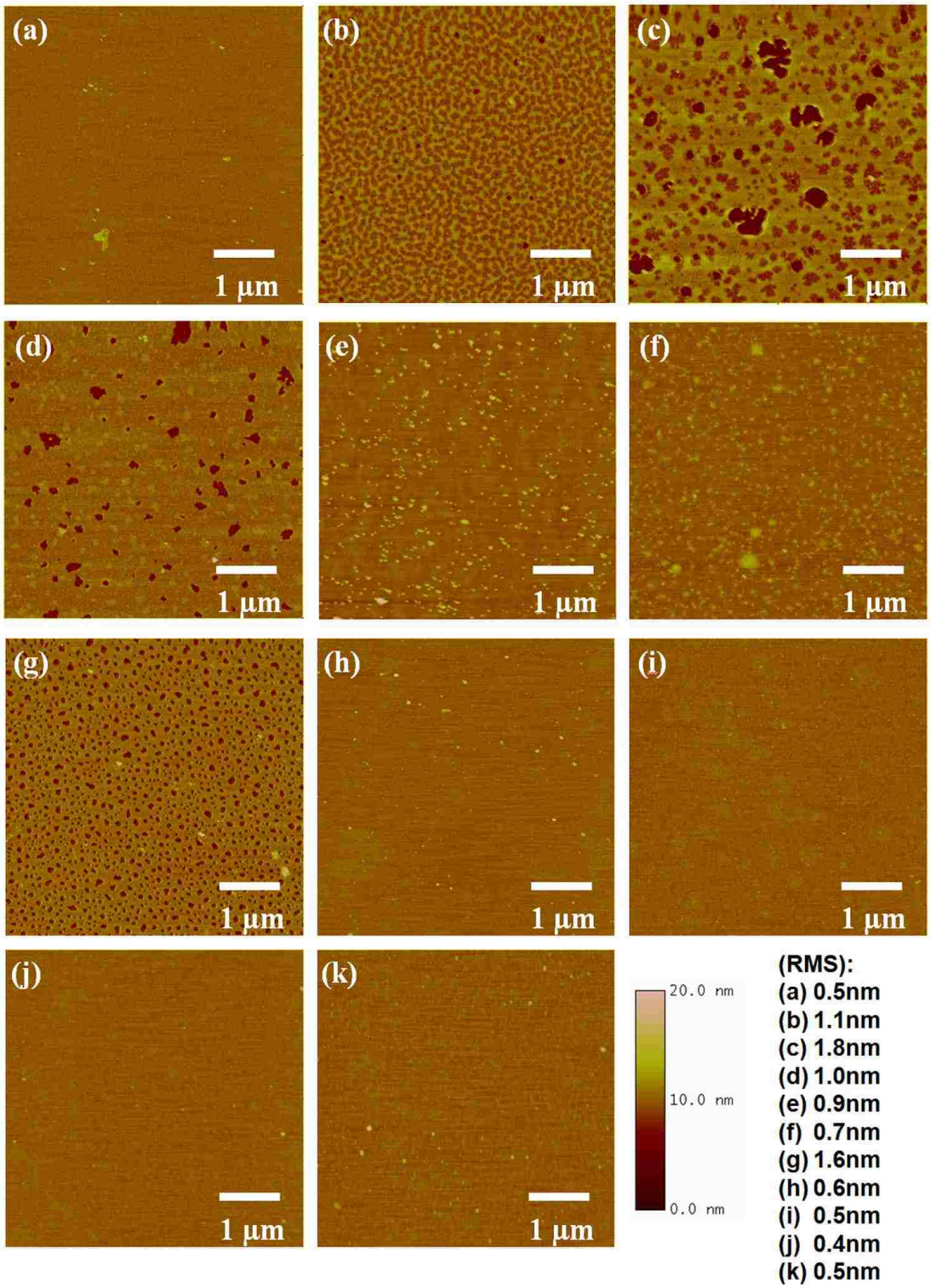

Figure 5.10 Topography (AFM, tapping mode, 5 × 5 µm^2) and root mean aquare (RMS) roughness of LB bilayers of polymer **2**: (a) on pure water, (b) on 0.1 mM PAA at pH 3.0 and (c) at pH 2.5; LB bilayer of **Calix6**: (d) on pure water, (e) on 0.1 mM PAA at pH 3.0 and (f) at pH 2.5; LB bilayers of polymer **1**: (g) on pure water, (h) on 0.1 mM PAA at pH 3.5, (i) at pH 3.0, (j) at pH 2.5 and (k) at pH 2.0.

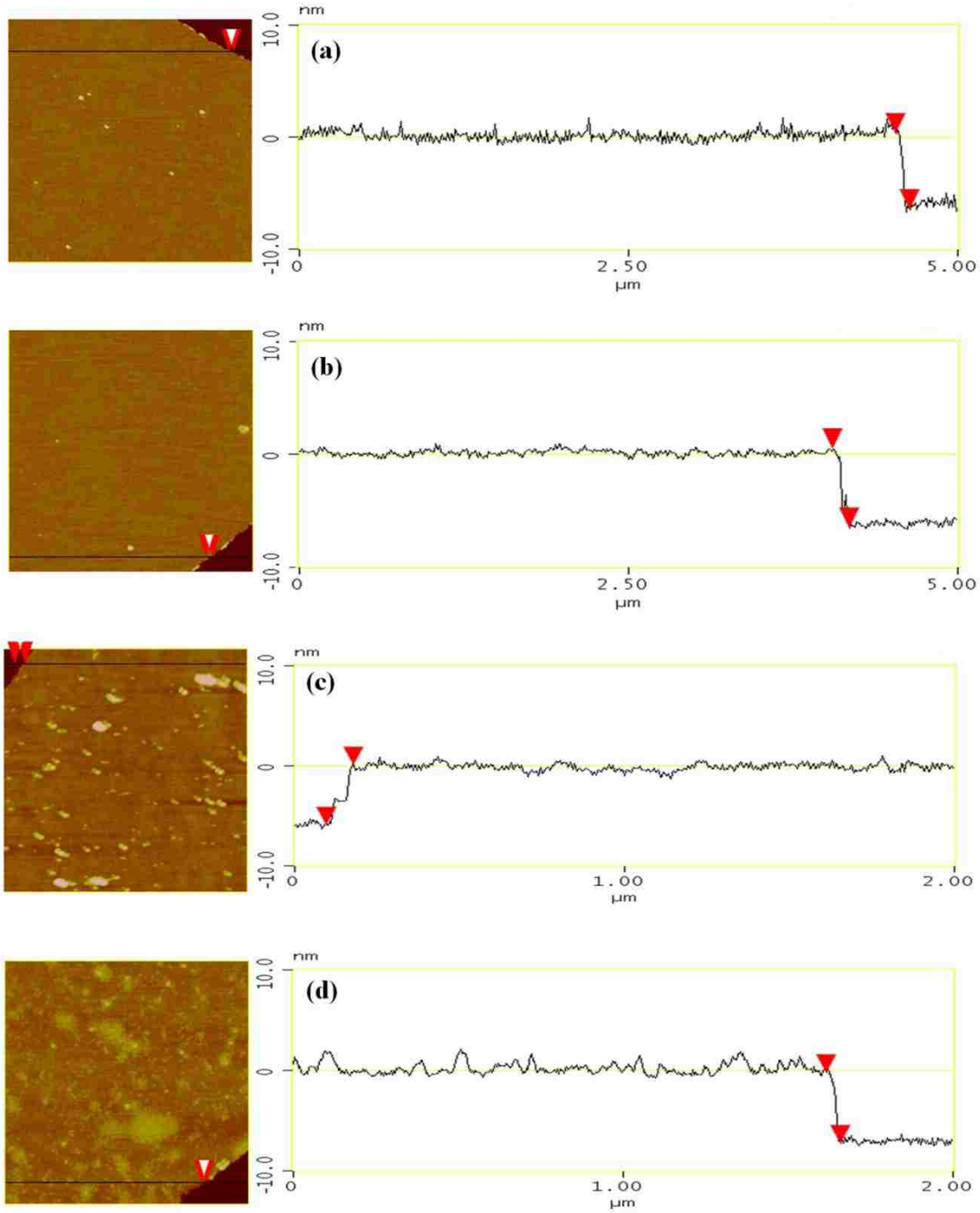

Figure 5.11 Step-height image and section profile showing the film thickness of PAA glued LB bilayers of polymer **1** (AFM, tapping mode, 5 × 5 μm^2): (a) over 0.1 mM PAA at pH 3.0 and (b) at pH 2.5; PAA glued LB bilayers of **Calix6** (AFM, tapping mode, 2 × 2 μm^2): (c) on 0.1 mM PAA at pH 3.0 and (d) at pH 2.5. (Note: Thicknesses are shown in Table 5.1)

5.3.2.3 Topographies of Unglued and PAA-Glued LB Bilayers as a Function of the Number of Ionic Sites Presented on the Surfactants

As shown in Figure 5.10 (a), (d) and (g), the unglued LB bilayer made of **2** had defect-free surfaces, while unglued LB bilayers of **1** and **Calix6** both rearranged after deposition and contained lots of defects. The fact that **2** had neutral head groups, while both **1** and **Calix6** had positively charged quaternary ammonium head groups, implies that the repulsion between charged head groups was the main driving force for this rearrangement. In contrast, PAA-incorporated bilayers of **2** showed signs of immiscibility and were full of defects [Figure 5.10 (b) and (c)], while PAA-glued bilayers of **1** and **Calix6** both exhibited defect-free surfaces. These results demonstrated the importance of having ionic sites on the surfactants for glued bilayers.

5.3.3 Confirm the Layered Structure of Unglued and PAA-glued LB Bilayers of 1 by XPS

X-ray Photon Spectroscopy (XPS) was used to determine the layered structure of the LB bilayers of **1**. The experiments were done by Ms. Jie Fu at Princeton University, following the procedures described in Chapter 2. Thus, three take-off angles ($\boldsymbol{\theta}$) (Figure 5.12), 30 º, 49 ºand 90 ºwere chosen for XPS scans. Figure 5.13 shows the survey spectra for unglued and PAA-glued LB bilayers of **1** at different take-off angles. After the survey scans (0-1100 ev), the peaks of interest, C, N and O in specific, were selected and scanned again under same conditions. The escape depth d_{escape} (*i.e.*, contributing 64% of the photoelectron signal) and sampling depth $d_{sampling}$ (*i.e.*, contributing 95% of the photoelectron signal) are related to the electron inelastic mean free path λ_{IMFP} (*i.e.*, the average distance traveled by an electron of a specific energy within a particular single-layered homogeneous amorphous solid between two successive inelastic scattering

events) by equations $d_{escape}=\lambda_{IMFP}Sin\theta$ and $d_{sampling}=3\lambda_{IMFP}Sin\theta$, respectively (Figure 5.12).[13] Assuming the kinetic energy of an electron is 1000 eV, the maximum electron inelastic mean free path λ_{IMFP} should be *ca.* 3 nm for organic polymers.[14] As a result, the maximum escape depth was *ca.* 3 nm, while the maximum sampling depth was *ca.* 9 nm. A summary of the escape depths and sampling depths at different take-off angles is shown in Table 5.2. The normalized elemental composition of C, N and O at different take-off angles is shown in Table 5.3, in which the total atomic compositions of carbon, oxygen and nitrogen were normalized to 100%.

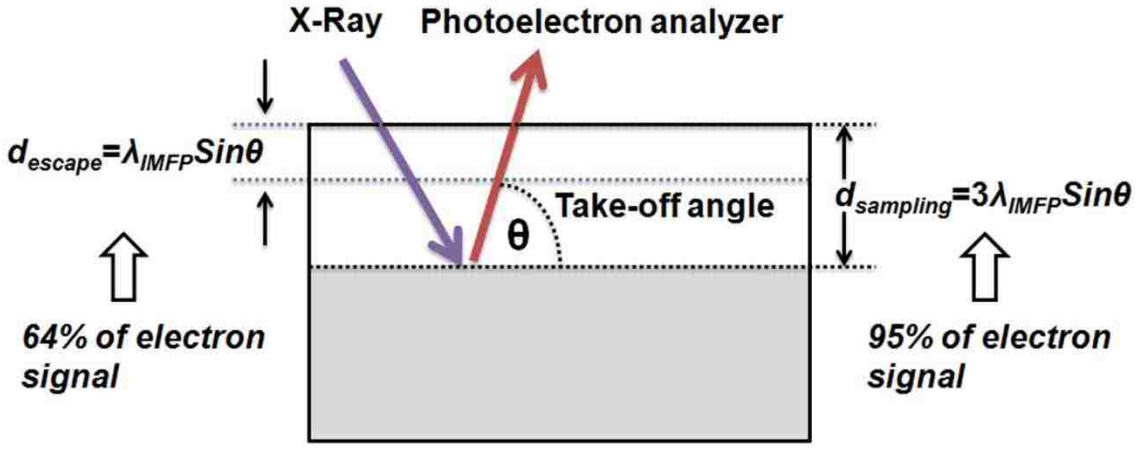

Figure 5.12 Schematic illustration of XPS measurement.

Table 5.2 Escape depths and sampling depths at different take-off angles

Take-off Angle	Escape Depth[a] (nm)	Sampling Depth[b] (nm)
30 º	1.5	4.5
49 º	2.3	6.9
90 º	3.0	9.0

[a]Escape depth is where 64% of the photoelectron signals can be detected. [b]Sampling depth is where 95% of the photoelectron signals can be detected.

Table 5.3 Normalized elemental composition determined by XPS.

Membrane	Take-off Angle	C% [c]	N% [c]	O% [c]
1[a]	30 º	68.7	0.8	30.5
	49 º	76.0	3.5	20.5
	90 º	76.7	4.0	19.3
1/PAA-3.0[b]	30 º	70.1	0.1	29.8
	49 º	70.5	2.0	27.5
	90 º	73.3	2.7	24.0

[a]Unglued LB bilayer of **1**. [b]PAA-glued LB bilayer of **1** at pH 3.0. [c]The atomic sensitivity factor (ASF) used for C, N, O were 0.296, 0.477 and 0.711, respectively, (provided by Ms. Jie Fu). The total atomic compositions of C, N and O were normalized to 100%.

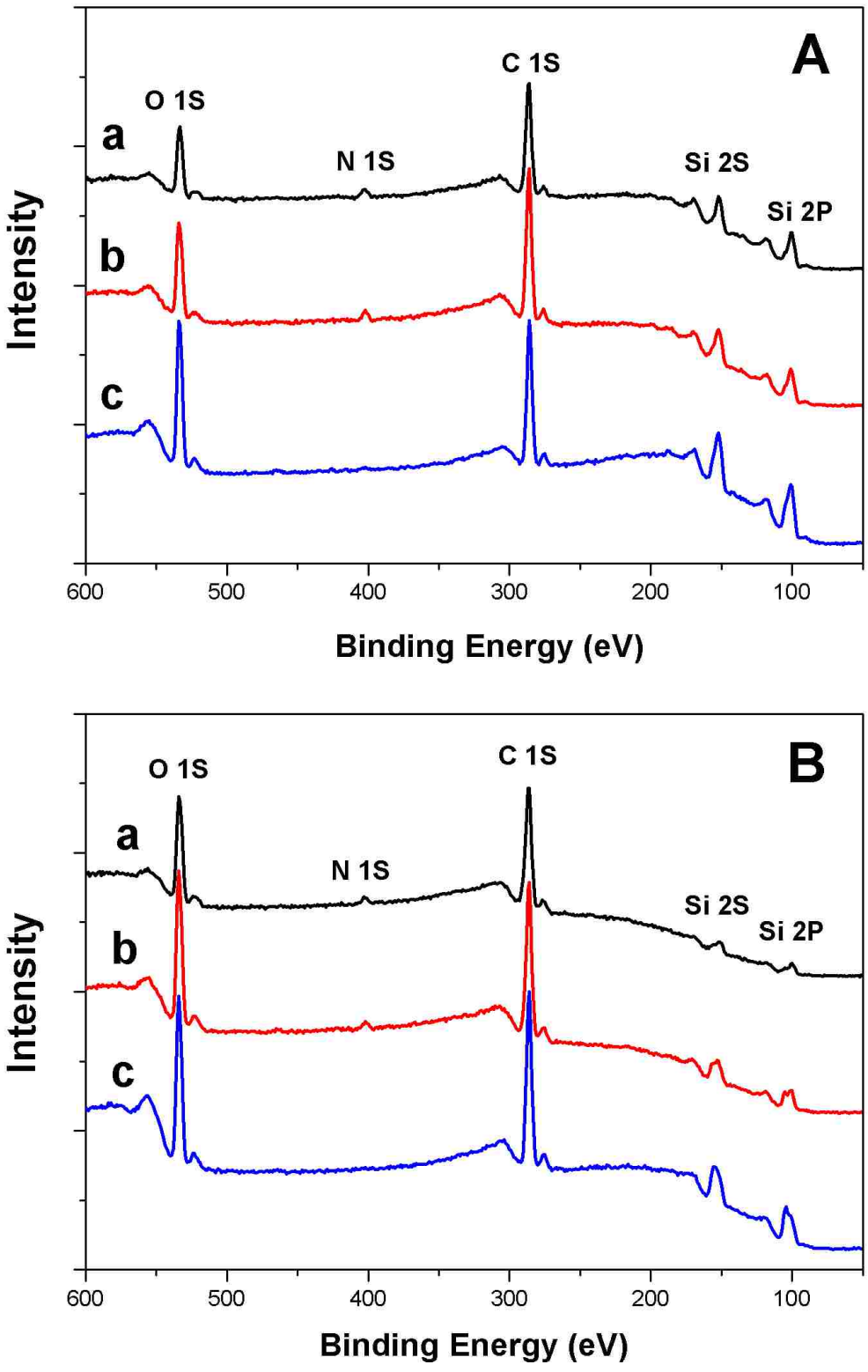

Figure 5.13 XPS survey spectra scanned for (A) unglued bilayer of **1** and (B) PAA-glued bilayer of **1** at pH 3.0: (a) 90 º, (b) 49 ºand (c) 30 º.

5.3.3.1 The Nitrogen Content of Unglued and PAA-glued LB Bilayers of 1 as a Function of the Take-off Angles.

As shown in Table 5.3, by increasing the take-off angles, the nitrogen content of both unglued and PAA-glued LB bilayers of **1** increased. This is in good agreement withpredicted layered structure of the LB bilayers of **1** (Figure 5.14). For instance, at a take-off angle of 30º, the escape depth (*i.e.*, contributing 64% of the photoelectron signals) is *ca.* 1.5 nm (Table 5.2), which is smaller than the monolayer thickness of the polymer **1** at both unglued and PAA-glued states (Table 5.1), thus the nitrogen was barely detected. In contrast, at a take-off angle of 90º, the escape depth is *ca.* 3 nm, which is larger than the monolayer thickness of the polymer 1, thus the nitrogen in quaternary ammonium groups was detected and the nitrogen content increased.

5.3.3.2 The Nitrogen Content of Unglued *versus* PAA-glued LB Bilayers of 1.

As is apparent, for the measurements that were taken at a specific take-off angle, the nitrogen content was always smaller for PAA-glued LB bilayers of **1** when compared with their unglued analogs. This is likely due to the incorporation of PAA into the LB bilayers of **1** increased the bilayer thickness, and lowered the number of quaternary ammonium groups that were detected. For instance, as shown in Figure 5.14, at a take-off angle of 90º, two layers of the quaternary ammonium groups in an unglued bilayer were within the escape depth (*ca.* 3 nm). In contrast, only one layer of quaternary ammonium groups in a PAA-glued bilayer was within the escape depth. As a result, the nitrogen content that was detected by the XPS was supposed to be larger in an unglued LB bilayer of **1**.

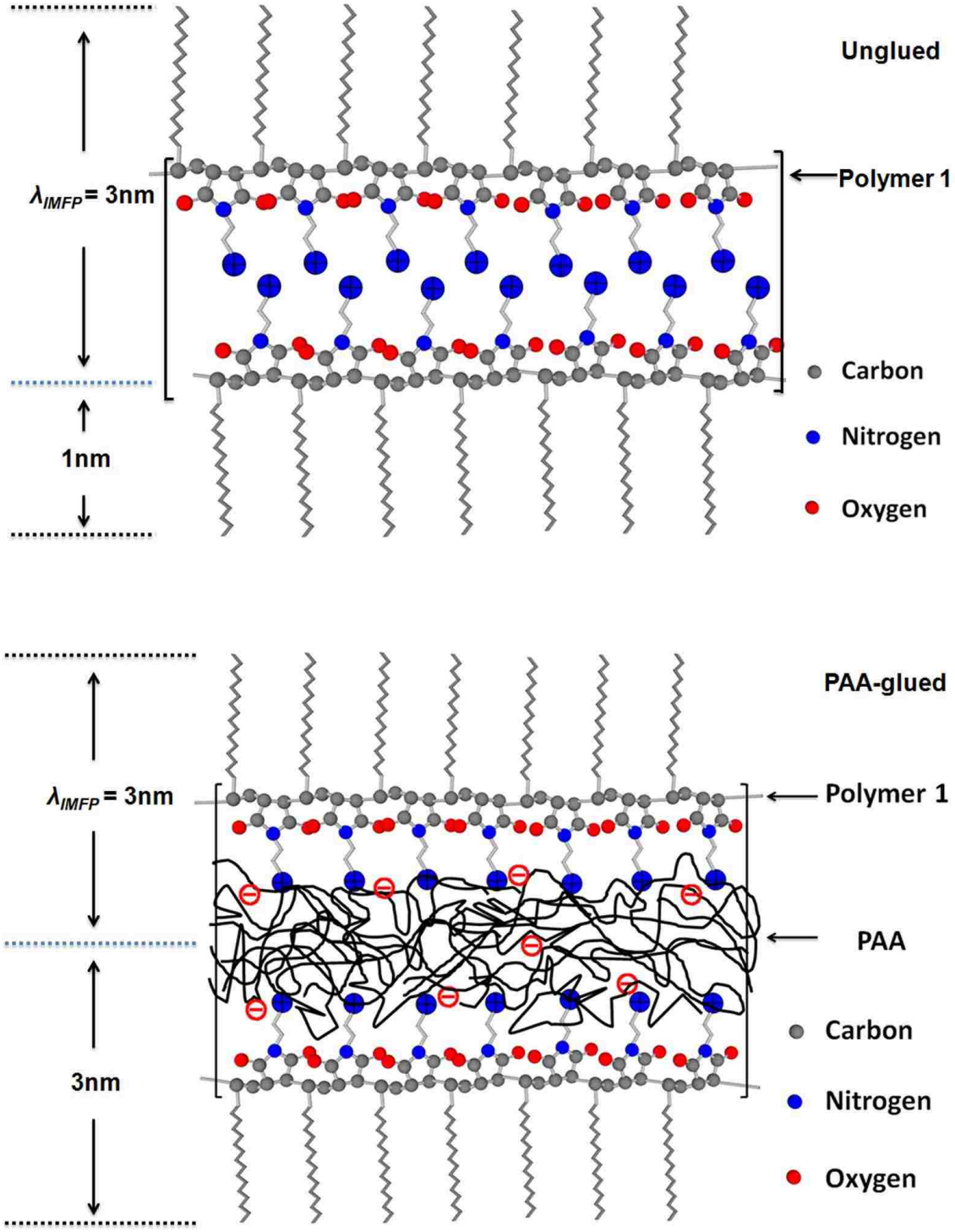

Figure 5.14 Layered structures of unglued and PAA-glued LB bilayers of **1**.

5.3.3.3 Why Survey Spectra Show Si 1s and Si 2s Signals?

According to the chemical structure of polymer **1** and PAA (Figure 5.2), they don't contain silicon. However, Si 1s and Si 2s signals existed in all spectra that were taken at different take-off angles (Figure 5.13). This is probably due to that the wafers were not fully covered by LB bilayers (Figure 5.15). Since the silicon wafers were always clamped to a holder during LB transfer, a part of the OTS layer was not covered by LB bilayers. Thus this part of the OTS layer and the SiO_2 layer beneath (both containing silicon) were exposed to the X-Ray during the measurement (Figure 5.15). As a result, Si 1s and Si 2s signals were shown in the survey spectra (Figure 5.13). [Note: At a take-off angle of 90 º, the size of the incidence X-ray on the sample plane is estimated to be *ca*. 2×2 cm^2, while the size of the sample itself is *ca*. 1.2×2.3 cm^2.]

In addition, for measurements that were done at higher take-off angles, for instance at 90 º, a second factor was also contributing to the emerging of Si 1s and Si 2s signals in the survey spectra. Since the sampling depth (*i.e.*, contributing 95% of the photoelectron signals) was *ca.* 9.0 nm at a take-off angle of 90 º, which was larger than the thicknesses of both unglued and PAA-glued LB bilayers of **1** (Tables 5.1 and 5.2), the photoelectrons from OTS and SiO_2 layers (both containing silicon), that were covered by LB bilayers, can also contribute to the final spectra.

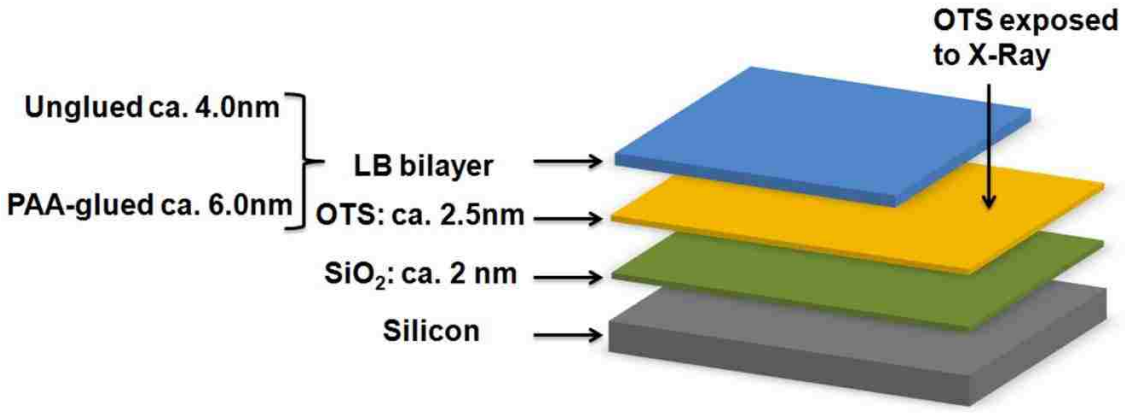

Figure 5.15 Illustration of the OTS-modified silicon wafer with a LB bilayer.

5.3.3.4 Why Was the Oxygen Content Higher Than Expected?

As shown in Table 5.3, the normalized oxygen content was *ca.* 30% at a take-off angle of 30 °for the unglued LB bilayer of **1**. However, based on the repeat unit formula of the polymer **1**, $C_{27}H_{52}N_2O_2Cl$, the ideal normalized content of oxygen in an unglued bilayer of **1** should be *ca.* 8.4%, which is smaller than observed content. We speculate that similar reasons that were discussed in the last section should account for this difference. Thus, the oxygen in the layers of OTS and SiO_2 that were not covered by LB bilayers could be detected by the XPS instrument at all take-off angles. In addition, for the measurements that were taken at higher take-off angles, the oxygen in the layers of OTS and SiO_2 that were covered by LB bilayers could also be detected in addition to the oxygen contained in polymer **1**. As a result, the total oxygen content was higher than expected. A similar trend was also observed in PAA-glued LB bilayers of **1** (Table 5.3).

5.3.4 Gas Permeation Properties

To determine the gas permeation properties of unglued and PAA-glued LB bilayers, LB films made of **1**, **2** and **Calix6** were deposited onto PTMSP cast films in unglued and

glued states. The procedures used for these depositions were as reported. (see detailed protocols in Chapter 2).[1] A pressure gradient of 40 psig was used for measuring three gaseous permeants: H_2, N_2 and CO_2. In Table 5.4 are shown the observed permeance values (P/l) for each gas, in which P is the permeability coefficient and l is the thickness of the composite membrane. The P/l has been calculated by dividing the observed flux (F) by the area of the membrane (A) and by the pressure gradient (p) that is used; that is, $P/l = F/(A \times p)$.

As is apparent, unglued LB bilayers of **1**, **2** and **Calix6** showed little barrier properties toward H_2, CO_2 and N_2 as compared with untreated PTMSP. This is also the case for PAA-incorporated bilayers of **2** at pH 3.0 and pH 2.5. The negligible barrier properties of the unglued LB bilayers of **1** and **Calix6**, and PAA-glued **2** at pH 3.0 and pH 2.5 can be explained by their topographies measured by AFM, which were full of defects. The fact that unglued LB bilayers of **2** had defect free surfaces but little barrier properties toward three gaseous permeants implies that the transient gaps within such LB bilayers were large in size.

In contrast, PAA-glued LB bilayers of **1** and **Calix-6** at various pH showed significant barrier properties toward H_2, CO_2 and N_2. The permeances of three gaseous permeants were $H_2 > CO_2 > N_2$. These results demonstrated that by ionically crosslinking of the surfactants with pendant ionic sites, PAA glue could tighten these LB bilayers.

Table 5.4 Observed permeances of H_2, CO_2 and N_2 and their selectivities (at 40 psig) across LB bilayers[a]

LB layers	H_2	CO_2	N_2	H_2/CO_2	CO_2/N_2
-----[b]	7.3×10^2	1.7×10^3	2.9×10^2	0.43	5.9
-----[b]	7.2×10^2	1.7×10^3	2.9×10^2	0.42	5.9
Calix6[c]	6.4×10^2	1.4×10^3	2.7×10^2	0.46	5.2
Calix6[c]	6.2×10^2	1.3×10^3	2.6×10^2	0.48	5.0
1[c]	5.8×10^2	1.3×10^3	1.9×10^2	0.45	6.8
1[c]	4.7×10^2	1.1×10^3	1.6×10^2	0.43	6.9
2[c]	5.6×10^2	1.3×10^3	1.7×10^2	0.43	7.6
2[c]	5.5×10^2	1.3×10^3	1.7×10^2	0.42	7.6
Calix6/PAA-3.5[d]	16	1.4	0.040	12	34
Calix6/PAA-3.5[d]	15	0.88	0.019	17	46
1/PAA-3.5[d]	13	0.66	0.016	20	42
1/PAA-3.5[d]	14	0.50	0.013	27	38
Calix6/PAA-3.0[e]	4.0	0.054	0.0023	74	23
Calix6/PAA-3.0[e]	5.7	0.081	0.0024	70	34
1/PAA-3.0[e]	5.9	0.062	<0.0023	95	>27
1/PAA-3.0[e]	5.6	0.049	<0.0023	1.1×10^2	>21
2/PAA-3.0[e]	5.7×10^2	1.2×10^3	1.3×10^2	0.47	9.2
2/PAA-3.0[e]	5.6×10^2	1.2×10^3	1.3×10^2	0.47	9.2
Calix6/PAA-2.5[f]	3.0	0.19	0.018	16	11
Calix6/PAA-2.5[f]	4.5	0.66	0.068	6.8	9.7
1/PAA-2.5[f]	2.9	0.012	<0.0023	2.4×10^2	>5.2
1/PAA-2.5[f]	2.6	0.013	0.0049	2.0×10^2	2.7
2/PAA-2.5[f]	5.7×10^2	1.2×10^3	1.2×10^2	0.48	10
2/PAA-2.5[f]	6.1×10^2	1.2×10^3	1.2×10^2	0.51	10
1/PAA-2.0[g]	4.0	0.13	0.0071	31	18
1/PAA-2.0[g]	4.9	0.34	0.020	14	17

[a]Permeances at ambient temperature, 10^6P/l (cm^3/cm^2-s-cm Hg), were calculated by dividing the observed flow rate by the area of the membrane(9.36 cm^2) and the pressure gradient (40 psi) employed, using *ca.* 30 μm thick PTMSP supports. All measurements were made at ambient temperatures. Average values were obtained from 5-10 independent measurements of the same sample; the error in each case was ±5%. Each membrane listed was prepared, independently.[b]Bare PTMSP support. [c]Pure water subphase. [d]At pH 3.5. [e]At pH 3.0. [f]At pH 2.5. [g]At pH 2.0. (NOTE: At pH 2.0, the LB transfer ratio for **1** on the down-trip was *ca.* 0.7 ± 0.1, while the up-trip was *ca.* 1.5 ± 0.1. All other transfer ratios were within 1.0 ± 0.1)

5.3.4.1 Gas Permeation Properties of PAA-glued LB Bilayers of 1 *versus* Calix6

As is apparent, at each pH tested, the H_2/CO_2 permeation selectivity of PAA-glued LB bilayers of **1** was larger than PAA-glued **Calix6** (Table 5.3). For instance, at pH 3.0, PAA-glued LB bilayers of **1** showed a H_2/CO_2 selectivity *ca.* 100, while PAA-glued **Calix6** showed a H_2/CO_2 selectivity *ca.* 70. At pH 2.5, PAA-glued LB bilayers of **1** showed a H_2/CO_2 selectivity *ca.* 200, while PAA-glued **Calix6** showed a H_2/CO_2 selectivity *ca.* 10. These results indicate that PAA-glued LB bilayers of **1** are tighter than those made from **Calix6**. Since all other factors were the same, the difference in the number of ionic sites presented by these surfactants appears to be responsible for the difference in the tightness of these LB films. Thus, a higher number of ionic sites within polymer **1** formed a higher degree of ionic crosslinking with PAA when compared to **Calix6**, and enhanced the tightness of the LB bilayers. These results also imply that a surfactant does not need to be porous to create LB films having high gas permeation selectivities.

5.3.4.2 The H_2/CO_2 Permeation Selectivity *versus* the Monolayer Cohesiveness and Bilayer Thickness.

As shown in Figure 5.8 and Table 5.4, similar trends were observed for the monolayer cohesivenesses and H_2/CO_2 permeation selectivities of PAA-glued **Calix6** as a function of the pH of PAA, which implies that higher monolayer cohesiveness may lead to tighter bilayers and higher H_2/CO_2 permeation selectivities.

However, as shown in Figure 5.16, the decrease of monolayer cohesiveness of PAA-glued **1** from pH 3.0 to 2.5 did not lead to a lower H_2/CO_2 permeation selectivity of the PAA-glued LB bilayer of **1**. This indicates that a second factor should be taken into consideration. We speculate that the thickness of the bilayers is this second factor. Thus,

the increase in the bilayer thickness from pH 3.0 to 2.5 may more than compensate for the loss in the cohesiveness of the PAA-glued bilayer assembly of **1**, which could lead to a higher H_2/CO_2 selectivity (Figure 5.16). In other words, these results may suggest that the tightness and the H_2/CO_2 permeation selectivity of a PAA-glued LB bilayer were influenced by both the monolayer cohesiveness and the bilayer thickness. In principle, we speculate that higher monolayer cohesiveness and thicker bilayers should lead to tighter bilayers and higher H_2/CO_2 permeation selectivities.

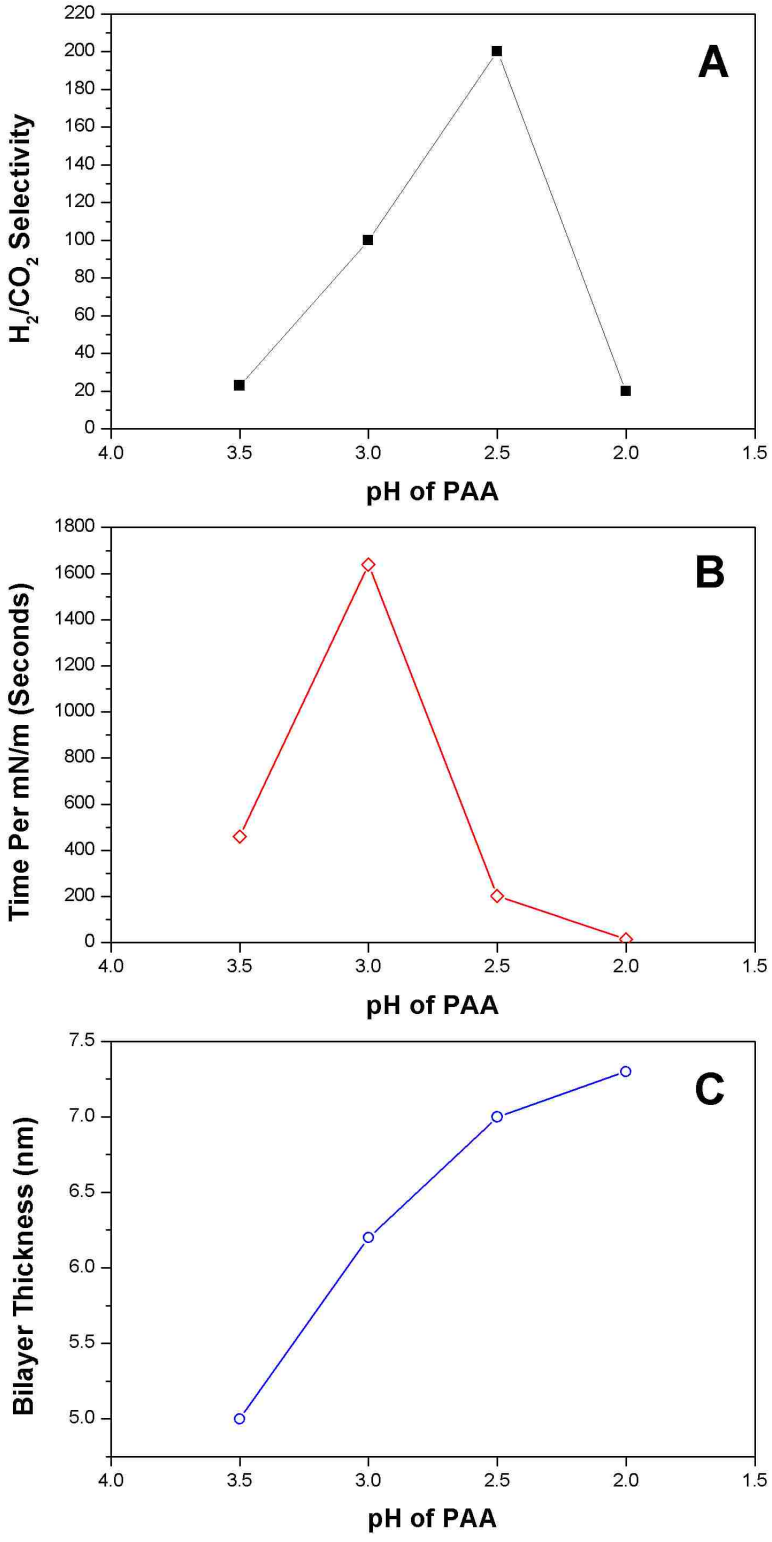

Figure 5.16 The monolayer and bilayer properties of PAA-glued **1** as a function of the pH of PAA: (A) H_2/CO_2 selectivities, (B) monolayer cohesivenesses and (C) bilayer thicknesses.

5.3.4.4 What Factors Affect Membrane Tightness

Figure 5.17 summarizes what we believe are the major factors that contribute to the tightening of LB films made from **1**. Basically, they are the same factors that affect the monolayer cohesiveness as shown in Figure 5.9. Thus, the main factors that contribute to the tighteness of these LB films are: (i) degree of ionic crosslinking between surfactant and polyelectrolyte; (ii) charge repulsion within polyelectrolytes; and (iii) the hydrogen bonding capability within polyelectrolytes.

Thus, increasing the degree of ionic crosslinking can enhance the monolayer cohesiveness. The way to enhance the degree of ionic crosslinking is either by increasing the charge density of the polyelectrolytes in the subphase, or by increasing the number of ionic sites presented on the surfactants (Figure 5.17). Furthermore, we believe that increasing the ionic sites presented on the surfactants should be better than increasing the charge density of the polyelectrolytes in the subphase, because increasing the latter could increase the charge repulsion and decrease the hydrogen bonding within polyelectrolytes.

Reducing the charge repulsion within polyelectrolytes could enhance the monolayer cohesiveness and increase the bilayer thickness, thus increase the tightness of the bilayer. The way to reduce the charge repulsion within polyelectrolytes in this study was to reduce the charge density of the PAA by decreasing the pH of PAA.

Just like reducing the charge repulsion within polyelectrolytes, increasing the hydrogen bonding within polyelectrolytes could also enhance the monolayer cohesiveness and increase the bilayer thickness, thus increase the tightness of the bilayer. The way to increase the hydrogen bonding within polyelectrolytes in this study was to reduce the pH

of PAA. As a result, most of the carboxylate groups were protonated, and a hydrogen bonding network could be formed effectively among the PAA chains.

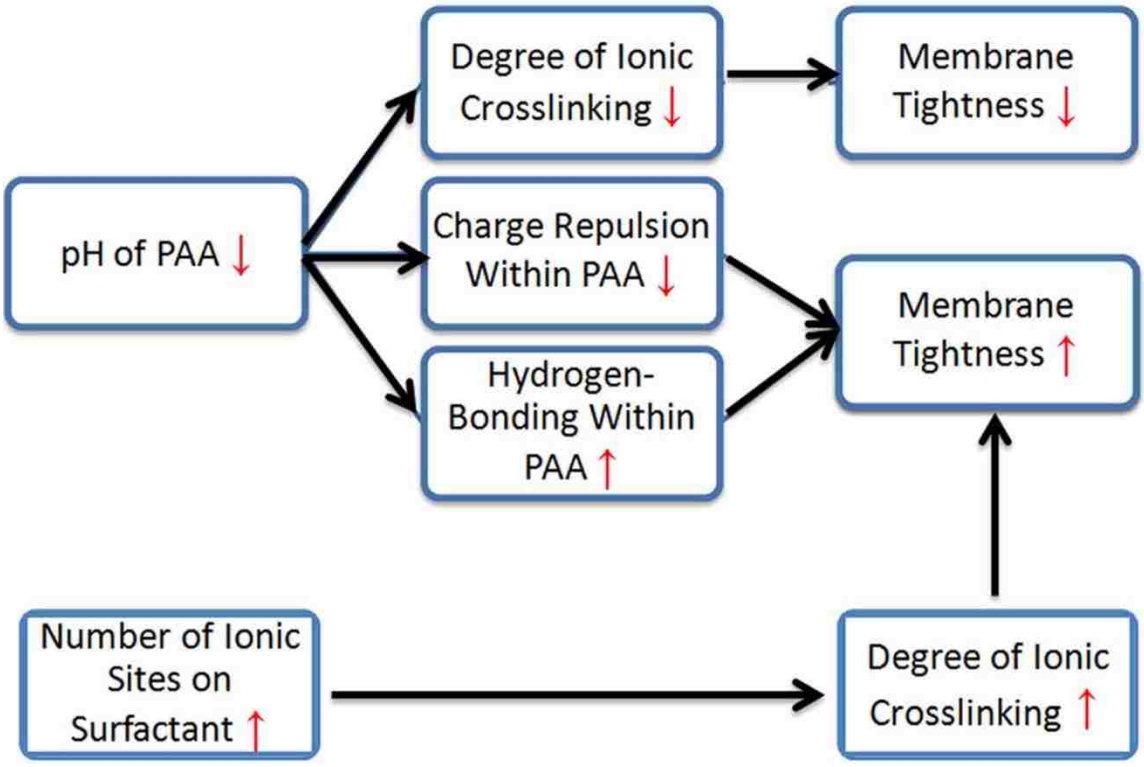

Figure 5.17 Factors that are likely to affect the tightness of PAA-glued bilayers.

5.3.4.5 Membrane Performances as Judged by the Upper-Bound Plot

To place their barrier properties into perspective, optimized PAA-glued bilayers of **1** and **Calix6** have been included in Robeson's upper-bound plot for H_2/CO_2 (Figure 5.13).[4] Here, the series-resistance model (*i.e.*, $1/[P/l]_{composite} = 1/[P/l]_{PTMSP} + 1/[P/l]_{LB}$) was used to calculate the intrinsic permeabilities of PAA-glued bilayers.[15] Thus, by measuring the permeance of PTMSP ($[P/l]_{PTMSP}$) and composite membranes ($[P/l]_{composite}$) separately, the intrinsic permeance value of the LB bilayers($[P/l]_{LB}$) can be calculated.[15] The intrinsic

permeability coefficient of the LB bilayers were calculated by the equation: $P_{LB} = [P/l]_{LB} \times l_{LB}$, in which l_{LB} is the thickness of the LB bilayers.

As seen in Figure 5.13, the intrinsic barrier properties of the PAA-glued LB bilayers made from **1** at pH 2.5 are exceptional, falling right on the current upper bound for H_2/CO_2, with their H_2/CO_2 selectivities of *ca.* 200, which are larger than any of the polymers reported to date. This implies that molecular sieving may be occurring in these bilayers.[4, 16] Further analysis will be given in the next section. The data for PAA-glued bilayers of **1** and **Calix6** at pH 3.0 lie below the upper bound, but are close to the upper bound.

The fact that the PAA-glued bilayers of **1** and **Calix6** had H_2/CO_2 permeation selectivities that are higher than almost any of the polymers reported to date, together with their extreme thinness, makes this class of films of potential interest for H_2/CO_2 separations.[2, 17]

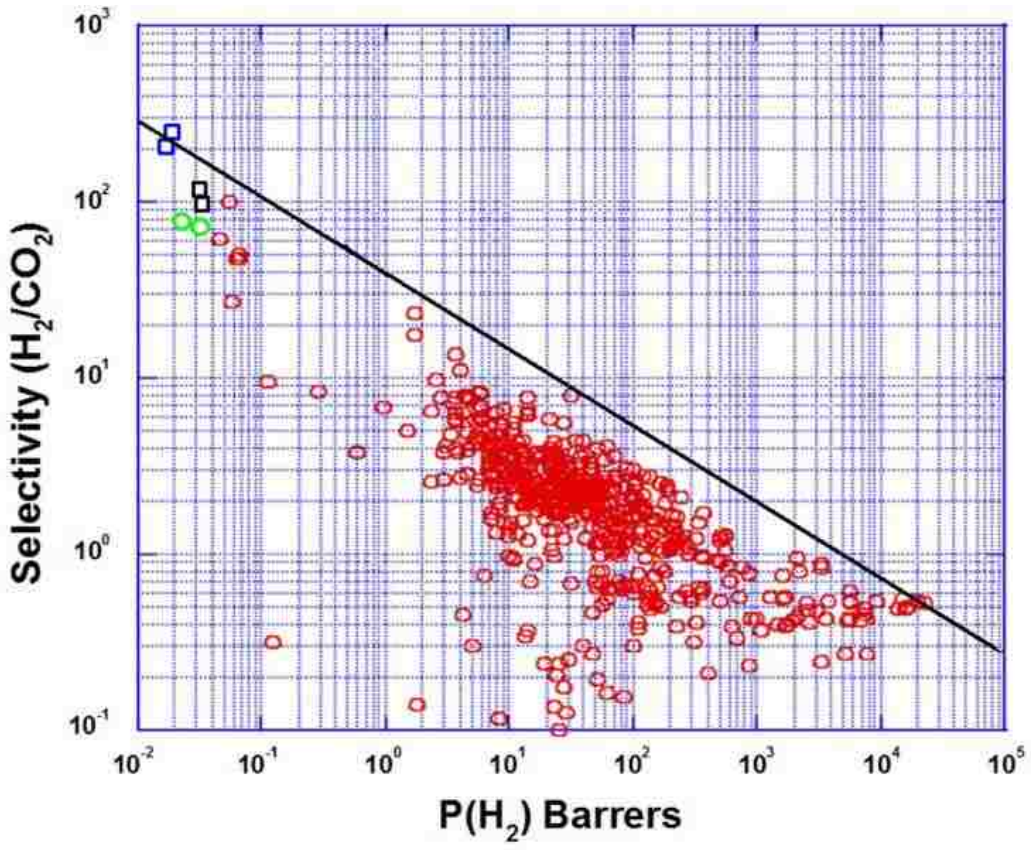

Figure 5.18 Upper-bound plot for H_2/CO_2 selectivity *versus* H_2 permeability, $P(H_2)$. Data in red are for homopolymers previously reported. Also included are the barrier properties for LB bilayers (calculated by use of the series resistance model) made from **1**+PAA, pH 2.5 (7 nm, open blue squares);**1** + PAA, pH 3.0 (6 nm, open black squares); **Calix6** + PAA, pH 3.0 (6 nm, open green circles). Figure adapted from reference 4, Copyright (2008), with permission from Elsevier.

5.3.4.6 Is Molecular Sieving Occurring?

First, assuming that the solution-diffusion mechanism controls the permeation of H_2, CO_2 and N_2 across these optimized PAA-glued bilayers of **1** and **Calix6**. Then, as discussed in Chapter 1, the gas selectivity of the membrane is defined as the product of diffusivity selectivity and solubility selectivity:[18]

$$\alpha_{ij}=(D_i/D_j)\times(S_i/S_j) \qquad (1)$$

Here, the diffusivity selectivity is related to the difference of the kinetic diameters of two gas permeants as shown in equation below: [19]

$$ln\left(\frac{D_i}{D_j}\right) = \frac{1-a}{RT} \cdot c \cdot (d_j^2 - d_i^2) \qquad (2)$$

Here, a and c are constants, while d_i and d_j are the kinetic diameters of two gas permeants.[19] Thus, the diffusivity selectivities for two gas pairs with similar size differences should be similar. Based on the kinetic diameters of H_2, CO_2 and N_2, that are 0.289 nm, 0.330 nm and 0.364 nm, respectively, the (d_{CO2}^2 - d_{H2}^2) is 0.0254 nm^2, while the (d_{N2}^2 - d_{CO2}^2) is 0.0236nm^2, which are close to each other.[20] [Note: Kinetic diameters of gases determined by zeolite molecular sieves are used in the calculation.] Thus, the diffusivity selectivity of (D_{H2}/D_{CO2}) should be similar to (D_{CO2}/D_{N2}). As a result, any difference between the permeation selectivities of H_2/CO_2 and CO_2/N_2 for these bilayers should be ascribed to the difference within solubility selectivities of two gas pairs.

In the case of PAA-glued bilayers of **1** and **Calix6** that are fabricated at pH 3.0, the H_2/CO_2 selectivities were slightly larger than CO_2/N_2 selectivities. This indicates that the relative solubility ratios of H_2/CO_2 and CO_2/N_2 in these bilayers are approximately the same, and the permeation of three gaseous permeants through the membrane was mainly controlled by diffusion.

In the case of PAA-glued bilayers of **1** that were fabricated at pH 2.5, the H_2/CO_2 selectivities were much larger than CO_2/N_2 selectivities. Here only a solubility of CO_2 that is smaller than the solubilities of H_2 and N_2 can explain the results. However, this is inconsistent with the general finding that the solubility of CO_2 is much higher than H_2 and N_2 in organic polymer membranes.[4, 20] Here, a molecular sieving model appears to provide a more reasonable explanation for these findings. Thus, in these bilayers, the

transient gaps were small enough to block the permeation of CO_2 and N_2 but not the permeation of H_2; hence, the exceptionally high H_2/CO_2 selectivities and low CO_2/N_2 selectivities that have been observed.

5.3.4.7 Is the PAA Layer Behaving as the Main Gas Barrier?

The current finding also implies that the main gas barrier is the PAA layer filled in between two surfactant layers. The reasoning is similar to that discussed in Chapter 4. In addition, the fact that increasing the thickness of PAA in PAA-glued LB bilayers of 1 (by decreasing the pH of PAA aqueous solution from 3.0 to 2.5) could improve the H_2/CO_2 selectivity serves as an additional evidence to support that the PAA layer is the main gas barrier. Nevertheless, as pointed out in Chapter 4, the intrinsic barrier properties of the pure PAA membrane are necessary to conclude that the main gas barrier is indeed the PAA layer.

5.4 Chapter Summary

In this chapter, the permeation properties of PAA-glued LB bilayers of **1**, **2** and **Calix6** under a variety of conditions have been investigated. The virtual absence of significant barrier properties for PAA-glued LB bilayers of **2**, and the exceptional performance of glued bilayers of **1**, highlight the need for high numbers of ionic sites per surfactant and ionic crosslinking for achieving high permeation selectivity. These findings also indicate that porous surfactants are not necessary to fabricate LB films with high gas permeation selectivities. Three main factors appear to be of primary importance in determining the barrier properties of ionically crosslinkied LB bilayers: (i) the degree of ionic crosslinking, (ii) charge repulsion, and (iii) hydrogen bonding among the polyelectrolyte chains. The fact that the permeation properties of PAA-glued LB bilayers of **1** that are

fabricated at pH 2.5 reach the upper bound for H_2/CO_2 suggests that molecular sieving is occurring in such LB bilayers. The current finding also indicates that the main gas barrier is the PAA layer filled in between two surfactant monolayers.

5.5 References

1. Wang, M. H.; Yi, S.; Janout, V.; Regen, S. L., A 7 nm thick polymeric membrane with a H_2/CO_2 selectivity of 200 that reaches the upper bound. *Chem. Mater.*, 2013, 25, (19), 3785-3787.
2. Shao, L.; Low, B. T.; Chung, T. S.; Greenberg, A. R., Polymeric membranes for the hydrogen economy: Contemporary approaches and prospects for the future. *J. Membr. Sci.*, 2009, 327, (1-2), 18-31.
3. Sanders, D. E.; Smith, Z. P.; Guo, R. L.; Robeson, L. M.; McGrath, J. E.; Paul, D. R.; Freeman, B. D., Energy-efficient polymeric gas separation membranes for a sustainable future: A review. *Polymer* 2013, 54, (18), 4729-4761.
4. Robeson, L. M., The upper bound revisited. *J. Membr. Sci.*, 2008, 320, (1-2), 390-400.
5. Wang, M. H.; Janout, V.; Regen, S. L., Gas Transport across hyperthin membranes. *Acc. Chem. Res.*, 2013, 46, (12), 2743-2754.
6. Wang, M. H.; Janout, V.; Regen, S. L., Hyper-thin organic membranes with exceptional H_2/CO_2 permeation selectivity: importance of ionic crosslinking and self-healing. *Chem. Commun.*, 2011, 47, (8), 2387-2389.
7. Wang, M. H.; Janout, V.; Regen, S. L., Glued Langmuir-Blodgett bilayers from calix[n]arenes: Influence of calix[n]arene size on ionic cross-linking, film thickness, and permeation selectivity. *Langmuir* 2010, 26, (15), 12988-12993.
8. Li, J. W.; Janout, V.; Regen, S. L., Glued Langmuir-Blodgett bilayers having unusually high He/CO_2 permeation selectivities. *Langmuir* 2005, 21, (5), 1676-1678.
9. McCullough, D. H.; Janout, V.; Li, J. W.; Hsu, J. T.; Truong, Q.; Wilusz, E.; Regen, S. L., Glued Langmuir-Blodgett bilayers from porous *versus* nonporous surfactants. *J. Am. Chem. Soc.*, 2004, 126, (32), 9916-9917.
10. Wang, Y.; Janout, V.; Regen, S. L., Polymer-enhanced stability of glued Langmuir-Blodgett monolayers. *Macromolecules* 2008, 41, (3), 497-500.

11. McAloney, R. A.; Sinyor, M.; Dudnik, V.; Goh, M. C., Atomic force microscopy studies of salt effects on polyelectrolyte multilayer film morphology. *Langmuir* 2001, 17, (21), 6655-6663.

12. Wang, Y.; Stedronsky, E.; Regen, S. L., Probing the gas permeability of an ionically cross-linked Langmuir-Blodgett bilayer with a "touch" of salt. *Langmuir*, **2008**, 24, 6279-6284.

13. Van Der Heide, P., *X-Ray photoelectron spectroscopy: An introduction to principles and applications,* John Wiely & Sons: Hoboken, NJ, 2012

14. Cumpson, P. J., Estimation of inelastic mean free paths for polymers and other organic materials: use of quantitative structure-property relationships. *Surf. Interface Anal.* 2001, 31, 23-34.

15. Rose, G. D.; Quinn, J. A., Composite membranes - permeation of gases through deposited monolayers. *Science* 1968, 159, (3815), 636-637.

16. Carta, M.; Malpass-Evans, R.; Croad, M.; Rogan, Y.; Jansen, J. C.; Bernardo, P.; Bazzarelli, F.; McKeown, N. B., An efficient polymer molecular sieve for membrane gas separations. *Science* 2013, 339, (6117), 303-307.

17. Ismail, A. F.; Yean, L. P., Review on the development of defect-free and ultrathin-skinned asymmetric membranes for gas separation through manipulation of phase inversion and rheological factors. *J. Appl. Polym. Sci.*, 2003, 88, (2), 442-451.

18. Wijmans, J. G.; Baker, R. W., The solution-diffusion model - a review. *J. Membr. Sci.*, 1995, 107, (1-2), 1-21.

19. Freeman, B. D., Basis of permeability/selectivity tradeoff relations in polymeric gas separation membranes. *Macromolecules* 1999, 32, (2), 375-380.

20. Baker, R. W., *Membrane technology and applications. 3rd ed.*; John Wiley & Sons: Chichester, West Sussex, 2012.

Chapter 6

Structurally Matched and Unmatched Polyelectrolyte Multilayers for Gas Separations[1]

This chapter includes material that has been reproduced in part with permission from reference 1. Copyright (2013) The Royal Society of Chemistry.

6.1 Introduction

Polyelectrolyte multilayers (PEMs) that are derived *via* the layer-by-layer (LbL) deposition method have attracted considerable attention over the past 20 years.[2, 3] Although PEMs have been of interest for applications involving electronics[4], catalysis[5], sensors[6], drug delivery[7, 8], antifouling *etc*.[2,9,10] Studies involving their gas barrier properties have been limited.[11-14]

Recently in our laboratory, we have studied PEMs made from several pairs of polyelectrolytes.[15, 16] These membranes showed impressive CO_2/N_2 selectivities in excess of 100, while their thicknesses were much less than 100 nm. Since poly(allylamine hydrochloride) (PAH) was common to these PEMs, and since primary amine groups are known to promote the facilitated transport of CO_2 through membranes, we hypothesized that these pendent primary amine groups contributed to the high CO_2/N_2 selectivities.[17]

To test this hypothesis, PEMs that are devoid of primary amine groups are investigated in this chapter. A secondary aim of this work was to examine the consequences of *structural matching* of polyelectrolytes (*i.e.*, the polycation and polyanion have the identical polymer backbones) on the gas permeation properties of PEMs. In principle, the miscibility of the polyelectroltyes should be improved by structural matching, thereby

reducing the average size of the transient gaps[18] and their permeability while increasing their permeation selectivity. Here, the transient gaps are the cavities between the polymer chain segments due to their thermal motion.[18] This excess space can also be referred to as free volume elements.[19] In addition to the effect of "structural matching", the effects of "molecular weight" and "ionic strength" on the gas permeation properties of the PEMs were also investigated. To gain further insight into these PEMs, the permeation properties of H_2 and O_2 were examined in addition to that of CO_2 and N_2.

6.2 Membrane Materials

As shown in Figure 6.1, each membrane consisted of polyelectrolyte multilayers (PEMs), an anchor layer and a poly[1-(trimethylsilyl)-1-propyne] (PTMSP) support. The structures of the polyelectroltyes, the anchoring surfactant and the support membrane are shown in Figure 6.2. Cast membranes made from PTMSP (Gelest, Inc.) were used as the ultra-permeable support. In order to introduce hydrophilicity to the PTMSP surface, an anchor layer made from a LB monolayer of **Calix6**, which was ionically crosslinked with poly(4-styrene sulfonate) (PSS or **2,** Polysciences, Inc), was deposited onto PTMSP prior to the deposition of the PEMs.

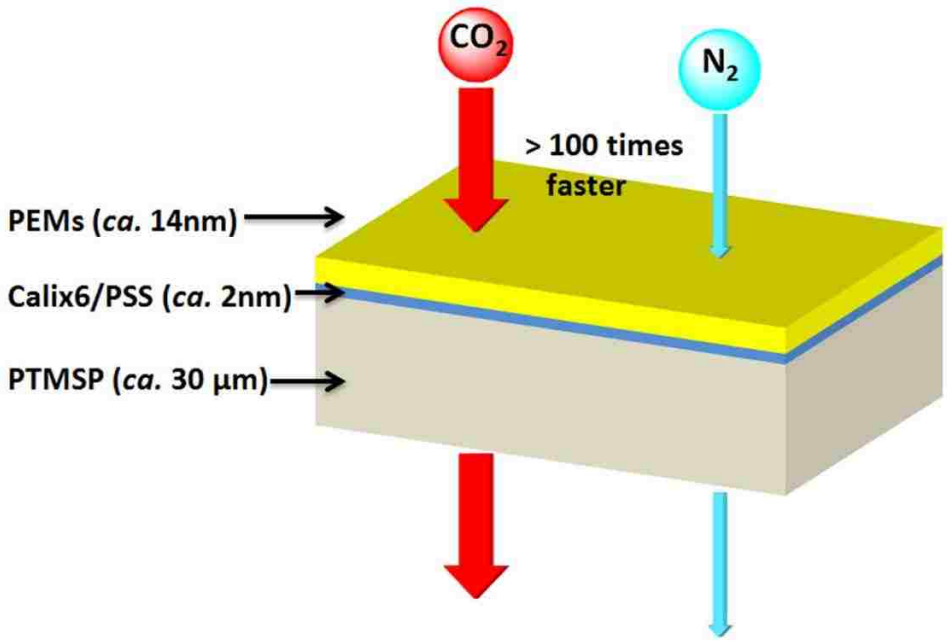

Figure 6.1 Schematic illustration of the membrane assembly.

Poly(diallyldimethylammonium chloride) (PDADMAC or **1**, Sigma-Aldrich Inc.) and poly(4-vinylbenzyltrimethylammonium chloride) (or **3**) were paired with PSS to construct hyperthin PEMs for this study. The synthesis of **3** has recently been reported.[1] Here, **3** and PSS were considered as a "structurally matched" pair since they have an identical polymer backbone, while PDADMAC and PSS were considered as a structurally unmatched pair.

Polyelectrolyte multilayers were fabricated using PDADMAC having average molecular weights of 8.5 kDa, 150 kDa and 450 kDa, PSS having an average molecular weight of 70 kDa, and **3** having an average molecular weight of 27 kDa. Specific depositing solutions that were used contained 15 mM of each polyelectrolyte (repeat unit concentration) either in the absence or in the presence of 0.1 M NaCl or 1.0 M NaCl.

Polyelectrolyte multilayers made from PDADMAC and PSS are denoted as $(\mathbf{1}_{Mw} + \mathbf{2})_n$, where **1** is PDADMAC and **2** represents PSS (Figure 6.2). The subscript Mw is the average molecular weight of PDADMAC, and n is the number of bilayers of (**1** + **2**). For example, PEMs made of PSS and PDADMAC (Mw, 450k) with a total number of layers of 27 is denoted as $(\mathbf{1}_{450k} + \mathbf{2})_{13.5}$, in which the outer layer of this PEMs is PDADMAC. For PEMs made of PSS and polycation **3**, similar nomenclature has been used.

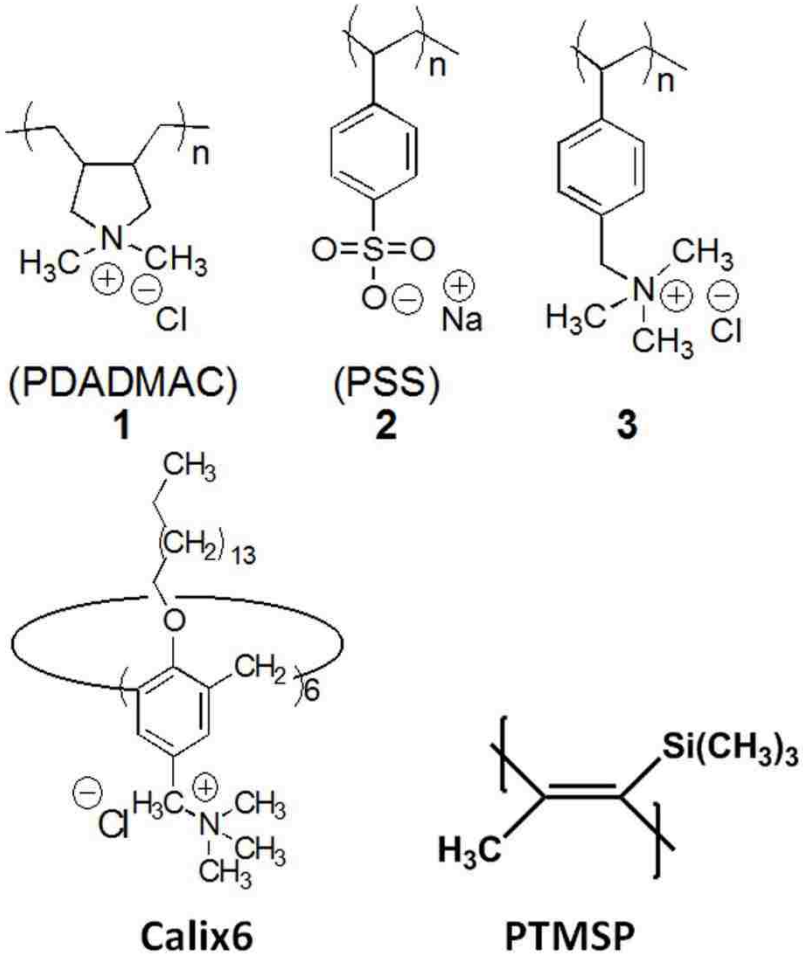

Figure 6.2 Structures of polyelectrolytes, **Calix6** (used as an anchor) and PTMSP (used as support material).

6.3 Results and Discussion

6.3.1 Thicknesses and Topographies of PEMs

To determine membrane thicknesses, PEMs were deposited onto silicon wafers that were first made hydrophobic by treatment with *n*-octadecyltrichlorosilane (OTS) to mimic the surface of PTMSP. A Langmuir-Blodgett (LB) monolayer of **Calix6** that had been ionically crosslinked with PSS was then deposited on the OTS surface to serve as an anchor layer. Experimental procedures that were used were similar to those described in the literature as well as in Chapter 2.[1,16] Film thicknesses were measured by both ellipsometry and by atomic force microscopy (AFM). [Note: a Solver Next AFM system from NT-MDT America Inc. was used for this research.] As shown in Table 6.1 and Figure 6.5, the step heights measured by AFM (by scratching the surface with a razor blade to remove the PEMs and the PSS-crosslinked **Calix6** LB monolayer) were in good agreement with the values determined from ellipsometry (NOTE: The results from AFM were consistent with OTS still on the surface under such conditions)[20-23] Figure 6.3 shows the ellipsometric film thicknesses that were determined as a function of the number of deposited layers. As is apparent, the thicknesses of PEMs grew linearly as the layers increased, under all conditions. In Figure 6.4 is shown the topographies of PEMs, which appeared to be free of defects.

6.3.1.1 The Effects of Polyelectrolyte Molecular Weight, Ionic Strength and Structurally Matching on the Thicknesses of PEMs

As shown in Figure 6.3, it is clear that the average thickness of each PEM layer made from PSS and PDADMAC was higher when higher average molecular weights were used. However, these differences were small. In contrast, increasing the ionic strength of polyelectrolyte solutions, by adding NaCl to the polyelectroyte solution greatly increased

the thickness of each polyelectrolyte layer. One possible explanation is that the NaCl weakens the charge repulsion between polycation chains or polyanion chains, by reducing the overall charge density of the polyelectrolyte chains. Thus the amount of polyelectrolytes adsorbed during each dipping process increased accordingly.[24]. The effect of structurally matching appeared to have little influence on the thicknesses of the polyelectrolyte layers based on a comparison between PEMs $(\mathbf{3}_{27k} + \mathbf{2})_{18}$ with that of $(\mathbf{1}_{8.5k} + \mathbf{2})_{18}$.

6.3.1.2 The Effects of Polyelectrolyte Molecular Weight, Ionic Strength and Structurally Matching on the Topographies of PEMs

Figure 6.4 shows the topographies of a series of PEMs. Based on these micrographs, it is clear that topographies of PEMs derived from PSS and PDADMAC with different molecular weights were similar. In contrast, the root mean square (RMS) roughness increased significantly when the NaCl concentration in solutions of PDADMAC was increased to 1.0 M. This increase in roughness may be related to the increase in the amount of polyeletrolyte adsorbed by substrate during each dipping process as discussed in the last section. Replacing PDADMAC with polycation **3** did not alter the topography of the PEMs, which was in consistent with the thickness results.

Table 6.1 Membrane thicknesses determined by ellipsometry and AFM

	Membrane[a]	Thickness[b] (ellipsometry, nm)	Thickness (AFM, nm)	RMS Roughness (AFM, nm)
NaCl Free	$(\mathbf{3}_{27k} + \mathbf{2})_{18}$	13.8 ± 0.2	13.3 ± 0.5	0.7
	$(\mathbf{1}_{8.5k} + \mathbf{2})_{18}$	14.2 ± 0.4	14.0 ± 0.6	1.3
	$(\mathbf{1}_{150k} + \mathbf{2})_{14}$	13.8 ± 0.5	13.7 ± 0.4	0.9
	$(\mathbf{1}_{450k} + \mathbf{2})_{13.5}$	13.8 ± 0.7	13.7 ± 0.3	0.7
0.1M NaCl	$(\mathbf{1}_{8.5k} + \mathbf{2})_{6.5}$	15.1 ± 0.2	14.7 ± 0.7	1.2
	$(\mathbf{1}_{150k} + \mathbf{2})_{5.5}$	14.8 ± 0.1	14.3 ± 0.9	1.5
	$(\mathbf{1}_{450k} + \mathbf{2})_{5}$	15.4 ± 0.2	14.7 ± 1.0	0.7
1.0M NaCl	$(\mathbf{1}_{8.5k} + \mathbf{2})_{3.5}$	18.4 ± 0.6	--	2.6
	$(\mathbf{1}_{150k} + \mathbf{2})_{3}$	18.5 ± 1.2	--	2.1
	$(\mathbf{1}_{450k} + \mathbf{2})_{2.5}$	17.0 ± 0.4	16.1 ± 1.4	2.0

[a]The subscripts in the parentheses are the average molecular weights of PDADMAC, the subscripts outside the parentheses are the number of bilayers of polycation and polyanion. [b]The thicknesses of PEMs that are summarized here do not include the thickness of the LB monolayer (*ca.* 2.3 nm). Error values given for film thicknesses represent one standard deviation based on five AFM and five ellipsometric measurements at different locations along the surface.

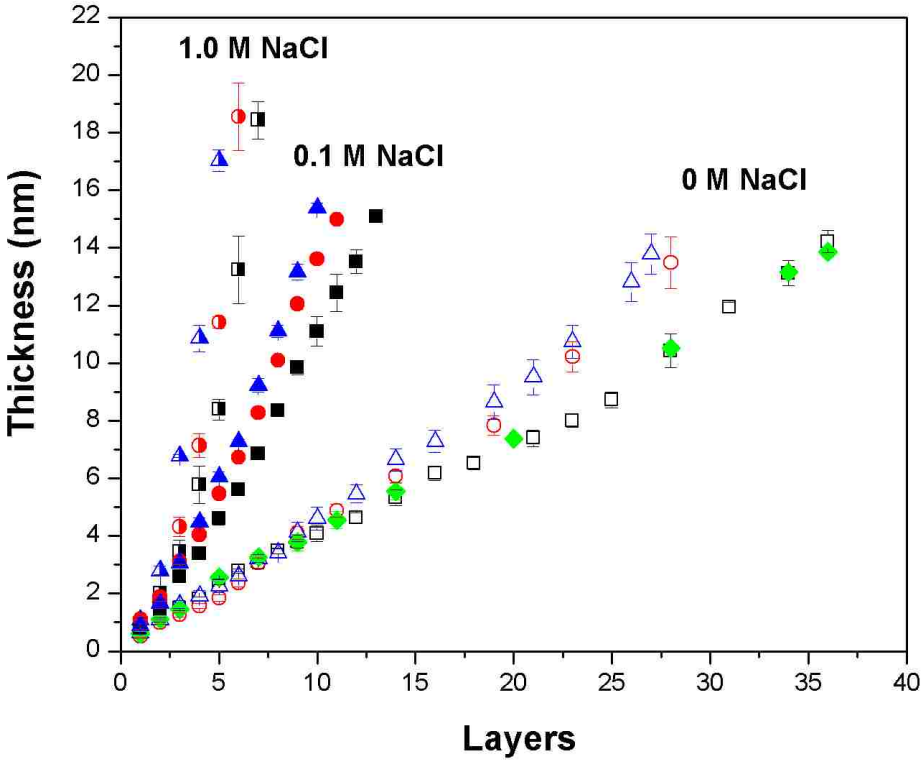

Figure 6.3 Ellipsometric membrane thicknesses *versus* number of alternating layers for PEMs. Formed without NaCl: **PSS** (Mw 70k) + **3** [(Mw 27K (♦)]; formed without NaCl: **PSS** (Mw 70k) + **PDADMAC** [Mw 8.5K (□),150K (○), and 450K (△)]; formed with 0.1M NaCl: **PSS** (Mw 70k) + **PDADMAC** [Mw 8.5K (■),150K (●), and 450K (▲)]; and formed with 1.0M NaCl: **PSS** (Mw 70k) + **PDADMAC** [Mw 8.5K (◨),150K (◨), and 450K (◭)].

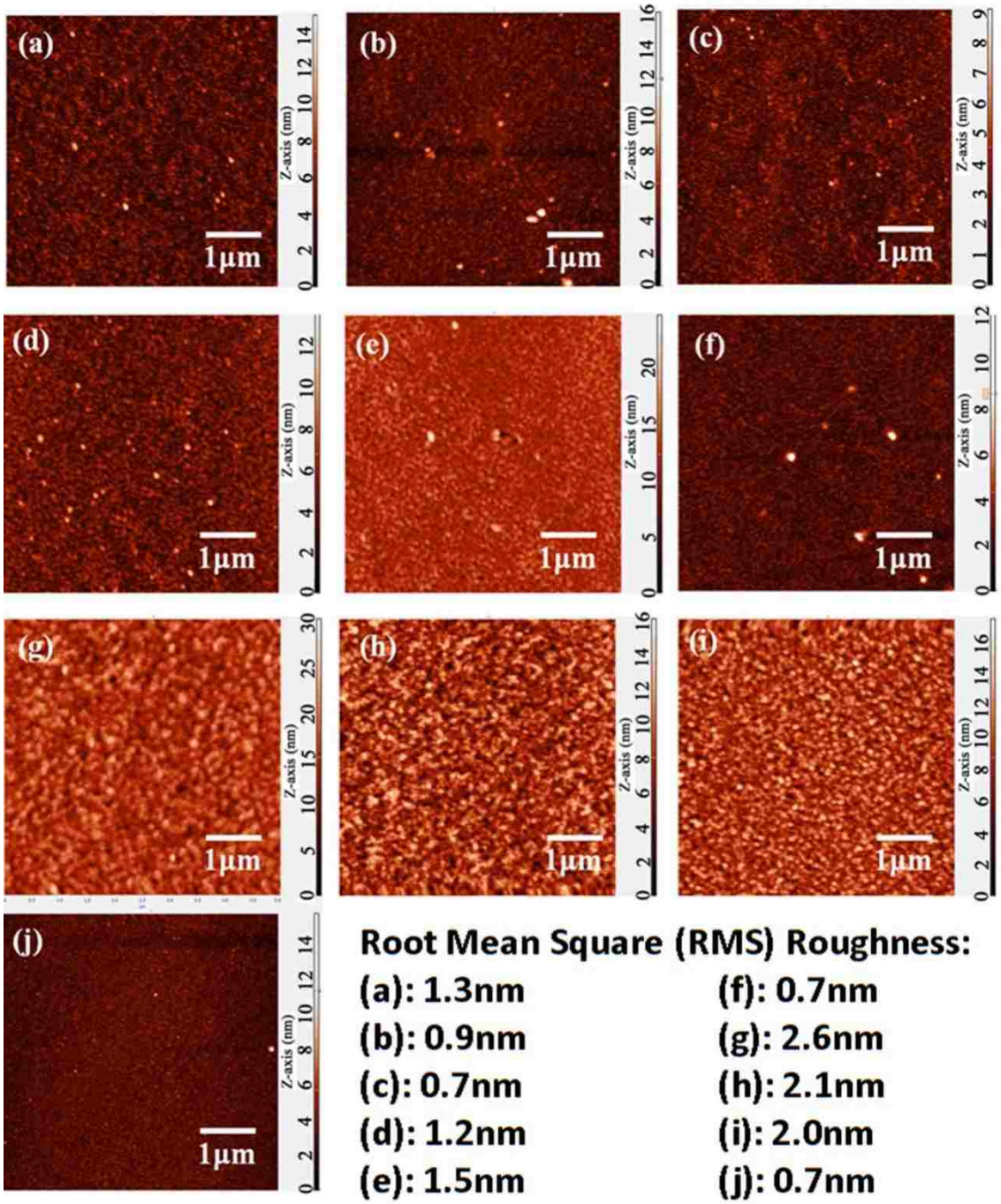

Figure 6.4 AFM Topography (tapping mode, 5 × 5 μm^2) and RMS roughness of PEMs. Formed without NaCl: (a), $(\mathbf{1}_{8.5k} + \mathbf{2})_{18}$; (b), $(\mathbf{1}_{150k} + \mathbf{2})_{14}$; and (c), $(\mathbf{1}_{450k} + \mathbf{2})_{13.5}$; formed with 0.1M NaCl: (d), $(\mathbf{1}_{8.5k} + \mathbf{2})_{6.5}$; (e), $(\mathbf{1}_{150k} + \mathbf{2})_{5.5}$; and (f), $(\mathbf{1}_{450k} + \mathbf{2})_{5}$; formed with 1.0M NaCl: (g), $(\mathbf{1}_{8.5k} + \mathbf{2})_{3.5}$; (h),$(1_{150k} + 2)_{3}$; and (i), $(1_{450k} + 2)_{2.5}$; and formed without NaCl: (j), $(\mathbf{3}_{27k} + \mathbf{2})_{18}$.

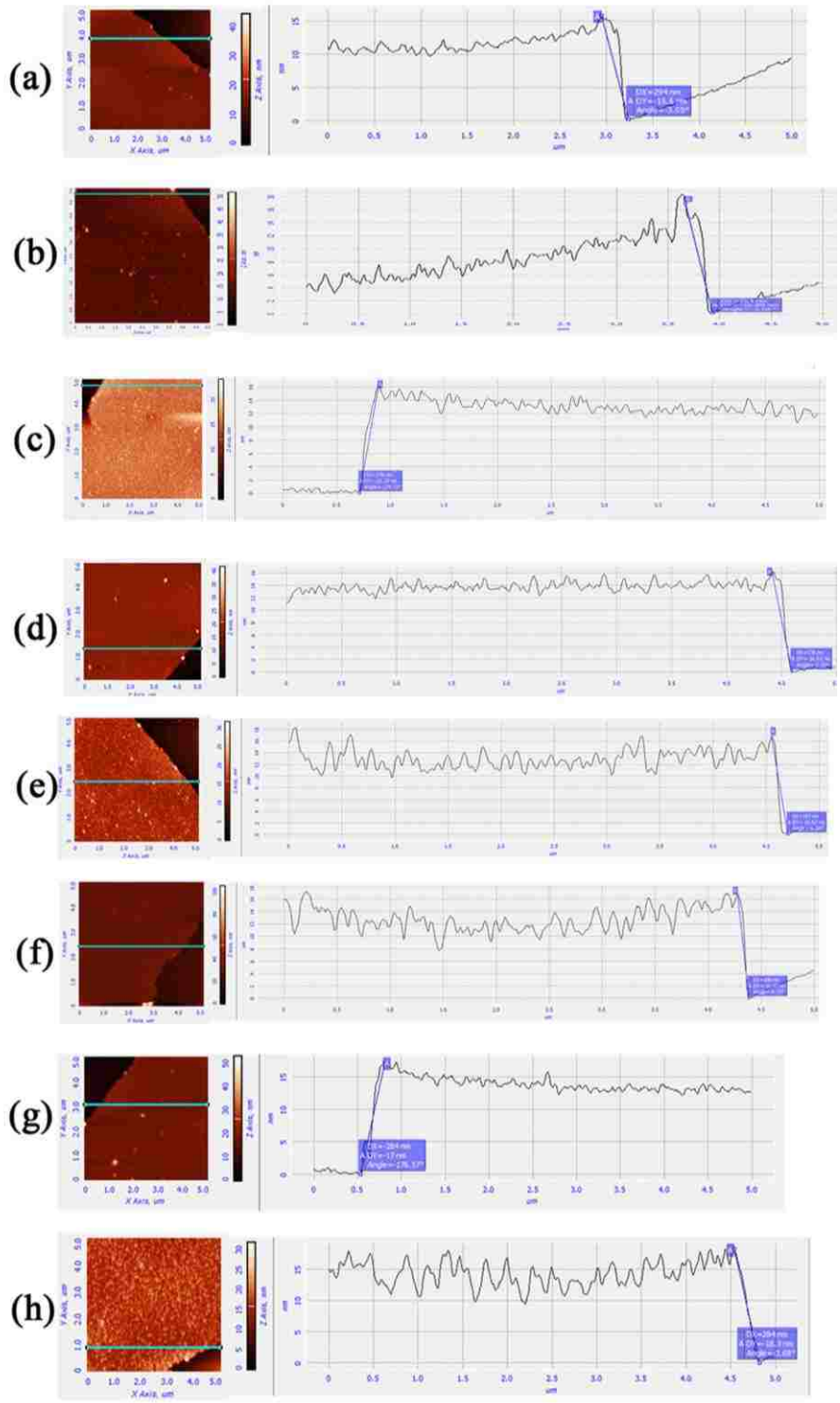

Figure 6.5 Step-**h**eight image and section profile (AFM, tapping mode, 5×5 μm^2) showing the thicknesses of PEMs (including a *ca.* 2.3 nm PSS-crosslinked **Calix6** LB monolayer): formed without NaCl: (a), $(\mathbf{3}_{27k} + \mathbf{2})_{18}$; (b), $(\mathbf{1}_{8.5k} + \mathbf{2})_{18}$; (c), $(\mathbf{1}_{150k} + \mathbf{2})_{14}$; and (d), $(\mathbf{1}_{450k} + \mathbf{2})_{13.5}$; formed with 0.1M NaCl: (e), $(\mathbf{1}_{8.5k} + \mathbf{2})_{6.5}$; (f), $(\mathbf{1}_{150k} + \mathbf{2})_{5.5}$; and (g), $(\mathbf{1}_{450k} + \mathbf{2})_{5}$; and formed with 1.0M NaCl: (h), $(\mathbf{1}_{450k} + \mathbf{2})_{2.5}$.

6.3.2 Gas Permeation Properties of PEMs

To determine the barrier properties of these membranes, a series of PEMs were deposited onto PTMSP cast membranes that were first surface-modified with a PSS-crosslinked LB monolayer of **Calix6** (Table 6.1). The thicknesses of the PEMs that were made in the absence of NaCl, in the presence of 0.1 M NaCl and in the presence of 1.0 M NaCl were *ca.* 14 nm, *ca.* 15 nm and *ca.* 18 nm, respectively (Table 6.1).

Table 6.2 shows the observed permeances (P/l) for H_2, CO_2, O_2 and N_2 across membranes that were fabricated in the absence of NaCl. Permeances that were determined for analogous PEMs made from **1** and **2** in the presence of 0.1 M NaCl and 1.0 M are summarized in Tables 6.3 and 6.4, respectively. A pressure gradient of 30 psig was employed. Here, P is the permeability coefficient and l is the thickness of the composite membrane, P/l has been derived by dividing the observed flux (F) by the area of the membrane (A) and by the pressure gradient (Δp) that was used; that is, $P/l = F/(A \times \Delta p)$. The gaseous permeants CO_2 and N_2 were investigated because the permeation selectivity of CO_2/N_2 is of practical interest for the CO_2 capture from flue gas.[25] H_2 and O_2 were measured to gain an additional perspective of their barrier properties, and because H_2/CO_2 and O_2/N_2 selectivities are of practical interests for the hydrogen production and nitrogen enrichment, respectively.[25, 26] As is apparent, the permeances of H_2, CO_2, O_2 and N_2 all reduced significantly when PEMs were deposited onto the PTMSP cast membranes. The permeances of the four gases were always $H_2 > CO_2 > O_2 > N_2$. Since the reduction in the flux for N_2 has been found to be much larger than for that of H_2, CO_2 and O_2 (Tables 6.2-6.4), the gas permeation selectivities of PEMs with respect

to H_2/N_2, CO_2/N_2 and O_2/N_2 increased substantially when compared to pristine PTMSP cast films.

As shown in Tables 6.2-6.4, these PEMs showed H_2/N_2 permeantion selectivities of *ca.* 200-400, CO_2/N_2 selectivities *ca.* 100-150, O_2/N_2 selectivities of *ca.* 8-11, and H_2/CO_2 selectivities *ca.* 2-4. The fact that all of the PEMs exhibited CO_2/N_2 selectivities that were greater than 100 clearly indicated that *the presence of primary amine groups is not required for a PEM to show high CO_2/N_2 permeation selectivity*.

In addition, Tables 6.5 and 6.6 show the gas permeation properties of PEMs fabricated in the absence and in the presence of 0.1 M NaCl using 10 psig as the pressure gradient. It is clear that the lower pressure gradient had little effect on the permeances as compared to Tables 6.2 and 6.3. However, the lower pressure gradient can lower the detectability of gas transport. For example, the N_2 flux for some of the PEMs were not detected at a 10 psig pressure gradient and were set at <0.1.

Table 6.2 Observed permeances and selectivities across hyper-thin membranes formed in the absence of NaCl.[a] (Measured at 30 psig)

Membranes[b]	H_2	CO_2	O_2	N_2	H_2/N_2	CO_2/N_2	O_2/N_2	H_2/CO_2
PTMSP[c]	6.2×10^2	1.5×10^3	3.7×10^2	2.6×10^2	2.4	5.7	1.5	0.43
PTMSP[c]	6.2×10^2	1.5×10^3	3.7×10^2	2.6×10^2	2.4	5.7	1.5	0.42
$(\mathbf{3}_{27k}+\mathbf{2})_{18}$	1.1×10^2	54	4.9	0.50	2.2×10^2	1.1×10^2	9.8	2.1
$(\mathbf{3}_{27k}+\mathbf{2})_{18}$	95	49	4.0	0.48	2.0×10^2	1.0×10^2	8.2	2.0
$(\mathbf{1}_{8.5k}+\mathbf{2})_{18}$	48	28	2.1	0.25	1.9×10^2	1.1×10^2	8.4	1.7
$(\mathbf{1}_{8.5k}+\mathbf{2})_{18}$	45	19	1.7	0.18	2.5×10^2	1.1×10^2	9.4	2.4
$(\mathbf{1}_{150k}+\mathbf{2})_{14}$	40	17	1.5	0.15	2.6×10^2	1.1×10^2	10	2.4
$(\mathbf{1}_{150k}+\mathbf{2})_{14}$	61	20	1.7	0.19	3.2×10^2	1.0×10^2	8.8	3.1
$(\mathbf{1}_{450k}+\mathbf{2})_{13.5}$	40	22	1.6	0.17	2.4×10^2	1.3×10^2	9.1	1.8
$(\mathbf{1}_{450k}+\mathbf{2})_{13.5}$	40	18	1.4	0.16	2.5×10^2	1.1×10^2	8.9	2.2

[a]Permeances at ambient temperature, $10^6 P/l$ (cm^3/cm^2-s-cmHg), were calculated by dividing the observed flow rate by the area of the membrane (9.36 cm^2) and the pressure gradient (30 psi) employed, using *ca.* 30 μm thick PTMSP supports. All measurements were made at ambient temperatures. Average values were obtained from 5-10 independent measurements; the error in each case was ±5%. [b]The subscript represents the total number of bilayers needed to reach a film thickness of *ca.* 14 nm. [c]PTMSP support with and without the LB anchor layer.

Table 6.3 Observed permeances and selectivities across hyper-thin membranes formed in the presence of 100 mM NaCl.[a] (Measured at 30 psig)

Membranes[b]	H_2	CO_2	O_2	N_2	H_2/N_2	CO_2/N_2	O_2/N_2	H_2/CO_2
PTMSP[c]	6.2×10^2	1.5×10^3	3.7×10^2	2.6×10^2	2.4	5.7	1.5	0.43
PTMSP[c]	6.2×10^2	1.5×10^3	3.7×10^2	2.6×10^2	2.4	5.7	1.5	0.42
$(\mathbf{1}_{8.5k}+\mathbf{2})_{6.5}$	33	19	1.3	0.16	2.0×10^2	1.2×10^2	8.3	1.7
$(\mathbf{1}_{8.5k}+\mathbf{2})_{6.5}$	34	15	1.2	0.11	3.1×10^2	1.3×10^2	11	2.3
$(\mathbf{1}_{150k}+\mathbf{2})_{5.5}$	34	12	0.85	0.08	4.3×10^2	1.5×10^2	11	2.9
$(\mathbf{1}_{150k}+\mathbf{2})_{5.5}$	29	9.9	0.82	0.08	3.6×10^2	1.2×10^2	10	2.9
$(\mathbf{1}_{450k}+\mathbf{2})_{5}$	36	16	1.2	0.11	3.3×10^2	1.4×10^2	10	2.3
$(\mathbf{1}_{450k}+\mathbf{2})_{5}$	33	14	0.92	0.13	3.0×10^2	1.1×10^2	7.1	2.3

[a]Permeances at ambient temperature, $10^6 P/l$ (cm^3/cm^2-s-cmHg), were calculated by dividing the observed flow rate by the area of the membrane (9.36 cm^2) and the pressure gradient (30 psi) employed, using *ca.* 30 μm thick PTMSP supports. All measurements were made at ambient temperatures. Average values were obtained from 5-10 independent measurements; the error in each case was ±5%. [b]The subscript represents the total number of bilayers needed to reach a film thickness of *ca.* 15 nm. [c]PTMSP support with and without the LB anchor layer.

Table 6.4 Observed permeances and selectivities across hyper-thin membranes formed in the presence of 1000 mM NaCl[a] (Measured at 30 psig)

Membranes[b]	H_2	CO_2	O_2	N_2	H_2/N_2	CO_2/N_2	O_2/N_2	H_2/CO_2
PTMSP[c]	6.2×10^2	1.5×10^3	3.7×10^2	2.6×10^2	2.4	5.7	1.5	0.43
PTMSP[c]	6.2×10^2	1.5×10^3	3.7×10^2	2.6×10^2	2.4	5.7	1.5	0.42
$(\mathbf{1}_{8.5k}+\mathbf{2})_{3.5}$	22	6.9	0.74	0.055	4.0×10^2	1.3×10^2	13	3.2
$(\mathbf{1}_{8.5k}+\mathbf{2})_{3.5}$	26	8.1	0.78	0.080	3.3×10^2	1.0×10^2	9.8	3.2
$(\mathbf{1}_{150k}+\mathbf{2})_{3}$	18	5.1	0.49	0.044	4.0×10^2	1.2×10^2	11	3.5
$(\mathbf{1}_{150k}+\mathbf{2})_{3}$	25	6.3	0.59	0.061	4.1×10^2	1.0×10^2	9.7	4.0
$(\mathbf{1}_{450k}+\mathbf{2})_{2.5}$	18	4.3	0.47	0.041	4.3×10^2	1.1×10^2	11	4.1
$(\mathbf{1}_{450k}+\mathbf{2})_{2.5}$	20	5.3	0.51	0.050	4.3×10^2	1.1×10^2	10	3.9

[a]Permeances at ambient temperature, $10^6 P/l$ (cm^3/cm^2-s-cmHg), were calculated by dividing the observed flow rate by the area of the membrane (9.36 cm^2) and the pressure gradient (30 psi) employed, using *ca.* 30 μm thick PTMSP supports. All measurements were made at ambient temperatures. Average values were obtained from 5-10 independent measurements; the error in each case was ±5%. [b]The subscript represents the total number of bilayers needed to reach a film thickness of *ca.* 15 nm. [c]PTMSP support with and without the LB anchor layer.

Table 6.5 Observed permeances and selectivities across hyper-thin membranes formed in the presence of 0 mM NaCl[a] (Measured at 10 psig)

Membranes[b]	H_2	CO_2	O_2	N_2	H_2/N_2	CO_2/N_2	O_2/N_2	H_2/CO_2
PTMSP[c]	6.2×10^2	1.5×10^3	3.7×10^2	2.6×10^2	2.4	5.7	1.5	0.43
PTMSP[c]	6.2×10^2	1.5×10^3	3.7×10^2	2.6×10^2	2.4	5.7	1.5	0.42
$(\mathbf{3}_{27k}+\mathbf{2})_{18}$	94	48	3.7	0.48	2.0×10^2	1.0×10^2	7.8	2.0
$(\mathbf{3}_{27k}+\mathbf{2})_{18}$	1.1×10^2	52	4.8	0.50	2.1×10^2	1.0×10^2	9.5	2.1
$(\mathbf{1}_{8.5k}+\mathbf{2})_{18}$	40	26	2.1	0.22	1.8×10^2	1.2×10^2	9.4	1.6
$(\mathbf{1}_{8.5k}+\mathbf{2})_{18}$	37	16	1.6	0.13	2.9×10^2	1.3×10^2	12	2.3
$(\mathbf{1}_{150k}+\mathbf{2})_{14}$	35	16	1.4	0.13	2.7×10^2	1.2×10^2	11	2.2
$(\mathbf{1}_{150k}+\mathbf{2})_{14}$	47	17	1.6	0.12	3.9×10^2	1.4×10^2	13	2.8
$(\mathbf{1}_{450k}+\mathbf{2})_{13.5}$	35	23	1.5	0.17	2.0×10^2	1.4×10^2	8.8	1.5
$(\mathbf{1}_{450k}+\mathbf{2})_{13.5}$	34.5	18	1.4	0.16	2.2×10^2	1.1×10^2	8.8	1.9

[a]Permeances at ambient temperature, $10^6 P/l$ (cm^3/cm^2-s-cmHg), were calculated by dividing the observed flow rate by the area of the membrane (9.36 cm^2) and the pressure gradient (10 psi) employed, using *ca.* 30 μm thick PTMSP supports. All measurements were made at ambient temperatures. Average values were obtained from 5-10 independent measurements; the error in each case was ±5%. [b]The subscript represents the total number of bilayers needed to reach a film thickness of *ca.* 15 nm. [c]PTMSP support with and without the LB anchor layer.

Table 6.6 Observed permeances and selectivities across hyper-thin membranes formed in the presence of 100 mM NaCl[a] (Measured at 10psig)

Membranes[b]	**H_2**	**CO_2**	**O_2**	**N_2**	**H_2/N_2**	**CO_2/N_2**	**O_2/N_2**	**H_2/CO_2**
PTMSP[c]	6.2×10^2	1.5×10^3	3.7×10^2	2.6×10^2	2.4	5.7	1.5	0.43
PTMSP[c]	6.2×10^2	1.5×10^3	3.7×10^2	2.6×10^2	2.4	5.7	1.5	0.42
$(\mathbf{1}_{8.5k}+\mathbf{2})_{6.5}$	28	17	1.1	0.11	2.5×10^2	1.5×10^2	10	1.7
$(\mathbf{1}_{8.5k}+\mathbf{2})_{6.5}$	29	13	0.95	0.11	2.8×10^2	1.2×10^2	8.9	2.3
$(\mathbf{1}_{150k}+\mathbf{2})_{5.5}$	29	9.3	0.84	<0.1	$>2.9\times10^2$	>93	>8.4	3.1
$(\mathbf{1}_{150k}+\mathbf{2})_{5.5}$	24	9.1	0.76	<0.1	$>2.4\times10^2$	>91	>7.6	2.6
$(\mathbf{1}_{450k}+\mathbf{2})_5$	28	14	1.1	<0.1	$>2.8\times10^2$	$>1.4\times10^2$	>11	2.0
$(\mathbf{1}_{450k}+\mathbf{2})_5$	27	12	0.85	0.12	2.3×10^2	1.0×10^2	7.3	2.3

[a]Permeances at ambient temperature, $10^6P/l$ (cm^3/cm^2-s-cm Hg), were calculated by dividing the observed flow rate by the area of the membrane (9.36 cm^2) and the pressure gradient (10 psi) employed, using *ca.* 30 μm thick PTMSP supports. All measurements were made at ambient temperatures. Average values were obtained from 5-10 independent measurements; the error in each case was ±5%. [b]The subscript represents the total number of bilayers needed to reach a film thickness of *ca.* 15 nm. [c]PTMSP support with and without the LB anchor layer.

6.3.2.1 The Effects of Polyelectrolyte Molecular Weight, Ionic Strength and Structurally Matching on the Permeation Properties of PEMs

As shown in Table 6.2, the permeances for PEMs made from PSS and PDADMAC with three different molecular weights in the absence of NaCl, were similar with respect to H_2, CO_2, O_2 and N_2. Also, the gas selectivities of H_2/N_2, CO_2/N_2, O_2/N_2 and H_2/CO_2 were similar. Similar trends were also found for PEMs made of PDADMAC and PSS in the presence of 0.1 M NaCl (Table 6.3) and 1.0 M NaCl (Table 6.4). These results indicate that changing the polyelectrolyte molecular weight had little influence on the gas barrier properties of these PEMs.

Comparing the gas permeation properties of PEMs made from PDADMAC and PSS with different concentrations of NaCl present (Table 6.2-6.4), it is clear that with NaCl present, the permeances of all gaseous permeants were slightly smaller. At the same time, the gas selectivity of H_2/N_2 increased modestly with an increase in the concentration of NaCl. These results imply that increasing the ionic strength could slightly tighten the PEMs.[19] However, the fact that the gas selectivities of CO_2/N_2, O_2/N_2 and H_2/CO_2 were almost unchanged, while the permeances of all gaseous permeants were reduced, indicates that increasing of ionic strength cannot improve the membrane gas separation properties.

A comparison of the permeation properties between structurally matched PEMs $(\mathbf{3}_{27k} + \mathbf{2})_{18}$ and structurally unmatched PEMs $(\mathbf{1}_{8.5k} + 2)_{18}$ reveals some interesting and unexpected findings (Table 6.2). As is apparent, the gas selectivities of these two PEMs were similar for H_2/N_2, CO_2/N_2, O_2/N_2 and H_2/CO_2. However, the permeances of $(\mathbf{3}_{27k} + \mathbf{2})_{18}$ were significantly higher than that of $(\mathbf{1}_{8.5k} + 2)_{18}$ (by a factor of 2). These results imply that the permeability of PEMs was increased by creating a structurally matched PEM, while its gas selectivities were retained. The origin of this effect is not presently clear. A possible reason is that the PEMs made of structurally matched pair of polyelectrolytes (*i.e.*, **3** + **2**) have transient gaps (or free volume elements) that are more uniform in size than structurally unmatched analogs (*i.e.*, **1** + **2**).

6.3.2.2 Membrane Performances as Judged by Upper-Bound Plots

To place the barrier properties of these hyperthin membranes into perspective, the intrinsic gas permeances of the PEMs were calculated using the series resistance model: $1/[P/l]_{composite} = 1/[P/l]_{PTMSP} + 1/[P/l]_{PEMs}$.[27] Here, the permeances of the composite and

the PTMSP support can be measured separately. The permeability of a PEM is then calculated by the equation: $P_{PEMs} = [P/l]_{PEMs} \times l_{PEMs}$, where l_{PEMs} is the thickness of the PEMs. The intrinsic permeation properties were then included in Robeson's upper-bound plots for H_2/N_2, CO_2/N_2, O_2/N_2 and H_2/CO_2 for further evaluation.[28] As is evident in Figure 6.6(b), the PEMs exhibited exceptionally high CO_2/N_2 selectivities and low permeabilities relative to a large number of polymeric membranes that have previously been reported. These results, together with their extreme thinness (< 20 nm), indicate that such PEMs may have potential as permeation selective layers in asymmetric membranes for CO_2/N_2 separation. Furthermore, these PEMs showed relatively high H_2/N_2 and O_2/N_2 selectivities [Figure 6.6 (a) and (c)]. However, the H_2/CO_2 selectivities of these PEMs were modest, while the permeabilities of H_2 were lower than most polymers for H_2/CO_2 separation [Figure 6.6 (d)].

In addition, as shown in Figure 6.6, the data points of PEMs made of **3** and PSS were closer to the upper bound than the PEMs made of PDADMAC and PSS in all upper-bound plots. The fact that the gas permeation properties of these PEMs lie well below the upper bounds for all four gas pairs indicates that gases permeate through such PEMs *via* a solution-diffusion process.

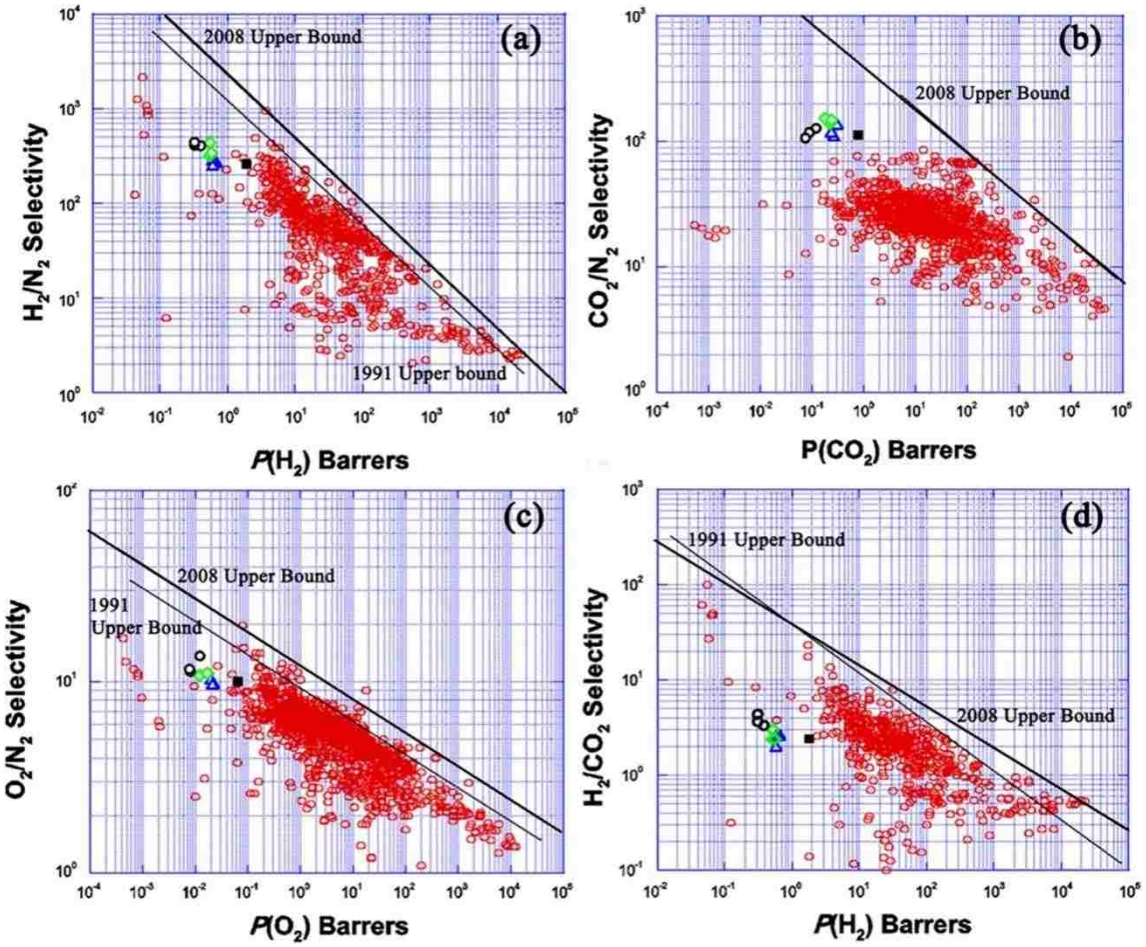

Figure 6.6 Upper-bound plots for: (a) H_2/N_2 selectivity *versus* H_2 permeability, $P(H_2)$; (b) CO_2/N_2 selectivity *versus* CO_2 permeability, $P(CO_2)$; (c) O_2/N_2 selectivity *versus* O_2 permeability, $P(O_2)$; and (d) H_2/CO_2 selectivity *versus* H_2 permeability, $P(H_2)$. The unit barrer equals to 10^{-10} $cm^3 \cdot cm/cm^2 \cdot s \cdot cmHg$. The data shown in red are for homopolymers that have been reported to date. Also included in this plot are data for PEMs formed from PSS plus **3** in the absence of NaCl (■), and PSS plus three different molecular weights of PDADMAC in the absence of NaCl (Δ), in the presence of 0.1 M NaCl (◊), and in the presence of 1.0M NaCl (○). Figures adapted from reference 28, Copyright (2008), with permission from Elsevier.

6.3.2.3 Why These PEMs Exhibit High CO_2/N_2 Selectivities But Low H_2/CO_2 Selectivities.

As shown in Tables 6.2-6.4, the CO_2/N_2 selectivities for all of the PEMs ranged between *ca.* 100 and 150, while the H_2/CO_2 selectivities of PEMs were only *ca.* 3. A relatively high solubility of CO_2 in these PEMs as compared to that of H_2 and N_2 can account for this difference.

As discussed in Chapter 1, according to the solution-diffusion mechanism, the gas selectivity of a membrane is defined as:[29]

$$\alpha_{ij}=(D_i/D_j)\times(S_i/S_j) \qquad (1)$$

For the diffusion component, the diffusivity selectivity is related to the difference of the kinetic diameters of two gas permeants as shown in equation below: [30]

$$ln\left(\frac{D_i}{D_j}\right)=\frac{1-a}{RT}\cdot c\cdot(d_j^2-d_i^2) \qquad (2)$$

Here *a* has a universal value of 0.64 for all polymers, and *c* is a constant depending on the type of polymer. A typical range of *c* is from 2.5×10^4 cal/(mol·nm^2) for ultra-permeable rubbery polymers to 1.1×10^5 cal/(mol·nm^2) for highly glassy polymers. The kinetic diameters for the two different gaseous permeant are then represented by d_i and d_j.[30] Thus, the diffusivity selectivities for two gas pairs with similar size differences should be similar.

For H_2, CO_2 and N_2, their kinetic diameters are 0.289 nm, 0.330 nm and 0.364 nm, respectively. Thus, the (d_{CO2}^2 - d_{H2}^2) is 0.0254 nm^2, while the (d_{N2}^2 - d_{CO2}^2) is 0.0236 nm^2, which are very close to each other.[31] [Note: Kinetic diameters of gases determined from zeolite molecular sives are used in the culculation.] As a result, the diffusivity selectivity of (D_{H2}/D_{CO2}) is expected to be similar to (D_{CO2}/D_{N2}). The fact that the CO_2/N_2

permeation selectivity is much greater than the H_2/CO_2 selectivity implies that the greater solubility of CO_2 relative to H_2 and N_2 is responsible for this difference; *i.e.*, $S_{CO2}/S_{N2} > S_{H2}/S_{CO2}$. This is in consistent with the fact that CO_2 usually have larger solubility in polymers than both H_2 and N_2.[28]

6.4 Chapter Summary

In this study, the gas-permeation properties for PEMs made of polyelectrolytes devoid of primary amine groups clearly demonstrated that the primary amine groups are not required to achieve high CO_2/N_2 permeation selectivities. In addition, this study also suggested that varying the molecular weights and ionic strength of the polyelectrolytes cannot improve the gas separation properties of the resulted PEMs. The fact that structural matching can enhance the permeability of a PEM without the loss of permeation selectivity was unexpected and will be subject to further investigations.

6.5 References

1. Wang, M. H.; Janout, V.; Regen, S. L., Unexpected barrier properties of structurally matched and unmatched polyelectrolyte multilayers. *Chem. Commun.,* **2013,** 49, (34), 3576-3578.

2. Decher, G.; Schlenoff, J. B., *Multilayer thin films*. Wiley-VCH Verlag &Co.: Weinheim, 2012.

3. Decher, G., Fuzzy nanoassemblies: Toward layered polymeric multicomposites. *Science* **1997,** 277, (5330), 1232-1237.

4. Xiang, Y.; Lu, S. F.; Jiang, S. P., Layer-by-layer self-assembly in the development of electrochemical energy conversion and storage devices from fuel cells to supercapacitors. *Chem. Soc. Rev.,* **2012,** 41, (21), 7291-7321.

5. Zhang, X.; Su, Z. H., Polyelectrolyte-multilayer-supported Au@Ag core-shell nanoparticles with high catalytic activity. *Adv. Mater.,* **2012,** 24, (33), 4574-4577.

6. Hammond, P. T., Form and function in multilayer assembly: New applications at the nanoscale. *Adv. Mater.,* **2004,** 16, (15), 1271-1293.

7. Tang, Z. Y.; Wang, Y.; Podsiadlo, P.; Kotov, N. A., Biomedical applications of layer-by-layer assembly: From biomimetics to tissue engineering. *Adv. Mater.,* **2006,** 18, (24), 3203-3224.

8. De Koker, S.; Hoogenboom, R.; De Geest, B. G., Polymeric multilayer capsules for drug delivery. *Chem. Soc. Rev.,* **2012,** 41, (7), 2867-2884.

9. Quinn, A.; Such, G. K.; Quinn, J. F.; Caruso, F., Polyelectrolyte blend multilayers: A versatile route to engineering interfaces and films. *Adv. Funct. Mater.,* **2008,** 18, (1), 17-26.

10. Ariga, K.; Hill, J. P.; Ji, Q. M., Layer-by-layer assembly as a versatile bottom-up nanofabrication technique for exploratory research and realistic application. *PCCP,* **2007,** 9, (19), 2319-2340.

11. Yang, Y. H.; Haile, M.; Park, Y. T.; Malek, F. A.; Grunlan, J. C., Super gas barrier of all-polymer multilayer thin films. *Macromolecules* **2011,** 44, (6), 1450-1459.

12. Sullivan, D. M.; Bruening, M. L., Ultrathin, gas-selective polyimide membranes prepared from multilayer polyelectrolyte films. *Chem. Mater.*, **2003,** 15, (1), 281-287.

13. van Ackern, F.; Krasemann, L.; Tieke, B., Ultrathin membranes for gas separation and pervaporation prepared upon electrostatic self-assembly of polyelectrolytes. *Thin Solid Films,* **1998,** 327, 762-766.

14. Levasalmi, J. M.; McCarthy, T. J., Poly(4-methyl-1-pentene)-supported polyelectrolyte multilayer films: Preparation and gas permeability. *Macromolecules* **1997,** 30, (6), 1752-1757.

15. Wang, Y.; Janout, V.; Regen, S. L., Creating poly(ethylene oxide)-based polyelectrolytes for thin film construction using an ionic linker strategy. *Chem. Mater.*, **2010,** 22, (4), 1285-1287.

16. Wang, Y.; Stedronsky, E.; Regen, S. L., Defects in a polyelectrolyte multilayer: The inside story. *J. Am. Chem. Soc.*, **2008,** 130, (49), 16510-16511.

17. Shishatskiy, S.; Pauls, J. R.; Nunes, S. P.; Peinemann, K. V., Quaternary ammonium membrane materials for CO_2 separation. *J. Membr. Sci.*, **2010,** 359, (1-2), 44-53.

18. Schmeling, N.; Konietzny, R.; Sieffert, D.; Rolling, P.; Staudt, C., Functionalized copolyimide membranes for the separation of gaseous and liquid mixtures. *Beilstein J. Org. Chem.*, **2010,** 6, 789-800.

19. Quinn, J. F.; Pas, S. J.; Quinn, A.; Yap, H. P.; Suzuki, R.; Tuomisto, F.; Shekibi, B. S.; Mardel, J. I.; Hill, A. J.; Caruso, F., Tailoring the chain packing in ultrathin polyelectrolyte films formed by sequential adsorption: Nanoscale probing by positron annihilation spectroscopy. *J. Am. Chem. Soc.*, **2012,** 134, (48), 19808-19819.

20. Wagner, K. C.; Wang, Y.; Regen, S. L.; Vezenov, D. V., Yield strength of glued Langmuir-Blodgett films determined by friction force microscopy. *PCCP,* **2013,** 15, (33), 14037-14046.

21. Sarno, D. M.; Martin, J. J.; Hira, S. M.; Timpson, C. J.; Gaffney, J. P.; Jones, W. E., Enhanced conductivity of thin film polyaniline by self-assembled transition metal complexes. *Langmuir* **2007,** 23, (2), 879-884.

22. Wang, Y.; Stedronsky, E.; Regen, S. L., Probing the gas permeability of an ionically cross-linked Langmuir-Blodgett bilayer with a "touch" of salt. *Langmuir*, **2008**, 24, 6279-6284.

23. McAloney, R. A.; Sinyor, M.; Dudnik, V.; Goh, M. C., Atomic force microscopy studies of salt effects on polyelectrolyte multilayer film morphology. *Langmuir* **2001,** 17, (21), 6655-6663.

24. Dubas, S. T.; Schlenoff, J. B., Factors controlling the growth of polyelectrolyte multilayers. *Macromolecules* **1999,** 32, (24), 8153-8160.

25. Sanders, D. E.; Smith, Z. P.; Guo, R. L.; Robeson, L. M.; McGrath, J. E.; Paul, D. R.; Freeman, B. D., Energy-efficient polymeric gas separation membranes for a sustainable future: A review. *Polymer* **2013,** 54, (18), 4729-4761.

26. Shao, L.; Low, B. T.; Chung, T. S.; Greenberg, A. R., Polymeric membranes for the hydrogen economy: Contemporary approaches and prospects for the future. *J. Membr. Sci.,* **2009,** 327, (1-2), 18-31.

27. Rose, G. D.; Quinn, J. A., Composite membranes - permeation of gases through deposited monolayers. *Science* **1968,** 159, (3815), 636-637.

28. Robeson, L. M., The upper bound revisited. *J. Membr. Sci.,* **2008,** 320, (1-2), 390-400.

29. Wijmans, J. G.; Baker, R. W., The solution-diffusion model - a review. *J. Membr. Sci.,* **1995,** 107, (1-2), 1-21.

30. Freeman, B. D., Basis of permeability/selectivity tradeoff relations in polymeric gas separation membranes. *Macromolecules* **1999,** 32, (2), 375-380.

31. Baker, R. W., *Membrane technology and applications*. *3rd ed.*; John Wiley & Sons: Chichester, West Sussex, 2012

Chapter 7

Conclusions and Recommendations

7.1 Conclusions

In this dissertation, the gas-permeation properties of two types of hyperthin membranes have been investigated: (i) Langmuir-Blodgett (LB) bilayers and (ii) polyelectrolyte multilayers (PEMs). The specific aims accomplished are summarized below.

7.1.1 Single Langmuir-Blodgett Bilayers

1) To Determine If Calix[n]arenes Act as Molecular Sieves.

The gas permeation properties of poly(4-styrene sulfonate) (PSS)-glued and poly(acrylic acid) (PAA)-glued calix[n]arene-based Langmuir-Blodgett (LB) bilayers were investigated to determine if the calix[n]arenes act as molecular sieves. The current findings support *a solution diffusion mechanism of transport and not molecular sieving*. (*i.e.*, the gaseous permeants pass through gaps between the individual calix[n]arenes and not through the pores within the calix[n]arenes).

2) To Determine Whether Porous Surfactants Are Necessary For Making Tight LB Bilayers.

The fact that the H_2/CO_2 permeation selectivities of PAA-glued LB bilayers of a non-porous surfactant polymer **1** were larger than those of a porous surfactant, **Calix6**, at each pH tested, clearly demonstrates that porous surfactants are not necessary for making tight LB bilayers.

3) To Understand What Factors Contribute to the Tightening of LB Bilayers.

By comparing the gas permeation properties of PSS-glued LB bilayers of calix[n]arenes, PAA-glued LB bilayers of calix[n]arenes and PAA-glued LB bilayers of

polymer **1**, three factors that are likely to affect the tightness of ionically crosslinked LB bilayers have been proposed: *(i) the degree of ionic crosslinking, (ii) charge repulsion, and (iii) hydrogen bonding among the polyelectrolyte chains*. In principle, a higher degree of ionic crosslinking, reduced charge repulsion and stronger hydrogen bonding among the polyelectrolyte chains should tighten the resulted LB bilayers. As a result, employing a surfactant bearing a large number of ionic sites (*e.g.*, polymer **1**) and a weak polyelectrolyte that can be optimized to have reduced charge repulsion and stronger hydrogen bonding (*e.g.*, PAA) are expected to increase the tightness of the LB bilayers.

4) To Determine if the Gas Permeation Properties of a Single LB Bilayer Can Reach the Upper Bound.

The fact that the intrinsic permeation properties of a PAA-glued single LB bilayer of polymer **1** lie on the H_2/CO_2 upper bound clearly demonstrates that the gas permeation properties of a single LB bilayer can reach the upper bound by carefully optimizing the choices of the surfactants and the conditions of the polyelectrolytes.

In addition to above accomplished aims, the studies carried out in Chapters 4 and 5 also imply that the PAA layer filled in between two surfactant monolayers in a PAA-glued LB bilayer is the main gas barrier.

7.1.2 Polyelectrolyte Multilayers

1) To Study the Effects of Molecular weight, Ionic Strength and "Structural Matching" on the Gas Permeation Properties of PEMs.

Based on the gas permeation properties of PEMs that were made from PSS and PDADMAC with different molecular weights and different ionic strengths, it is clear that varying the molecular weight and ionic strength of the polyelectrolytes solutions cannot significantly improve their gas separation properties. In contrast, replacing PDADMAC

with a structurally matched polyelectrolyte **3** (*i.e.*, with respect to PSS) afforded PEMs with significantly increased permeabilities while retaining the CO_2/N_2 permeation selectivities, which was unexpected and will be subject to further investigations.

2) To Understand the Origin of High CO_2/N_2 Selectivities of PEMs.

The comparison between the CO_2/N_2 permeation selectivities and H_2/CO_2 permeation selectivities of these PEMs suggests that the larger solubility of CO_2 with respect to H_2 and N_2 in such PEMs is the reason leads to the high CO_2/N_2 permeation selectivities.

7.2 Recommendations

7.2.1 Creating Graphene Oxide-Based Langmuir-Blodgett Films to Improve Water Vapor Resistance

One draw-back of the ionically crosslinked LB bilayers studied above is that these membranes lose gas permeation selectivities quickly after introducing water vapor into the feed gas stream. To overcome this weakness, a more water vapor-resist material should be considered. Recently, hyperthin membranes that were made from graphene oxide (GO) (Figure 7.1) by various non-LB methods showed impressive gas permeation properties. In addition, the gas permeation properties of such membranes were barely affected by the existence of water vapor.[1, 2] This fact together with GO's ability to form LB films suggests that GO-based LB films may afford high H_2/CO_2 permeation selectivities that are not affected by the water vapor.[3, 4]

In Figure 7.2 is shown a proposed scheme of a hyperthin GO-based LB film that is supported by a poly[(1-trimethylsilyl)-1-propyne] (PTMSP) cast membrane. The structures are shown in Figure 7.3. Since GO bears negative charges, the PTMSP cast membrane should be modified with a monolayer of PSS-glued **Calix6**, followed by an

additional layer of positively charged polyelectrolyte poly(diallyldimethylammonium chloride) (PDADMAC) layer, in order to ionically crosslink a GO layer. It should then be possible to deposit either a monolayer or multilayers of GO onto such support in the absence or in the presence of a "glue" (*i.e.*, PDADMAC, to ionically crosslink monolayers of GO together), using protocols similar to the literatures.[3]

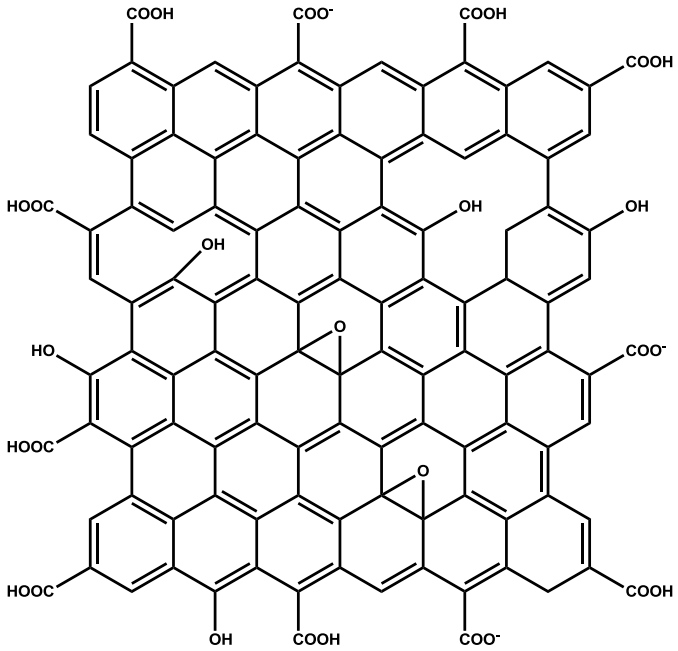

Figure 7.1 The structural model of the graphene oxide.

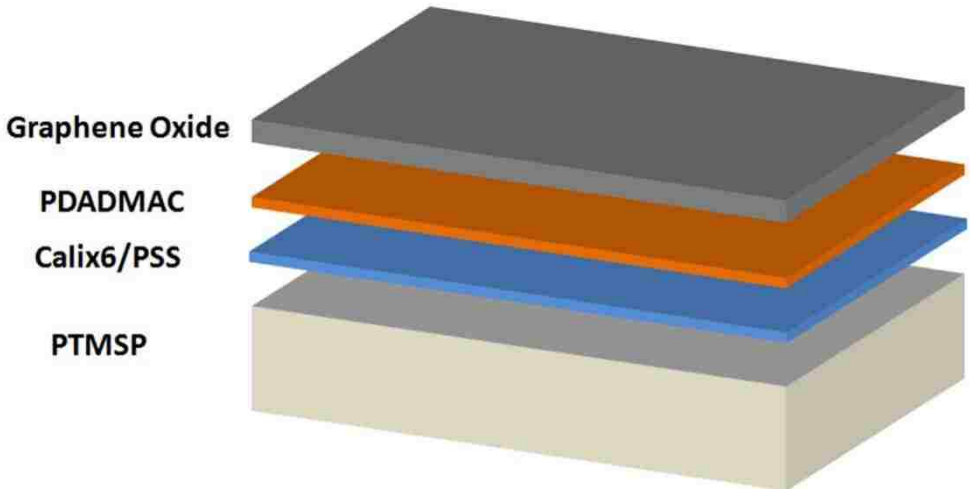

Figure 7.2 Illustration of a graphene oxide-based LB film on a hydrophilically modified PTMSP cast membrane.

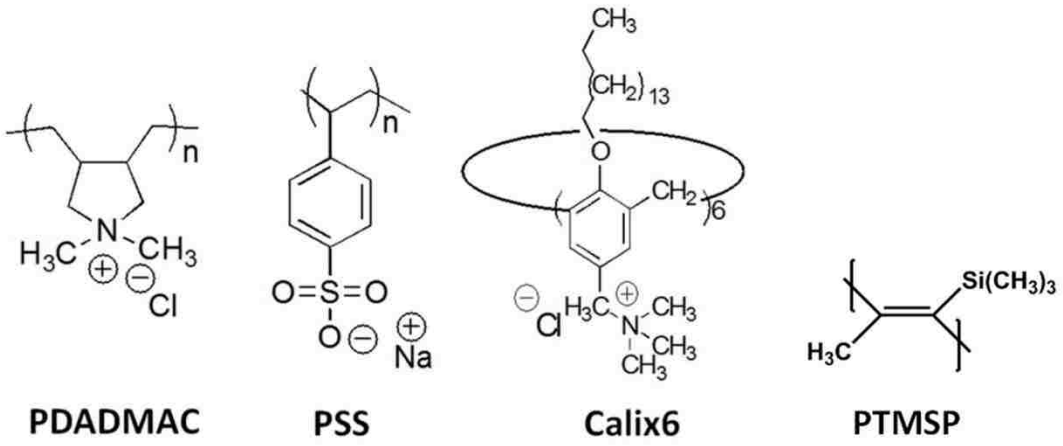

Figure 7.3 Structures of polyelectrolytes PDADMAC and PSS, surfactant **Calix6** and support material PTMSP

7.2.2 Introducing Bulky Pendent Groups into Polyelectrolyte Multilayers to Increase Gas Permeabilities

A recent publication has shown that incorporating bulky groups into copolyimides greatly increased the permeabilities of CO_2 and N_2, while retaining the CO_2/N_2 selectivities.[5] The authors suggested that this was probably due to the gain of fractional free volume (FFV) caused by the presence of bulky pendent groups.[5] This result suggests that gas permeabilities may also be enhanced by introducing bulky pendent groups into PEMs. Figure 7.4 shows a scheme to synthesize polycation **4** bearing bulky groups derived from N,N-dimethylaniline. The fractional free volume (FFV) is expected to be related to the ratio of m:n, which can be adjusted by controlling the amount of N,N-dimethylaniline that is used in the reaction.

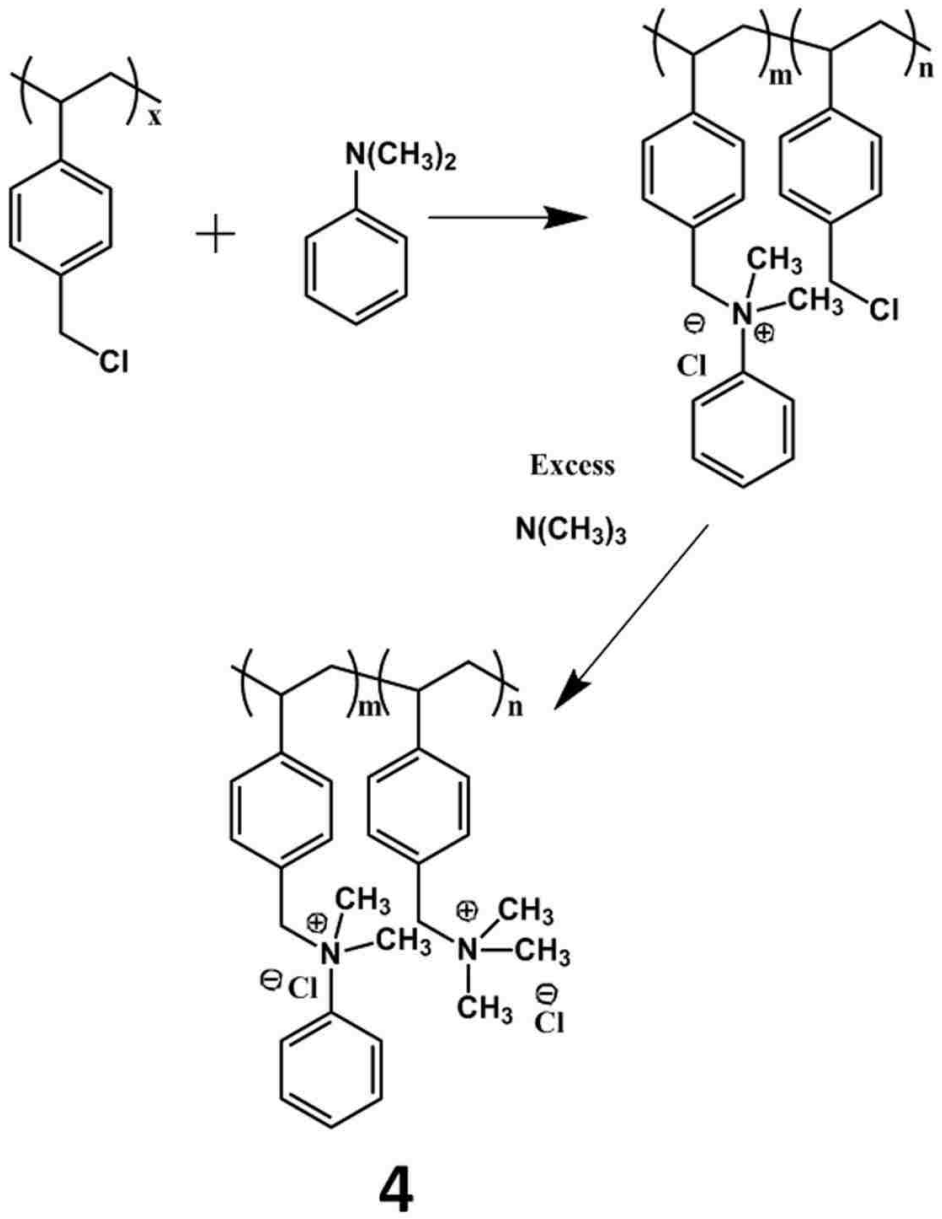

Figure 7.4 Scheme of synthesizing polyelectrolyte **4**.

7.2.3 Measuring the Intrinsic Gas Permeation Properties of PSS and PAA Membranes

The studies carried out in this dissertation suggest that the PSS layer in a PSS-glued LB bilayer made minor contribution to the gas barrier properties of the LB film, while the PAA layer in a PAA-glued LB bilayer is the main gas barrier. Whether these suggestions

are ture or not can be determined by measuring the intrinsic gas permeation properties of PSS and PAA membranes and making comparison with that of PSS or PAA-glued LB bilayers.

A solution-casting (as discussed in Chapter 2 for the casting of PTMSP membranes) or a spin-coating technique may be employed to coat PSS or PAA thin membranes on PTMSP cast films.[6] Thus the intrinsic barrier properties of PSS or PAA can be obtained by using series-resistance model.[7]

7.3 References

1. Li, H.; Song, Z. N.; Zhang, X. J.; Huang, Y.; Li, S. G.; Mao, Y. T.; Ploehn, H. J.; Bao, Y.; Yu, M., Ultrathin, molecular-sieving graphene oxide membranes for selective hydrogen separation. *Science* **2013,** 342, (6154), 95-98.
2. Kim, H. W.; Yoon, H. W.; Yoon, S. M.; Yoo, B. M.; Ahn, B. K.; Cho, Y. H.; Shin, H. J.; Yang, H.; Paik, U.; Kwon, S.; Choi, J. Y.; Park, H. B., Selective gas transport through few-layered graphene and graphene oxide membranes. *Science* **2013,** 342, (6154), 91-95.
3. Cote, L. J.; Kim, F.; Huang, J. X., Langmuir-Blodgett assembly of graphite oxide single layers. *J. Am. Chem. Soc.* **2009,** 131, (3), 1043-1049.
4. Li, X. L.; Zhang, G. Y.; Bai, X. D.; Sun, X. M.; Wang, X. R.; Wang, E.; Dai, H. J., Highly conducting graphene sheets and Langmuir-Blodgett films. *Nature Nanotech.* **2008,** 3, (9), 538-542.
5. Maya, E. M.; Garcia-Yoldi, I.; Lozano, A. E.; de la Campa, J. G.; de Abajo, J., Synthesis, characterization, and gas separation properties of novel copolyimides containing adamantyl ester pendant groups. *Macromolecules* **2011,** 44, (8), 2780-2790.
6. Jiang, P.; McFarland, M. J., Large-scale fabrication of wafer-size colloidal crystals, macroporous polymers and nanocomposites by spin-coating. *J. Am. Chem. Soc.*, **2004**, 126, (42), 13778-13786
7. Rose, G. D.; Quinn, J. A., Composite membranes - permeation of gases through deposited monolayers. *Science* 1968, 159, (3815), 636-637.

Vita

Education

Ph.D. in Polymer Science and Engineering **May, 2014**

Lehigh University, Department of Chemistry, Bethlehem, PA

Cumulative GPA: 3.90/4.00

M.S. in Materials Chemistry and Physics **July, 2008**

Shanghai Institute of Ceramics, Chinese Academy of Sciences (CAS), Shanghai, China

First year study finished in University of Science and Technology of China, Hefei, China

Cumulative GPA: 3.85/4.00

B.S. in Chemistry **June, 2005**

East China Normal University, Department of Chemistry, Shanghai, China
Ranking: Top 3 out of 114 students, Chemistry Class of 2005

High School **June, 2001**

Fenghua Middle School, Fenghua, Zhejiang, China

Research and Practical Experiences

Graduate Research

In Prof. Steven L. Regen's group, Lehigh University **2009 - Present**

Ph.D. Dissertation: Hyperthin organic membranes for gas separations.

- Developing calixarene and polymer based Langmuir-Blodgett (LB) films with ultra-high H_2/CO_2 permeation selectivity.
- Fabricating polyelectrolytes multilayers with ultra-high CO_2/N_2 selectivity.

Graduate Research

In Prof. Qian Liu's group, Shanghai Institute of Ceramics, CAS **2006 - 2008**

M.S. Thesis: Preparation and characterization of N-containing compounds and composites using mesoporous materials.

Undergraduate Research

In Prof. Yongkui Shan's group, East China Normal University **2004 - 2005**

B.S. Thesis: Preparation and characterization of composite semiconductor photocatalysts.

Undergraduate Research

In Prof. Qiying Zhang's group, East China Normal University **2003 - 2004**

Research Topic: Synthesis of a azo-containing visualization reagent and its application in detecting trace lithium.

Volunteer

In 16th International Conference of Solid State Ionics, Shanghai, China **July, 2007**

Intern

In China Technology Center of General Electric (GE), Shanghai, China **Spring, 2005**

Awards and Honors

Excellence in Polymer Science & Engineering Award **October, 2012**
(By Society of Plastic Engineers-Lehigh Valley)

Newton W. & Constance B. Buch Fellowship, Lehigh University **2011 - 2012**

Outstanding Scholarship from Chinese Academy of Sciences **2005 - 2008**

Excellent All-round Student of Chinese Academy of Sciences **2005 - 2006**

Shanghai Outstanding College and University Graduate of the year **June, 2005**

Academic Scholarship from East China Normal University (2nd Prize) **2002 - 2004**

Excellent Student Leader of East China Normal University **2002 - 2003**

National Scholarship of China (2nd Prize) **2002**

Academic Scholarship from East China Normal University (1st Prize) **2001 - 2002**

Excellent All-round Student of East China Normal University **2001 – 2002**

Journal Publications

1. Cen Lin, Qibin Chen, Song Yi, **Minghui Wang** and Steven L. Regen, "Polyelectrolyte Multilayers on PTMSP as Asymmetric Membranes for Gas Separations: Langmuir-Blodgett *versus* Self-Assembly Methods of Anchoring", *Langmuir*, 2014, DOI: 10.1021/ la404660f.

2. **Minghui Wang**, Song Yi, Vaclav Janout and Steven L. Regen, "A 7nm Thick Polymeric Membrane With A H_2/CO_2 Selectivity of 200 That Reaches the Upper Bound", *Chemistry of Materials*, 2013, *25* (19), 3785-3787.

3. **Minghui Wang**, Vaclav Janout and Steven L. Regen, "Unexpected Barrier Properties of Structurally Matched and Unmatched Polyelectrolyte Multilayers", *Chemical Communications*, 2013, 49, 3576-3578.

4. **Minghui Wang**, Vaclav Janout and Steven L. Regen, "Gas Transport across Hyper-Thin Membranes", *Accounts of Chemical Research*, 2013, *46* (12), 2743-2754.

5. **Minghui Wang**, Vaclav Janout and Steven L. Regen, "Minimizing Defects in Polymer-Based Langmuir-Blodgett Monolayers and Bilayers *via* Gluing", *Langmuir*, 2012, *28* (10), 4614-4617.

6. Mauricio F. Misdrahi, **Minghui Wang**, Chullikkattil P. Pradeep, Tianbo Liu, *et al*., "Amphiphilic Properties of Dumbbell-Shaped Inorganic-Organic-Inorganic Molecular Hybrid Materials in Solution and at an Interface", *Langmuir*, 2011, *27* (15), 9193-9202.

7. Trevor A. Daly, **Minghui Wang** and Steven L. Regen, "The Origin of Cholesterol's Condensing Effect", *Langmuir*, 2011, *27* (6), 2159-2161.

8. **Minghui Wang**, Vaclav Janout and Steven L. Regen, "Hyper-thin Organic Membranes with Exceptional H2/CO2 Permeation Selectivity: Importance of Ionic Crosslinking and Self-healing", Chemical Communications, 2011, 47, 2387-2389.

9. **Minghui Wang**, Vaclav Janout and Steven L. Regen, "Glued Langmuir−Blodgett Bilayers from Calix[*n*]arenes: Influence of Calix[*n*]arene Size on Ionic Cross-Linking, Film Thickness, and Permeation Selectivity", *Langmuir*, 2010, *26* (15), 12988–12993.

10. Vaclav Janout, Serhan Turkyilmaz, **Minghui Wang**, Yao Wang, Yuichi Manaka and Steven L. Regen, "An Upside Down View of Cholesterol's Condensing Effect: Does Surface Occupancy Play a Role?", *Langmuir*, 2010, *26* (8), 5316–5318.

11. **Minghui Wang**, Qian liu, Jiacheng Wang, Tongping Xiu, "Highly Ordered Mesoporous Silicon Oxynitride from Carbothermal Reduction Nitridation with Nanocasting Procedure", *Journal of the American Ceramic Society*, 2008, *91*(7), 2405-2408.

Presentation, Book Chapter and Patent

- **Minghui Wang**, Vaclav Janout & Steven L. Regen, "Minimizing Defects in Ultrathin Polymer-based Langmuir-Blodgett films *via* Gluing", 244th National Meeting of American Chemical Society, Philadelphia, PA, August 2012. (Poster)
- Tongping Xiu, Qian Liu, **Minghui Wang** & Qiang Yan, "Rod-Like β-Sialon Powder Prepared by a New N_2-Assisted Carbothermal Reduction of Carbon and Aluminum Nanocasted Mesoporous Silica", *Ceramic Transactions, 2010, Vol 210, Ceramic Materials and Components for Energy and Environmental Applications*, (eds D. Jiang, Y. Zeng, M. Singh and J. Heinrich), John Wiley & Sons, Inc., Hoboken, NJ, USA. 403-406
- Qian Liu, Qiang Yan & **Minghui Wang**, "Preparation of High-purity β-Sialon Ceramic Powders", Patent No. CN101698610A, 2010 (In Chinese)